Characterisation of Resistance to Everolimus in Acute Lymphoblastic Leukemia

Jordan Basnett

A thesis submitted in fulfilment of the requirements for the degree of

DOCTOR OF PHILOSOPHY

Faculty of Medicine
The University of Sydney

2016

Statement of Authenticity

This thesis is submitted to the University of Sydney in fulfilment of the requirement for the Degree of Doctor of Philosophy. The work presented in this thesis is, to the best of my knowledge and belief, original except as acknowledged in the text. I hereby declare that I have not submitted this material, either in full or in part, for a degree at this or any other institution.

Jordan Basnett

Date: 17 October 2016

Acknowledgements

This PhD has been a rollercoaster of a journey full of mixed emotions and would not have been possible without the help and support of a number of people. Firstly, I don't think I can fully say how much I appreciate the endless support provided by my supervisor A/Prof Linda Bendall. This project was not easy or simple and I would like to thank you for your patience and persistence to make me grow as a scientist and for putting up with all my "weird results" I always seemed to generate. I would also like to thank you for always being available to answer my many, many questions and for the enlightening discussions we had, some even about science. I also am greatly appreciative of the financial support offered you by during this difficult time in the science industry. Next, I would like to thank my co-supervisor Prof Ken Bradstock who was able to provide a clinical interpretation of my data and keep my work focus on the patient outcome.

I would also like to thank the members of the Leukemia Cell Biology and Cell Therapies labs over the years, especially Rob, Rana, Jacky, and Shiva, as well the lovely smurfies Renee (Old Renee/Cake Renee) and Jane (coffee Jane). I can't being to say how much I appreciate your support and guide in both conducting experiments, interpreting results and in general life as a scientist. But more importantly, I would like to thank you for our countless procrastinating discussions and many, many laughs that made the time spent of this thesis bearable.

I would also like to extend my appreciation to Joey for his assistance in all things DNA/RNA related and for trying to help me workout those weird questions I would always manage to ask him. I can't forget to say my thanks to my dear Eve. Your help and patience with me during my PhD help immensely with the proteomics aspect of

this thesis. All those long hours spot picking and mass spec'ing were made all the more enjoyable by having you there with me, I will greatly miss our chats and laughs.

To my friends and family, thank you for supporting me throughout this thesis and put up my somewhat hermit like lifestyle and intermittent phone calls. And lastly, I would like to thank Michelle, you stuck by and somehow managed to put up with me during a very stressful and trying period, thank you for your endless love and support.

Abstract

Acute Lymphoblastic Leukemia (ALL) is the most common childhood cancer. Disease relapse following treatment still occurs in a significant minority of children and the majority of adult patients. The inability to further intensify current treatments due to dose limiting toxicities of chemotherapeutic agents demands the development of new agents. One exciting new treatment, is the mTOR inhibitor everolimus. Preclinical studies using everolimus, while promising, revealed that resistance can emerge following prolonged treatment *in vivo*.

This study uses ALL xenografts that have developed resistance to everolimus by long-term exposure *in vivo*. This unique resource, combined with proteomic and transcriptome sequencing technology, allows a global approach to analyse the complex biological mechanisms behind the development of resistance to everolimus in ALL.

The expression of RNA and protein, the cell cycle distribution of everolimus resistant xenografts as well as the Kaplan Meier survival curves was vastly different between the two ALL xenografts analysed in this study. This indicates that resistance to everolimus is likely to have developed through different mechanisms. The cell cycle distribution of everolimus resistant ALL xenografts also differed depending on the tissues from which they were isolated. Leukemia cells may home to different tissue specific microenvironments that express specific factors that support ALL growth and survival to varying degrees. Furthermore, while individual genes were dissimilar between the two xenografts, there was a common regulation in pathways involved in cellular adhesion and the cytoskeleton. Proteomic sequencing identified 3 proteins possibly involved in everolimus resistance; PDLIM1, Vimentin and Stathmin-1. These proteins are involved with the cytoskeleton and may have a role in the adhesion,

migration and cell cycle, yet their exact role in the development of resistance to everolimus is yet to be confirmed.

We were unable to correlate the possible mechanisms of resistance identified in the murine model to ALL patients after acute everolimus exposure. We identified a decrease in the expression of the oncogenic micro-RNA, miR-21, though, this was likely due to the immunosuppressive effects of everolimus and did not correlate to patient outcome.

Table of Contents

Abbreviations

2D-DIGE	2 Dimensional Difference In Gel Electrophoresis
4EBP1	4E binding protein 1
ALL	Acute lymphoblastic leukemia
BCA assay	Bicinchoninic acid assay
BrdU	Bromodeoxyuridine
eIF4E	eukaryotic initiation factor 4E
FDR	False Discovery Rate
GSEA	Gene Set Enrichment Analysis
HSC	Hematopoietic stem cell
ITG	Integrin
LC-MSMS	Liquid Chromatography with tandem Mass Spectrometry
MALDI	Matrix Adsorption Laser Desorption and Ionisation
mTOR	Mammalian target of rapamycin
mTORC1	Mammalian target of rapamycin complex 1
mTORC2	Mammalian target of rapamycin complex 2
PCA	Principal component analysis
Ph– ALL	Philadelphia negative ALL
Ph+ ALL	Philadelphia positive ALL
qRT-PCR	Quantitative Reverse Transcription Polymerase Chain Reaction
Rapalog	Rapamycin analogue
RNAseq	RNA sequencing
S6K1	p70 S6 kinase 1
S6RP	S6 ribosomal protein
(xenograft)-R	denotes the everolimus resistant form of the xenograft
(xenograft)-S	denotes the everolimus sensitive form of the xenograft

CHAPTER 1 INTRODUCTION

1.1 Hematopoiesis

Hematopoiesis is a complex process where pluripotent hematopoietic stem cells (HSC) divide and differentiate along lineage specific pathways into the cells which normally comprise the blood [2, 3]. HSCs give rise to two known oligo-lineage progenitor cells, the common lymphoid and common myeloid progenitor cells, and these progenitors are restricted in their differentiation and proliferation capabilities. The common lymphoid progenitor (CLP), is the oligo-lineage progenitor which gives rise to lymphoid population, namely B-cells, T-cells, and NK-cells. The common myeloid progenitor (CMP) further differentiates into two progenitor cells, the granulo-monocyte progenitor, which gives rise to the granulocytic and monocytic lineages, and

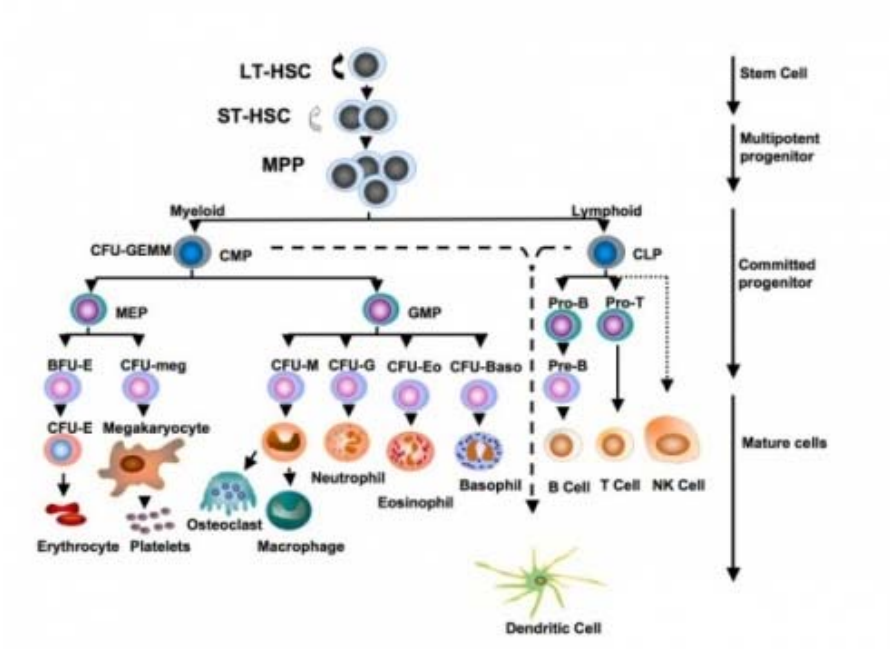

Figure 1.1 Hematopoietic Stem Cells have the pluripotent ability to divide and differentiate into the cells which normally comprise the blood. Reproduced from [1].

the megakaryocyte-erythroid progenitors which gives rise to cells of the erythrocytic and megakaryocytic lineages (Figure 1). Nevertheless, the common myeloid progenitors retain the potential to differentiate into the B-cell lineage at an extremely low frequency [4].

In 1978, Schofield et al described a specialised microenvironment within the bone marrow where HSC reside, which they termed the HSC niche [5, 6]. The supporting cells of the bone marrow create this niche and express and/or secrete factors that are required for HSC maintenance, quiescence and differentiation [2, 4]. HSC interactions with the niche and the supporting cells determine whether they remain stem cells, commit and differentiate or undergo apoptotic cell death [4, 7, 8].

1.2 Normal lymphocyte development

As HSCs develop into mature lymphocytes, they progressively lose multi-lineage and self-renewal potential and simultaneously gain the cellular and immunophenotypic features associated with the lymphoid lineage [9, 10]. The developing lymphocytes require contact with surrounding cells of the bone marrow microenvironment for continued growth and survival (Figure 1.2) and factors expressed and/or secreted by the microenvironment promote commitment to a particular lineage and mature along specific pathways. As the cells mature they move out of the bone marrow into the peripheral circulation.

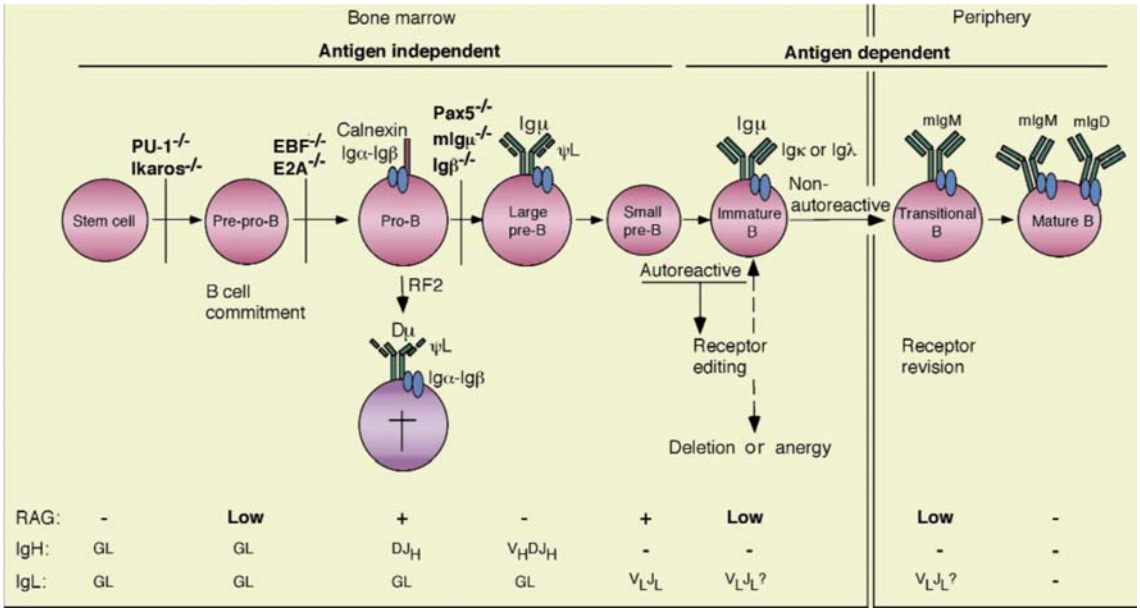

Figure 1.2 Normal B-cell development. Reproduced from [11]. IgH (heavy) and IgL (light) chain loci. GL, locus in the germline configuration.

Perhaps one of the most important secreted factors for B-lymphopoiesis is the chemokine CXCL12. It was first discovered to be a growth stimulating factor for pre-B cells [12] and is required for the retention of HSC and B-cell progenitors within the bone marrow [9]. CXCL12 is produced by a variety of cells within the bone marrow microenvironment including CXCL12-abundant reticular (CAR) cells, endothelial cells and osteoblastic cells [13, 14]. The receptor for CXCL12, CXCR4, is highly expressed on hematopoietic cells and the binding of the ligand stimulates the cell survival pathways. A gradient of CXCL12 exists within the bone marrow, with higher levels being present compared to the peripheral blood. This is a positive gradient that functions to retain the HSC within the bone marrow pool [13, 14]. Mice lacking CXCL12 or its receptor CXCR4 are non-viable with both lymphopoiesis and myelopoieisis being severely diminished in the foetal liver and bone marrow [15].

Members of the TGF-β superfamily play important roles in maintaining HSC and B-lymphopoiesis. The superfamily consists of more than 20 members including

transforming growth factor beta (TGF-β) 1–3, the bone morphogenic proteins (BMP) 2 and 7, growth and differentiation factors (GDF) 1-15, activin and Nodal [14].

TGF-β is one of the most potent inhibitors of HSC growth and is produced by a number of cells within the bone marrow microenvironment such as non-myelinating Schwann cells and megakaryocytes [16, 17]. The growth and survival of HSC pool is regulated by TGF-β in a bidirectional manner. High concentrations of the cytokine strongly induces HSC quiescence, while lower concentrations promotes the proliferation of myeloid precursors and inhibits the growth of lymphoid precursors [16].

Normal lymphocyte development in the murine bone marrow is highly dependent on the activity of IL-7 and FMS-like tyrosine kinase 3 (FLT-3, CD135), with loss of either of these cytokines arresting murine lymphocyte development [14, 18, 19]. In contrast, the role of IL-7 in humans is different, where while it is absolutely required for T-cell lymphopoiesis [14, 20] and induces proliferation of human B-cell precursors in vitro [14], it is not required for B-cell development.

In humans, FLT3 (CD135) is expressed on HSCs and early precursors of all lineages. While the exact role of FLT3 in human hematopoiesis remains unclear, it is postulated to play an important role in the survival of the HSC and precursor cells [21]. On the other hand, the expression of FLT3 in mice is restricted to the multipotent and lymphoid progenitors and is not expressed in self-renewing stem cells [21, 22].

Nevertheless, the bone marrow microenvironment is a highly complex biological system. The structure and factors expressed by the niche is not completely understood, and new discoveries are consistently being made. While the factors mentioned above are crucial for lymphocyte development, a far greater number of

factors may be responsible for the regulation of the growth and survival of both normal and malignant lymphocytes *in vivo*.

1.3 Acute Lymphoblastic Leukemia

1.3.1 Definition

Acute lymphoblastic leukemia (ALL) is characterised by the uncontrolled proliferation of lymphoblasts, within the bone marrow. As the malignant lymphoblasts increase in number, there is a concomitant decrease in the space available for normal hematopoietic cells, resulting in a reduction of normal hematopoiesis. Therefore patients often present with fatigue (anaemia), bleeding (thrombocytopenia) and recurrent infections (neutropenia), while the extensive cellular expansion can produce bone pain. The bone marrow is involved in all cases of ALL and diagnosis is made when the nucleated cell portion of the bone marrow is comprised of at least 20% malignant lymphoblasts. Extramedullary involvement is a common feature and may involve the central nervous system, lymph nodes, spleen, liver, and in males, the testes.

1.3.2 Incidence

ALL is the most common childhood malignancy in children under 15 years of age and accounts for approximately 31.9% of all childhood cancers diagnosed in the United States of America in the years 1992 to 2004, with a higher incidence rate for males than females [23]. There has been a significant increase in the event free survival for children with ALL, though females continue to obtain higher survival rates compared to males. Recent data has shown the five-year event free survival has increased to 85.6% and 87.1% for males and females respectively [24, 25].

The incidence of ALL in adults is much lower than in children, and while modern chemotherapeutic intervention has improved patient survival, the prognosis for these patients is far worse than that for children [26]. Adult ALL is generally associated with unfavourable genetic alterations, such as a high incidence of Philadelphia chromosome positive (Ph+) disease. Adult disease may also be complicated by age related co-morbidities [26-28].

1.3.3 Classification of ALL

Diagnosis of ALL is dependent on the guidelines by the World Health Organisation that uses immunophenotyping, cytogenetics and morphology to classify the leukemias. Identification of surface markers on leukemic cells also allows them to be classified according to the stage of maturation and also to be differentiated from normal cells (Table 1.1). The latter enables the tracking of the malignant cells throughout treatment and the detection of minimal residual disease [29]. Cytogenetic abnormalities are found in 70% of adults and 90% of children with ALL [28] and play a large role in the risk stratification of ALL patients into risk categories. Common cytogenetic abnormalities associated with adult and paediatric B-lineage ALL are summarised in Table 1.2.

1.3.4 Current Therapy

The therapeutic options available for patients with ALL are dependant on factors such as their age, cytogenetic abnormalities and risk status. The cornerstone of all therapy is a complex, multi-agent approach that aims to eradicate the bulk of the leukemic cells, induce remission and restore normal hematopoiesis.

Table 1.1 Common ALL phenotypes and expression of immunological markers (adapted from [28]).

B Lineage

Subtype	Immunophenotype
Pro-B	CD19+, CD22+, CD79a+
Pre-B	CD19+, CD22+, CD79a+, CD10+, clg
Mature	CD19+, CD22+, CD79a+, CD10+, slg, CD20(+/-)

T Lineage

Subtype	Immunophenotype
Pro-thymocyte	CD7+, CD2-, CD5-
Immature	CD7+, CD2 or CD5+, CD3-
Mature	CD7+, CD2+, CD5+, CD3+

CD – cluster of differentiation, c-Ig – cytoplasmic immunoglobulin, sIg – surface immunoglobulin.

Table 1.2 Common chromosomal abnormalities found in adult and pediatric ALL patients (adapted from [28, 30, 31])

Cytogenetics	Gene	Adult	Children
t(9;22)(q34;q11)	BCR-ABL1	25-30%	2-5%
t(1;14)(p32;q11)	TAL-1	12-26%	3%
t(v;11)(v;q23)	MLL	10%	8%
t(10;14)(q24;q11)	HOX11	8%	1%
t(12;21)(p13;q22	TEL-AML1	1-4%	25%
t(8;14), t(2;8), t(8;22)	C-MYC	4%	2%
t(1;19)(q23;p13)	E2A-PBX1	3%	6%
t(5;15)(q35;q32)	HOX11L2	1%	1%
t(5;14)(q31;q32)	IL3-IGH	<1%	<1%
Focal deletions/mutations of 7p12.2	IKZF1	-	15%
Dic(9;20)	CDKN2a	0.5%	2-3%
Deletion on 22q22	ERG	-	3-7%
Hyperdiploidy (more than 50 chromosomes)	-	<9%	25-30%
Hypodiploidy (less than 44 chromosomes)	-	2%	1%
N/A	BCR-ABL1-Like	21-27%	15%

CNS involvement is uncommon at diagnosis but intrathecal chemotherapy may be included in first line treatment if the patient is considered to be a high risk of developing CNS disease. The overall survival rate of paediatric patients following induction chemotherapy is 90%, though this is dependent on early intensification and consolidation of therapy [32-34]. Adolescent and young adults (AYA) patients with ALL have an increased prevalence of poor risk factors, such as the Ph+, hypodiploidy, complex karyotypes and a higher incidence of T-cell ALL [28]. While the recent adoption of paediatric treatment protocols, including the use of asparaginase, has improved outcomes for AYA patients [35], the survival rates remain inferior to paediatric patients treated with the same protocols.

The survival of adults with ALL has improved significantly over the last decade with remission rates rising to 85-90% and overall survival rates of 40-50% [27, 36-38]. Superior chemotherapy regimens and the adoption of stem cell transplant into front line therapy, have made substantial contributions to increasing patient survival. However, poor risk factors including unfavourable cytogenetics, and a high rate of relapse, continue to limit favourable patient outcomes. Historically, Ph+ disease was associated with poor patient prognosis, a high risk of relapse, and a five year survival rate of only 5-10% with chemotherapy alone [39]. The development of the BCR/ABL tyrosine kinase inhibitors (TKI) such as imantinib, dasatinib, nilotinib and ponatinib has significantly improved the response of Ph+ ALL, when combined with conventional chemotherapy [28].

Recently, a new sub-group of ALL has been identified. These Philadelphia-like (Ph-like) cases have a similar gene expression profile to Ph+ ALL, but do not carry the BCR/ABL translocation [40]. Deletions or mutations in IZKF1, a lymphoid transcription factor, are features of both Ph-like and BCR/ABL positive ALL. Moreover,

approximately 50% of Ph-like ALL cases contain a mutation in CRLF2, which is highly associated with mutations of members of the Janus Kinase (JAK) family [31, 41, 42]. Ph-like ALL represents approximately 15% of paediatric and 27% of AYA patients with ALL and is associated with a poor patient outcome and a higher rate of relapse than other BCR/ABL negative subtypes [42, 43]. A study by Roberts et al profiled the genome of 1725 patients with ALL (154 of which had Ph-like ALL) and found 91% of the patients with Ph-like ALL, also harboured other kinase-activating mutations [40]. Therefore, clinically approved tyrosine kinase inhibitors may be beneficial in treating Ph-like ALL. However, a larger clinical trial where tyrosine kinase inhibitors are added to current protocols based mutations detected in individual Ph-like patients must be performed to assess effects on patient outcome.

1.3.5 New directions in ALL therapy

Monoclonal antibodies such as those directed against CD20, CD22, CD52, and CD19 have demonstrated the power of immunotherapy to complement current chemotherapeutic regimens and improve patient survival. [44-46]. Two new promising immunotherapy options in ALL are CAR (Chimeric Antigen Receptor) cells [47-52] and BiTE (Bispecific T-cell Engaging) antibodies [47, 53-58].

Both CAR cell and BiTE antibodies have successfully been used in several clinical trials in both adults and children with promising results [47, 55-58]. However, their use in patients with ALL results significant toxicities, particularly a ‘cytokine storm’ which eventuates when used in patients with high tumour load [47]. Therefore more clinical trials are required for both immunotherapy options before their implementation in mainstream clinical treatment of ALL.

1.3.6 Issues with current therapy

Currently, the treatment of ALL is a long, arduous process and results in significant toxicity to normal tissues due to the relative non-specific action of chemotherapeutic compounds. Moreover, the efficacy of treatments is severely hampered by the development of resistance and often leads to refractory relapses and poor patient survival. Two major hypotheses exist as to how ALL cells develop resistance to chemotherapeutic compounds. ALL cells may develop resistance through the acquisition of resistance conferring mutations during chemotherapy, or such mutations may have been present in a sub-population of ALL clones at diagnosis. Extended treatment selects these clones allowing them to become the dominant population and leading to relapsed disease that is resistant to chemotherapy [59, 60].

The development of new therapeutic options, such as immunotherapy and targeted pathway inhibition, has great potential in improving patient survival. However, these treatments remain in the experimental stage and carry significant risks associated with their use. Further investigation into these upcoming immunotherapy and pathway specific inhibitors is required overcome treatment related resistance and to maximise patient outcome.

1.4 Mammalian Target of Rapamycin (mTOR)

Cell growth is a tightly controlled process involving numerous signalling pathways that can become dysregulated in malignant disease. One such pathway is that involving the mammalian target of rapamycin (mTOR), a ubiquitously expressed serine/threonine kinase that is involved in important cellular processes such as proliferation, protein synthesis, survival and metabolic activity [61, 62].

mTOR is a highly conserved protein, with humans, mice and rats sharing approximately 95% homology in amino acid sequence. The N-terminus of the protein contains up to 20 tandemly repeated HEAT domains (Huntingtin, Elongation factor 3, A subunit of PP2A and TOR) as well as a FAT (FRAP-ATM-TRRAP) domain. While the C-terminus of mTOR contains a catalytic kinase domain, putative auto-inhibitory domain (negative repressor domain, NRD), the FK binding protein 12 (FKBP12)-rapamycin binding domain (FRB) and FATC (FAT C-terminus) domain (Figure 1.3). As this portion of the protein is homologous to PI3K, mTOR is considered to be part of the same family of kinases, the PIKK (PI3K-related protein kinase) family [64-67].

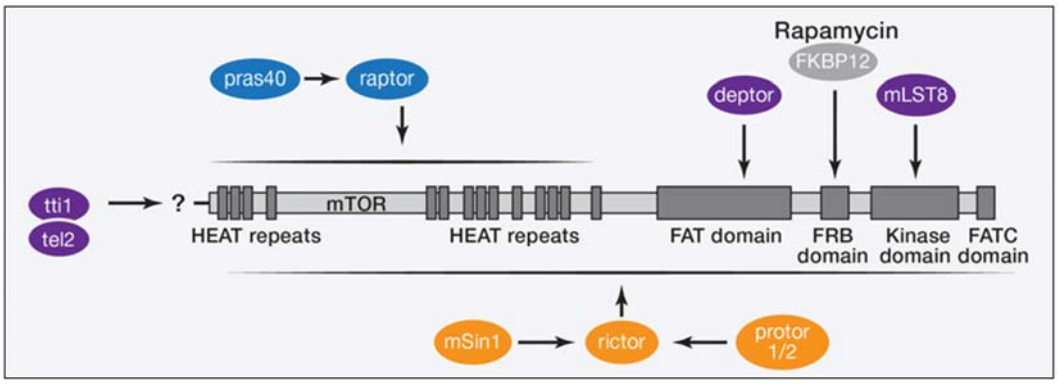

Figure 1.3 The protein structure of the mammalian target of rapamycin (mTOR). Reproduced from [63].

1.4.1 mTORC1

Two complexes are formed using mTOR; mTORC1 and mTORC2, with each recruiting different subunits and having distinct roles within the cell (Figure 1.4). The first complex, mTORC1, arises from the association between mTOR and FKBP12 which further recruits the following proteins; RAPTOR (regulatory associated protein of

mTOR), PRAS40 (proline rich AKT substrate 40) and DEPTOR (DEP-domain containing mTOR-interacting protein [68]). GβL (g-protein β-subunit like protein), otherwise known as mammalian LST8 (mLST8), is also recruited and its binding to the catalytic domain of mTORC1 being necessary for full catalytic activity [69]. The role of RAPTOR in the formation and activity of the mTORC1 complex remains unclear, however, it has been proposed that RAPTOR has a tug-of-war style relationship with GβL. Under nutrient deficient conditions raptor binds strongly to mTOR thereby inhibiting it. Conversely in nutrient rich conditions GβL displaces RAPTOR allowing kinase activation [70].

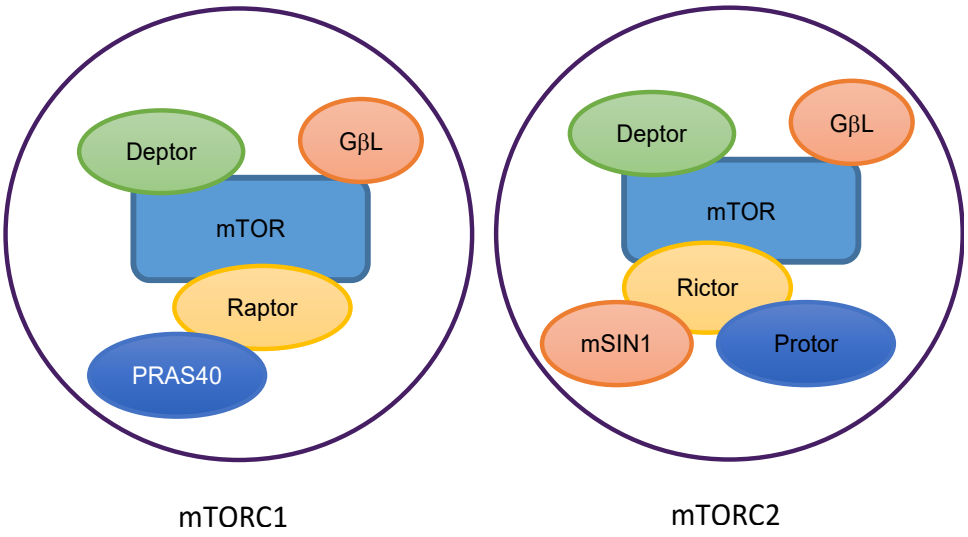

Figure 1.4 Composition of the two mTOR complexes, mTOR1 and mTORC2.

There are two methods by which the mTORC1 may be activated: 1) by extracellular growth factors and their receptors or 2) by fluctuations in the metabolic status of the cell such as cellular energy status, nutrient availability or hypoxia. The proteins TSC1

(also known as hamartin) and TSC2 (also known as tuberin) form a complex that controls cellular growth and regulates the activity of mTOR [71, 72] (Figure 1.5). TSC1 stabilizes TSC2 by preventing its degradation by the ubiquitin pathway. The GAP (GTPase-activating protein) domain of TSC2 activates the small G-protein Rheb (Ras homologue enriched in brain) that catalyses the conversion GTP to GDP [72]. Activated Akt inhibits the TSC1/2 complex allowing the accumulation of GTP within the cell. The accumulated GTP activates mTORC1, although the mechanism behind this activation is not fully understood [73, 74].

The translation of mRNA is tightly regulated at the rate-limiting step where the ribosome is recruited to the 5' end of the mRNA. The 5' end of all nuclear transcribed mRNA's possess the cap structure m^7GTP (7-methylguanosine), which is recognized by the eukaryotic initiation factor 4E (eIF4E) [75]. This leads to a complex being formed with other initiation factors and leading to the binding of the 40S ribosome and the initiation of translation. The 4E-Binding protein family (4EBP), of which 4EBP1 is the most extensively studied, restricts the recruitment of the translation complex to initiation factor eIF4E, thus controlling the rate of translation. Under basal conditions, 4EBP1 remains bound to eIF4E in its hypo-phosphorylated form, and upon activation, the phosphorylation of 4EBP1 by mTORC1, leads to its dissociation from eIF4E, allowing the recruitment of the protein complex and mRNA translation [75, 76].

The synthesis of new proteins is paramount for the continual survival of a cell, and the downstream effects of mTORC1 signalling to the S6 kinases, co-ordinates this process. Mammalian cells contain two S6 kinases, S6K1 and S6K2, that have conserved phosphorylation domains but are encoded by separate genes [76]. Un-phosphorylated S6K remains bound to the initiation factor eIF3, and phosphorylation of S6K on Thr389 by mTORC1, results in its dissociation from eIF3 [75]. The activity

of S6K1 is dependent on multiple phosphorylation events, including phosphorylation on Thr229 and Ser411, however, initial phosphorylation on Thr389 by mTOR, is essential for full activation [77-79]. mTOR binds to a specific site within the N-terminus of S6K1 called the TOR signalling (TOS) motif. This site is essential as deletion or functional inactivation of this motif prevents mTOR binding and subsequent phosphorylation of S6K [66]. Interestingly, S6K1 is involved in a negative feedback loop linked the activity of Akt through its phosphorylation RICTOR, a subunit of mTORC2 [80].

Phosphoinositide Dependent Kinase 1 (PDK1) is responsible for the phosphorylation of Thr229 in the kinase domain of S6K1, however, phosphorylation of Thr389 is required prior to the PDK1-mediated phosphorylation of Thr229 [64]. Meanwhile, the phosphorylation of Ser411 is required for the mTOR mediated phosphorylation of Thr389 and subsequent activation of the kinase [81]. S6K subsequently phosphorylates several substrates involved in the translation of mRNA and in protein biosynthesis, such as eIF4B, PDCD4 (programmed cell death 4), SKAR (S6K1 ALY/REF-like substrate), eEF2K (Eukaryotic elongation factor-2 kinase), CCTβ (T-complex protein 1 subunit beta), NCBP80 (Nuclear cap-binding protein subunit 1), and p70-RPS6 (ribosomal protein S6) [75].

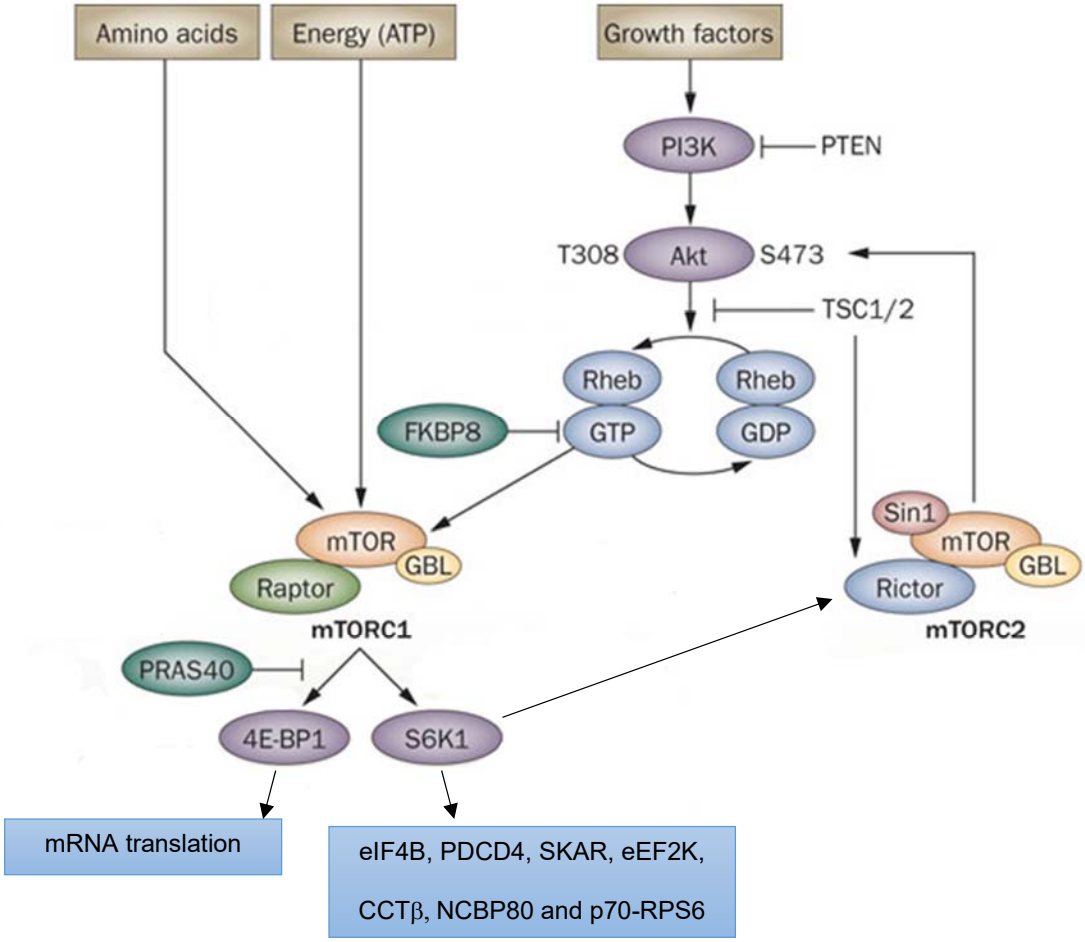

Figure 1.5. The PI3KAkt/mTOR signalling pathway (adapted from [75, 82, 83]).

1.4.2 mTORC2

mTORC2 is a distinct complex from mTORC1. In contrast to mTORC1, it does not require mTOR to first bind FKBP12 and so is relatively insensitive to rapamycin, although, prolonged treatment with rapamycin can inhibit mTORC2 in some cell types [83, 84]. As with mTORC1, mTORC2 is comprised of mTOR, mLST8 and DEPTOR, but specifically recruits mSIN1, Protor and RICTOR (rapamycin insensitive companion of mTOR). [83, 85, 86] (Figure 1.4). In contrast to mTORC1, mTORC2 requires an intact TSC1/2 complex for activation by growth factors [87]. The TSC1/2 complex associates with rictor and activates mTORC2 independently of the GAP activity of TSC2 towards Rheb (Figure 1.5) [83].

mTORC2 is responsible for the allosteric activation of Akt by phosphorylation of Ser473 which increases the specificity of Akt towards its substrates [88]. Phosphorylation of Akt on Ser473 is indicative of mTORC2 activation by stimuli such as growth factors and hormones. Mouse embryonic fibroblasts (MEFs) with defective mTORC2 signalling due to deletion of Sin1, rictor or mLST8 are unable to phosphorylate Akt on Ser473. These cells have normal Akt activity as it can still be activated by phosphorylation of its T-Loop domain on Thr308, however, they demonstrate reduced activity on downstream targets [88].

The AGC group of kinases (Protein kinase A, G and C families) all share conserved Thr-Pro-Pro residues within their turn motif. Thr450 of Akt is within such a motif and is solely phosphorylated by mTORC2 during the synthesis of nascent Akt while the peptide is still attached to the ribosome. This modification is essential for the stability of the protein by allowing the C-terminus to anchor to the kinase domain [83]. Moreover, the lack of turn motif phosphorylation in mTORC2 disrupted cells leads to ubiquitination and degradation of the newly synthesized Akt.

mTORC2 is also phosphorylates Ser422 within the hydrophobic motif of the AGC kinase SGK1. Disruption of mTORC2 signalling leads to defective activation of SGK1 due to diminished phosphorylation and activation of the hydrophobic motif [83, 89]. Unlike SGK1, phosphorylation of the hydrophobic motif of protein kinase c (PKC) does not require mTORC2 as it can also occur by auto-phosphorylation, although, phosphorylation of the turn motif is highly dependent on mTORC2 and disruption of mTORC2 signalling leads to diminished phosphorylation and decreased PKC expression [83].

1.4.3 Role of mTOR in leukemia

The mTOR signalling pathway plays a pivotal role in the growth and proliferation of cells through the coordination of many metabolic processes such as energy levels, nutrient availability and extracellular growth factors (Figure 1.5) [63, 82, 90, 91] . One of the key hallmarks of cancer is the uncontrolled proliferation in the absence of growth signals. It is of no surprise then, that the Akt/ mTOR pathway is aberrantly activated in many malignancies including breast, prostate and ovarian cancers as well as acute and chronic leukemias [67, 85, 92, 93].

In contrast to solid tumours, the frequency of copy number variations leading to activation of the mTOR pathways is significantly lower in ALL [93]. Additionally, activating mutations in Akt and deletions in PTEN are not common in B-ALL, indeed PTEN appears to be essential for the survival of B-ALL cells in vivo [94, 95]. In contrast, PTEN abnormalities are a common feature of T-ALL [96] and the Akt/mTOR pathway may be activated through aberrant Notch-1 signalling in T-ALL [97-99] and by direct interaction with BCR/ABL in Ph+ B-ALL [100]. It is not fully understood how Notch-1 activates mTOR, though it is speculated to occur indirectly through c-myc or through crosstalk with other pathways such as those involving as insulin growth factor receptor and IL-7 receptor α [101, 102].

Despite the lack of activating mutations, mTOR is frequently hyper-activated in B and T-ALL [103]. Contact between ALL and the bone marrow microenvironment is highly important for their continued growth and survival [104]. Given that mTOR is influenced by extracellular factors such as CXCL12, IL7 and TSLP, deregulation of the production of these factors by bone marrow microenvironment can result signalling through the Akt/mTOR pathway [105-108].

Although the use of tyrosine kinase inhibitors (TKIs) against the BCR/ABL fusion gene has significantly improved treatment of Ph+ disease, the development of resistance to the inhibitors limits their efficacy. One possible mechanism of resistance, is the activation of the mTOR pathway by BCR/ABL [109]. Indeed, the combination of rapamycin with imatinib demonstrated improved growth inhibition and cell death, overcoming the resistance conferring mutation in BCR/ABL, T315I [109, 110]. Additionally, hyper-active mTOR signalling has also been correlated to rearrangements of the CRLF2 gene, seen in Ph-like ALL. The combination of an mTOR inhibitor with a JAK2 inhibitor may be effective in treating this high risk ALL subtype [41, 111].

While much of the role of mTOR in cancer has been associated with changes to upstream oncogenes, there is evidence to suggest its downstream effectors, S6K1 and 4EBP1, may also play a role in cancer and have been correlated to poor patient prognosis, despite regular mTOR function [112-114]. The eIF4E/4EBP1 axis is finely regulated, with both increases and decreases being correlated with cancer cell growth and drug resistance [115, 116]. Moreover, the concentration of eIF4E is highly important, with increased expression driving tumorigenic programs [117] and may confer resistance to active site mTOR inhibitors [118]. On the other hand, little is known about the role of S6K1 in cancer. A recent study has suggested that that S6K1 may regulate the metabolic requirements for BCR/ABL positive chronic myelogenous leukemia cell survival [119] and may have prognostic value in breast cancer [120].

By comparison, less is known about the role of mTORC2 in leukemia. The activity of mTORC2 in increased in the prostate cancer cell line PC3, the breast cancer line MCF7, as well as several types of glioma [121, 122]. The increased mTORC2 activity

in these cells is correlated to the elevation in the expression of the mTORC2 specific sub-unit, RICTOR, promoting the proliferation and metastatic potential of the cells.

1.4.4 Targeting mTOR in leukemia

Extensive pre-clinical investigation of the use of mTOR inhibitors in ALL has highlighted their efficacy in decreasing cell proliferation and inducing autophagy and/or cell death [123-126]. Rapamycin and its analogues are reported to induce cell death by the classical apoptosis pathways. However additional pathways appear to be recruited, but these pathways have not been fully characterised and further investigation is required [127, 128]. Inhibition of mTOR also impacts the cell cycle process by inhibiting key cell cycle proteins such as pRb, Ki67 and PCNA, resulting in the arrest of the cell cycle in G1, although this appears to be a dose dependant process [125, 129]. *In vivo*, inhibition of mTOR is efficacious in extending the survival of mice engrafted with human ALL xenografts [128, 130] and is synergistic with current chemotherapeutic compounds such as methotrexate, vincristine and ionising radiation [124, 128, 129, 131], indicating the ability of mTOR inhibitors to be incorporated into current chemotherapy regimens.

Several clinical trials have demonstrated the safety and efficacy of everolimus in hematological malignancies [100, 132]. However, clinical evidence of the safety and efficacy in ALL is lacking. Recently, two clinical trials have demonstrated that everolimus is well tolerated in conjunction with conventional chemotherapy and has moderate efficacy, particularly in T-ALL [133, 134]. Currently, there are a number of

clinical trials investigating the efficacy of rapamycin and its derivatives in combination with current chemotherapy for the treatment of leukemia (Table 1.3).

Table 1.3 Current clinical trials into the use of mTOR inhibitors in Leukemia (Adapted from [100])

Drug	Disease	Clinical activity	Current clinical trials
Sirolimus	AML	CR not observed as a single agent 24% ORR with MEC chemotherapy	Sirolimus and azacitidine (NCT01869114) Sirolimus, idarubicin, and cytarabine (NCT01822015)
	ALL	CR not observed as a single agent	Sirolimus and multi-agent chemotherapy (NCT01658007) Sirolimus and methotrexate (NCT01162551)
Temsirolimus	AML	21% CR with temsirolimus and clofarabine	Temsirolimus and chemotherapy (NCT01611116)
	ALL		Temsirolimus and multi-agent chemotherapy (NCT01403415), Temsirolimus with etopiside and cyclophosphamide (NCT01614197)
	CML		Temsirolimus and imatinib (NCT00101088)
Everolimus	AML	68% CR with everolimus and 7+3 chemotherapy	Everolimus and midostaurin (NCT00819546)
	ALL		Everolimus and multi-agent chemotherapy (NCT01523977)
	CML		Everolimus and imatinib (NCT00093639)

Abbreviations: AML – Acute Myeloid Leukemia, ALL – Acute Lymphoid Leukemia, CML – Chronic Myeloid Leukemia, CR – Complete remission, MEC: mitoxantrone, etoposide, cytarabine, ORR: overall response rate.

1.5 Resistance to mTOR inhibition

The model of the mechanism of action for rapamycin was developed in yeast in the early 1990's [135, 136] and it quickly became apparent that these cells acquire genetic mutations that confer resistance to mTOR inhibition [137-139]. Further research demonstrated similar mechanisms of resistance in mammalian cells as those

observed in yeast. However, transplantation of rapamycin resistant mammalian cell lines generated *in vitro* in mice showed a restoration of sensitivity [140], indicating the complex nature of acquired resistance.

Recently, everolimus resistance has been documented following chronic exposure to the mTOR inhibitor in renal cell carcinoma and prostate cancer cell lines [141-143], although clinically, little has been documented regarding resistance to rapamycin or its analogues. Several hypotheses exist as to possible mechanism by which cells may become resistant to mTOR inhibition. The majority of these were determined using the stereotypical mTOR inhibitor rapamycin; however, may be more broadly applicable to rapalogs due to similar mechanism of action.

1.5.1 Mutations in FKBP12

Rapalogs have a well-defined mechanism of action in first binding FKBP12, then binding the FKBP12 binding domain of mTOR, thus inhibiting the formation of the active complex. Mutations in the either the FKBP12 protein, which would prevent rapalog binding, or mutations in mTOR preventing the binding of the FKBP12-rapalog complex, would impart resistance. This particular mechanism was first discovered in the yeast *S.cerevisiae* where sub-strains of the yeast were resistant to growth inhibition by rapamycin. Resistant yeast strains had mutations in the FKBP12 and/or TOR proteins resulting in decreased rapamycin binding [137, 144]. Similar mutations were identified in murine mast cells [139] and T-cell lymphoma cell lines [138] where reduced binding affinity for rapamycin by FKBP12 conferred high-level resistance.

1.5.2 Mutations in S6 kinase 1

Rapamycin induced inhibition of mTORC1 leads to the rapid dephosphorylation of Thr389 in S6K1, and due to hierarchal phosphorylation events, results in decreased

phosphorylation on subsequent residues such as Thr229 and Ser411 [81, 145]. Therefore, mutations in these critical regions such as Thr389 to glutamic acid, render S6K1 insensitive to the effects of rapamycin [146].

mTORC1 interacts with a specific motif of S6K1, the TOS motif, and deletion or functional inactivation of this motif prevents mTOR induced phosphorylation of S6K1 at Thr389. Interestingly, co-deletion of the carboxy-terminus of S6K1 slightly rescues the phosphorylation of Thr389, and also prevents its decrease by rapamycin [66, 77]. However, deletion of the carboxy-terminus alone only imparts partial resistance to rapamycin. Suppression of rictor through siRNA abrogates the resistance to rapamycin in the carboxy-terminus knockout S6K1, but does not impact on phosphorylation of wild type S6K1 [77]. This indicates that mTORC2 is also able to phosphorylate and activate S6K1, though to a somewhat lesser extent than mTORC1, and the carboxy-terminus contains an inhibitory motif that restricts this in wild type S6K1.

There is little evidence to show that S6K can impart resistance to mTOR inhibitors in patients, however, there is evidence that it may play a part in the development of resistance to other treatments. In two breast cancer studies patients who responded poorly to endocrine inhibitor therapy [147] and neoadjuvant chemotherapy [148] displayed increased S6K1 activity. It is clear that S6K has the potential to impart resistance to many therapeutic options including mTOR inhibition, and it would not be surprising to see S6K1 correlated to the development of resistance in patients.

1.5.3 Defect in the ratio of eIF4E to 4EBP1

The initiation factor eIF4E is crucial for regulating the initiation of mRNA transcription and early work determined its role in cellular growth and malignant transformation

[149-151]. eIF4E is inhibited by 4EBP1 and overexpression of eIF4E is associated with increased tumour progression and has been reported in a number of malignancies such as head and neck [152], breast [153, 154], and gastrointestinal carcinomas [155]. In addition, phosphorylation of eIF4E at Ser209 reduces its affinity for 4EBP1, resulting in a relative increase in free eIF4E that promotes mRNA translation [156].

The down regulation or inactivation of the inhibitory protein 4EBP1, by decreased translation or hyper-phosphorylation, is another mechanism by which eIF4E may become deregulated and reduced 4EBP1 activity has been correlated with rapamycin resistance [157]. While the levels of eIF4E may remain unchanged, decreased levels of 4EBP1 result in increased free eIF4E and increased eIF4E activity. The ratio between eIF4E and 4EBP1 may be indicative of how tumours respond to mTOR inhibition, with high cellular 4EBP1 correlating with a more favourable outcome.

1.5.4 Akt negative feedback loop

Despite strong pre-clinical evidence, many clinical trials involving the allosteric inhibition of mTOR by rapamycin, or its first generation analogues, have demonstrated only modest efficacy [158]. Recently, a negative feedback loop has been discovered whereby inhibition of mTOR may result in the activation of the Akt signalling cascade in some cell types [63, 159-162]. However, the mechanism behind the increased Akt activation following mTOR inhibition remains elusive. Given mTOR negatively regulates the downstream signalling of growth factors such as Insulin receptor substrate-1 (IRS1), growth factor receptor bound protein 10 (Grb10) and platelet derived growth factors (PDGFR's) [63], inactivation of mTOR may lead to the subsequent increase in the ability of these growth factors to signal on to their respective receptor tyrosine kinases, leading to downstream activation of Akt (Figure

1.6). Furthermore, the second mTOR complex (mTORC2) is associated with its own feedback look with Akt. Akt phosphorylates the mTORC2 subunit SIN1 at Thr86, enhancing the mTORC2 kinase activity. Active mTORC2 is responsible for the phosphorylation of Akt on S473, leading to the full activation of Akt [163].

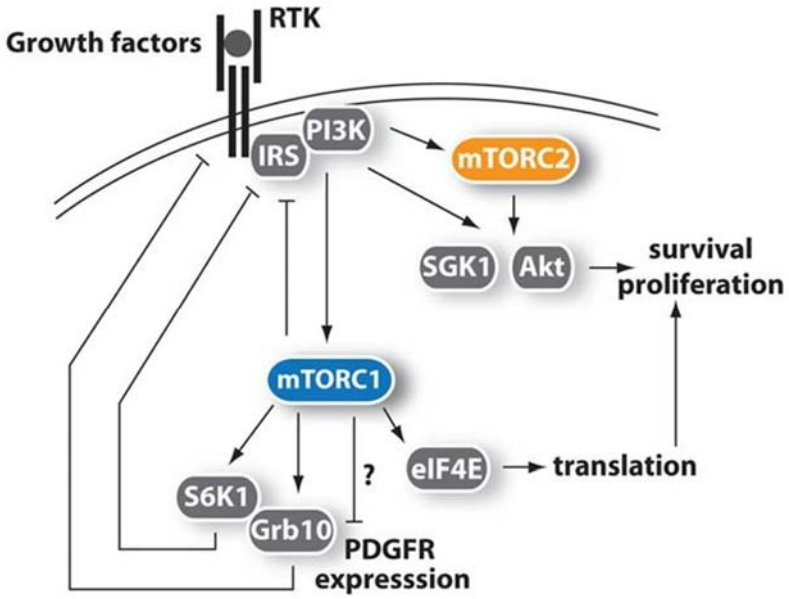

Figure 1.6 mTOR negative feedback loop with Akt. Reproduced from [63].

1.5.5 PP2A Related Phosphatases

The mammalian protein phosphatase 2A (PP2A) is a family of serine/threonine phosphatases involved in many cellular processes including oncogenic transformation [164, 165]. The PP2A complex contains a dimeric core composed of a structural A subunit and a catalytic C subunit, that associates with a diverse array of regulatory B subunits [166]. The PP2A complex in intrinsically intertwined in many kinase cascades including the mTOR signalling cascade where it affects the downstream targets S6K1 and 4EBP1 [166, 167]. The *in vitro* response to rapamycin has been correlated with

components of the PP2A complex such as the A4 and B55β subunits. Treatment of Jurkat cells with rapamycin leads to the dissociation of the A4 sub-unit from the catalytic subunit. Transfection of exogenous A4 into Jurkat cells confers resistance to rapamycin [168]. Loss of the B55β subunit in colorectal cancer confers resistance to rapamycin through a compensatory mechanism involving MYC and PDK1. Re-expression of B55β restores sensitivity to rapamycin by abrogating these compensatory pathways [169]. However, transfection of the α4 subunit into Raji cells did not confer resistance to rapamycin and other studies have failed reproduce the rapamycin induced dissociation of the A4 subunit seen in other mammalian cell types [168], leaving the association of PP2A to resistance to mTOR inhibition uncertain.

1.5.6 Cellular Adhesion

Adhesion to a supportive microenvironment confers resistance to chemotherapeutic compounds in many malignancies, including ALL [170-172]. Integrins are a crucial component of ALL meditated adhesion to the bone marrow microenvironment [173, 174], and disruption of integrin binding can overcome resistance to chemotherapy and improve outcome [175]. Moreover, the development of resistance to the mTOR inhibitors everolimus and temsirolimus has been correlated to changes in expression of integrins and cellular adhesion [176, 177]. However, whether the altered integrin expression and adhesion potential of the cells resulted in the development of resistance or if it is altered after resistance has developed remains uncertain.

Focal adhesion kinase (FAK/PTK2) plays an important role in adhesion and migration downstream of integrin mediated signalling [178-180], and inhibition of FAK is able to synergize with the mTOR inhibitor everolimus to improve patient response in an *in vivo* setting [181]. While evidence that FAK is involved in the development of resistance to

everolimus is lacking, the synergy between FAK inhibitors and everolimus indicates that FAK inhibitors may be beneficial in overcoming everolimus resistance.

1.5.7 Cell cycle regulation

Everolimus elicits a cell cycle arrest in the G_0/G_1 stage of the cell cycle in *in vitro* cell models of leukemia [129], bladder cancer [182] and pancreatic neuroendocrine tumours [183], while a G_2M arrest was reported in the oral cancer cell line SCC4 [184].

The *in* vitro development of resistance to everolimus in renal cell carcinoma and pancreatic cancer was associated with increased expression of cell cycle regulating protein complexes CDK2-CyclinA and CDK1-CyclinB. These complexes are crucial for cell cycle to occur with increased levels overcoming the inhibitory effects of everolimus on the cell cycle resulting in cell cycle progression [143, 185]. The importance of the cell cycle in the development of resistance to everolimus is further evidenced by the restoration of sensitivity upon the inhibition of these crucial cell cycle complexes. Tsuar et al were able to restore sensitivity to everolimus and slow the growth of prostate cancer cells *in vitro* by knock down either CDK1 or Cyclin B with siRNA [143]. Likewise, decreased CDK2 and cyclinA expression in renal cell carcinoma cells by the histone deacetylase inhibitor valproic acid abrogated resistance to everolimus [185]. However, knockdown of CDK1/Cyclin B did not fully restore everolimus sensitivity and the HDAC family have many crucial roles in cell homeostasis. Indicating that, while regulation of the cell cycle may be involved in resistance to mTOR inhibition, they are not solely responsible for the development of resistance.

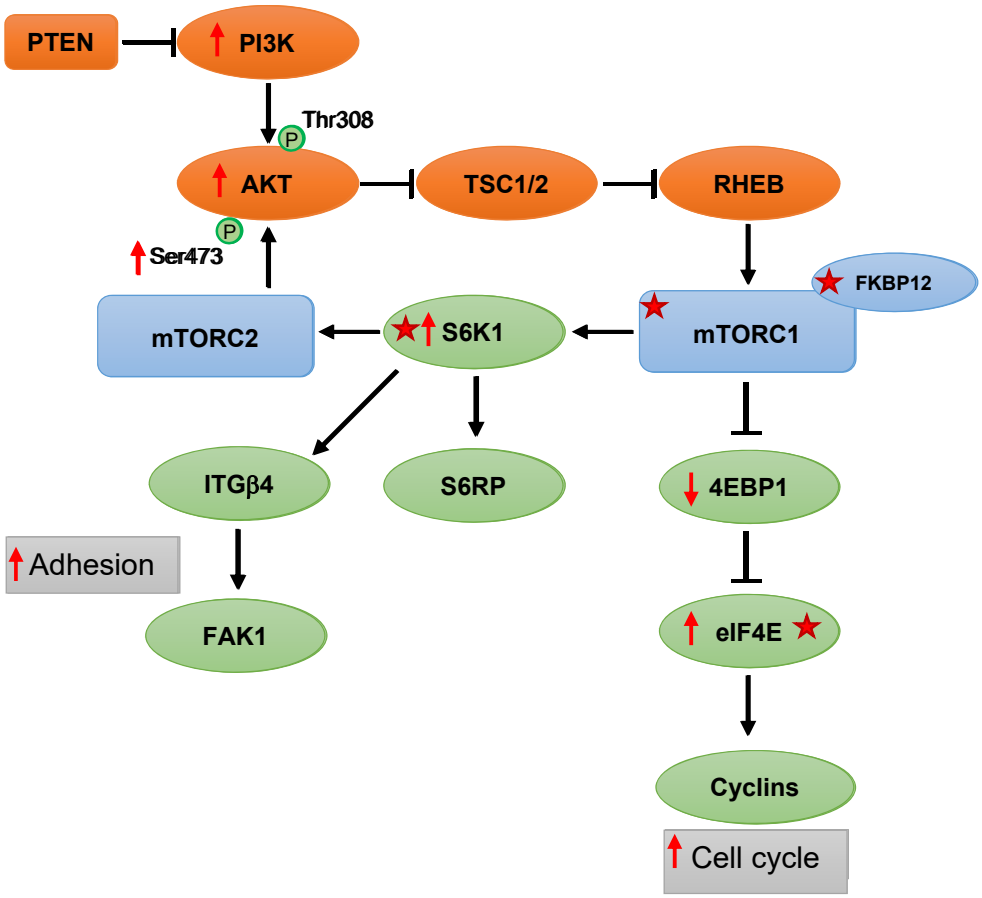

Figure 1.7 Predicted sources of resistance to rapamycin and its analogues in the mTOR pathway. Mutations (stars) and changes to protein expression (arrows) predicted to confer to mTOR inhibition (Adapted from [168, 186, 187]).

1.6 Significance

The mTOR signalling complex is hyperactive in many malignancies and effective pharmacological inhibition could synergize with existing chemotherapy to increase patient survival. The rapamycin analogue everolimus, is effective in treating mice engrafted with human ALL xenografts alone and when used in combination with conventional chemotherapy [65, 128].

Resistance to everolimus has been found in many malignancies treated with mTOR inhibitors both in vivo and in vitro. Long-term administration of everolimus to mice with pre-B ALL has led to the development of resistance that is maintained upon secondary transplantation of cells from treated mice (unpublished data). While a number of mechanisms have been proposed to be responsible to the development of resistance, there was no common mechanism of resistance between different types of mammalian cell. Understanding the mechanisms by which cells become resistant to mTOR inhibition may not only provide increased therapeutic efficacy of such inhibitors, but also provide insights into the resistance mechanisms to other kinase inhibitors.

1.7 Hypotheses and Aims

1.7.1 Hypotheses

Comparing the genome and proteome of everolimus resistant cells to sensitive cells will provide new insights into mechanisms behind the development of resistance to everolimus *in vivo*.

1.7.2 Aims

1. To characterise changes in to the transcriptome and proteome in ALL xenografts upon the development of resistance to everolimus.
2. To identify a common mechanism behind the development of resistance to everolimus in ALL.
3. To determine whether patients with ALL receiving everolimus in conjunction with chemotherapy display evidence of resistance development.

CHAPTER 2 MATERIALS AND METHODS

2.1 MATERIALS

2.1.1 Patient Derived Xenografts

Table 2.1 Characteristics of patient derived xenografts

ID	Age/Sex	Immunophenotype	Cytogenetics
1196	8/F	CD34- CD19+ CD10+	46 XX -19,del(19), t(1;19)(q23p13)
1345	5/F	CD34- CD19+ CD10+	45XX, dup(1)(q42q25),del(3)(q21), -9, del(9)(p22), t(18;20)(q21;q13.1)
2055	1.5/F	CD34+ CD19+ CD10+	45,X,T(X;1)(P22;P36),-9,T(12;12)(P11;Q11.2),ADD(20)(Q12)

2.1.2 Tissue Culture

Roswell Park Memorial Institute (RPMI) 1640 and phosphate buffered saline (PBS) were purchased from Lonza (Sydney, NSW, Australia). Fetal bovine serum, L-glutamine and trypsin-EDTA were purchased from Sigma-Aldrich (Sydney, NSW, Australia). ^{51}Chromium Radionuclide 1mCi (37MBq) Sodium Chromate in Normal Saline (pH 8-10) was purchased from Perkin Elmer (Melbourne, Vic, Australia).

2.1.3 Antibodies

Anti-human phospho-CDK1 (Thr161), CDK1, phospho-CDK2 (Thr160), CDK2, phospho-STMN (Ser38), phospho-PKCδ, PDKδ, PKACα, phospho-eEF2, eEF2, and ITGα6 were purchased from Cell signaling technology (Boston, MA, USA). Anti-human STMN, phospho-STMN (Ser16), phospho-STMN (Ser63), phospho-S6K1 (Ser411), phospho-S6K1 (Thr229), S6K1, ELF2, ITGα6-Phycoerythrin (PE), anti-mouse horse radish peroxidase (HRP) and anti-rabbit-Alexa Fluor 405 (AF405) were purchased

from Abcam (Melbourne, Vic, Australia). Anti-human GAPDH, ITGα8- allophycocyanin (APC), ITGβ4-Alexa fluor 488 (AF488) and ITGα6 (Clone GoH3) were purchased from R&D systems (Minnesota, USA). Anti-β–actin was purchased from Sigma-Aldrich, anti-rabbit HRP from Dako (Melbourne, Vic, Australia), goat anti-rabbit pacific blue (PB) and anti-mouse CD45-fluorescein isothiocyanate (FITC) from Life Technologies (Melbourne, Vic, Australia). Anti-human CD19-PE and CD29-PE, rat IgG2a isotype and APC BrdU flow kit were purchased from BD Biosciences (Sydney, NSW, Australia). Anti-human ITGβ1 (4B4) was purchased from Beckman Coulter (Sydney, NSW, Australia) and mouse IgG1 isotype from Biolegend (San Diego, CA, USA)

2.1.4 RNA

TRIzol reagent, SuperScript III, TaqMan hsa-miR-21 gene expression assay, MultiScribe reverse transcriptase and TaqMan Universal PCR master mix (no UNG) were purchased from Life Technologies. ISOLATE II RNA mini extraction kit, ISOLATE II plasmid mini kit, Tetro cDNA synthesis kit, and SensiFAST qRT-PCR master mix were purchased from Bioline (Sydney, NSW, Australia).

RNeasy Mini kit, QIAquick gel extraction kit, RT² Profiler PCR Array Human miR-21 Targets, RT2 First Strand kit, RC3 reverse transcriptase and RT2 SYBR green mastermix were all purchased from Qiagen (Limburg, Venlo, Netherlands). TargetAmp-Nano labelling kit was procured from Epicenter (Madison, WI, USA) and the HumanHT-12v4 Bead expression chip from Illumina (San Diego, CA, USA).

Phusion High fidelity DNA polymerase was purchased from New England Biosciences (Massachusetts, USA), kanamycin from Astral Scientific (Sydney Australia) and the restriction enzymes EcoRI and BamHI as well as T4 DNA ligase and JM109 cells from Promega (Sydney, NSW, Australia).

Sanger sequencing was performed by the AGRF (Sydney, Australia) and transciptome sequencing by Axeq Technologies (Seoul, Korea). Agilent bioanalyser analysis was performed by the The Westmead Institute for Medical Research Genomics Facility.

2.1.5 Primers

Table 2.2 cDNA primers

Gene	Detection Primer	Cloning Primer
DYRK1a	FWD 5'CAACTGCTCCCCTGAGAAAA, REV 5'AACCCATTCTTGCTCCACAC	FWD 5'CTTCGAATTCCAACTGCTCCCCTGAGAAAA, REV 5'GGTGGATCCAACCCATTCTTGCTCCACAC
CHEK1	FWD 5'GAAGAAGCAGTCGCAGTGAA REV 5'CTTCGAATTCGAAGAAGCAGTCGCAGTGAA	FWD 5'CTTCGAATTCGAAGAAGCAGTCGCAGTGAA REV 5'GGTGGATCCTCCACAGGACCAAACATCAA
ATG5	FWD 5'TGGGCCATCAATCGGAAACT REV 5'TCTGTTGGCTGTGGGATGAT	FWD 5'CTTCGAATTCTGGGCCATCAATCGGAAACT REV 5'GGTGGATCCTCTGTTGGCTGTGGGATGAT
PKN2	FWD 5'TGAGTCTCCCTTTCCTGGTG REV 5'GGTTCTCGAGGTGGAGTCAG	FWD 5'CTTCGAATTCTGAGTCTCCCTTTCCTGGTG REV 5'GGTGGATCCGGTTCTCGAGGTGGAGTCAG
MLL5	FWD 5'ATCAGGCGGTCTTGTACACC REV 5'TTGTTGGTCGTTCCTTCACA	FWD 5'CTTCGAATTCATCAGGCGGTCTTGTACACC REV 5'GGTGGATCCTTGTTGGTCGTTCCTTCACA
ITGα6	FWD: 5'TCATGGATCTGCAAATGGAA, REV: 5'AGGGAACCAACAGCAACATC	N/A
ITGα8	FWD: 5'GAACGCAACAACAAGGGATT, REV: 5'CTCAAGACGTGGAACTGCAA	N/A
PTK2	FWD 5' CATGCCCTCAACCAGGGATT REV 5' CACGCTGTCCGAAGTACAGT	N/A
ACTN1	FWD 5' TGATATTGGCAACGACCCCC REV 5' GCCTGGAATGTCACTACCCC	N/A
CDK6	FWD 5' ACAGAGCACCCGAAGTCTTG REV 5' CTGGGAGTCCAATCACGTCC	N/A

AKAP12	FWD 5’ CGCCACCAAGCTCCTACAGA REV 5’ GTGATGTCGTGAACAACCGC	N/A
PRKCB1	FWD 5’ CTGTGCCACCAGAAGGAAGT REV 5’ TGGTCGTCTTTTCTTCCGGG	N/A
EIF4e3	FWD 5’ AGTAATGCAAAGGGTGGCGT REV 5’ TCCCCGATGGTTGCTAACAG	N/A
EPAS1	FWD 5’ GCTTCCTGCGAACACACAAG REV 5’ GGTCACCACGGCAATGAAAC	N/A
PTAR	FWD 5’ ACTTTACCACTGCATGGAAC REV 5’GGCGAGTTTTCCCAGATGTA	N/A
PTEN	FWD 5’ CCGTTACCTGTGTGTGGTGA REV 5’ AGGTTTCCTCTGGTCCTGGT	N/A
BMPR2	FWD 5’ GGACGCATGGAATATTTGCT REV 5’ CCCAGTCACTTGTGTGGAGA	N/A
USP34	FWD 5’ ACATCAAAGTGGAGGTAGTGACA REV 5’ CACCACTGTTGGCAGTTTCG	N/A
PELI1	FWD 5’ GGCTCAGCAGAGAGGAAAAA REV 5’ ACAATGTTGCACCACAGAGG	N/A
RHOB	FWD 5’ CTCATGTGCTTCTCGGTGGA REV 5’ TGGGCACATTGGGACAGAAG	N/A
GAPDH	FWD: 5’GAGTCAACGGATTTGGTCGT, REV: 5’TTGATTTTGGAGGGATCTCG	N/A

2.1.6 Proteomics

cOmplete ULTRA and PhosSTOP protease inhibitor tablets were purchased from Roche (Sydney, NSW, Australia), BCA colorimetric assay from Pierce (Waltham, MA, USA) and 0.4 μm nitrocellulose membrane from Merck Millipore (Melbourne, Vic, Australia). Clarity chemiluminescent substrate (ECL), coomassie G-250, and 17cm,

pH 3-10 IPG strips were purchased from Bio-RAD (Sydney, NSW, Australia) and Trypsin Gold from Promega. 2D-Clean-up kit, 2D Quant kit, IPG buffer pH3-10 and GELoader tips were purchased from GE Life sciences (Sydney, NSW, Australia), 3 Dye 2D DIGE labelling Kit from Lumiprobe (Hallandale Beach, FL, USA) and 20 x 20cm, 4-16% gradient, bis-TRIS polyacrylamide gel in low fluorescent glass plates from Jule Biotechnologies (Milford, CT, USA)

Triethylammoniumbicarbonate (TEAB), Formaldehyde, ^{13}C formaldehyde in deuterated water, cyanoborohydride, cyanoborodeuteride, formic acid and α-cyano-4-hydroxycinnamic acid were purchased from Sigma-Aldrich. C18 reverse phase cartridges were purchased from (Waters, Australia), 3M Empore C18 filter membrane (Supelco, USA) and 100 nm Reprosil-Pur 120 C18 AQ resin from Masch GmbH (Ammerbuch-Entringen, Germany) and POROS 20 R2 reverse phase resin from Life Technologies. Dithiotherol (DTT), iodoacetimide, Acetonitrile, ammonium bicarbonate and TFA (trifluoroacetic acid) were all purchased from Sigma-Aldrich.

2.1.7 Drugs

Everolimus and placebo were provided by Novartis (Basil, Switzerland). Harmine was purchased from Abcam.

2.1.8 Animals

NOD/SCIDγc$^{-/-}$ (NSG) mice were bred in the Westmead Hospital Animal Care Facility.

2.1.9 Software

The software packages GenomeStudio (Illumina) Partek Genomics Suite (Partek, St Louis, MO, USA), Metacore (Thompson Reuters, Sydney, NSW, Australia), GSEA (Broad institute, MIT, Cambridge, MA, USA), ImageLab (Bio-RAD), DeCyder (GE

Healthcare), MicroBeta scintillation plate counter (Perkin Elmer), ProteinPilot (SCIEX, Framingham, MA, USA), Prism 6 (GraphPad, La Jolla, CA, USA) and SPSS statistics 22 (IBM, Armonk, NY, USA) were used for data analysis.

2.2 METHODS

2.2.1 Tissue Culture

RPMI media was supplemented with 10% FBS and 1 mM L-glutamine (cRPMI). Cells were incubated at 37°C in 5% CO_2.

For removal of adherent cells, the supernatant was removed and remaining cells washed with PBS. Cells were incubated with trypsin-EDTA at 37°C for 10-30 min or until the adherent layer detached. Cells were harvested and pelleted by centrifuging at 400 x *g* for 5 min then resuspended in fresh cRPMI media.

2.2.2 Isolation of human leukemia xenografts from murine tissues

Peripheral blood, femurs and spleens were collected from sacrificed animals and single cell suspensions prepared as previously described [128]. Briefly, spleens were gently pushed through a 70 μm filter with 10 mL of cRPMI. Bone marrow was isolated from femurs by removing distal ends of the femur and flushing central marrow with a 25 gauge needle and 1 mL of cRPMI. Red blood cells were removed by incubating with red cell lysis buffer consisting of 10 mM $KHCO_3$, 155 mM NH_4Cl and 126μM EDTA at pH 7 and remaining cells were washed by centrifugation at 400 x *g*.

2.2.3 RNA extraction with TRIzol

RNA was extracted using TRIzol reagent according to manufacturer instructions. Up to 10 million cells were lysed by resuspending the cell pellet in 1 mL of TRIzol reagent. Two hundred microliters of chloroform was added, then tubes vigorously shaken by hand for 15 s. Samples were incubated at room temperature (RT) for 2 min then centrifuged for 15 min at 12000 x *g* at 4°C. The top aqueous layer was carefully removed and placed in a fresh RNase free tube to which 0.5 mL of isopropyl alcohol

was added. Samples were incubated for 10 min at RT and then centrifuged for 10 min at 12000 x *g* at 4°C. The supernatant was carefully discarded and the pellet was washed with 1 mL of 75% ethanol, briefly mixed and the centrifuged at 7500 x *g* for 5 min at 4°C. The supernatant was discarded, the pellet air-dried and then resuspended in 20 μL of RNase free water.

2.2.4 RNA Extraction with commercial kits

Total RNA was extracted with the Isolate II RNA mini kit according to manufacturer's instructions. Contaminating DNA was removed from samples by an on-column DNase digestion step.

2.2.5 Bioanalyser

RNA integrity was determined using the TotalRNA nano chip and the Bioanalyzer 2100 (Agilent, California, USA). The concentration of RNA and DNA was calculated by UV nanophotometer (Implen, Germany). RNA with an integrity number (RIN) greater than 7 and an absorbance ratio at 260 nm and 280 nm (A260/280) of between 1.8 and 2 was deemed satisfactory for amplification.

2.2.6 Microarray

RNA was amplified and biotinylated using TargetAmp-Nano labelling kit. RNA (300 ng) was reverse transcribed to produce cDNA by incubating samples with SuperScript III and T7 Oligo(dT)18 primers at 50°C for 30 min. The second strand was subsequently synthesized using TargetAmp-Nano 2nd-Strand DNA Polymerase by incubating samples at 65°C for 10 min. Biotinylated mRNA was then transcribed from the synthesized cDNA by incubation with T7 RNA polymerase and biotin-UTP at 42°C

for 4 h. Excess cDNA was removed from samples by incubating with DNase I at 37°C for 15 min. Samples were then purified with RNeasy Mini kit.

Biotinylated RNA was hybridised to a HumanHT-12v4 Bead expression chip by the The Westmead Institute for Medical Research Genomics Facility according to manufacturer's instructions and scanned using Illumina BeadArray Reader.

Array data was imported into GenomeStudio corrected for background signals and normalised to the mean signal of each sample (average normalisation). Gene set enrichment analysis carried out using GSEA software.

2.2.7 Quantitative real time PCR

cDNA was reverse transcribed from 300 ng of RNA using Tetro reverse transcriptase by incubating samples with Oligo (dT)18 primers at 45°C for 30min. The reverse transcriptase was inactivated by incubating samples at 85°C for 5 min. cDNA was combined with SensiFAST qRT-PCR master mix and forward and reverse primers (f.c. 200 nM) The relative expression of target genes was quantitated using a standard curve generated from serially diluted cDNA. Reactions were performed on the Bio-RAD CFX96 real time PCR machine (The Westmead Institute for Medical Research) using a 2 step cycling protocol with the following cycling conditions: hot start 95°C for 2 min, 40 cycles of 5 s at 95°C and 15 s at 60°C. Fluorescence data was collected in the SYBR channel at the end of each cycle. A melt curve was generated at the completion of the cycles. The expression of indicated genes was normalised to GAPDH expression.

2.2.8 Protein extraction

Cell pellets were lysed with a lysis buffer consisting of 10 mM TRIS-HCl, 150 mM sodium chloride, 1 mM EDTA, 2 mM sodium molybdate, 10 mM sodium fluoride, 1% v/v Triton X-100, cOmplete ULTRA and PhosSTOP tablets. Samples were rotated at 4°C for half an hour then centrifuged for 10 min at 12,000 x *g*. Supernatants were transferred to fresh tubes and protein quantified by BCA colorimetric assay.

2.2.9 Immunoblotting

Twenty micrograms of protein was combined with 5 μl of 3x Laemmli buffer and heat denatured in a water bath at 95°C for 10 min. Samples were loaded onto 10% bis-TRIS SDS-PAGE gels with a 4% stack and run at 120 volts until the dye front reached the end of the gel. Proteins were transferred onto a 0.4 μm nitrocellulose membrane by wet transfer for 2.5 h at 300 mAmp. Transfer of protein was confirmed by staining the membranes with 0.1% Ponceau S in 1% acetic acid, for 1 min with gentle agitation. Membranes were washed briefly in 1x TBS containing 0.1% Tween-20 (TTBS) and then blocked with 5% skim milk powder in TTBS for 1 h at RT with gentle agitation.

Primary antibody was diluted in 5% BSA in TTBS and incubated with membranes at 4°C overnight with gentle agitation. Membranes were washed to remove unbound antibody and then probed with the secondary antibody conjugated to HRP for 1.5 h at RT with gentle agitation. Membranes were again washed to remove unbound antibody. Membranes were incubated with Clarity ECL for 1 min and then imaged using the ChemiDoc MP imaging system (Bio-RAD).

Membranes were stripped of bound primary and secondary antibodies by incubating blots in 0.4% SDS, 0.06M TRIS-HCl and 0.008% v/v β-mercaptoethanol for 0.5 h at

55°C with gentle rocking. Membranes were washed briefly in 1x TBS containing 0.1% Tween-20 (TTBS) and were then re-probed with a second primary antibody.

2.2.10 Statistics

Two tailed non-paired t-tests were performed using Microsoft Excel. Kaplan Meier survival curves were generated with GraphPad Prism and log ranked (Mantel-Cox) test performed on data. One-way and Two-way ANOVA analysis was performed by Partek Genomics Suite. P-values ≤ 0.05 were considered statistically significant.

2.2.11 Ethics Approval

All mouse experimental protocols were approved by the Westmead Hospital Animal Ethics Committee. All patients enrolled in clinical trial conducted by MD Anderson Cancer Center signed an informed consent form approved by the Institutional Review Board of University of Texas / MD Anderson Cancer Center (clinicaltrials.gov identifier: NCT00968253).

CHAPTER 3 NEXT GENERATION SEQUENCING OF EVEROLIMUS RESISTANT ALL XENOGRAFTS

3.1 INTRODUCTION

A pre-clinical study conducted by Crazzolara et al [128] evaluated the efficacy of everolimus in a murine xenograft model of human ALL. The survival of mice engrafted with human ALL xenografts was significantly extended with administration of everolimus as a single agent, and in the case of one xenograft eradicated the leukemia. However, despite this very promising efficacy in the treatment of leukemia *in vivo*, clinical use of everolimus is likely to be in combination with established chemotherapy regimens [188, 189]. Indeed, the survival of mice engrafted with human ALL xenografts and treated with everolimus in conjunction with the chemotherapeutic agent vincristine, was significantly extended over either agent alone [128, 129].

A preliminary investigation of the effects of long-term administration of everolimus was conducted prior to the commencement of this project. Human ALL xenograft cells were harvested from mice that succumbed to ALL despite continuous treatment with everolimus. When these cells were re-engrafted into secondary recipients, the extension in survival elicited by everolimus was significantly reduced compared to everolimus naïve cells, indicating the development of resistance (unpublished data, Fig 3.5). This resistance development severely limits the therapeutic potential of everolimus and must be investigated so that patients may benefit from the anti-tumor properties of mTOR inhibition.

ALL exists as a heterogeneous clonal population with sub-clones arising from a common parental clone with a driving mutation [190, 191]. Relapse and drug

resistance is proposed to occur by the selection of a pre-existing resistant clone or through the acquisition of a resistance conferring mutation [192-194].

Resistance to everolimus has not been described in ALL, though parallels may be drawn from studies with everolimus, and its parental compound rapamycin, in other mammalian cell models. The mechanism by which these cells acquire resistance is not universal, though mutations in genes such as FKBP12 (the binding partner for everolimus) and S6K1 (a downstream target of mTOR) may confer resistance [138, 139, 147, 148]. Next generation sequencing of the transcriptome (RNAseq) gives not only insight into the actively transcribed genes but also any mutations, splice variants and gene fusions that have occurred within cells. RNAseq has previously been used to determine mechanisms of drug resistance to conventional chemotherapeutic compounds in leukemia cells [195]. This chapter aimed to characterise the transcriptome of everolimus resistant ALL cells to determine possible mechanisms by which resistance has been acquired.

3.2 METHODS

3.2.1 Transcriptome sequencing

RNA was extracted and its quality determined as described in 2.2.3 and 2.2.4 respectively. RNA (5 μg), with a RIN > 6 and A260/280 > 1.8, was precipitated by adding 0.1 volumes of 3 M sodium acetate (pH 7-8) then 2 volumes of ice cold 100% ethanol. Samples were sent to Axeq Technologies (Seoul, Korea) for transcriptome sequencing using Illumina HiSeq 2000 and the 100bp paired end sequencing method. Sequence alignment and analysis (Gene expression, SNP, INDEL, fusion gene, slice variant) was performed by Axeq.

3.2.2 Cloning and Sanger sequencing

Reverse transcribed cDNA was amplified by PCR using Phusion high fidelity DNA polymerase and gene specific primers containing restriction sites for EcoRI and BamHI on the forward and reverse primers respectively (Table 2.2). PCR products were separated using agarose gel electrophoresis and correct products excised then purified using the QIAquick gel extraction kit. Purified PCR products and cloning vector (pEGFP-N1) were digested with EcoRI and BamHI restriction enzymes by incubating products with 1x digestion buffer, 1 μg/μL of acetylated BSA and 5 U of restriction enzyme in a 20 μL reaction at 37°C for 1 h. Digested products and vector were purified by from agarose gels using the QIAquick gel extraction kit. Products were ligated into the cloning vector using T4 DNA ligase overnight at 4°C. Competent E-coli JM109 cells were transformed with ligated vectors and selected on agar plates containing kanamycin (60 μg/mL). Colonies were picked and incubated in 5 mL of lysogeny broth containing kanamycin (60 μg/mL). Plasmid DNA was extracted using the ISOLATE II plasmid mini kit and sent for Sanger sequencing with the AGRF.

3.2.3 Adhesion

Human bone marrow stroma (HuBMS.hTERT) was seeded onto sterile white optiplate-96 microtitre plates with transparent bases and grown to confluence, as determined by light microscopy. White optiplate-96 microtitre plates were coated with 1 μg/well of laminin by incubation at 4°C overnight. Microplates coated with laminin were washed twice with PBS and non-specific binding was blocked by incubating wells with 1% BSA for 2 h at 37°C. Excess BSA was removed through two washes with PBS.

Cells were labelled with 100 μCi of ^{51}chromium in 100 μL phenol red free cRPMI supplemented with 10% FBS and 1 mM L-glutamine for 90 min at 37°C. Cells were washed twice with phenol red free cRPMI. Cells were resuspended at $1x10^5$/mL in phenol red free cRPMI and 100 μL added per well (minus the 100% control). Plates were centrifuged at 250 x *g* for 5 min then incubated at 37°C for 1 h. Non-adherent cells were gently removed by three washes with PBS. The cells for the 100% control were added to respective wells and 100 μL of phenol red free cRPMI was added to each of the remaining wells. Cells were lysed with 50 μL of a 3% TritonX-100 solution. The transparent base of optiplates were covered with a white adhesive layer and adherent cells were analyzed by adding 100 μL of microscint40 to each well and reading plates with the Microbeta2 scintillation counter.

3.3 RESULTS

3.3.1 Gene expression

RNA was isolated from the everolimus resistant xenograft 1345-R and its matched sensitive control 1345-S, and sent to Axeq technologies for transcriptome sequencing. Gene expression data was subsequently filtered by removing genes that were not expressed in any sample from the analysis. A total of 13204 genes were quantified and their expression in 1345-R was normalised to the parental xenograft, 1345-S. Everolimus resistant cells had 593 genes upregulated and 578 genes downregulated greater than 2 fold over the sensitive xenograft. Three of the top 15 genes (MLLT4, ITGa6, ITGa8) upregulated in the 1345-R cells are involved in cellular adhesion (Table 3.1) and the top down regulated gene (ADAM23) has anti-adhesive properties (Table 3.2). Moreover, 4 genes that control gene expression either by forming transcription factor complexes (FOSB, EGR2, FOS) or by affecting alternative splicing of RNA (AFF2) were upregulated in the 1345-R xenograft. Resistant cells down regulated 3 genes implicated in cell death (Table 3.2), CDIP and RNF133B are involved with p53 dependent cell death, while RNF130 is suggested to have a role in the death of hematopoietic cells.

GSEA did not identify any gene sets as being significantly enriched in 1345-R cells as compared to the sensitive parental cells. Fifty pathway maps (Table 3.3 and Appendix Table A.3) and 18 process networks (Table 3.4) that were significantly enriched in 1345-R cells, with an FDR < 25%, were identified using Metacore analysis. Consistent with the observations made with the gene expression data, six of the pathway maps and 2 of the process networks involved cellular adhesion.

Table 3.1. The 15 most upregulated genes in the transcriptome of xenograft 1345-R (for full table see Appendix Table A.1).

Gene ID	Gene Name	Ratio R/S	Function
MLLT4	Mixed-Lineage Leukemia Translocated To, 4	53.97	Cell-Cell adhesion
ITGa6	Integrin alpha 6	45.62	Adhesion to laminin
CR1	Complement component receptor 1	44.91	Complement cascade
H1F0	H1 histone family, member 0	35.49	Histone present in cells that are in terminal stages of differentiation or that have low rates of cell division
LOC100130992	uncharacterized LOC100130992	28.62	Affiliated with non-coding RNA
JMJD7-PLA2G4B	Jumonji Domain Containing 7-Phospholipase A2, Group IVB (Cytosolic) Read-Through	27.94	Calcium-dependent phospholipase A2
RAI14	Retanoic acid induced 14	27.5	Novel retinal pigment
FOSB	FBJ Murine Osteosarcoma Viral Oncogene Homolog B	25.69	Enhances DNA binding of Jun proteins
ITGa8	Integrin alplha 8	20	Cell-Cell adhesion
NOS1	Nitric oxide synthase 1	17.82	Produces nitric oxide
EGR2	Early growth response 2	17.69	Transcription factor
NR4A1	Nuclear Receptor Subfamily 4, Group A, Member 1	17.11	May inhibit NF-kappa-B transactivation of IL2.
FOS	FBJ Murine Osteosarcoma Viral Oncogene Homolog	17.1	Part of Jun/AP-1 transcription factor complex
TTC28	Tetratricopeptide repeat protein 28	16.41	Possible role in condensation of spindle midzone microtubules
AFF2	AF4/FMR2 Family, Member 2	15.53	RNA binding protein. Possible alternate splicing role.

Table 3.2. The 15 most down regulated genes in the transcriptome of xenograft 1345-R (for full table see Appendix Table A.2).

Gene ID	Gene Name	Ratio R/S	Function
ADAM23	ADAM Metallopeptidase Domain 23	-176.58	Non-catalytic metalloprotease-like protein
LRRC26	Leucine Rich Repeat Containing 26	-79.74	aux of BK-a channel
PHOSPHO2-KLHL23	PHOSPHO2-KLHL23 Readthrough	-31.9	Phosphatase function
SNHG5	Small Nucleolar RNA Host Gene 5	-23.69	snoRNA, affliated with non-coding RNA
SNHG4	Small Nucleolar RNA Host Gene 4	-17.34	snoRNA, affiliated with non-coding RNA
RNF130	Ring Finger Protein 130	-13.86	Possible role in cell death of hematopoietic cells
MOCS2	Molybdenum Cofactor Synthesis 2	-13.19	sulfur carrier required for molybdopterin biosynthesis
HSD17B8	Hydroxysteroid (17-Beta) Dehydrogenase 8	-12.9	Steroid regulation
SHOX2	Short stature homeobox 2	-12.89	Possible growth regulator
SPG20	Spastic Paraplegia 20	-12.04	Possible endosomal trafficking and/or microtubule dynamics
LOC100133957	uncharacterized LOC100133957, transcript variant 1	-11.91	affiliated with non-coding RNA
CDIP1 (C16orf5)	Cell Death-Inducing P53 Target 1	-11.58	p53 apoptotic effector
RNF144B	Ring finger protein 144B	-11.52	p53 dependent but caspase-independent apoptosis
ODF2L	Outer Dense Fiber Of Sperm Tails 2-Like	-11.03	cytoskeletal
GUSBP2	Glucuronidase, Beta Pseudogene 2	-10.86	pseudogene

Table 3.3. The 20 most significantly enriched Metacore pathway maps in the transcriptome data (for full table see Appendix Table A.3).

Pathway map	pValue	FDR
Transcription_Role of AP-1 in regulation of cellular metabolism	1.181E-07	8.988E-05
Cytoskeleton remodeling_Cytoskeleton remodeling	2.572E-06	9.798E-04
Cytoskeleton remodeling_TGF, WNT and cytoskeletal remodeling	8.890E-06	2.258E-03
Inhibition of neutrophil migration by proresolving lipid mediators in COPD	2.459E-05	6.432E-03
Reproduction_GnRH signaling	3.363E-05	6.398E-03
NETosis in SLE	8.139E-05	1.038E-02
Cell adhesion_Integrin-mediated cell adhesion and migration	1.057E-04	1.153E-02
Neurophysiological process_Corticoliberin signaling via CRHR1	1.113E-04	1.154E-02
Immune response_ETV3 affect on CSF1-promoted macrophage differentiation	1.316E-04	1.154E-02
Transcription_Role of VDR in regulation of genes involved in osteoporosis	1.365E-04	1.154E-02
Immune response_HSP60 and HSP70/ TLR signaling pathway	2.181E-04	1.618E-02
HBV signaling via protein kinases leading to HCC	2.524E-04	1.618E-02
Immune response_MIF-induced cell adhesion, migration and angiogenesis	2.918E-04	1.618E-02
Immune response_MIF - the neuroendocrine-macrophage connector	2.918E-04	1.618E-02
Development_Keratinocyte differentiation	2.977E-04	1.618E-02
Role of Endothelin-1 in inflammation and vasoconstriction in Sickle cell disease	3.748E-04	1.724E-02
Development_Regulation of cytoskeleton proteins in oligodendrocyte differentiation and myelination	4.002E-04	1.724E-02
Stimulation of TGF-beta signaling in lung cancer	4.078E-04	1.724E-02
Cell adhesion_Chemokines and adhesion	4.318E-04	2.057E-02
Immune response_MIF-mediated glucocorticoid regulation	4.696E-04	1.787E-02

Table 3.4 Metacore networks maps significantly enriched in the transcriptome of the resistant xenograft.

Network	pValue	FDR
Cytoskeleton_Regulation of cytoskeleton rearrangement	2.729E-05	4.339E-03
Muscle contraction	5.703E-05	4.534E-03
Cell adhesion_Cadherins	2.835E-04	1.298E-02
Protein folding_Folding in normal condition	3.251E-04	1.298E-02
Cell adhesion_Integrin-mediated cell-matrix adhesion	5.572E-04	2.570E-02
Neurophysiological process_Corticoliberin signaling	1.080E-03	2.734E-02
Cytoskeleton_Actin filaments	1.173E-03	2.734E-02
Development_Skeletal muscle development	1.336E-03	3.721E-02
Proliferation_Positive regulation cell proliferation	1.762E-03	5.569E-02
Immune response_Antigen presentation	2.559E-03	4.639E-02
Signal Transduction_TGF-beta, GDF and Activin signaling	3.730E-03	7.366E-02
Translation_Translation in mitochondria	6.584E-03	9.850E-02
Cytoskeleton_Cytoplasmic microtubules	7.230E-03	9.850E-02
Inflammation_MIF signaling	1.160E-02	1.359E-01
Development_Keratinocyte differentiation	1.290E-02	1.359E-01
Immune response_Phagosome in antigen presentation	1.291E-02	1.359E-01
Development_Blood vessel morphogenesis	1.882E-02	2.066E-01
Proteolysis_ECM remodeling	2.665E-02	2.492E-01

3.3.2 Mutations in resistant xenograft 1345-R

Four genes (CHEK1, DYRK1A, ATG5 and PKN2) with documented roles in malignancy were found to have novel heterozygous mutations in both untreated and everolimus treated 1345-R cells that were not detected within the sensitive parental xenograft (Table 3.5). CHEK1 had single base mutation that was predicted to have a significant impact on protein function with a BLOSUM score of -3, while the remaining genes had a single base pair insertion.

The mutation observed in DYRK1a is predicted to result in the truncation of the protein at amino acid (a.a.) 119, leading to a complete loss in function. To determine whether inactivation of DYRK1a confers resistance to everolimus, a pharmacological inhibitor of DYRK1a, harmine, was combined with a sub-lethal dose of everolimus and the viability and proliferation of NALM6 assessed *in vitro*. Harmine induced a dose dependent G_1 arrest by 24 h, but no further effect was observed with the combination with 8 μM of everolimus (Figure 3.1 A). Similarly, harmine did not prevent the loss of viability induced by everolimus at 24 h (Figure 3.1 B).

As inhibition of DYRK1a by harmine was unable to confer resistance to everolimus in NALM6 cells, we sought to confirm the mutations found in 1345-R cells (Table 3.5). Genes were amplified by PCR using a high fidelity polymerase and cloned into a sequencing vector. Ten clones of each gene were sequenced however none of the 4 mutations were confirmed in 1345-R cells (Figure 3.2).

Table 3.5 Mutations identified in 1345-R cells by transcriptome sequencing

Gene ID	Gene Name	Zygosity	Mutation and Blosum score	Function	Predicted impact on protein	Reported impact in cancer
CHEK1	Checkpoint kinase 1	Heterozygous	Single base mutation T → G at bp 353 aa119 Val → Gly. blossom -3. Mutation in protein kinase domain and claspin binding region.	Checkpoint mediated cell cycle arrest in response to DNA damage.	Altered downstream signaling	Potential drug target for B-cell lymphomas / leukemia, neuroblastoma and some breast and lung cancers
DYRK1A	Dual specificity tyrosine-phosphorylation-regulated kinase 1A	Heterozygous	1 bp insertion at bp 318. Predicted truncation at amino acid 119 of 754	May play a role in a signaling pathway regulating cell proliferation.	Loss of kinase domain, ATP binding domain, and bipartite nuclear localization signal motif.	Increased expression associated with AMKL, decrease associated with T-ALL.
ATG5	Autophagy protein 5	Heterozygous	1bp insertion, frameshift mutation at aa233, stop codon at aa244 of 275	E3 ubiquitin ligase, required for autophagy	Possible impact on protein folding	Depletion can generate autophagy deficient neoplasms in vivo.
PKN2	PKC-related serine/threonine-protein kinase N2	Heterozygous	1bp insertion at amino acid 928, stop codon at amino acid 944; region 917-977 necessary for catalytic activity	Plays a role in the regulation of cell cycle progression, actin cytoskeleton assembly, cell migration, cell adhesion, tumor cell invasion and transcription activation signaling processes.	Altered catalytic activity	PRK2/PKN2, a Ser/Thr kinase and Rho/Rac effector protein, is an essential regulator of both entry into mitosis and exit from cytokinesis.

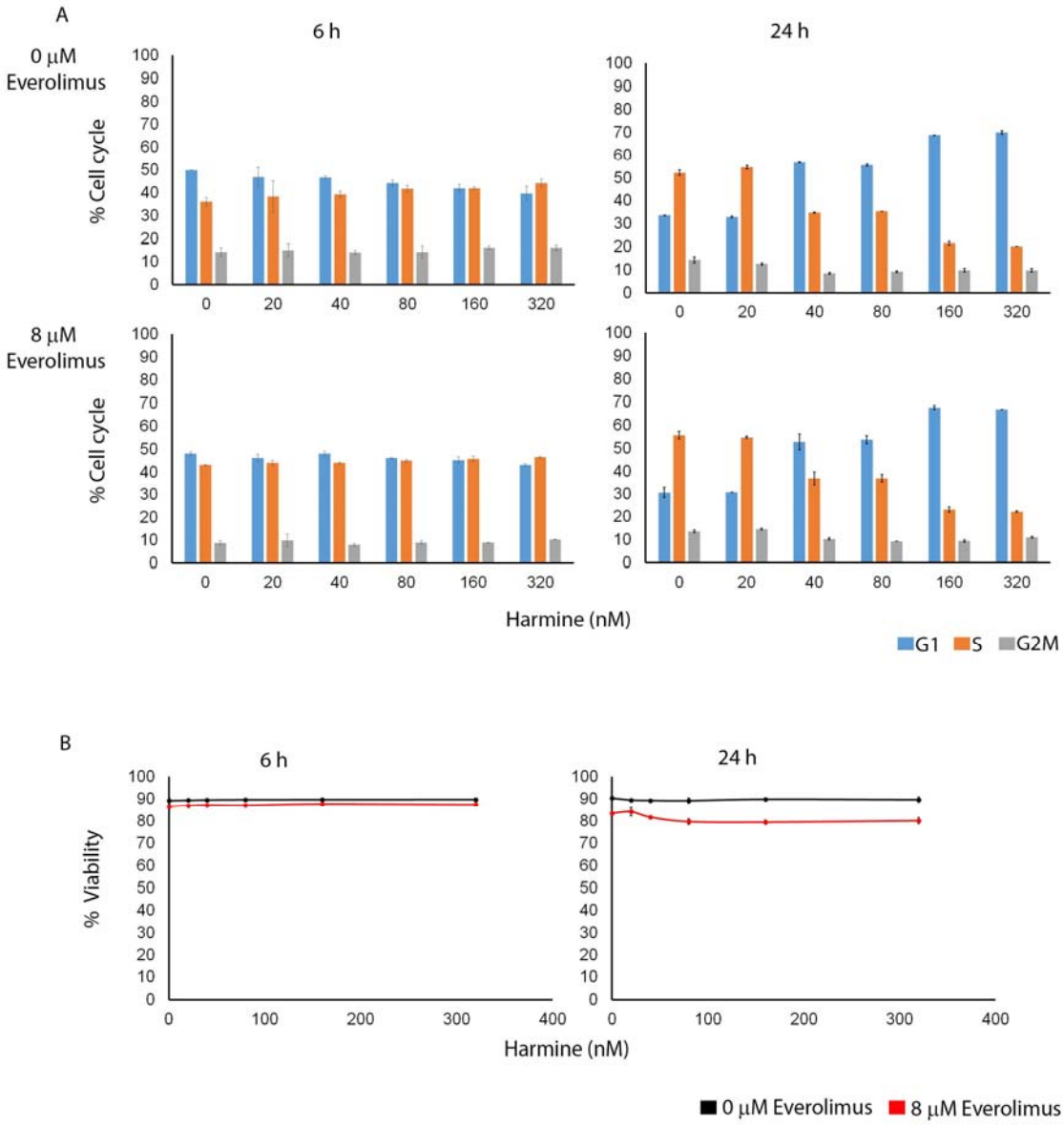

Figure 3.1 Effects of DYRK1a inhibition by harmine on NALM6 cells. Cells were cultured with increasing doses of harmine alone and in combination with 8 mM everolimus and analysed for cell cycle distribution (A) and viability (B). Error bars represent the standard deviation of the mean of 2 independent experiments.

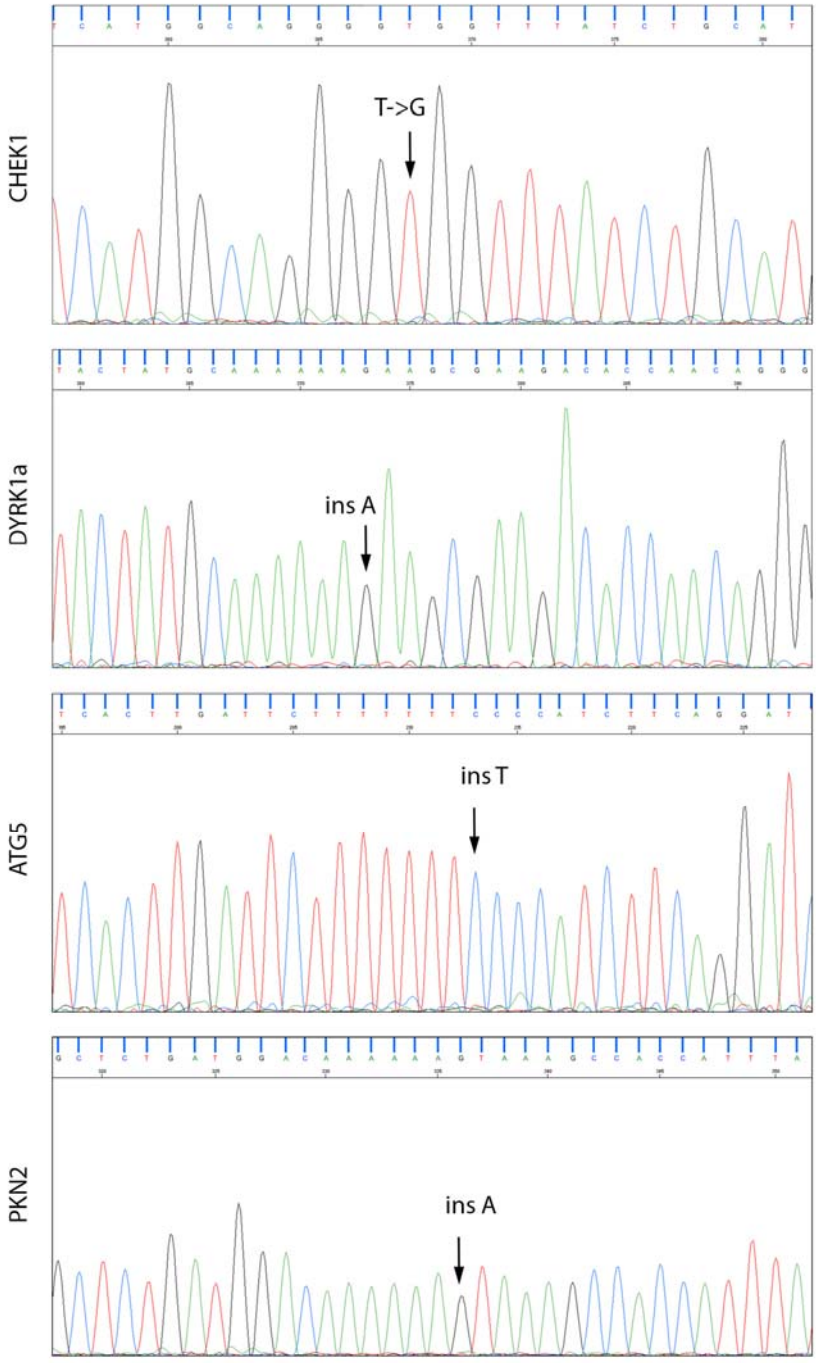

Figure 3.2 Sanger sequencing of 1345-R RNA. Region surrounding the predicted mutation site of each gene was PCR amplified and cloned into pEGFP-N1 expression vector. Arrows indicate predicted mutation. Data shown is a representative of 10 clones sequenced for each gene.

3.3.3 Integrin expression

To investigate the enrichment of adhesion related networks and pathways, the expression of adhesion molecules associated with these pathways was explored. The two most regulated were integrins alpha 6 and 8 being increased by 45.62 and 20 fold according to the transcriptome data. Quantitative Real time PCR (qRT-PCR) was used to confirm the increase in expression of the integrins alpha 6 (ITGα6) and alpha 8 (ITGα8) detected by transcriptome sequencing in 1345-R cells. ITGα6 was significantly increased 93 fold in the resistant 1345-R xenograft cells, as compared to the sensitive parental cells (Figure 3.3), however, there was a large variation in expression in resistant cells harvested from different mice. The expression of ITGα8 was too low to be detected by qRT-PCR and therefore its regulation could not be confirmed.

ITGα6 could not be detected by immunoblotting, therefore flow cytometry was used to confirm protein expression. Strong expression of ITGα6 was detected on the pre-B ALL cell line NALM6, however, no ITGα6 could be detected on the surface of either sensitive or resistant 1345 cells (Figure 3.4). However, intracellular staining for ITGα6 revealed higher expression in 1345-R than 1345-S cells, confirming the RNA results. The increase in ITGα6 expression in 1345-R cells is restricted to the intracellular compartment where it cannot elicit its adhesive capabilities, making it unlikely that it is involved in resistance to mTOR inhibition by everolimus.

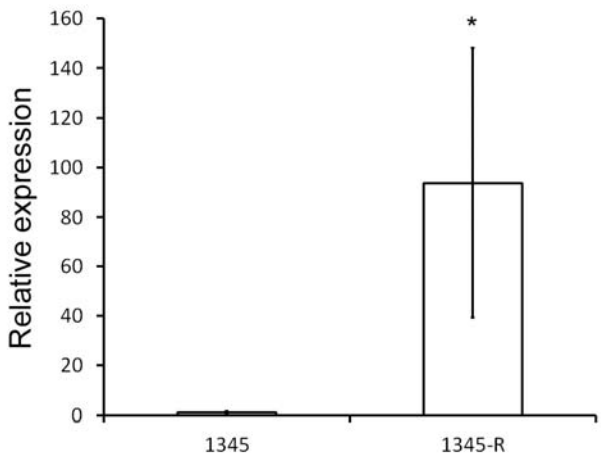

Figure 3.3 1345-R cells have increased ITGα6 expression. ITGα6 expression relative to GAPDH and normalized to 1345. Error bars represent the standard deviation of the mean of biological triplicates. * p=0.0012

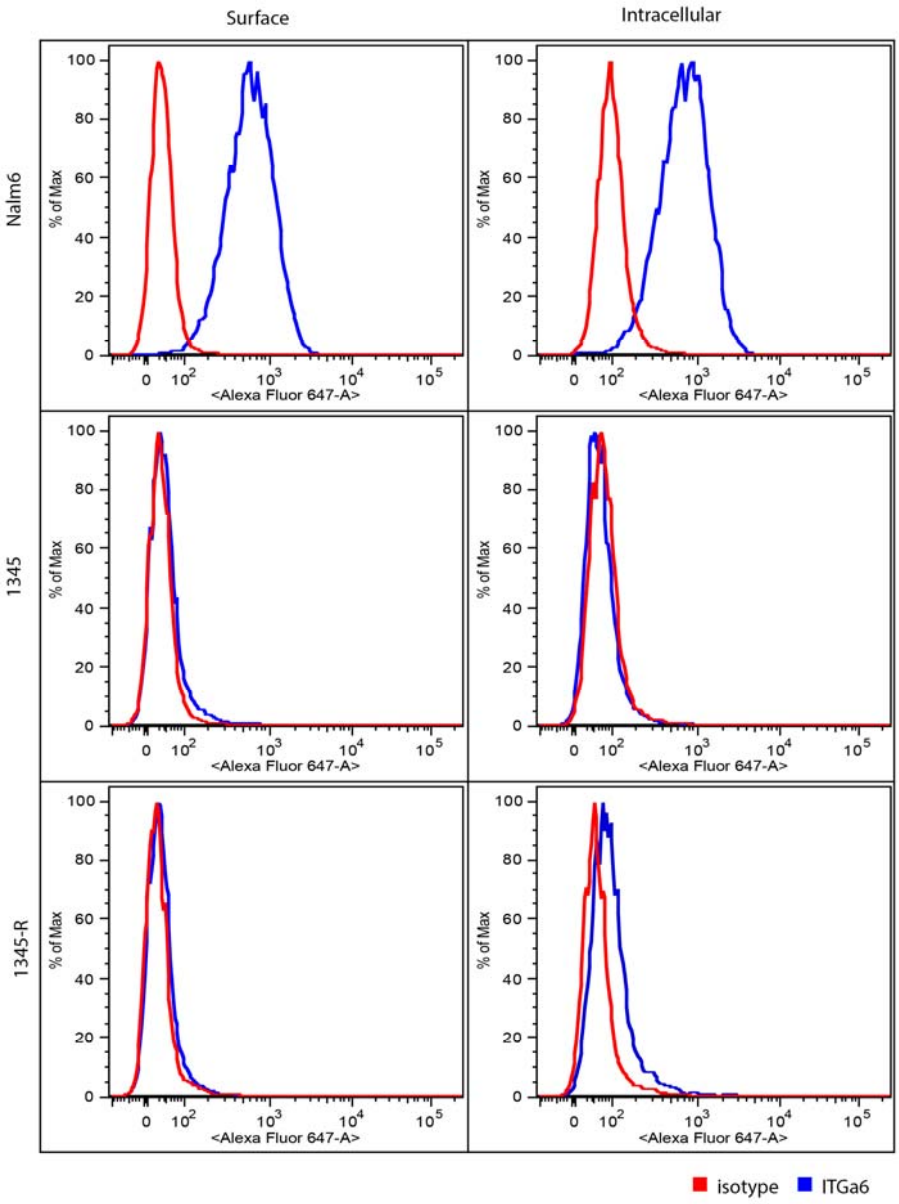

Figure 3.4 Expression of ITGα6 expression in leukemia cells as detected by GoH3 antibody. Surface and intracellular expression of ITGα6 was assessed on sensitive and resistant 1345 cells. ITGα6 (GoH3) is represented by the blue histogram while the isotype control

3.3.4 Generation of additional resistant xenografts

In order to expand the number xenografts analysed, an additional 2 xenografts, 1196, and 2055 were evaluated for their capability to develop resistance to everolimus *in vivo* (Figure 3.5). Everolimus was efficacious in extending the survival of animals engrafted with both xenografts, and re-engraftment of 2055 cells harvested from animals pre-treated with everolimus resulted in a reduction in the survival extension to 27 days (green and purple lines), from 41 days in mice having previously received placebo (red and blue lines), indicating the development of resistance in these cells ($p < 0.0001$). In mice engrafted with 2055 cells from placebo and everolimus pre-treated animals, the fraction of leukemia in the peripheral blood reached 1% in both simultaneously and as such, received treatments at the same time. Interestingly, however, cells from the everolimus pre-treated animals expanded at a slower rate, irrespective of whether the mice subsequently received placebo or everolimus. This is in contrast to the effect of resistance observed in 1345-R where mice more rapidly succumbed to the resistant xenograft. The xenograft 1196 did not develop resistance with the everolimus-induced survival extension being unchanged following serial transplantation and continuous everolimus exposure.

The difference in the kinetics of the sensitive and resistant forms of the ALL xenografts, raised concerns about potential contamination. Therefore, short tandem repeat profiling of 9 loci was undertaken on the resistant and sensitive cells according to the ATCC guidelines to verify the origin of the resistant xenografts [196]. Both 1345-R and 2055-R xenografts shared identical tandem repeat profiles as their sensitive forms, 1345-S and 2055-S respectively, (Figure 3.6) indicating that both resistant xenografts arose from sensitive parental cells.

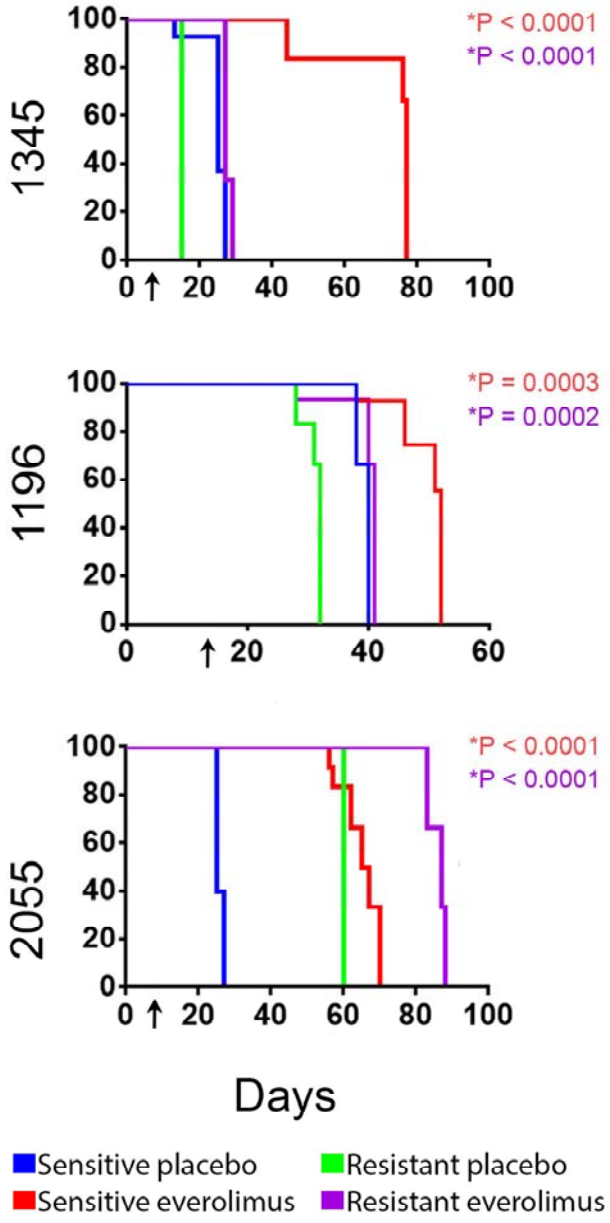

Figure 3.5 Development of resistance to mTOR inhibition by everolimus in human ALL xenografts in NSG mice. NOD/SCID mice engrafted with the indicated human ALL xenografts were treated as shown when blasts in the peripheral blood reached greater than 1%. Kaplan Meier plots shown with the p values indicating significant extensions in survival compared to each xenografts respective placebo control, determined using a Gehan-Breslow-Wilcoxon test. Arrows indicate the days when treatment commenced.

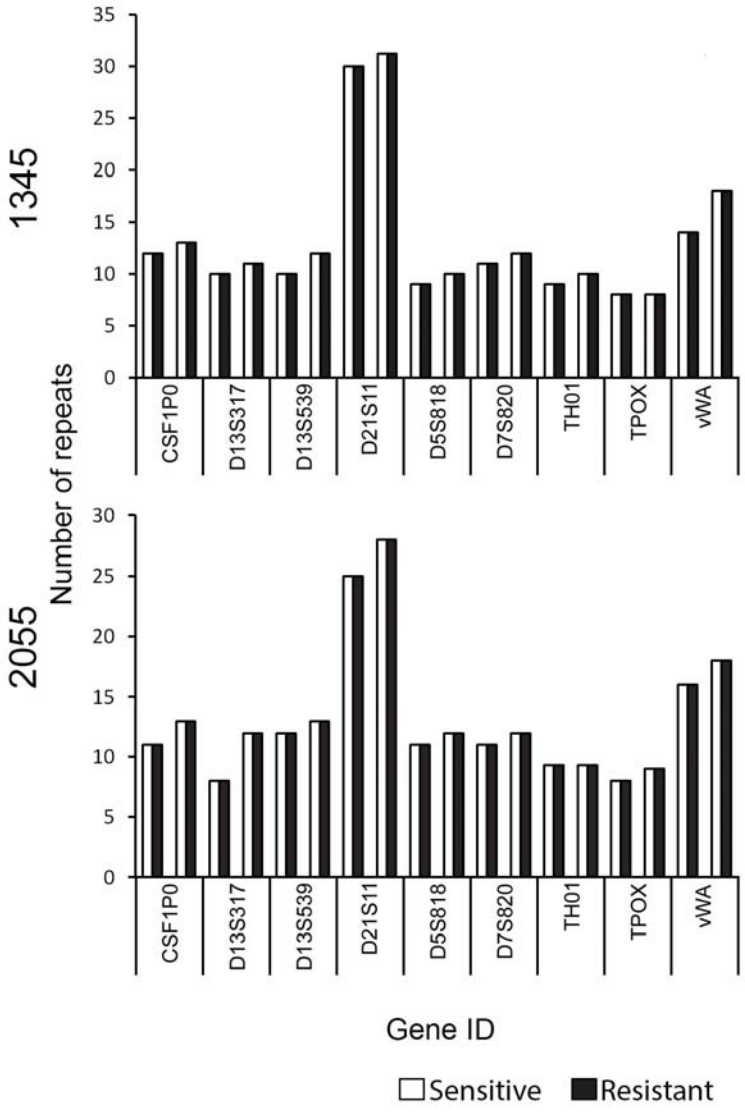

Figure 3.6 STR analysis of everolimus resistant ALL xenografts. DNA from xenografts was sequenced for 11 short tandem repeats and the number of copies in each allele compared between sensitive and resistant xenografts.

3.3.5 Microarray

Transcriptome sequencing revealed resistance to everolimus induced numerous alterations to gene expression, however, the sample size had limited statistical power. Therefore we analysed RNA from the newly generated 2055-S and 2055-R, along with 1345-S and 1345-R, with and without everolimus treatment by microarray. Mice were either engrafted with resistant ALL xenografts or their sensitive parental cells and once leukemia reached approximately 50% in the peripheral blood, mice received a single dose of everolimus or placebo and were sacrificed after 24 h. RNA was isolated from spleen cells (2.2.3), amplified, biotinylated and hybridized to a HumanHT-12v4 bead expression chip (2.2.6).

Gene expression data obtained from the microarray was imported into GenomeStudio software and normalised for background with the average normalisation parameter. Gene lists were obtained by collapsing probes by average expression and exported into a Microsoft Excel spreadsheet. Genes were filtered by excluding those that were not significantly detected in at least 2 of the 3 mice from any group. Xenograft 1345-S and 2055-S had 15022 and 15765 genes remaining respectively after the filter was applied, and these genes were subjected to gene set enrichment analysis using the curated oncology (C2) gene set dataset.

No gene sets were significantly enriched with a FDR of less than 25% when 1345-R and 1345-S cells were compared (Table 3.6). On the other hand, the development of resistance in 2055 resulted in the enrichment of 1063 genes sets in 2055-R and 467 in 2055-S cells. (Table 3.6). Due to the lack of similarity in the changes in gene expression in the two xenografts upon the development of resistance, the effect of everolimus treatment on gene expression was considered. Two gene sets were

enriched following everolimus treatment in both the untreated and resistant 1345 xenograft. Of interest was the negative correlation with the BIOCARTA_AKT_PATHWAY in treated 1345-S cells (Table 3.8). This gene set was not significantly regulated in 1345-R cells, although a trend was observed, suggesting a reduced effect on this pathway in the resistant cells. While everolimus administration negatively enriched a similar number of gene sets in 1345-R and 2055-R (344 and 290 respectively, Table 3.6), there was no similarity in the gene sets enriched (Tables 3.8 and 3.9).

Table 3.6 Number of gene sets significantly enriched with a FDR of less than 25% in microarray data.

Comparisons	Xenograft	
	1345	2055
Sensitive	0	467
Resistant	0	1063
Sensitive untreated	2	0
Sensitive 24hr Everolimus	2	9
Resistant untreated	344	290
Resistant 24hr Everolimus	0	0

Table 3.7 Gene set enrichment analysis of differential gene expression found by microarray associated with resistance in two human ALL xenografts

1345

	NAME	NES	NOM p-val	FDR q-val
1345-S	REACTOME_CELL_CELL_JUNCTION_ORGANIZATION	1.636	0.000	1.000
	MENSSEN_MYC_TARGETS	1.624	0.000	1.000
	KIM_ALL_DISORDERS_DURATION_CORR_DN	1.604	0.000	1.000
	CREIGHTON_AKT1_SIGNALING_VIA_MTOR_DN	1.581	0.000	1.000
	REACTOME_DESTABILIZATION_OF_MRNA_BY_AUF1_HNRNP_D0	1.565	0.109	1.000
1345-R	PID_HDAC_CLASSIII_PATHWAY	-1.407	0.000	0.441
	PID_IL1_PATHWAY	-1.407	0.000	0.441
	PID_AR_NONGENOMIC_PATHWAY	-1.407	0.000	0.442
	DELPUECH_FOXO3_TARGETS_DN	-1.407	0.192	0.443
	OUELLET_CULTURED_OVARIAN_CANCER_INVASIVE_VS_LMP_UP	-1.405	0.000	0.443

2055

	NAME	ES	NOM p-val	FDR q-val
2055-S	MARTINEZ_RESPONSE_TO_TRABECTEDIN_UP	2.141	0.000	0.054
	REACTOME_APC_C_CDC20_MEDIATED_DEGRADATION_OF_CYCLIN_B	2.134	0.000	0.054
	BASSO_CD40_SIGNALING_DN	2.075	0.000	0.054
	XU_HGF_TARGETS_REPRESSED_BY_AKT1_DN	2.066	0.000	0.054
	CHIANG_LIVER_CANCER_SUBCLASS_INTERFERON_DN	2.031	0.000	0.079
2055-R	PID_ILK_PATHWAY	-2.081	0.000	0.188
	BARIS_THYROID_CANCER_DN	-2.033	0.000	0.240
	REACTOME_MUSCLE_CONTRACTION	-1.949	0.000	0.345
	RASHI_RESPONSE_TO_IONIZING_RADIATION_2	-1.943	0.000	0.283
	LANDIS_BREAST_CANCER_PROGRESSION_DN	-1.936	0.000	0.257

Table 3.8 Gene set enrichment analysis of differentially expressed genes found by microarray following everolimus treatment of sensitive and resistant 1345

1345

	NAME	ES	NOM p-val	FDR q-val
UN	AMIT_SERUM_RESPONSE_40_MCF10A	1.844	0.000	0.214
	CROONQUIST_NRAS_VS_STROMAL_STIMULATION_DN	1.826	0.000	0.233
	REACTOME_CHOLESTEROL_BIOSYNTHESIS	1.880	0.000	0.262
	CHUANG_OXIDATIVE_STRESS_RESPONSE_UP	1.741	0.000	0.265
	LEE_AGING_NEOCORTEX_UP	1.746	0.000	0.289
Eve	BRACHAT_RESPONSE_TO_METHOTREXATE_UP	-1.990	0.000	0.054
	BIOCARTA_AKT_PATHWAY	-1.899	0.000	0.105
	REACTOME_SIGNALING_BY_NOTCH1	-1.755	0.000	0.360
	ZHU_CMV_8_HR_DN	-1.654	0.000	0.393
	XU_HGF_TARGETS_INDUCED_BY_AKT1_48HR_DN	-1.655	0.000	0.412

1345-R

	NAME	ES	NOM p-val	FDR q-val
UN	WONG_PROTEASOME_GENE_MODULE	1.881	0.000	0.078
	YAO_TEMPORAL_RESPONSE_TO_PROGESTERONE_CLUSTER_14	1.816	0.000	0.211
	KEGG_PURINE_METABOLISM	1.812	0.000	0.157
	KIM_MYC_AMPLIFICATION_TARGETS_UP	1.800	0.000	0.169
	REACTOME_REGULATION_OF_MITOTIC_CELL_CYCLE	1.785	0.000	0.201
Eve	BIOCARTA_AKT_PATHWAY	-1.820	0.000	0.487
	PID_IL2_STAT5_PATHWAY	-1.768	0.000	0.671
	WAMUNYOKOLI_OVARIAN_CANCER_GRADES_1_2_DN	-1.735	0.000	0.958
	SMIRNOV_RESPONSE_TO_IR_2HR_DN	-1.708	0.000	1.000
	ZHAN_MULTIPLE_MYELOMA_PR_DN	-1.690	0.000	1.000

Table 3.9 Gene set enrichment analysis of differentially genes by microarray following everolimus treatment of sensitive and resistant 2055

2055

	NAME	NES	NOM p-val	FDR q-val
UN	ZHAN_LATE_DIFFERENTIATION_GENES_DN	1.791	0.000	0.259
	BIOCARTA_G2_PATHWAY	1.775	0.000	0.266
	BUCKANOVICH_T_LYMPHOCYTE_HOMING_ON_TUMOR_DN	1.769	0.000	0.271
	ODONNELL_METASTASIS_UP	1.480	0.000	0.286
	GINESTIER_BREAST_CANCER_20Q13_AMPLIFICATION_UP	1.481	0.000	0.287
Eve	REACTOME_NONSENSE_MEDIATED_DECAY_ENHANCED_BY_THE_EXON_JUNCTION_COMPLEX	-1.793	0.000	0.066
	REACTOME_TRANSLATION	-1.804	0.000	0.075
	REACTOME_FORMATION_OF_THE_TERNARY_COMPLEX_AND_SUBSEQUENTLY_THE_43S_COMPLEX	-1.744	0.000	0.086
	REACTOME_INFLUENZA_VIRAL_RNA_TRANSCRIPTION_AND_REPLICATION	-1.823	0.000	0.089
	REACTOME_3_UTR_MEDIATED_TRANSLATIONAL_REGULATION	-1.710	0.000	0.105

2055-R

	NAME	NES	NOM p-val	FDR q-val
UN	KEGG_AMINOACYL_TRNA_BIOSYNTHESIS	1.507	0.000	0.192
	ZHAN_MULTIPLE_MYELOMA_CD1_VS_CD2_UP	1.505	0.000	0.192
	REACTOME_PACKAGING_OF_TELOMERE_ENDS	1.507	0.000	0.193
	SOTIRIOU_BREAST_CANCER_GRADE_1_VS_3_UP	1.506	0.000	0.193
	NAKAMURA_TUMOR_ZONE_PERIPHERAL_VS_CENTRAL_UP	1.507	0.000	0.193
Eve	COLIN_PILOCYTIC_ASTROCYTOMA_VS_GLIOBLASTOMA_DN	-1.699	0.000	1.000
	LEE_INTRATHYMIC_T_PROGENITOR	-1.692	0.000	1.000
	HOEBEKE_LYMPHOID_STEM_CELL_UP	-1.662	0.000	1.000
	BRACHAT_RESPONSE_TO_METHOTREXATE_UP	-1.609	0.000	1.000
	POMEROY_MEDULLOBLASTOMA_PROGNOSIS_UP	-1.600	0.000	1.000

A list of genes significantly detected by the microarray analysis of both everolimus resistant xenografts was imported into Partek genomics suite. Principal component analysis (PCA) indicated the major source of variation within the 1345 xenograft set was based on how the xenografts responded to everolimus treatment rather than the development of resistance (Figure 3.7 A). Conversely, resistance to everolimus was the major source of variation between the 2055 xenograft set (Figure 3.7 B). Similarly, hierarchical clustering of the significantly detected genes clustered in 1345-S by treatment (Figure 3.8 A) and 2055 by resistance (Figure 3.8 B), further emphasising the difference in the development of resistance between these two xenografts. This suggests that changes in baseline gene expression are important for resistance in 2055 while changes in the response to everolimus is important for resistance in 1345.

Differential regulation of genes was detected with the Partek genomics suite by means of a 2-way ANOVA using the method of moments and comparing groups by the Fisher's Least Significant Difference method on Log2 transformed data. Lists that contained genes significantly altered by everolimus treatment and the development of resistance, were generated for each xenograft. Everolimus treatment of 1345-S and 1345-R significantly altered the expression of 4833 and 3547 genes respectively, with 2531 genes being regulated in common (Figure 3.9 A). Fewer genes were significantly regulated by treatment in 2055-S and 2055-R with 1792 and 1534 respectively being altered, 505 being common between the two xenografts (Figure 3.9 B). Compared to their respective sensitive parental controls, 762 genes were regulated in common between both 1345-R and 2055-R (Figure 3.9 C). Treatment of the resistant xenografts with everolimus commonly altered the expression of 441 genes (Figure 3.9 D).

The 762 genes commonly regulated in both 1345-R and 2055-R (Figure 3.9 C intersection) could potentially indicate a similarity in the development of resistance to everolimus. To assess what pathways these genes were involved in, the list of genes was interrogated using Metacore and GSEA. GSEA was unable to identify enrichment of any gene sets in the commonly regulated genes, however, Metacore identified 20 pathway maps (Table 3.10) and 15 process networks (Table 3.11) that were significantly enriched with a FDR of less than 25%. Pathways associated with cellular adhesion and cytoskeletal regulation were prominent in both process networks and pathways maps of everolimus resistant cells.

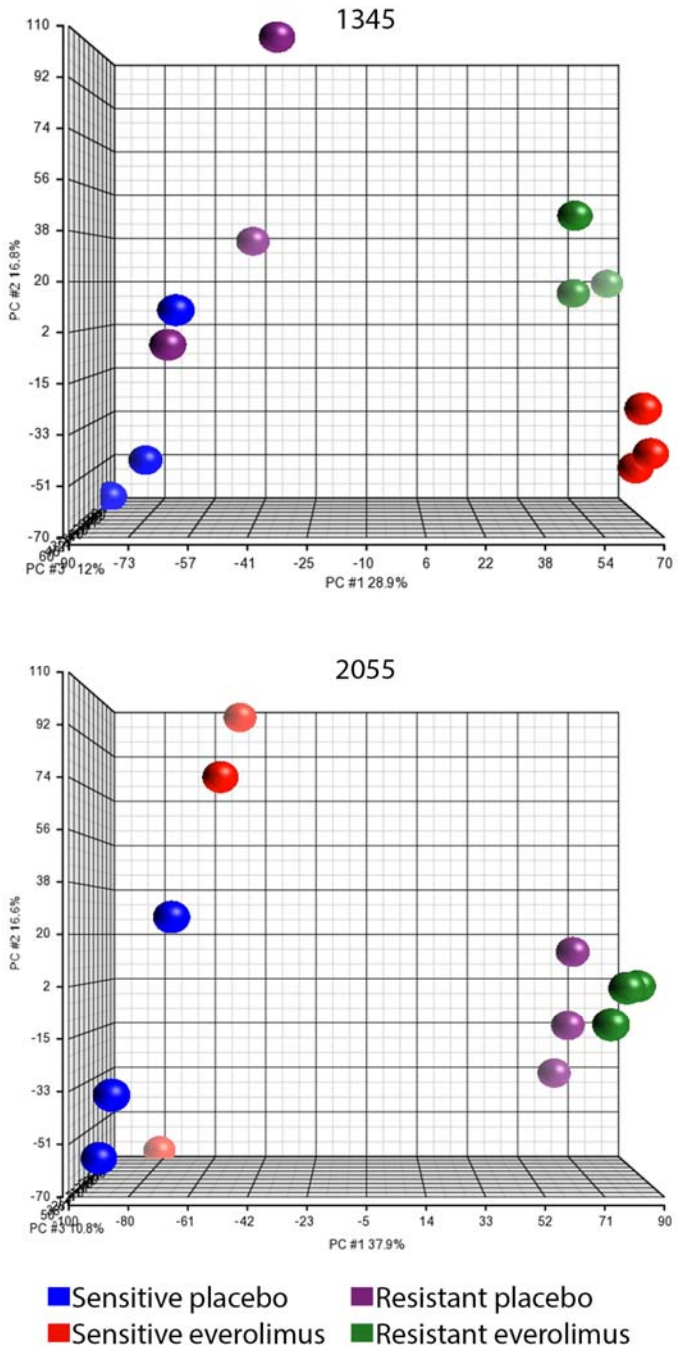

Figure 3.7 Principal component analysis (PCA) of microarray data. RNA was isolated from mice engrafted with sensitive and resistant 1345 (A) and 2055 (B). Mice were untreated (blue and red dots) or received everolimus 24 h before cull (green and purple dots). RNA was analyzed by microarray and expression data was imported into Partek genomics suite and samples separated by PCA analysis. Samples were run in biological triplicate.

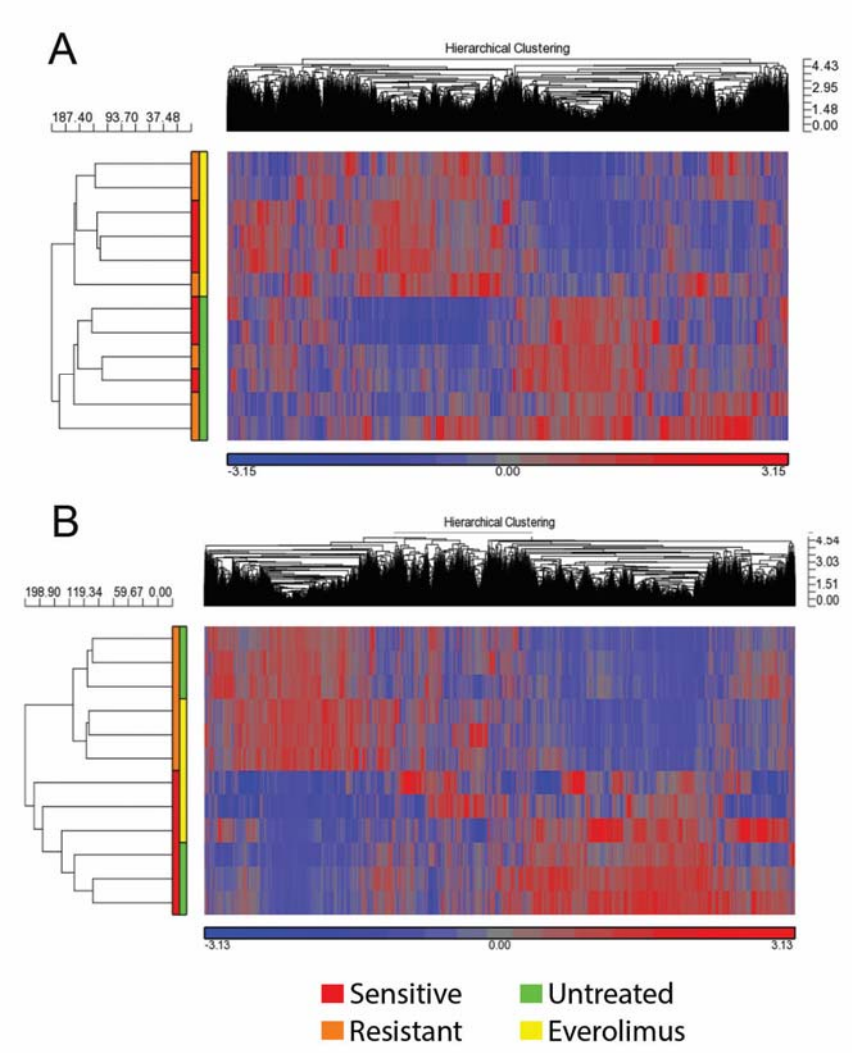

Figure 3.8 Hierarchical clustering of microarray data from 1345 and 2055 ALL xenografts. RNA was isolated from mice engrafted with sensitive and resistant 1345 (A) and 2055 (B). Mice were untreated (red and orange bars) or received everolimus 24 h before cull (green and yellow bars). RNA was analyzed by microarray and expression data was imported into Partek genomics suite. Hierarchical clustering was performed on Samples (rows) and genes (columns) using Euclidean dissimilarity and the average linkage method. Samples were run in biological triplicate.

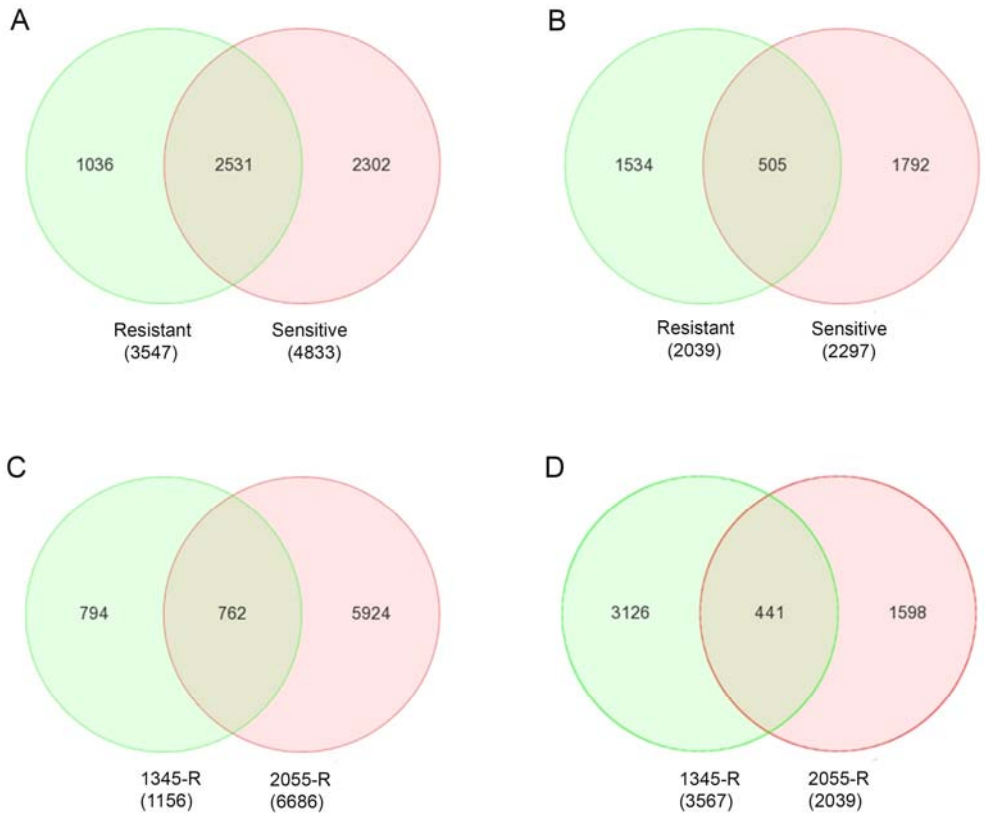

Figure 3.9 Venn diagram of commonly expressed genes. Partek genomics suite was used to detect differentially expressed genes and compare generated lists between different comparison groups. Expression of genes significantly altered by everolimus treatment was compared between the sensitive and resistant 1345 (A) and 2055 (B) ALL xenografts. Genes that were significantly different in both resistant xenografts compared to their relative sensitive parental controls (C) and common genes in resistant xenografts when treated with everolimus (D) were also compared.

Table 3.10 Metacore pathway maps of genes commonly regulated in everolimus resistant xenografts.

Maps	p-value	FDR
Cell adhesion_Cadherin-mediated cell adhesion	8.935E-06	8.206E-04
Cell adhesion_Chemokines and adhesion	1.641E-05	8.206E-04
Cell adhesion_Histamine H1 receptor signaling in the interruption of cell barrier integrity	4.787E-05	1.596E-03
Development_Role of proteases in hematopoietic stem cell mobilization	3.745E-04	9.363E-03
Cytoskeleton remodeling_Cytoskeleton remodeling	5.477E-04	9.870E-03
Cell adhesion_Endothelial cell contacts by non-junctional mechanisms	6.718E-04	9.870E-03
Cytoskeleton remodeling_TGF, WNT and cytoskeletal remodeling	7.013E-04	9.870E-03
Cell adhesion_Endothelial cell contacts by junctional mechanisms	7.896E-04	9.870E-03
Development_Osteopontin signaling in osteoclasts	1.053E-03	1.124E-02
Cytoskeleton remodeling_Fibronectin-binding integrins in cell motility	1.124E-03	1.124E-02
Role of growth factor receptors transactivation by Hyaluronic acid / CD44 signaling in tumor progression	1.433E-03	1.303E-02
Development_Astrocyte differentiation from adult stem cells	1.870E-03	1.559E-02
Cell adhesion_Integrin-mediated cell adhesion and migration	2.684E-03	1.997E-02
Cytoskeleton remodeling_Integrin outside-in signaling	2.796E-03	1.997E-02
Cell adhesion_Role of CDK5 in cell adhesion	1.460E-02	9.731E-02
Development_Role of G-CSF in hematopoietic stem cell mobilization	3.375E-02	1.124E-01
Cytoskeleton remodeling_ESR1 action on cytoskeleton remodeling and cell migration	3.533E-02	1.124E-01
Development_GDNF signaling	3.848E-02	1.124E-01
Development_Slit-Robo signaling	4.788E-02	1.124E-01
Cytoskeleton remodeling_Reverse signaling by ephrin B	4.944E-02	1.124E-01

Abbreviations: FDR- False discovery rate

Table 3.11 Metacore process networks of genes commonly regulated in everolimus resistant xenografts.

Networks	p-value	FDR
Cell adhesion_Cadherins	2.170E-05	1.302E-03
Cell adhesion_Platelet aggregation	1.732E-03	3.021E-02
Cell adhesion_Cell junctions	1.899E-03	3.021E-02
Cytoskeleton_Actin filaments	2.571E-03	3.021E-02
Cytoskeleton_Regulation of cytoskeleton rearrangement	2.962E-03	3.021E-02
Cell adhesion_Synaptic contact	3.021E-03	3.021E-02
Cell adhesion_Cell-matrix interactions	4.936E-03	3.597E-02
Cell adhesion_Integrin-mediated cell-matrix adhesion	5.190E-03	3.597E-02
Inflammation_Protein C signaling	5.396E-03	3.597E-02
Cell adhesion_Glycoconjugates	1.633E-02	9.796E-02
Cell adhesion_Platelet-endothelium-leucocyte interactions	1.973E-02	1.076E-01
Cytoskeleton_Intermediate filaments	2.982E-02	1.491E-01
Cytoskeleton_Macropinocytosis and its regulation	3.259E-02	1.504E-01
Signal Transduction_BMP and GDF signaling	3.693E-02	1.583E-01
Development_Blood vessel morphogenesis	3.961E-02	1.584E-01

Abbreviations: FDR- False discovery rate

3.3.6 qRT-PCR confirmation of changed expression

Of the 762 genes commonly altered in both resistant xenografts, 80 were mutually increased (≥1.5 fold) and 47 decreased (≤1.5 fold) over their respective sensitive controls (Table 3.12). A significant increase in the expression of 7 genes was confirmed in 2055-R cells (Figure 3.10 A) though one gene, PTAR, while similarly increased in 2055-R cells, failed to achieve significance. The expression of FAK (PTK2), CDK6, EPAS1 and AKAP12 was increased in 1345-R cells, however the difference was not significant (Figure 3.10 B).

Table 3.12 Top 25 commonly regulated genes in everolimus resistant xenografts by microarray (for full table see Appendix A.4).

Upregulated			Downregulated		
Gene	**FC 2055-R**	**FC 1345-R**	**Gene**	**FC 2055-R**	**FC 1345-R**
PTGDR	68.43	13.98	BEST3	105.20	1.72
GIMAP4	63.79	19.19	ADAMTSL2	56.99	3.07
LOC442597	30.28	3.41	CXORF57	56.64	2.83
NOG	18.73	2.04	ADAM23	53.59	4.65
SDK2	18.27	5.39	FAM127A	41.22	2.00
ZYX	17.00	1.73	DCBLD2	25.09	2.00
FAK	16.40	12.96	ALDH7A1	24.69	3.61
ACTN1	15.10	3.08	WBP5	24.29	1.67
GYPC	14.27	1.51	TMSB15A	21.15	0.91
ARMCX1	12.68	7.87	ALOX5	18.06	3.04
HS.570988	12.63	2.69	VMD2L3	17.31	1.73
SLC2A5	12.24	1.99	ZNF70	17.15	16.68
LOC646786	12.17	4.63	PTPRZ1	15.03	2.48
SLC4A11	11.23	1.91	BCL2L11	14.48	2.01
GOLGB1	8.61	2.81	SKAP1	13.87	2.56
SH3BP4	6.65	3.19	TRIB1	12.49	2.53
TNS3	6.27	3.45	RBM9	11.31	2.11
TBC1D4	5.88	1.58	IL9R	7.19	1.54
RAI14	5.68	3.12	MYOM2	6.94	1.56
RASD1	4.83	2.75	NFIA	6.04	0.15
C10ORF47	4.79	3.30	OXCT2	5.96	1.65
DMXL2	4.74	2.10	SERINC2	5.74	1.98
SPNS3	4.68	1.94	RAPGEF3	5.55	4.61
AKAP12	4.57	2.39	PLCH2	5.36	2.14
EIF4E3	4.54	6.01	FM01	5.30	2.48

Abbreviations: FC – Fold change

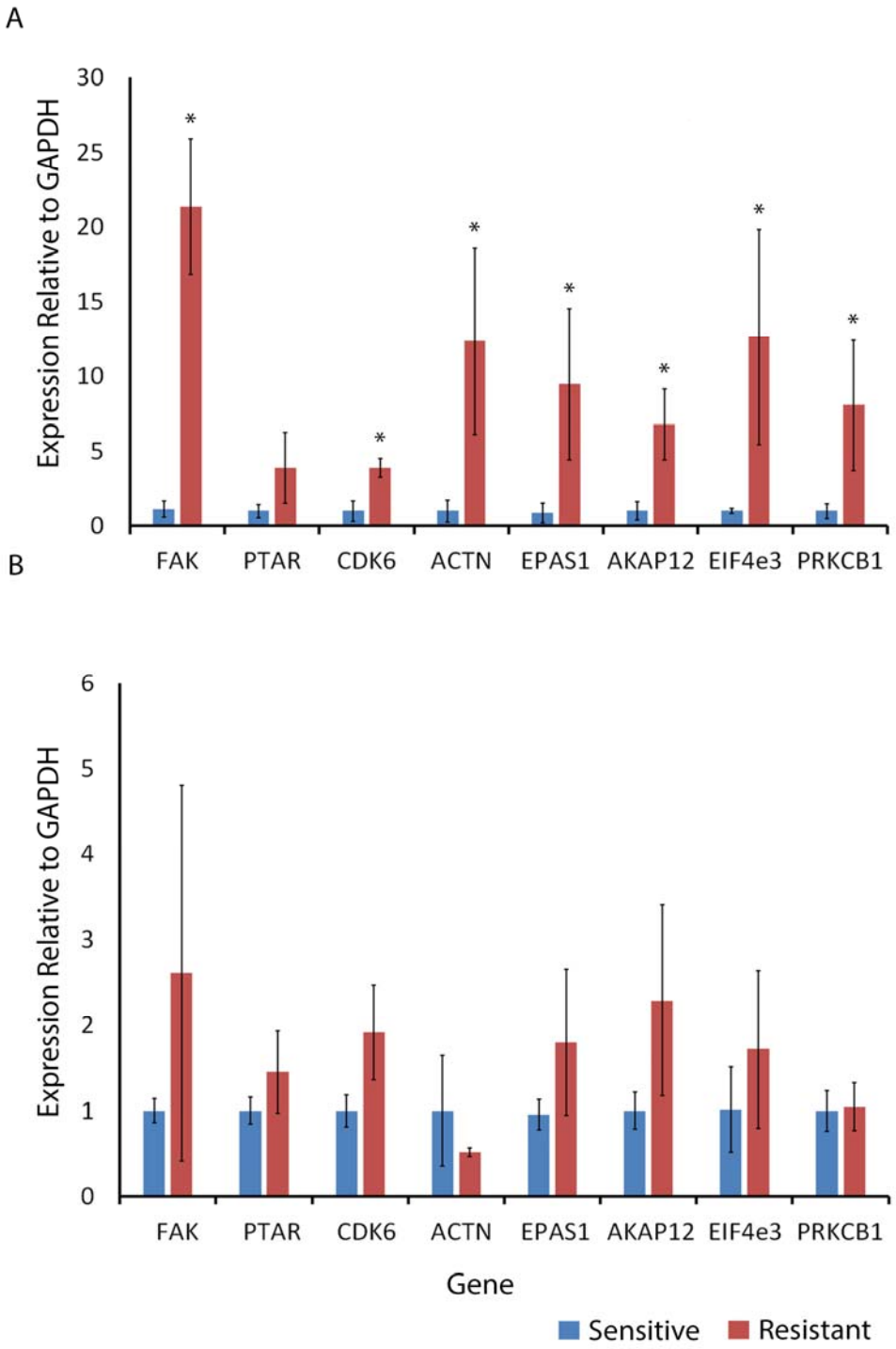

Figure 3.10 RT-PCR confirmation of altered gene expression detected in array analysis of resistant xenografts. Expression of indicated genes was assessed in RNA from mice engrafted with sensitive (blue) and resistant (red) 2055 (A) and 1345 (B). Error bars represent the standard deviation of the mean biological triplicates, data normalized to sensitive xenografts, * $p<0.05$.

3.5.7 Correlation of transcriptome sequencing and microarray

The list of genes significantly altered by resistance in 1345 and 2055 as detected by microarray was compared to the list generated from transcriptome sequencing. A total of 36 genes were identified by both techniques and of those genes, 33 were similarly altered in both the degree and directionality (Table 3.13). Analysis of the pathway maps (Table 3.14) and process networks (Table 3.15) associated with these genes, revealed and enrichment in adhesion related pathways. However, the relatively small gene list used to generate these pathways meant that only a few genes were involved in each pathway, limiting the reliability of the pathways generated.

Table 3.13 Genes commonly regulated in resistant xenografts found by microarray and transcriptome.

Gene	Gene Name	2055-R (microarray	1345-R (microarray	1345-R (transcriptome)
ACTN1	Actinin alpha 1	15.10121	3.081514	2.195555
ADAM23	ADAM Metallopeptidase Domain 23	-53.5883	-4.64562	-176.576
ALOX5	Arachidonate 5-lipoxygenase	-18.064	-3.0368	-6.52093
BEST3	Bestrophin 3	-105.202	-1.71758	-7.13469
C11ORF75	Single-Pass Membrane Protein With Coiled-Coil Domains 4	2.186602	4.152587	5.232009
CD163L1	CD163 Molecule-Like 1	-4.82464	-2.39797	-6.68956
CD200	OX-2 membrane glycoprotein	1.902462	1.513213	2.368478
CTNNA1	Catenin alpha-1	4.048169	5.428412	10.03516
DCBLD2	Discoidin, CUB and LCCL domain-containing protein 2	-25.0897	-1.99505	-3.76471
DDX60	DEAD (Asp-Glu-Ala-Asp) Box Polypeptide 60	-1.80541	-2.64506	-3.06109
FAM127A	Family With Sequence Similarity 127, Member A	-41.2189	-2.00215	-2.39869
FAM164A	Family With Sequence Similarity 164, Member A	-3.03256	-2.93756	-4.11349
FLJ22536	hypothetical locus LOC401237	4.442485	2.634444	3.0411
GATS	Stromal Antigen 3 Opposite Strand	2.362571	1.634139	2.597726
HIST1H1B	Histone Cluster 1, H1b	-2.37669	-1.60532	-2.00687
HIST1H1D	Histone Cluster 1, H1d	-1.92065	-1.60837	2.840239
KBTBD11	Kelch Repeat And BTB (POZ) Domain Containing 11	1.527067	2.711003	3.434046
LAX1	Lymphocyte Transmembrane Adaptor 1	1.795586	3.329376	2.615507
MVP	Major Vault Protein	1.582479	2.751358	3.116274
NEIL1	Nei Endonuclease VIII-Like 1	-5.18819	-1.58733	4.673198
OXCT2	3-Oxoacid CoA Transferase 2	-5.96289	-1.65187	-4.82785
PRKCB	Protein Kinase C, Beta	4.467857	1.521046	2.139201
PTGDR	Prostaglandin D2 Receptor	68.42667	13.98083	15.14209
PTK2	Protein tyrosine kinase 2 (FAK1)	16.40453	12.96064	4.562393
PTPRF	Protein Tyrosine Phosphatase, Receptor Type, F	2.22575	2.153346	3.226891
RAI14	Retinoic Acid Induced 14	5.684875	3.119224	27.49589
RASD1	RAS, Dexamethasone-Induced 1	4.82974	2.749402	6.451487
RHOB	Ras Homolog Family Member B	-4.44211	-2.3474	6.016126
SDK2	Sidekick Celltune Adhesion Molecule 2	18.2686	5.393328	12.31393
SPNS3	Spinster Homolog 3	4.676926	1.939586	3.125965
TM6SF1	Transmembrane 6 Superfamily Member 1	1.923002	5.365719	2.288218
TMEM136	Transmembrane Protein 136	2.684557	1.533716	2.853364
TMEM44	Transmembrane Protein 44	2.557675	1.619264	2.303991
WBP5	WW Domain Binding Protein 5	-24.2946	-1.6746	-2.90655
ZNF154	Zinc Finger Protein 154	4.208378	2.643361	7.111662
ZYX	Zyxin	17.00392	1.726505	3.249487

Table 3.14 Top 15 pathway maps of genes commonly regulated in resistant xenografts found by microarray and transcriptome (for full table see Appendix A.5).

Maps	p-value	FDR
Cell adhesion_Cadherin-mediated cell adhesion	1.058E-05	9.154E-04
Cell adhesion_Chemokines and adhesion	2.068E-05	9.154E-04
Cytoskeleton remodeling_Cytoskeleton remodeling	2.237E-05	9.154E-04sc
HBV signaling via protein kinases leading to HCC	2.876E-05	9.154E-04
Development_Gastrin in differentiation of the gastric mucosa	3.390E-05	9.154E-04
Cell adhesion_Histamine H1 receptor signaling in the interruption of cell barrier integrity	5.661E-05	1.274E-03
Cell adhesion_Integrin-mediated cell adhesion and migration	6.879E-05	1.327E-03
Muscle contraction_Oxytocin signaling in uterus and mammary gland	1.482E-04	2.501E-03
Development_VEGF signaling via VEGFR2 - generic cascades	3.649E-04	5.473E-03
Cell adhesion_Endothelial cell contacts by non-junctional mechanisms	7.481E-04	9.891E-03
Cytoskeleton remodeling_TGF, WNT and cytoskeletal remodeling	8.257E-04	9.891E-03
Cell adhesion_Endothelial cell contacts by junctional mechanisms	8.792E-04	9.891E-03
Cytoskeleton remodeling_Fibronectin-binding integrins in cell motility	1.252E-03	1.207E-02
NETosis in SLE	1.252E-03	1.207E-02
Neurophysiological process_Thyroliberin in cell hyperpolarization and excitability	1.595E-03	1.436E-02

Abbreviations: FDR – false discovery rate.

Table 3.15 Top 15 process networks of genes commonly regulated in resistant xenografts found by microarray and transcriptome (for full table see Appendix A.6).

Networks	p-value	FDR
Cell adhesion_Cadherins	8.305E-09	5.647E-07
Cell adhesion_Cell junctions	5.071E-05	1.724E-03
Cytoskeleton_Regulation of cytoskeleton rearrangement	9.073E-05	2.057E-03
Cell adhesion_Integrin-mediated cell-matrix adhesion	1.900E-04	3.230E-03
Development_Neuromuscular junction	5.246E-04	7.134E-03
Cytoskeleton_Actin filaments	1.033E-03	1.143E-02
Signal transduction_Oxytocin signaling	1.420E-03	1.143E-02
Cell cycle_G1-S Growth factor regulation	1.513E-03	1.143E-02
Cell adhesion_Amyloid proteins	1.513E-03	1.143E-02
Signal Transduction_Cholecystokinin signaling	2.589E-03	1.688E-02
Inflammation_Protein C signaling	2.731E-03	1.688E-02
Cell adhesion_Platelet aggregation	7.931E-03	4.444E-02
Cell adhesion_Glycoconjugates	8.496E-03	4.444E-02
Muscle contraction	1.017E-02	4.939E-02
Cell adhesion_Synaptic contact	1.202E-02	5.451E-02

Abbreviations: FDR – false discovery rate.

3.3.8 Adhesion

Genes involved with cellular adhesion were found to be upregulated in everolimus resistant xenografts by RNAseq and microarray. Furthermore, pathway mapping with Metacore identified an enrichment of adhesion pathways and networks. To confirm the increased adhesive capabilities of resistant cells, 1345-R and 2055-R xenografts adhesion assays were performed using the immortalised human bone marrow stromal cell line HuBMS.hTERT. Resistant 1345-R cells demonstrated significantly greater adhesion to human bone marrow stroma than the sensitive xenograft. A similar trend towards increased adhesion with resistance was observed with 2055, although the difference was not significant (Figure 3.11).

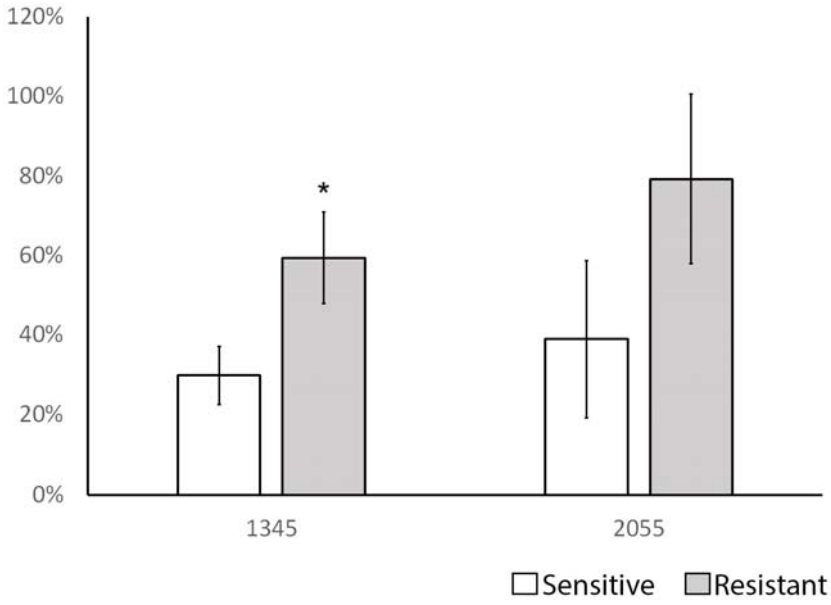

Figure 3.11 Adhesion of 1345 and 1345-R cells to human HuBMS.hTERT stromal cells. Cells were labelled with ^{51}Cromium and allowed to adhere to HuBMS.hTERT cells for 1 h. Adherent cells were counted by Microbeta 2 scintillation counter. Error bars represent the standard deviation of the mean from 2 independent experiments performed in quadruplicate. * p=0.01.

3.4 DISCUSSION

Relapse and drug resistance continue to plague patient survival in both paediatric and adult patients with ALL. Resistance to everolimus may occur through the acquisition of resistance conferring mutations during treatment, or through the selection of pre-existing sub-clones containing such mutations.

Several mutations were identified that were solely present within the resistant ALL xenograft 1345-R, however, none of the mutations could be confirmed by Sanger sequencing. The proposed mutations in the transcriptome sequencing occurred within single nucleotide rich regions. Errors in sequencing and inaccurate mapping of reads to the reference genome may have led to the false identification of mutated base pairs. The transcriptome is highly complex and sequencing technology is currently limited by technical and bioinformatics 'noise' that may have confounding effects on data obtained. Mapping the sequencing reads to the reference genome and library preparation are significant sources of error within RNAseq, and there is still room for improvement in these areas in order to maximise the quality of data obtained from sequencing of the transcriptome [197]. Large datasets are required to overcome current limitations of RNAseq technology and our limited sample number necessitated the use of alternative techniques to analyse the transcriptome of everolimus resistant xenograft.

A recurring theme in the analysis of the gene expression dataset of everolimus resistant cells was adhesion. Increased adhesion has been previously reported to occur in cells resistant to mTOR inhibition but a causal role has not yet been established [176, 181, 198]. Adhesion to the bone marrow microenvironment is critical for the growth and survival of ALL cells *in vivo* and *in vitro* [104, 107].

Changes to the expression of crucial adhesion factors such as VLA-4 [175, 199] and CD44 [200] are implicated in the development of drug resistance in ALL. Furthermore, increased adhesion to the bone marrow microenvironment has been shown to provide cells with a means by which to escape chemotherapy [170-172] and disruption of the adhesive interactions or factors that retain cells within the microenvironment, significantly improves the therapeutic effect of chemotherapy in pre-clinical models of ALL [175, 201].

The dissimilarity in survival curves of the two everolimus resistant xenografts suggests differences in the mechanisms underlying resistance in these xenografts. However, we identified 762 genes regulated in common between both everolimus resistant xenografts, and these genes were enriched for pathways involved in cellular adhesion. As adhesion is paramount for the survival of ALL cells, and has previously been demonstrated to associate to mTOR inhibitor resistance in other cancer cell models *in vitro* [176, 177], it is a potential common mechanism by which these xenografts have developed resistance to everolimus.

The transcript of the integrin, ITGα6, is increased in everolimus resistant 1345-R cells, however, this failed to translate to an increase of surface expression of the protein and therefore is unlikely to impact on the adhesion of the resistant cells. Regardless, both 1345-R and 2055-R were more adherent to human bone marrow stroma *in vitro* than their sensitive parental counterparts, and adhesion mediated intracellular signalling pathways enriched in the everolimus resistant xenografts. The expression of focal adhesion kinase (FAK/PTK2) was increased in both resistant xenografts as were pathways involving reorganisation of the actin cytoskeleton. FAK has a well-documented role in facilitating adhesion and migration downstream of integrin-mediated intracellular signalling regulating focal adhesions and directed migration by

reorganising the actin cytoskeleton [178-180, 202]. Cytoskeleton remodelling is an important process for adhesion and cellular migration [203, 204] and perturbation of Rho GTPases, regulators of cytoskeleton dynamics, can impair the adhesion ITGα4 mediated adhesion of multiple myeloma cells in response to SDF-1α [205].

Recently, the overexpression of FAK has been correlated with resistance to mTOR inhibition by everolimus in pancreatic neuroendocrine tumours and inhibition of FAK synergised with everolimus *in vitro* [181]. Similarly, genetic deletion or pharmacological inhibition of FAK sensitised PTEN null T-ALL cells to inhibition of the PI3K/mTOR pathway [206] and synergized with tyrosine kinase inhibitors in BCR/ABL positive ALL [207]. While overcoming everolimus resistant by inhibition of FAK remains to be seen, the FAK inhibitor defactinib is currently in several clinical trials including a phase II clinical trial for mesothelioma (NCT01870609) and a phase I trial for ovarian cancer (NCT01778803), making combination therapy with everolimus rapidly translatable.

Despite adhesion signalling being prominent in everolimus resistant cells, the exact surface factors involved is yet to be determined. The efficacy of combining of FAK inhibitors with everolimus in other cell models highlights the potential for their combination to overcome resistance to everolimus in ALL and offers an attractive target for future investigation.

CHAPTER 4 PROTEOMIC ANALYSIS OF EVEROLIMUS RESISTANT ALL XENOGRAFTS

4.1 INTRODUCTION

Early work on resistance to mTOR inhibition by rapamycin indicated that resistance can be conferred by deregulation of several proteins in the mTOR pathway. Alterations in the expression and/or function of proteins upstream of mTOR, such as FKBP12 [138, 139], or the downstream targets of mTOR, S6K1 [146, 208]) and 4EBP1 [157], facilitated resistance through various mechanisms. However, a common mechanism behind resistance to everolimus among these cell models could not be identified, suggesting multiple factors outside of the Akt/mTOR signalling pathway may be involved in the development of resistance to mTOR inhibitors.

While sequencing the genome and/or transcriptome of malignant cells gives insight into the genetic basis of cancer, it may not correlate to the functional proteome of the cell. Complex protein-protein interactions and post-translational modifications make it difficult to correlate the changes at the nucleotide level to the effects seen in disease states [209-211]. Recent advances in proteomic technology have improved the ability to accurately identify and quantify protein expression. Mass spectrometry is a highly sensitive proteomic technique and its use may have implications for the clinical management of malignancies by improving classification and stratification, the discovery of biomarkers and characterisation of resistance to chemotherapy [212-215].

This chapter aimed to correlate everolimus resistance development in ALL with previously identified mechanisms of resistance from prior investigations in other cancer cell models. The proteome of everolimus resistant xenografts was compared

to that of sensitive ALL xenografts in order to characterise the changes associated with the development of resistance and identify possible drivers of resistance to everolimus.

4.2 METHODS

4.2.1 2 Dimensional - Difference In Gel Electrophoresis (2D-DIGE)

Protein from the spleens of mice bearing sensitive and resistant xenografts were purified using the 2D-Clean-up kit and then quantified using the 2-D Quant kit. Fifty micrograms of protein from sensitive and resistance cells were fluorescently labelled with the 3Dye 2D DIGE labelling Kit, alternating Cy3 and Cy5 dyes between samples to eliminate label bias from analysis. An internal standard was created by labelling a pool of 25 μg of each sample with Cy2. Proteins were labelled with 400 pmol/μl of each respective dye for 30 min on ice, in the dark, after which the reaction was quenched with 10 mM lysine on ice for 30 min, in the dark. Proteins labelled with Cy2, Cy3 and Cy5 were combined into a single tube and proteins were reduced with 40 mM DTT at RT for 20 min, then alkylated with 80 mM iodoacetimide at RT for 20 min. Immobilized pH gradient (IPG) buffer pH 3-10 was added to samples (final concentration (f.c.) 0.5% v/v) before passively rehydrating 17cm, pH 3-10 IPG strips. Isoelectric focusing was carried out using Ettan IPGphor II (GE Healthcare) using the protocol in Table 4.1.

Table 4.1. 2D-DIGE isoelectric focusing profile

Voltage (V)	Type	Time
400	Gradient	1 min
400	Step	5 h
8000	Gradient	3 h
8000	Step	11 h
400	Gradient	2 h
400	Step	14 h (hold overnight

IPG strips were prepared for second dimension SDS-PAGE by equilibrating strips with 40 mM DTT in equilibration buffer (50 μM Tris-HCl (pH 8.8), 6 M urea, 30% (v/v) glycerol, 2% (v/v) SDS and 0.5% (v/v) bromophenol blue) for 20 min with gentle rocking followed by 80 mM iodoacetimide in equilibration buffer for 20 min with gentle rocking. Strips were then loaded onto a 20 x 20 cm, 8-16% gradient, bis-TRIS polyacrylamide gel between low fluorescent glass plates and proteins separated using the protocol in Table 4.2.

Table 4.2. SDS-PAGE profile for second dimension separation of 2D-DIGE.

Current (mAmp/gel)	Time
16	1.25 h
20	1.5 h
24	4 h (or until the dye front reached the end of the gel)

To visualize and quantify fluorescent protein spots, gels were scanned while between the low flouorescent glass plates using the Typhoon Trio variable mode imager (GE Life sciences) and analyzed with DeCyder software (GE life sciences). Gels were removed from glass plates and fixed for 1 h in a solution of 10% (v/v) methanol and 7% (v/v) acetic acid, and stained with a modified colloidal Coomassie blue protocol “blue silver” (0.12% (w/v) Coomassie G-250, 10% (v/v) ammonium sulfate, 10% (v/v) phosphoric acid, and 20% (v/v) methanol) [216] to visualize protein spots. Proteins that were significantly different in fluorescent images were identified on the Coomassie stained gels and excised for identification by MALDI MS/MS.

Gel pieces were de-stained in a 25% (v/v) acetonitrile (ACN) in 50 mM ammonium bicarbonate then dehydrated by washing twice with 100% ACN. Gel pieces were dried by vacuum centrifugation and in gel digestion of proteins performed by rehydrating gel pieces with 12 ng/μl of Trypsin Gold in 50 mM ammonium bicarbonate and incubating at 4°C for 1 h. Excess trypsin was removed and 20 μl of fresh 50 mM ammonium bicarbonate added for overnight incubation at 37°C. Peptides were extracted by adding 0.5% (v/v) TFA in 10% (v/v) ACN and incubating for 15 min in a water bath ultrasonicator (Ultrasonics Australia). The supernatant was collected, vacuum centrifuged and reconstituted in 0.5% (v/v) TFA. Samples were combined at a ratio of 1:1 with 5 μg/ml of a matrix (α-cyano-4-hydroxycinnamic acid) in 0.5% TFA (v/v) in 70% (v/v) ACN, spotted onto a MALDI sample plate and run on the SCIEX TOF/TOF 5800 MALDI (SCIEX, Massachusetts, USA). Spectra were analyzed with ProteinPilot software using the mascot method and interrogated against the UNIPROT database.

4.2.2 Dimethyl Labelling

Two hundred micrograms of protein was isolated from matched sensitive and resistant xenografts with lysis buffer containing 10 mM TRIS-HCl, 150 mM sodium chloride and 1% (v/v) Triton X-100 for half an hour at 4°C. Lysates were clarified by centrifugation at 12000 x *g* for 10 min at 4°C, supernatant collected and urea added to a f.c. of 6 M. Protein was reduced with DTT (f.c. 9.5 mM) in 100 mM ammonium bicarbonate for 30 min and alkylated with iodoacetemide (f.c. 32 mM) in 100 mM ammonium bicarbonate for 30 min. The urea concentration was reduced to 2 M with 50 mM ammonium bicarbonate and protein digested with Tryspin Gold (promega) at a trypsin to protein ratio of 1:25 overnight at 37°C. A second digestion was performed by adding additional trypsin at a ratio of 1:25 and incubating for a further 2 h at 37°C.

The trypsinised protein mixture was acidified with formic acid (FA) at f.c. of 1% (v/v) and peptides were purified with a C18 reverse phase cartridge. Cartridges were activated with 0.5% (v/v) FA in 70% (v/v) ACN before use. Samples were loaded onto the column and washed twice with 0.5% (v/v) FA. Peptides were first eluted with 0.5% (v/v) FA and 70% (v/v) ACN, followed by a second elution with 0.5% (v/v) FA and 90% (v/v) ACN. Samples were dried by vacuum centrifuge and re-suspended in 1 M triethylammoniumbicarbonate (TEAB) buffer, then diluted to 170 mM with MilliQ water and dimethyl labelling was carried out, as described by Boersema et al [217] (Figure 4.1), to add light and heavy methyl groups to the primary amines of peptides.

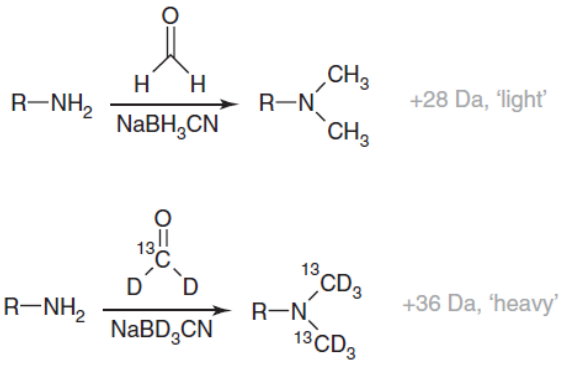

Figure 4.1. Labelling schema of triplex dimethyl labelling of primary amines (adapted from Boresema et al [217])

Briefly, 5 μL of a 10% (v/v) solution of formaldehyde (light) or ^{13}C formaldehyde in deuterated water (heavy) was added to samples and incubated by shaking at RT for 10 min. One molar cyanoborohydride (light) and cyanoborodeuteride (heavy) was added to appropriate tubes and incubated by shaking at RT for 20 min. The reaction was quenched by adding 25% (v/v) ammonium hydroxide and acidified with FA (f.c. 2%). Samples were pooled, dried by vacuum centrifugation and resuspended 10 mM KH_2PO_4 in 25% ACN at a pH of 3.

To remove contaminating Triton-X100, samples were loaded peptides onto POROS20 strong cation exchange (SCX) resin that had non-specific binding sites blocked with 10 μg of BSA. Columns were washed 4 times with 10 mM KH_2PO_4 in 25% ACN at pH3 then peptides eluted with 500 mM KCl in 10 mM KH_2PO_4 in 25% ACN at pH3. Supelco C18 reverse phase columns were activated with 70% ACN in 0.5% FA then washed with 0.5% FA. Samples were then bound to the column and washed three with 0.5% FA to remove salts added to samples by the SCX procedure. Peptides were firstly eluted with 0.5% (v/v) FA in 70% (v/v) ACN and any residual peptide eluted with 0.5% (v/v) FA in 90% ACN. Samples were dried by vacuum centrifugation and re-suspended in 0.1% (v/v) FA.

Samples were loaded into the SCIEX TripleTOF 5600 using a 40 cm column, packed with 100 nm Reprosil-Pur 120 C18 AQ resin and run for 240 min at a flow rate of 350 nl/min with the gradient in Table 4.3.

Table 4.3. LC-MS/MS gradient profile

Time	% Formic Acid	% ACN
0	98	2
3	98	2
15	88	12
180	70	30
215	40	60
225	5	95
230	5	95
235	98	2
240	98	2

Spectra were analysed and quantified with ProteinPilot using the paragon method.

4.2.3 Statistics

SPSS was used to calculate the T-statistic using the formula:

averageLogFoldChange / (standard deviation LogFold Change / (square root(N))).

A one sample t-test was then used to calculate the significant protein fold change in SPSS with n-1 degrees of freedom using the formula: 2*(1-CDF.T(Abs(T),N-1)).

4.3 RESULTS

4.3.1 Expression and activation of Akt in everolimus resistant xenografts

Aberrant Akt activity can confer resistance to mTOR inhibitors such as rapamycin and everolimus [160]. Akt is activated by a number or phosphorylation events, most importantly on Thr308 and Ser473. Phosphorylation of Akt on Thr308 activates the kinase and is the main regulator of the activity of Akt [218], whereas phosphorylation of Ser473 is a marker of the activation of a negative feedback loop involving mTORC2 [219, 220].

The two everolimus resistant xenografts had different expression and phosphorylation profiles of Akt. Where 1345-R had unaltered Akt expression compared to 1345-S, the expression of Akt was increased in xenograft 2055-R (Figure 4.2 C, G). The phosphorylation on Thr308 was not affected by the development of resistance to everolimus in either xenograft, however, the increase in basal Akt in 2055-R led to a decrease in the ratio of phosphorylated to total Akt in resistant cells (Figure 4.2 H). As with the sensitive parental xenografts, administration of everolimus for 24 h decreased the phosphorylation on Thr308, however, the decrease was only statistically significant in 2055-S cells when compared to actin (Figure 4.2 B and F) and 1345-S cells when the ratio of phosphorylated to total Akt was considered (Figure 4.2 D and H).

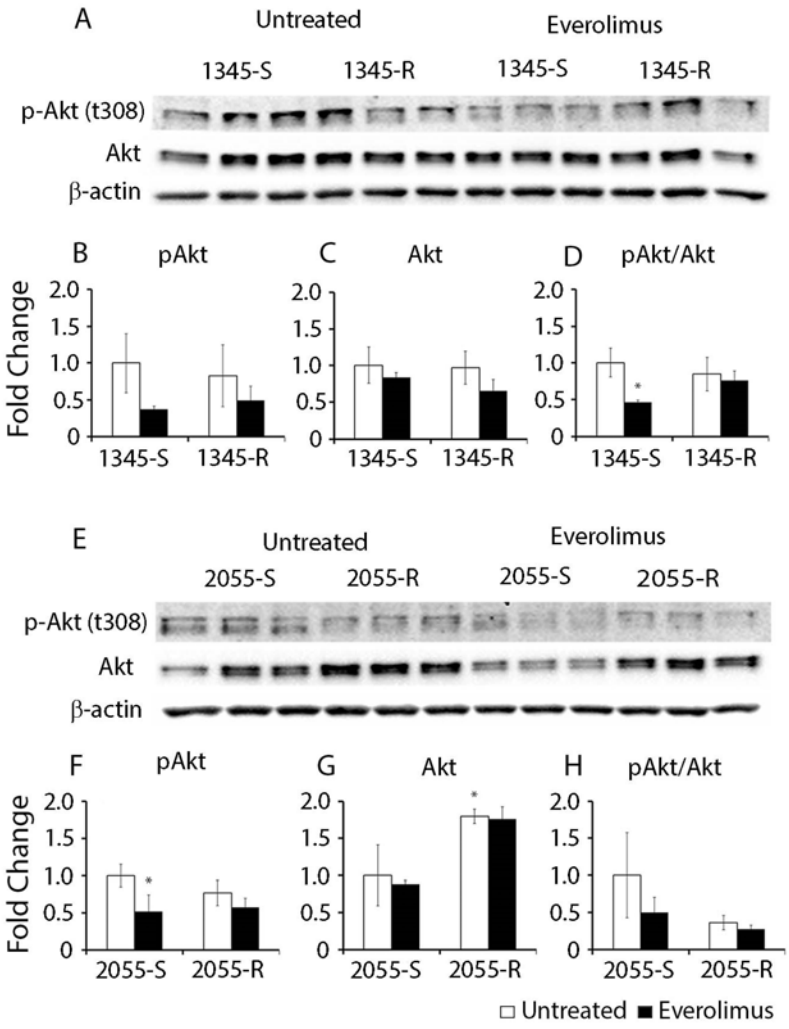

Figure 4.2 Expression of Akt and phosphorylation of Thr308 in everolimus sensitive and resistant ALL cells, with and without everolimus treatment. Protein isolated from resistant xenografts and matched sensitive controls 1345-R and 1345-S (A), 2055-S and 2055-R (E), with and without treatment with everolimus. Blots were probed with antibodies against phosphorylated Akt on Thr308 and total Akt, with β-actin used as a loading control. Band intensity was used to quantify the total amount of phosphorylated Akt on Thr308 (B, F), total Akt (C, G) and ratio of phosphorylated Akt to total protein (D, H). Lysates were run in biological triplicates using students 2 tailed unpaired t-test comparing against untreated sensitive cells (* $p < 0.05$) and untreated resistant cells (# $p < 0.05$).

The phosphorylation of Akt on Ser473 was increased in the sensitive xenografts 1345-S and 2055-S following everolimus treatment (Figure 4.3 B, F), although statistical significance was not achieved. This signifies the possible activation of the negative feedback loop in both of the sensitive xenografts upon mTORC1 inhibition by everolimus. Phosphorylation of Akt on Ser473 was higher in 1345-R cells (Figure 4.3 C) but not 2055-R (Figure 4.3 G) as compared to respective sensitive cells. The resistant xenografts respond to everolimus differently to their respective parental xenografts, in that the increase in phosphorylation on Ser473 was no longer apparent. As with phosphorylation of Thr308, the increased basal Akt levels in 2055-R led to a decrease in the relative proportion of phosphorylated protein (Figure 4.3 H).

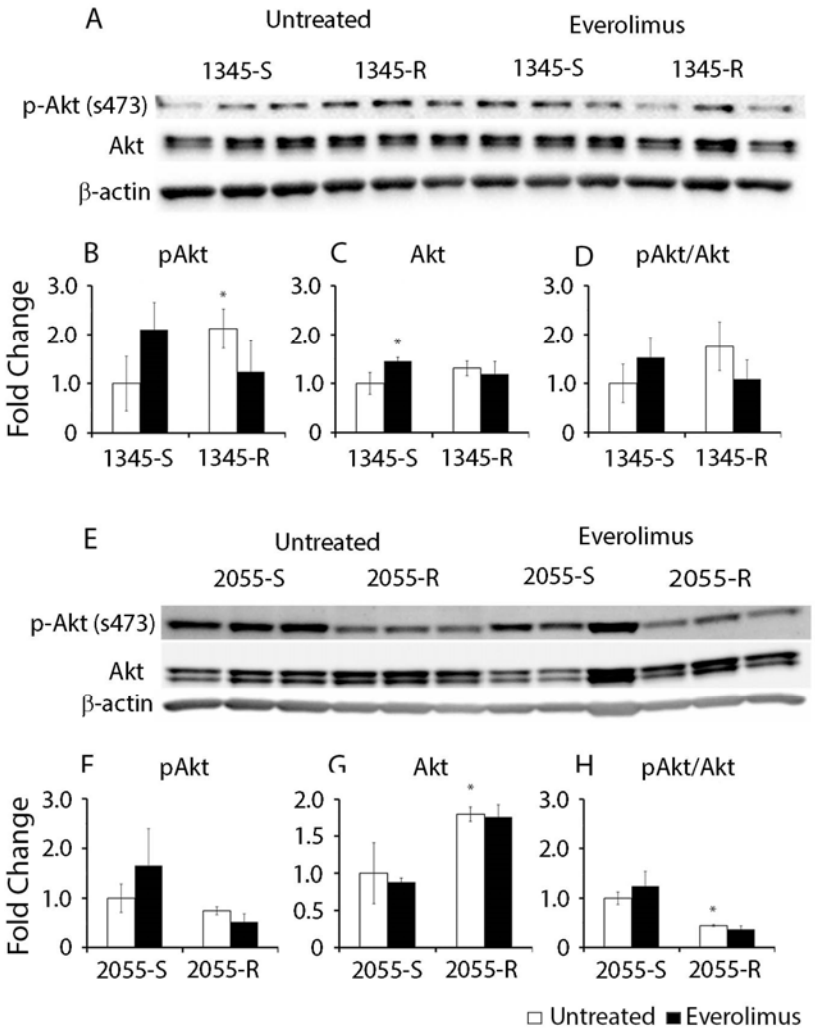

Figure 4.3 Expression of Akt and phosphorylation of Ser473 in everolimus sensitive and resistant ALL cells with and without everolimus treatment. Protein isolated from resistant xenografts and matched sensitive controls 1345-R and 1345-S (A), 2055-S and 2055-R (E), with and without treatment with everolimus. Blots were probed with antibodies against phosphorylated Akt on Ser473 and total Akt, with β-actin used as a loading control. Band intensity was used to quantify the total amount of phosphorylated Akt on Ser473 (B, F), total Akt (C, G) and ratio of phosphorylated Akt to total protein (D, H). Lysates were run in biological triplicates using students 2 tailed unpaired t-test comparing against untreated sensitive cells (* $p < 0.05$) and untreated resistant cells (# $p < 0.05$).

4.3.2 Expression and activation of the downstream targets of mTOR in everolimus resistant xenografts

Previous studies have implicated deregulation of the downstream effectors of mTOR such as S6K1 and 4EBP1 in the development of resistance to mTOR inhibitors. Unfortunately, it was not possible to accurately detect the expression or phosphorylation of S6K1 due to lack of specificity of commercially available antibodies, therefore we examined its downstream effector, S6 ribosomal protein (S6RP), as a marker of its activity.

The phosphorylation of S6RP on Ser235/236 was reduced in both parental 1345-S and 2055-S xenografts following everolimus administration (Figure 4.4 B, F), indicating successful inhibition of mTOR activity. However, resistance to everolimus elicited conflicting responses from the two resistant xenografts. While the total amount of S6RP was not altered in the resistant 1345-R cells compared to their sensitive parental controls (Figure 4.4 C), the amount of phosphorylation on Ser235/236 and the ratio of phosphorylated protein were significantly reduced (Figure 4.4 B and D). In contrast, the total amount of S6RP was significantly reduced in xenograft 2055-R (Figure 4.4 G), whereas, phosphorylation of Ser235/236 was significantly increased in resistant cells (Figure 4.4 F). This resulted in a 60 fold increase in the ratio of phosphorylated protein in 2055-R cells (Figure 4.4 H). Unlike the everolimus sensitive xenografts, the expression and phosphorylation of S6RP in both 1345-R and 2055-R was unaffected by treatment with everolimus (Figure 4.4 B-D, F-H).

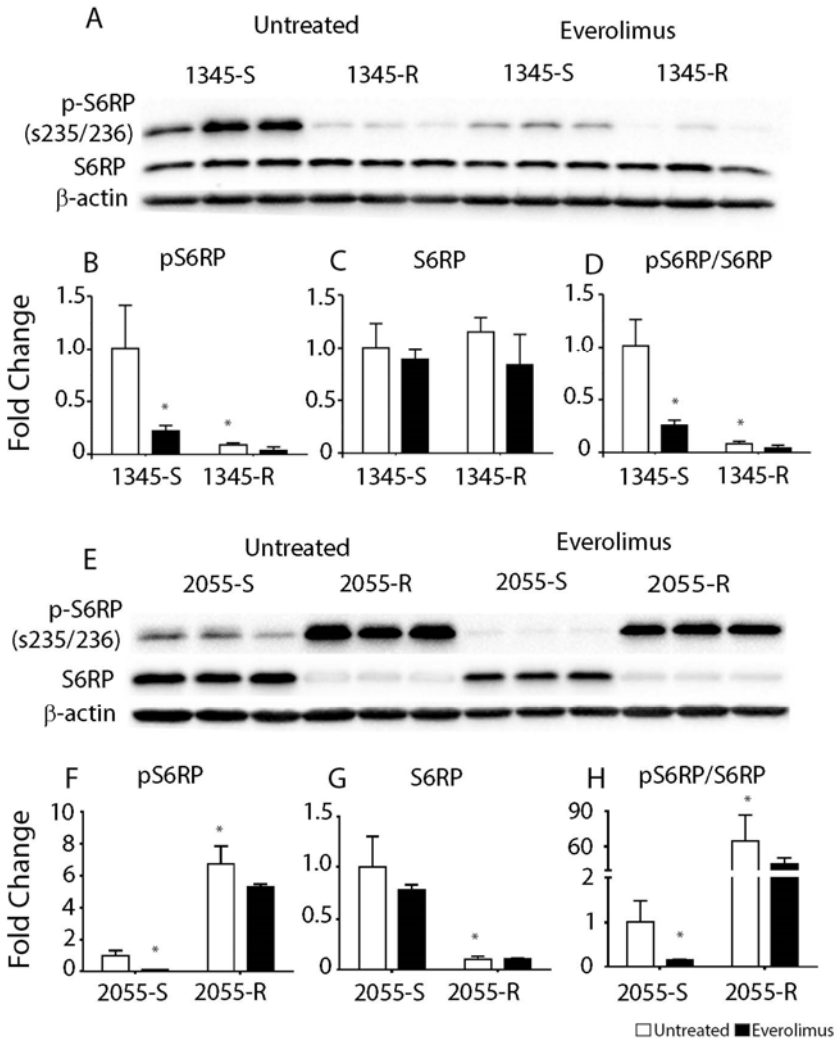

Figure 4.4 Expression of S6RP and phosphorylation of Ser235/236 in everolimus sensitive and resistant ALL cells with and without everolimus treatment. Protein isolated from resistant xenografts and matched sensitive controls 1345-R and 1345-S (A), 2055-S and 2055-R (E), with and without treatment with everolimus. Blots were probed with antibodies against phosphorylated S6RP on Ser235/236 and total S6RP, with β-actin used as a loading control. Band intensity was used to quantify the total amount of phosphorylated S6RP on Ser235/236 (B, F), total S6RP (C, G) and ratio of phosphorylated S6RP to total protein (D, H). Lysates were run in biological triplicates using students 2 tailed unpaired t-test comparing against untreated sensitive cells (* $p < 0.05$) and untreated resistant cells (# $p < 0.05$).

The expression of 4EBP1 was significantly reduced in 2055-S treated with everolimus (Figure 4.5 G) but was unaltered in 1345-S cells (Figure 4.5 C). Both everolimus resistant 1345-R and 2055-R xenografts had significantly increased expression of 4EBP1 (Figure 4.5 C, G). The sensitive xenografts failed to demonstrate any regulation of 4EBP1 phosphorylation following exposure to everolimus (Figure 4.5 B, F). While the resistant xenograft 1345-R behaved similarly to its sensitive counterpart (Figure 4.5 B), the phosphorylation of Ser37/46 was significantly reduced in 2055-R cells (Figure 4.5 F). Due to the increase in basal expression of 4EBP1 in everolimus resistant xenografts, the relative ratio of phosphorylated protein was reduced in both xenografts, although this only reached statistical significance in 2055-R (Figure 4.5 D, H).

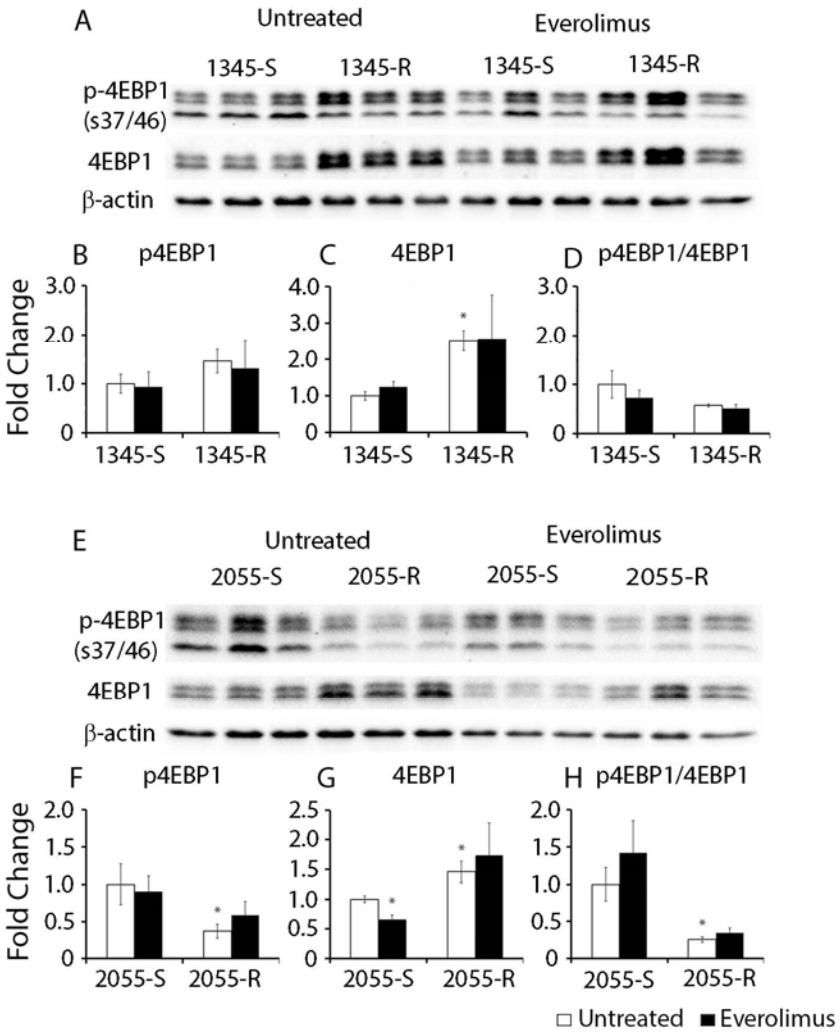

Figure 4.5 Expression of 4EBP1 and phosphorylation of Ser37/46 in everolimus sensitive and resistant ALL cells with and without everolimus treatment. Protein isolated from resistant xenografts and matched sensitive controls 1345-R and 1345-S (A), 2055-S and 2055-R (E), with and without treatment with everolimus. Blots were probed with antibodies against phosphorylated 4EBP1 on Ser37/46 and total 4EBP1, with β-actin used as a loading control. Band intensity was used to quantify the total amount of phosphorylated Akt on Ser37/46 (B, F), total Akt (C, G) and ratio of phosphorylated Akt to total protein (D, H). Lysates were run in biological triplicates using students 2 tailed unpaired t-test comparing against untreated sensitive cells (* $p < 0.05$) and untreated resistant cells (# $p < 0.05$).

4.3.3 Effects of resistance on the proteome of 1345 cells

Individual protein analysis by immunoblotting yielded inconsistent expression data between the two everolimus resistant xenografts. To gain a global understanding of the proteomic changes induced in the ALL xenografts by resistance to everolimus we undertook preliminary shotgun proteomic sequencing using 2D-DIGE. Fluorescent labels are used to directly correlate protein expression between 1345 and 1345-R relative to an internal standard, which comprised of an equal amount of protein from both xenografts (Figure 4.6). Samples were labelled with fluorescent dyes and proteins were separated in two dimensions to identify individual proteins (Figure 4.7).

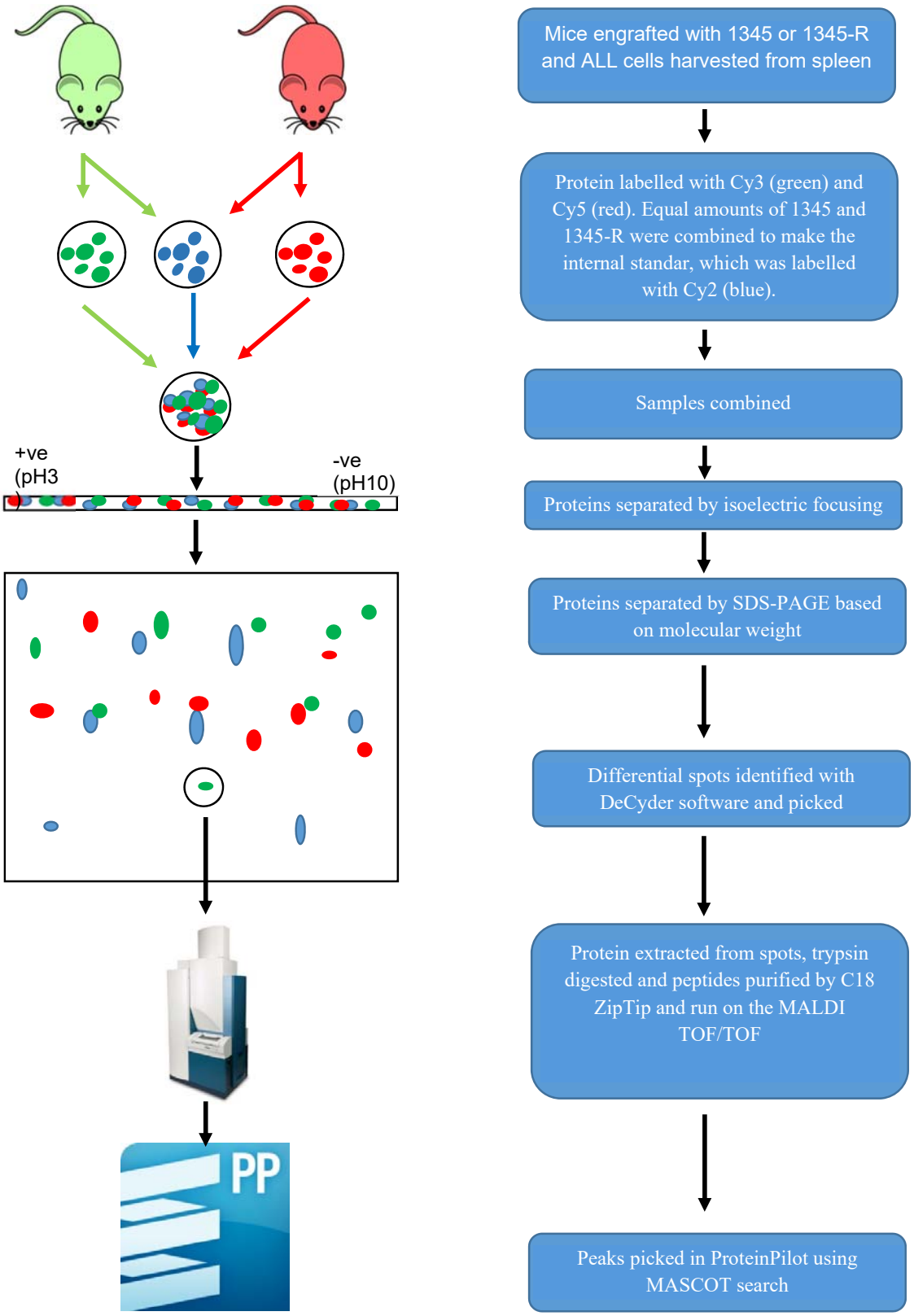

Figure 4.6 Work flow for the isolation and labelling schema for protein analysis for 2D-DIGE.

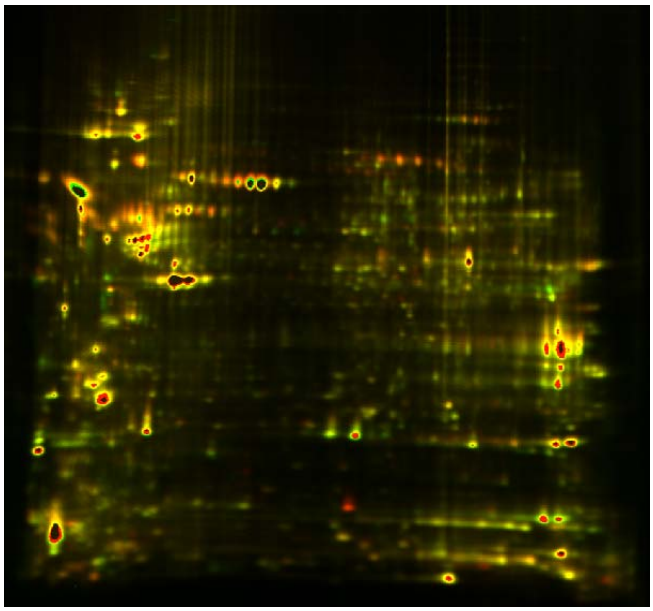

Figure 4.7 Representative 2D-DIGE image. Protein was first separated by isoelectric point on an 18 cm, non-linear, pH 3-10 isoelectric focusing strip. Separation on the second dimension was carried out on a 20 cm SDS-PAGE gel with a gradient of 8-16%. Shown here are protein isolated form 1345-R (green) v 1345 (red) relative to the fluorescence of the internal standard.

Proteins that were significantly regulated greater than 1.5 fold in either direction in resistant xenografts across 3 biological replicates were marked for identification by MALDI mass spectrometry. Forty six protein spots were significantly regulated in everolimus resistant xenograft 1345-R, and of those 11 proteins were successfully isolated and identified by MALDI (Table 4.4). To characterise the difference in response of the resistant and sensitive xenografts to everolimus, protein was extracted from the spleens of mice following 24 h treatment with the drug.

Table 4.4 Proteins identified by 2D-DIGE that are differentially regulated in 1345-R

Protein Name	Symbol	FC	P value	MW (kDa)	PI
Hemoglobin b	HBB	-2.65	0.0100	15.9	6.74
Hemoglobin alpha 2	HBA2	-2.62	0.0380	15.3	8.72
Hemoglobin alpha 1	HBA1	-2.62	0.0380	15.3	8.72
26S protease regulatory subunit 7	PRS7	-2.3	0.0200	48.6	5.71
Acidic leucine-rich nuclear phosphoprotein 23 family member E	AN32E	-2.07	0.0180	30.7	3.76
Tuberin-specific chaperone A	TBCA	-1.94	0.0240	12.85	5.25
PDZ and LIM domain protein 1	PDLIM1	-1.82	0.0200	36.1	6.56
serum albumin	ALBU	-1.61	0.0140	69.3	5.92
kininogen-1	KNG1	-1.53	0.0056	71.9	6.34
myotrophin	MTPN	1.53	0.0110	12.9	5.27
WD repeat-containing protein 1	WDR1	1.66	0.0140	50.7	6.04

FC – Fold change, MW – molecular weight, PI – isoelectric point.

Samples were again analysed by 2D-DIGE and 33 protein spots were differentially regulated between the two samples. Of these spots, we successfully identified 16 proteins with MALDI mass spectrometry (Table 4.5). Interestingly, 2D-DIGE identified 2 proteins with documented roles in cancer. The expression of the first, PDLIM1, was decreased in 1345-R cells and further decreased following everolimus treatment (Table 4.4 and 4.5) and while its function is not yet fully elucidated, it has been implicated in metastasis and disease progression [221]. The second protein identified was stathmin. (Table 4.5). Stathmin, which was upregulated in 1345-R cells, regulates important cell processes such as microtubule dynamics and the cell cycle [222, 223]. Stathmin is over expressed in many malignancies of different origins and may be involved in the development of resistance to chemotherapy by breast cancer cells and epithelial cancer cell lines [224, 225]. The effect of stathmin expression in resistance to everolimus in ALL is explored further in Chapter 5.

Table 4.5 Proteins identified by 2D-DIGE that are differentially regulated in 1345-R following everolimus treatment

Protein Name	Symbol	FC	P value	MW (kDa)	PI
heterogeneous nuclear ribonucleoprotein H	HNRNPH1	-1.98	0.029	49.2	5.89
isocitrate dehydrogenase 2	IDH2	-1.72	0.012	50.1	8.88
phosphoglycerate kinase 1	PGK1	-1.72	0.012	44.6	8.3
PDZ and LIM domain protein 1	PDLIM1	-1.71	0.019	36.1	6.56
high mobility group protein B2	HMGB2	-1.53	0.042	23.9	7.77
X-ray repair cross complementing protein 6	XRCC6	-1.38	0.038	69.8	6.23
Heat shock protein 60	HSP60	1.64	0.014	61	5.7
Moesin	MSN	1.71	0.0033	67.8	6.08
PRO2619 (serum albumin)	ALB	1.72	0.0034	69.3	5.92
annexin A2	ANXA2	1.73	0.067	38.6	7.57
Heat shock protein 10	HSP10	1.75	0.034	10.9	8.89
PRO2619 (serum albumin)	ALB	1.81	0.0084	69.3	5.92
truncated lactoferrin	LTF	2.04	0.011	78.2	8.5
elongation factor 2	EEF2	2.04	0.043	62.7	6.27
elongation factor 2	EEF2	2.07	0.016	62.7	6.27
stathmin	STMN	2.24	0.0019	17.32	5.75

FC – Fold change, MW – molecular weight, PI – isoelectric point.

4.3.4 LC-MSMS with dimethyl labelling

While 2D-DIGE technology successfully separated and quantified the proteomic changes in cells, it is limited by the need to visualise the spots by Coomassie blue staining. For this reason, we undertook a more sensitive whole cell lysate proteomic analysis by combining liquid chromatography with tandem mass spectrometry (LC-MS/MS). To quantify differences between everolimus resistant and sensitive ALL xenografts, we used an off-line labelling method to add methyl groups to lysine residues on peptide fragments [226] (Figure 4.8). LC-MS/MS successfully identified similar numbers of peptide spectra (Figure 4.9 A) and ProteinPilot matched those spectra to a similar number of proteins (Figure 4.9 B) in each comparison group. However, there was a large variation in the identified spectra between the biological replicates included in each sample group.

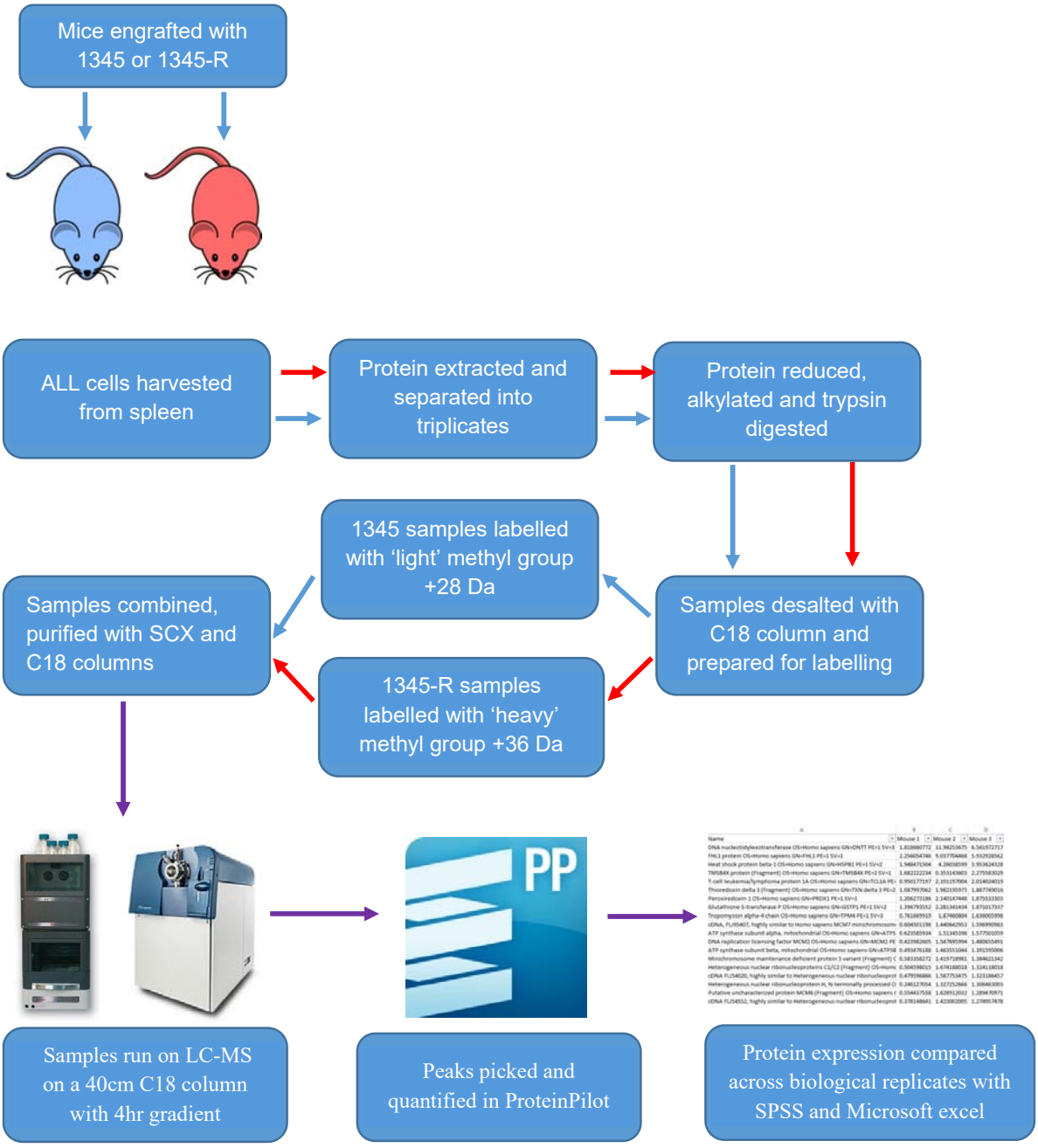

Figure 4.8 Work flow for the isolation and labelling schema for protein analysis by LC-MS/MS with dimethylation labelling.

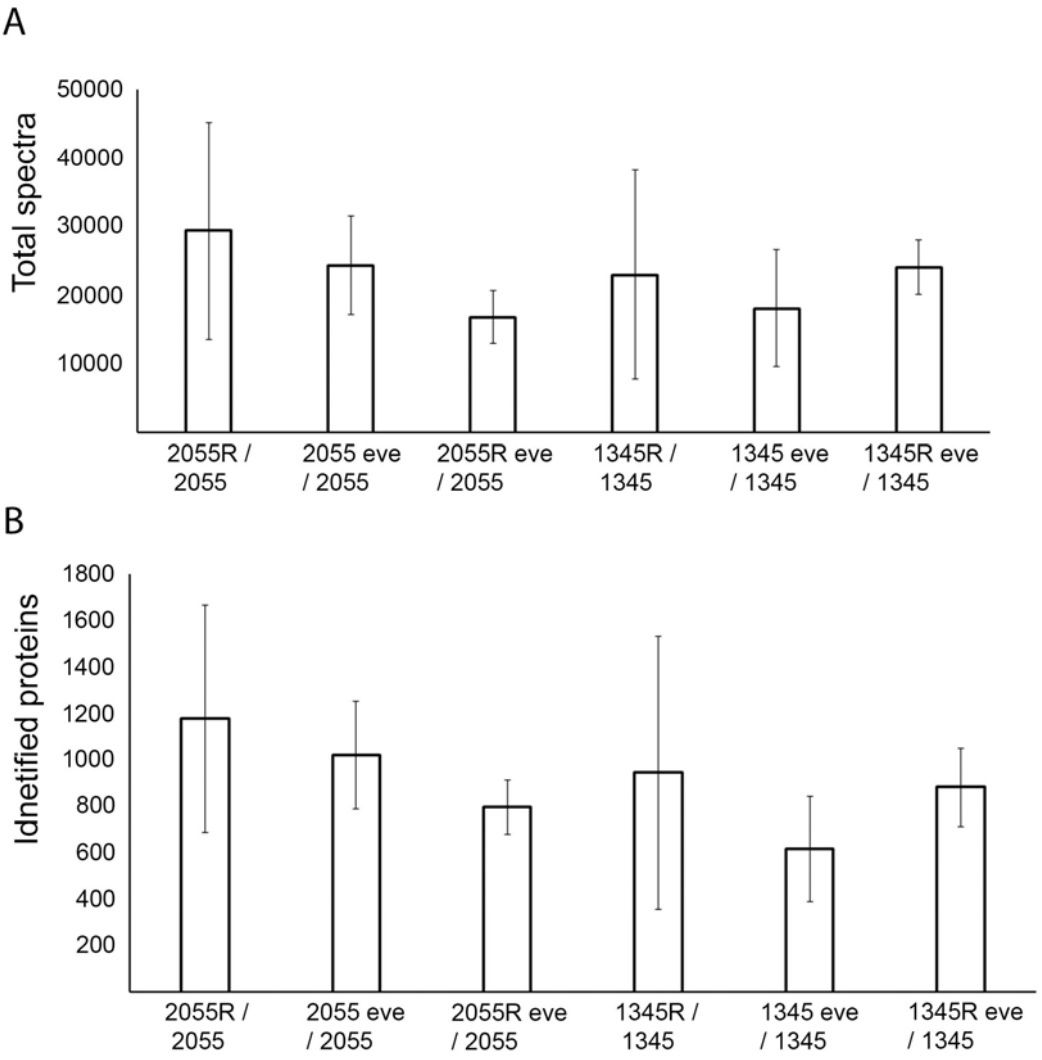

Figure 4.9 Summary of total spectra and identified proteins across all analysis groups. Data is shown as the average and standard deviation of technical and biological triplicates for both everolimus resistant xenografts with and without treatment.

Proteins differentially regulated in everolimus resistant ALL xenografts were identified by enumerating fold changes in proteins across biological replicates using the statistical program SPSS. The expression of proteins was averaged across all proteins identified in each technical replicate and Log2 transformed. The T-statistic was calculated on the Log2 transformed data and significantly altered proteins were determined with a one sample t-test, with N minus 1 degrees of freedom.

A large number of proteins were differentially expressed in xenograft 2055-R compared to the parental xenograft 2055-S. Three hundred and three proteins were significantly identified to be up or down regulated in at least one of the biological replicates. Of these proteins, 62 were significantly regulated with N-1 degrees of freedom (Figure 4.10). Pathway analysis with Metacore revealed 16 pathway maps (Table 4.6) and 4 process networks (Table 4.7) that were significantly enriched within the regulated proteins. In particular, pathways involved with DNA damage, protein translation and metabolic process were enriched in resistant cells.

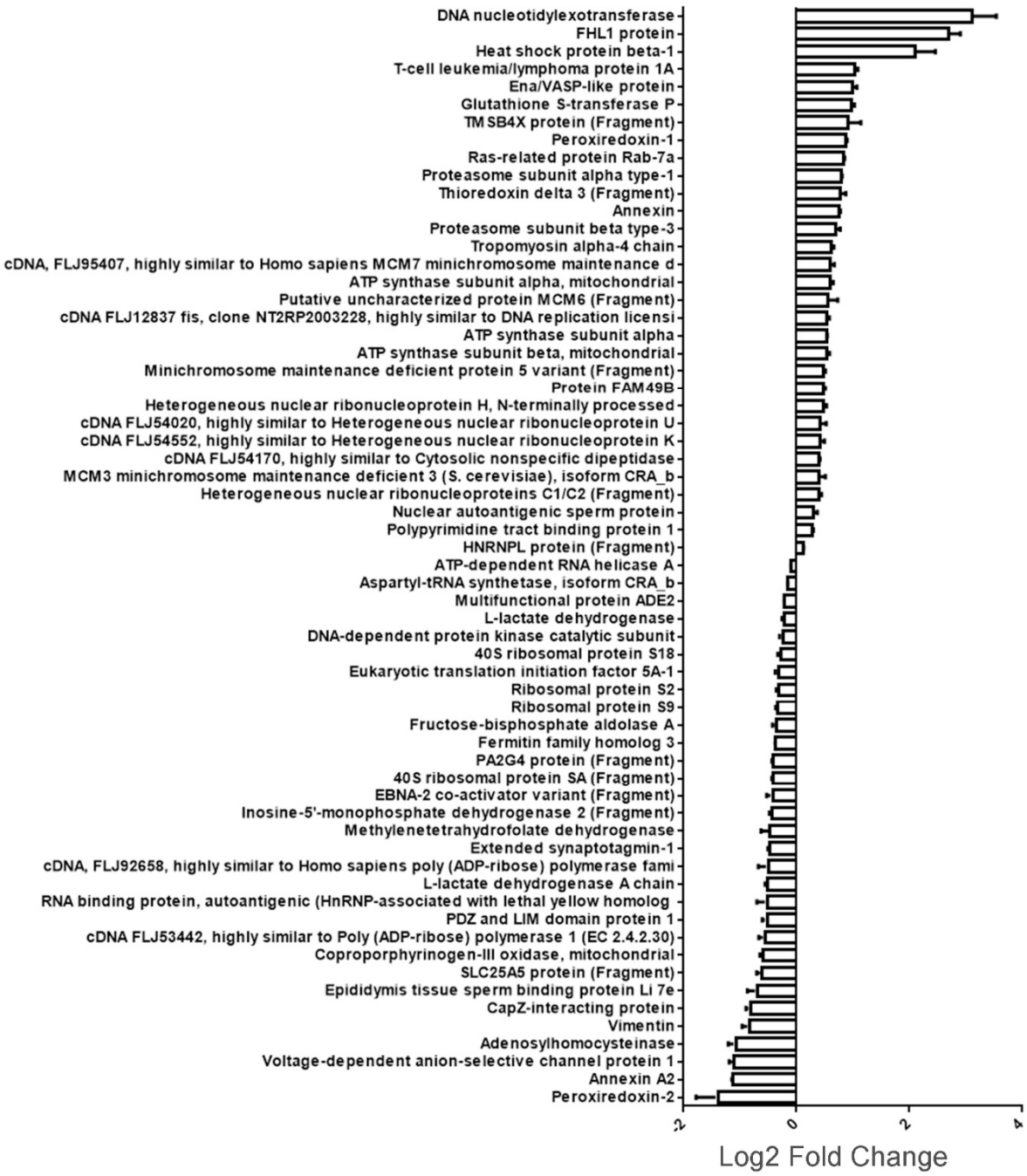

Figure 4.10 Proteins significantly differentially regulated in everolimus resistant ALL xenograft 2055-R. The log of the fold change was compared across biological replicates and significance calculated using the t-statistic and a one sided t-test with n-1 degrees of freedom.

Table 4.6 Metacore pathway maps significantly enriched in the proteome of the resistant xenograft 2055-R.

Maps	pValue	FDR
Neurophysiological process_Dynein-dynactin motor complex in axonal transport in neurons	4.764E-03	9.288E-02
L-Alanine, L-cysteine, and L-methionine metabolism	5.115E-03	9.288E-02
L-Alanine, L-Cysteine, and L-Methionine metabolism / Human version	5.477E-03	9.288E-02
Oxidative stress_Role of Sirtuin1 and PGC1-alpha in activation of antioxidant defense system	5.852E-03	9.288E-02
Transcription_Sirtuin6 regulation and functions	6.635E-03	9.288E-02
Aspartate and asparagine metabolism	8.560E-03	9.987E-02
Oxidative phosphorylation	1.715E-02	1.315E-01
DNA damage_DNA-damage-induced responses	1.728E-02	1.315E-01
Transport_Macropinocytosis	2.298E-02	1.315E-01
Apoptosis and survival_DNA-damage-induced apoptosis	2.864E-02	1.315E-01
wtCFTR and deltaF508 traffic / Late endosome and lysosome (normal and CF)	3.052E-02	1.315E-01
DNA damage_NHEJ mechanisms of DSBs repair	3.615E-02	1.315E-01
wtCFTR traffic / Sorting endosome formation (normal)	4.360E-02	1.315E-01
Glycolysis and gluconeogenesis p.3	4.545E-02	1.315E-01
Cytoskeleton remodeling_Neurofilaments	4.730E-02	1.315E-01
Cell adhesion_Endothelial cell contacts by junctional mechanisms	4.915E-02	1.315E-01

Table 4.7 Metacore networks maps significantly enriched in the transcriptome of the resistant xenograft 2055-R.

Networks	pValue	Min FDR
Response to hypoxia and oxidative stress	3.044E-03	5.083E-02
Translation_Translation initiation	3.619E-03	5.083E-02
Cytoskeleton_Actin filaments	4.013E-03	5.083E-02
Translation_Elongation-Termination	1.073E-02	1.019E-01

Large biological variation in comparing 1345-R to its parental xenograft, resulted in the reduction of the number of proteins significantly identified across the biological replicates. In total 146 proteins were identified and of those, only 3 were found to be significantly regulated (Figure 4.11).

Eleven proteins were regulated in both resistant xenografts if the lack of statistical significance was ignored for xenograft 1345 (Table 4.8). Six of those proteins were regulated in the same direction in both xenografts and of particular interest was the similar down regulation of the proteins PDLIM1 and vimentin.

Despite everolimus having known effects on protein expression, we were unable significantly detect any meaningful differences in the regulation of proteins in either xenograft, following acute everolimus exposure, irrespective of resistance status (Table 4.9).

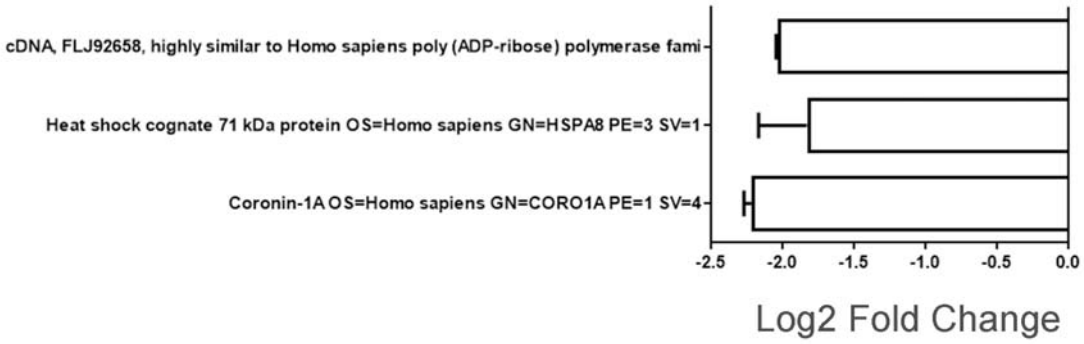

Figure 4.11 Proteins significantly differentially regulated in everolimus resistant ALL xenograft 1345-R. The log of the fold change was compared across biological replicates and significance calculated using the t-statistic and a one sided t-test with n-1 degrees of freedom.

Table 4.8 Proteins regulated in common between the everolimus resistant xenografts 1345-R and 2055-R.

Name	2055-R			1345-R		
	Avg log F.C.	Stdev log F.C.	Pval	Avg log F.C.	Stdev log F.C.	Pval
Actin related protein 2/3 complex, subunit 1B, 41kDa	0.303	0.079	0.116	-0.897	0.642	0.298
Annexin	-0.541	0.252	0.203	-0.680	0.729	0.413
cDNA, FLJ92658, highly similar to Homo sapiens poly (ADP-ribose) polymerase family, member 1 (PARP1), mRNA	-0.493	0.179	0.041	-2.018	0.026	0.006
EBNA-2 co-activator variant (Fragment)	-0.416	0.107	0.021	0.069	0.711	0.913
Epididymis tissue sperm binding protein Li 7e	-0.688	0.174	0.021	0.401	0.070	0.078
High mobility group protein B1	0.142	0.097	0.126	0.322	0.725	0.643
Histone cluster 1, H1e	-1.293	0.315	0.108	0.301	1.297	0.798
IQ motif containing GTPase activating protein 1	-0.228	0.052	0.102	-0.354	0.736	0.492
L-lactate dehydrogenase	-0.205	0.042	0.014	-0.125	0.450	0.762
PDZ and LIM domain protein 1	-0.514	0.085	0.009	-0.512	0.228	0.060
Vimentin	-0.825	0.132	0.008	-0.367	0.604	0.548

F.C. – fold change, Pval – p-value.

Table 4.9 Proteins regulated by treatment in everolimus sensitive and resistant ALL xenografts.

1345-S	Avg log F.C.	Stdev log F.C.	N	T	P
Nucleolin	0.23	0.76	2	0.42	0.75
Thymosin alpha-1	0.47	1.69	2	0.40	0.76
Aspartate--tRNA ligase, cytoplasmic	0.32	0.14	2	3.19	0.19

1345-R	Avg log F.C.	Stdev log F.C.	N	T	P
L-lactate dehydrogenase	0.552	0.258	2	3.03	0.20
Glyceraldehyde-3-phosphate dehydrogenase	-0.163	0.152	2	-1.51	0.37
Heterogeneous nuclear ribonucleoprotein AB isoform a variant (Fragment)	0.279	1.322	2	0.30	0.82
Cofilin-1	0.117	0.785	3	0.26	0.82
Voltage-dependent anion-selective channel protein 1	-0.114	0.745	2	-0.22	0.86

2055-S	Avg log F.C.	Stdev log F.C.	N	T	P
Voltage-dependent anion-selective channel protein 1	0.04	0.36	2	0.17	0.89
High mobility group protein B1	-0.18	0.41	2	-0.61	0.65
Ribosomal protein L4 variant (Fragment)	0.32	0.46	2	0.97	0.51

2055-R	Avg log F.C.	Stdev log F.C.	N	T	P
Ribosomal protein L5 variant (Fragment)	0.14	0.85	2	0.24	0.85
MYH9 variant protein	-0.23	0.11	2	-2.94	0.21
60S ribosomal protein L6	0.88	0.13	2	9.49	0.07

F.C. – fold change, N- number of samples, T – t-statistic, P – p-value.

4.4 DISCUSSION

There are many hypotheses as to the mechanism of resistance to mTOR inhibitors such as everolimus, though, most theories centre on the dysregulation of protein expression or function [143, 146, 157, 176, 177, 208, 219, 227]. Proteomics technology has improved immensely over the last decade and is capable of discovering novel cancer biomarkers [228-231], and identifying proteins involved in resistance to chemotherapeutic agents [209, 213, 232-236].

Several possible resistance mediators have been identified in other mammalian cell models. These include increased activity of Akt and S6K1 and downregulation of 4EBP1 [157, 220]. Inhibition of the mTORC1 complex by rapamycin and its analogues (rapalogs) is known to activate a negative feedback, driven by mTORC2 and S6K1 [220]. Phosphorylation of Akt on Ser473 is a marker of activation of this negative feedback loop which then leads to the activation of other cellular growth and survival pathways such as the MAPK pathway [219]. The negative feedback loop appeared to be activated by everolimus treatment of the sensitive ALL xenografts in this study. This response to everolimus was no longer apparent in the resistant xenografts, although 1345-R had increased basal phosphorylation of Ser473 suggesting this pathway is already activated in 1345-R cells. Interestingly 1345-R cells had activated Akt Ser473 in the absence of everolimus, suggesting that this may be the mechanism of resistance. However, treatment with everolimus reduced the phosphorylation of Akt on Ser473, questioning the role of the negative feedback loop in resistance to everolimus in this ALL sample. Further studies with additional xenografts would be required to clarify if the feedback loop is indeed involved in the development of resistance.

Dysregulation of the downstream mTOR substrates S6K1 and 4EBP1, may contribute to the resistance permitting downstream signalling irrespective of mTOR inhibition [157, 237]. Due to the relatively lack of specificity of commercially available antibodies against S6K1 and its phosphorylation sites, we used S6RP as a marker of its activity. Interestingly, there was a striking contrast in the regulation of S6RP between the two everolimus resistant xenografts. Moreover, contrary to reports that downregulation of 4EBP1 results in resistance to rapamycin [157], the expression of 4EBP1 was upregulated in both everolimus resistant ALL xenografts.

The discrepancy between previously published mechanisms of resistance to mTOR inhibitors [146, 157, 208] and the difference between the two xenografts, raises questions as to whether these proteins are involved in the development of resistance to everolimus and whether the effects observed in these xenografts are the cause or as a result of the development of resistance.

These discrepancies required a more global approach to understand how resistance developed in these cells. Analysing the proteome of everolimus resistant ALL xenografts identified 3 interesting targets, stathmin, vimentin and PDZ and LIM domain contain protein 1 (PDLIM1), that may contribute to the development of resistance to mTOR. Firstly, stathmin, an important regulator of microtubules and the cell cycle, is increased in many malignancies such as leukemia/lymphoma, breast cancer and prostate cancer [238-241]. Moreover, it has documented roles in the development of resistance to chemotherapy in *in vitro* models of breast cancer [224] and in cervical squamous cancer cells [209]. The expression of stathmin was increased in the everolimus resistant xenograft 1345-R and due to its effects on the cell cycle, may be involved in the increased disease progression of 1345-R *in vivo* (Figure 3.3). The

differences in cell cycle between the everolimus resistant xenografts and the impacts of stathmin on the cell cycle are examined in the next chapter.

The second protein identified by proteomic sequencing of resistant xenografts was vimentin. Vimentin is a major component of intermediate filaments and is involved in cell motility, the maintenance of cell shape and the formation of focal adhesions [242, 243]. Vimentin is over-expressed in various malignancies such as prostate cancer, gastrointestinal tumours, CNS tumours, breast cancer, malignant melanoma, lung cancer and correlates to increased tumour growth, metastasis and a poor prognosis [244-246]. The development of resistance to doxorubicin in breast cancer cells [245], resistance to the CHOP chemotherapy regimen in diffuse large B-cell lymphoma [247] and cisplatin resistance in ovarian cancer [248] and lung adenocarcinoma [249] have all been attributed to an increase in the expression of vimentin. However, as the expression of vimentin is decreased in our resistant xenografts, the role vimentin plays in resistance to everolimus in ALL remains unclear.

Finally, PDLIM1 was downregulated in everolimus resistant xenografts and was reproducibly identified with both 2D-DIGE and LC-MS/MS. The exact function of PDLIM1 remains uncertain, but it appears to be involved in formation of stress fibres, focal adhesions and the recruitment of proteins to the cytoskeleton through the association with cytoskeletal proteins such as alpha actinin and E-cadherin [221, 250-252]. Recently, PDLIM1 has been associated with the cancer metastases and disease progression, however, there are conflicting reports as to how PDLIM1 functions in malignant cells. One report states that PDLIM1 is downregulated in highly metastatic colorectal cancer, liver metastases and is a marker of a more aggressive disease [221]. Moreover, PDLIM1 is able to stabilize the E-cadherin and β-catenin complex and loss of PDLIM1 promotes the expression of markers of epithelial-mesenchymal

transition [221]. In contrast, another study suggests that overexpression of PDLIM1 in breast cancer is correlated to the progression of the disease [253]. PDLIM1 was consistently downregulated in everolimus resistant xenografts across multiple techniques and in two separate ALL xenografts. This strongly supports a role for PDLIM1 in everolimus resistance, however, as the role of this protein is still being investigated, how the effects are elicited remains to be determined.

Despite all the promising advances in the field of proteomics, many obstacles remain before it becomes routine in the clinic [228, 254, 255]. Two shotgun based proteomic techniques were utilized in this study and each came with their own inherent strengths and weaknesses. 2D-DIGE allows the separation of individual proteins on 2 dimensions, allowing for highly sensitive protein separation and quantification. However, only relatively small amounts of protein are able to be loaded on the first dimension, and there is an under-representation of highly hydrophobic proteins [256, 257]. Moreover, identification of the individual protein spots requires visualisation by Coomassie blue staining, thus lowly expressed proteins are often not identified with mass spectrometry. Therefore, only a small proportion of differentially expressed proteins found by the fluorescent Cy dyes were able to be correlated to spots visualised by Coomassie staining.

The second technique employed in this study separated proteins based on their hydrophobicity using high performance liquid chromatography (HPLC) coupled with tandem mass spectrometry (LC-MC/MS). LC-MS/MS is more sensitive than 2D-DIGE and is able to detect lowly abundant peptides and therefore, overcome some of the limitations associated with the gel based technique [258]. Yet, many factors such as the complexity of the lysate, tryptic digestion and under-sampling of data, limit the reproducibility between mass spectrometry runs [259, 260]. Multiple sample runs may

increase the number of peptides sampled by the mass spectrometer, although, abundant proteins tend to be analysed repeatedly thus decreasing the chance of identifying lowly abundant proteins [259].

ALL resistant xenografts were prepared in technical triplicate and biological triplicate to reduce the pitfalls of LC-MS/MS and to maximise the number and confidence of protein identification. While a similar number of peptides were identified in all samples, there was a large variation between technical replicates. Traditional cell lysis buffers containing urea resulted in a gelatinous lysate, most likely as a result of high nuclear content of ALL cells causing extraneous DNA to aggregate in the tube. To overcome this, samples were first lysed with a buffer containing Triton X-100, prior to the addition of the urea, which eliminated the problem with lysate preparation. To remove the contaminating Triton X-100, peptides were purified with strong anion exchange prior to samples being run on the mass spectrometer. Label based proteomics requires additional cleaning steps compared to non-label based proteomics prior to running samples on the mass spectrometer. The addition of extra purification measures to remove the contaminating TritonX-100, may have resulted in the loss of peptides and impacted on the identification of proteins.

Labelling of lysine residue with methyl groups allows for samples to be run concurrently and changes in protein expression may be directly quantified between samples, though correlation between replicates remained troublesome. One possible mechanism to reduce variability across replicates is to use a similar normalisation procedure as used in SILAC experiments, termed SUPER-SILAC. This involves adding an internal standard with a third label to samples to improve protein detection and quantification [261-263].

This study attempted to correlate changes in the expression of proteins to resistance to everolimus in ALL xenografts. Although some potential factors involved in the development of resistance to everolimus were identified, post-translational modifications such as phosphorylation, can have profound effects on protein function and add another layer of complexity in characterising the roles of proteins in resistance to everolimus. Higher level bioinformatics analysis, further refinement of experimental procedures, analysis of post-translation modification and increased number of samples may improve the identification and quantification of proteins involved in the development of everolimus resistance in ALL.

CHAPTER 5 *IN VIVO* CELL CYCLE ANALYSIS OF EVEROLIMUS RESISTANT ALL XENOGRAFTS

5.1 INTRODUCTION

The engraftment kinetics of the everolimus resistant ALL xenografts 1345-R and 2055-R, was similar to the respective sensitive parental cells, with leukemia detected in peripheral blood and treatment commenced in all groups simultaneously. However, once leukemia was established, the leukaemic burden increased at a vastly different rate both in respect to the parental cells and between the two resistant xenografts. Moreover, the response of the xenografts to everolimus administration differed greatly between the two resistant xenografts (Chapter 3.3.4). The difference between the cell growth of the resistant xenografts (2055-R and 1345-R) and their sensitive counterparts may be due to changes in cell cycle regulation resulting from the development of resistance.

Primary patient ALL cells are notoriously difficult to culture and require the presence of a supportive stromal layer to survive *in vitro* [104, 264]. However, both the sensitive and resistant xenografts analysed in this study could not be cultured *in vitro* despite the presence of the human bone marrow stroma (data not shown). For this reason the cell cycle status of everolimus resistant and sensitive ALL xenografts was analysed *in vivo* by using the thymidine analogue, 5-bromo-2'-deoxyuridine (BrdU). BrdU is incorporated into cycling cells during S phase and short term administration can be used to determine the cell cycle status when coupled with the DNA marker 7AAD using flow cytometry [129, 265, 266].

Initial proteomic investigations demonstrated that the microtubule regulating protein stathmin was increased in everolimus resistant 1345-R cells. Stathmin expression is

increased in many malignancies such as leukemia/lymphoma, breast cancer and prostate cancer, and is correlated to a metastatic phenotype [238-241]. Stathmin has microtubule destabilizing activity mediated by binding and sequestering alpha/beta-tubulin heterodimers [223, 267]. The activity of stathmin is regulated by a series of phosphorylation events [268] that occur progressively as cells transition through the cell cycle [223]. These specific inhibitory phosphorylation events are required for the disassembly of mitotic spindle and appropriate exit from mitosis (Figure 5.1) [269]. Stathmin expression is higher in actively proliferating cells, such as hematopoietic progenitors and malignant cells [270]. Stathmin expression is upregulated in many malignancies and is correlated to resistance to chemotherapy [225, 271]. Phosphorylation of Ser25, mediated by MAPK, and Ser38, carried out by the cyclin dependent kinases CDK1 and CDK2 [223] does not completely inhibit stathmin activity, instead appearing to be pre-requisite sites for further phosphorylation on Ser16 and Ser63 [272]. Phosphorylation at Ser16, mediated by Ca2+/calmodulin-dependent kinase IV (CaMK IV) and Ser63 by PKA [223] elicit the most potent effects on stathmin, with phosphorylation of these sites completely abolishing tubulin binding [268].

This chapter aims to determine the cell cycle status of everolimus resistant ALL xenografts and the effects of everolimus on the cell cycle kinetics. It also examines the expression and phosphorylation status of proteins involved in the cell cycle and correlates these with cell cycle distribution.

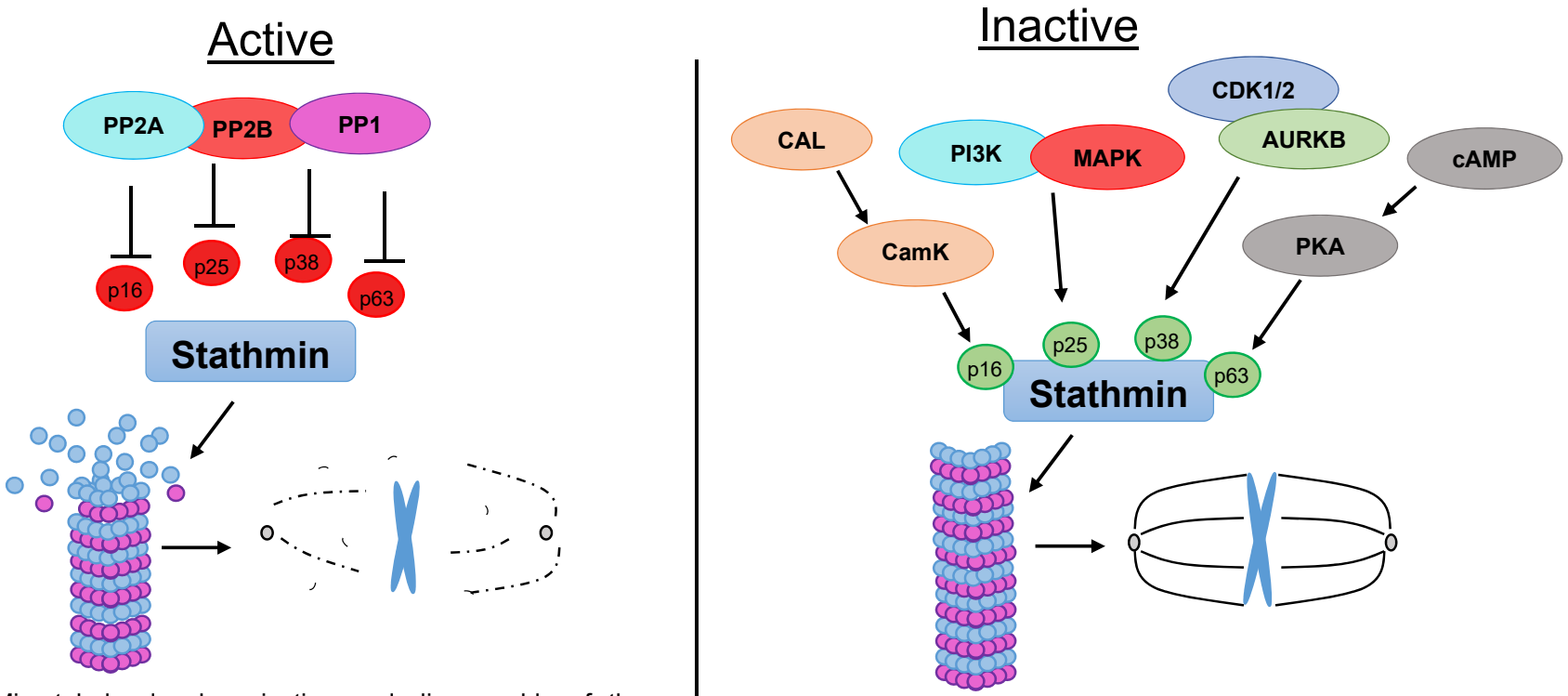

Microtubule depolymerisation and disassembly of the mitotic spindle

Microtubule polymerisation and assembly of the mitotic spindle

Figure 5.1 Stathmin signalling. Stathmin may be phosphorylated and inactivated on Ser sites by calmodulin (CALM) and Ca2+/calmodulin kinases, phosphoinositide 3-kinase (PI3K), mitogen-activated protein kinases (MAPKs)), cyclin-dependent kinases (CDKs), aurora kinase B (AURKB), protein kinase A (PKA) , leading to the stability of the microtubule and the formation of the mitotic spindle. On the other hand, Stathmin 1 may be dephosphorylated by protein phosphatase 2A (PP2A), protein phosphatase 2B (PP2B) or protein phosphatase 1 (PP1), resulting in the activation of stathmin and the instability of microtubules and dissolution of the mitotic spindle.

5.2 METHODS

5.2.1 *In vivo* cell cycle

NSG mice were engrafted with 2-5 x 10^6 patient derived xenografts cells, in which resistance to everolimus had been established by prolonged *in vivo* exposure, or a matched sensitive parental xenograft. Leukaemic engraftment was assessed by weekly tail vein bleeds and flow cytometry using antibodies to human CD19 and mouse CD45. Once mice had greater than 50% leukaemic blasts in their peripheral blood, they were treated once with everolimus (5 mg/kg) or a placebo by oral gavage 24 h prior to cull. Mice also received 100 μl of BrdU (10 mg/ml) by IP injection, 1 h prior to cull.

Peripheral blood, femurs and spleens were collected from sacrificed animals and single cell suspensions prepared as described in Chapter 2.2.2. Following red cell lysis, remaining cells were stained with antibodies against human CD19 and mouse CD45 to identify human leukemia cells. Cells were fixed and permeabilized by sequential incubation for 10 min with BD Cytofix/Cytoperm buffer (RT), Cytoperm Plus (4°C), and BD Cytofix/Cytoperm (RT), washing with BD wash solution between incubation steps with each buffer. BrdU epitopes were exposed by treating cells with 30 mg of DNase per million cells in a total volume of 100 μl then fluorescently labelled with a BrdU antibody conjugated with APC. For intracellular evaluation of stathmin, 1 x 10^6 BrdU labelled with incubated with rabbit antibodies specific for stathmin or its phosphorylation sites at Ser38 or Ser63. Bound primary antibodies were detected with anti-rabbit pacific blue. 7-AAD (f.c. 20 μg/ml) was added 10 minutes prior to running samples on the BD LSRFortessa. Analysis was carried out using Flowjo software (Treestar).

5.3 RESULTS

5.3.1 *In vivo* assessment of cell cycle

The baseline cell cycle status and the effects of administration of everolimus were assessed in sensitive and resistant xenografts using the BrdU method of *in vivo* cell cycle analysis. Flow cytometry was used to identify human CD19 leukemic cells and the cell cycle distribution and incorporation of BrdU into these cells was analysed in the blood, spleen and bone marrow as shown in Figure 5.2.

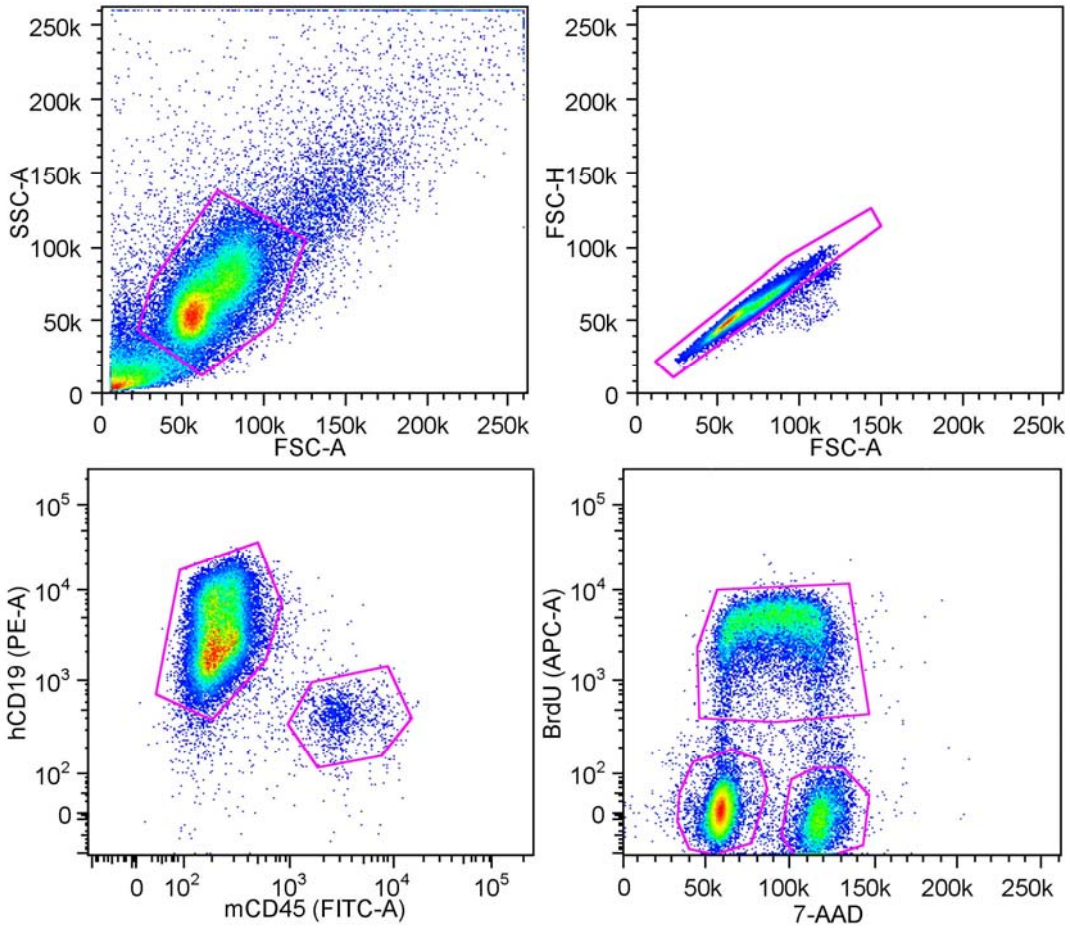

Figure 5.2. The gating strategy used for the assessment of cell cycle by BrdU incorporation in everolimus sensitive and resistant ALL xenografts *in vivo*. Top Left panel: ungated cells are shown on a FCS-A vs. SSC-A dot plot. The viable cell population is identified by the gate shown. Top right panel: cells gated from the top left panel are shown on a FSC-A vs. FSC-H dot plot. Doublets and aggregates are identified, and excluded by the gate shown. Bottom left panel: cells gated from the doublet exclusion date are shown on a human CD19 (PE) and mouse CD45 (FITC) dot plot, human leukaemia cells are identified by the gate shown. Bottom right panel: human leukaemia cells are shown on a 7-AAD vs. APC-A dot plot. The upper gate defines cells positive for BrdU and therefore in S phase at the time of the BrdU pulse, the lower left gate, cells in $G_{0/1}$ and the lower right gate those in G_2M.

In vivo, the xenograft 1345-R was more proliferative as compared to the parental xenograft 1345-S, but surprisingly, 2055-R was less proliferative than the sensitive 2055-S. The increase proliferation of 1345-R cells correlated with a significant reduction it the proportion of cells in $G_{0/1}$ in all tissues. Furthermore, a statistically significant increase in S phase and G_2M cells was observed in the spleen and blood respectively (Figure 5.3 A). Administration of everolimus elicited an accumulation of cells in $G_{0/1}$ in 1345-S and 1345-R cells. As a result the treated resistant cells had a similar cell cycle profile to that of untreated sensitive cells. While 1345-R cells remain sensitive to the anti-proliferative effects of everolimus the increased basal proliferation of these cells meant that even in the presence of the drug the cells continued to proliferate strongly.

2055-R cells had a smaller proportion of actively cycling cells, a finding consistent with the slower growth of these cells in vivo (Figure 3.3). Both the everolimus resistant and sensitive 2055 xenografts had a limited proportion of cells actively cycling in the peripheral blood, however, the proportion of 2055-R cells in $G_{0/1}$ was significantly higher (Figure 5.3 B). In contrast to 1345-R, 2055-R cells appeared less proliferative than the sensitive 2055-S cells, particularly in the spleen and bone with the majority of cells being in the $G_{0/1}$ phase of the cell cycle. Everolimus administration resulted in an accumulation of 2055-S in $G_{0/1}$ in all tissues analysed. While everolimus similarly affected 2055-R cells in the spleen, it had no effect on cells recovered from the blood and the bone marrow. While proliferating more slowly, 2055-R cells are less sensitive to everolimus-induced inhibition of proliferation.

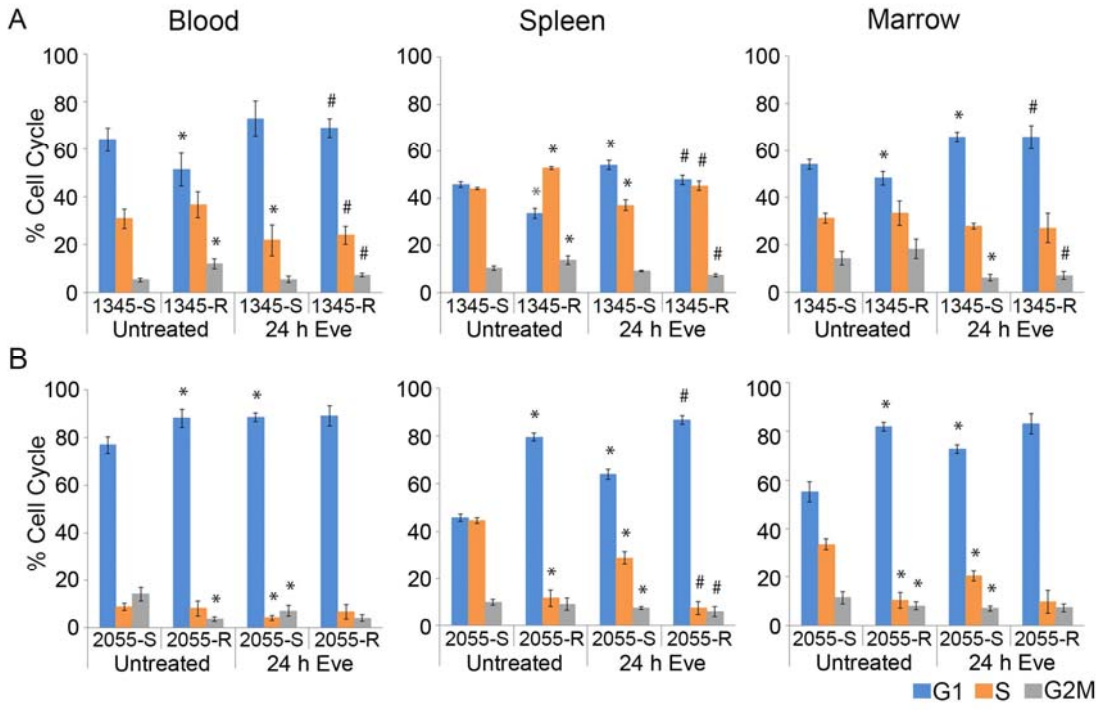

Figure 5.3 Resistance to everolimus alters the cell cycle *in vivo*. Cell cycle distribution of ALL cells isolated from the peripheral blood, spleen and bone marrow of mice engrafted with everolimus sensitive or resistant 1345 (A) or 2055 (B) ALL xenografts. Blue bars represent cells in G_1 phase, orange bars represent cells in S phase and grey bars represent cells in G_2M phase. The mean ± SD of six mice is shown for each xenograft. Students 2 tailed t-test comparing untreated sensitive cells (*$p < 0.05$) to untreated resistant cells (#$p < 0.05$).

5.3.2 Expression of stathmin in everolimus resistant ALL

Preliminary proteomic investigation identified the upregulation of the microtubule regulating protein stathmin in the everolimus resistant xenograft 1345-R. Although expression of stathmin is strikingly over expressed in 1345-S and 1345-R relative to peripheral blood mononuclear cells (PBMCs), no difference was observed upon development of resistance when examined by western blotting (Figure 5.4). However, using the same methodology, 2055-R demonstrated increased expression of stathmin (Figure 5.5 E).

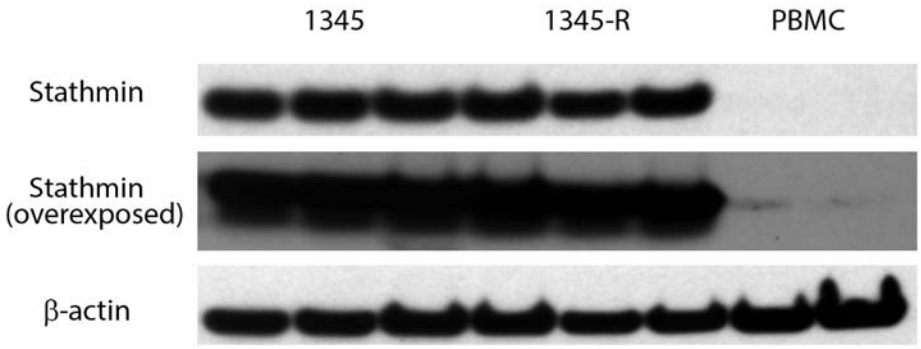

Figure 5.4 Stathmin is over expressed in 1345-S and 1345-R cells. Protein was isolated from spleen cells recovered from mice engrafted with resistant xenografts or matched sensitive controls (1345-R and 1345-S) as well as PBMC from healthy donors. Blots were sequentially probed with antibodies against stathmin with β-actin used as a loading control.

Since the activity of stathmin is regulated by phosphorylation events, it is possible that the differentially expressed spot observed on the 2D-DIGE in chapter 4 represented a particular phosphorylated form. Therefore the phosphorylation of stathmin on Ser38, the prerequisite phosphorylation site, and Ser63, the strongest inhibitory site were assessed in both xenografts. The phosphorylation on Ser38 was the same in 1345-S and 1345-R cells (Figure 5.5 B – D), though phosphorylation of Ser63 was significantly decreased (Figure 5.6 B - D). In contrast, the amount of phosphorylation on Ser38 (Figure 5.5 F) and amount and proportion of stathmin phosphorylated on Ser63 (Figure 5.6 F and H) were significantly increased in everolimus resistant 2055-R cells. In both xenografts, treatment with everolimus had opposing effects on the phosphorylation of the two serine residues, with Ser38 tending to be decreased (Figure 5.5 B and F) while there was increased phosphorylation of Ser63 (Figure 5.6 B and F).

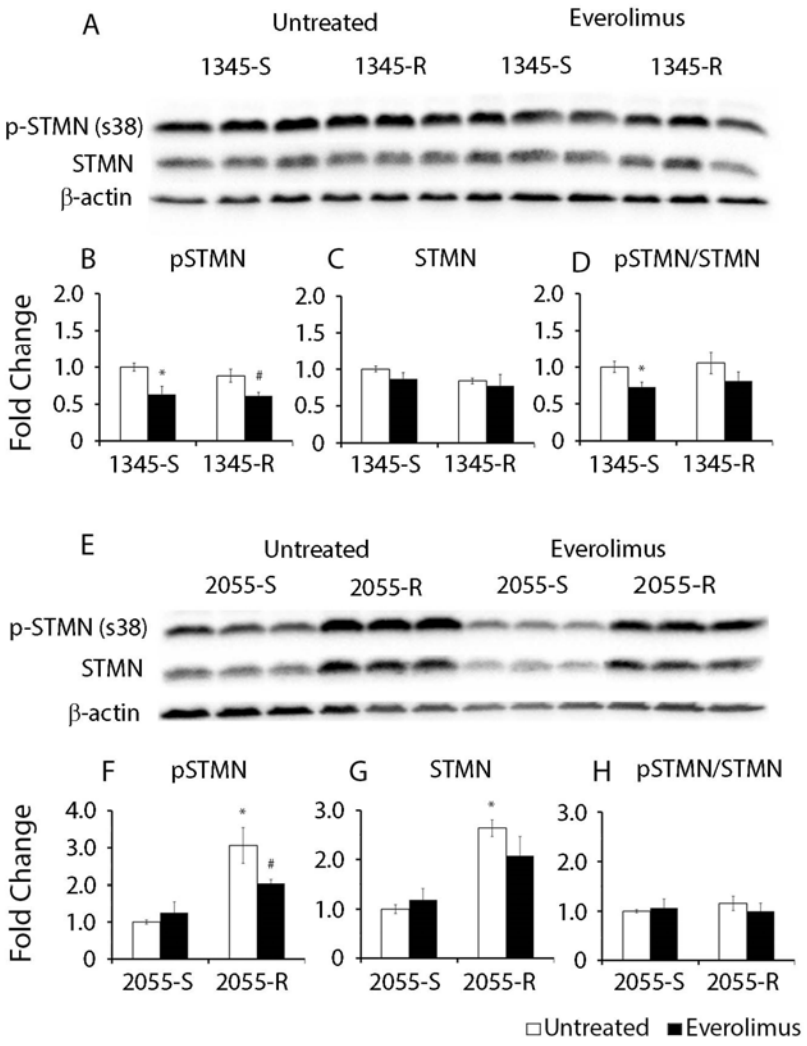

Figure 5.5 Expression of stathmin and phosphorylation of Ser38 in everolimus sensitive and resistant ALL cells with or without everolimus treatment. Protein was isolated from cells recovered from mouse spleens bearing resistant or matched sensitive xenografts: 1345-R and 1345-S (A), 2055-S and 2055-R (B). Mice had been treated with everolimus or vehicle 24 h prior to sacrifice. Blots were sequentially probed with antibodies against stathmin phosphorylated on Ser38, total stathmin, and β-actin, which was used as a loading control. Band intensity was used to quantify stathmin phosphorylated on Ser38 (B, F) and total stathmin (C, G) and ratio of phosphorylated to total stathmin calculated (D, H). Lysates were run in biological triplicates using students 2 tailed unpaired t-test. * $p < 0.05$ when comparing to untreated sensitive cells, # $p < 0.05$ when comparing to untreated resistant cells.

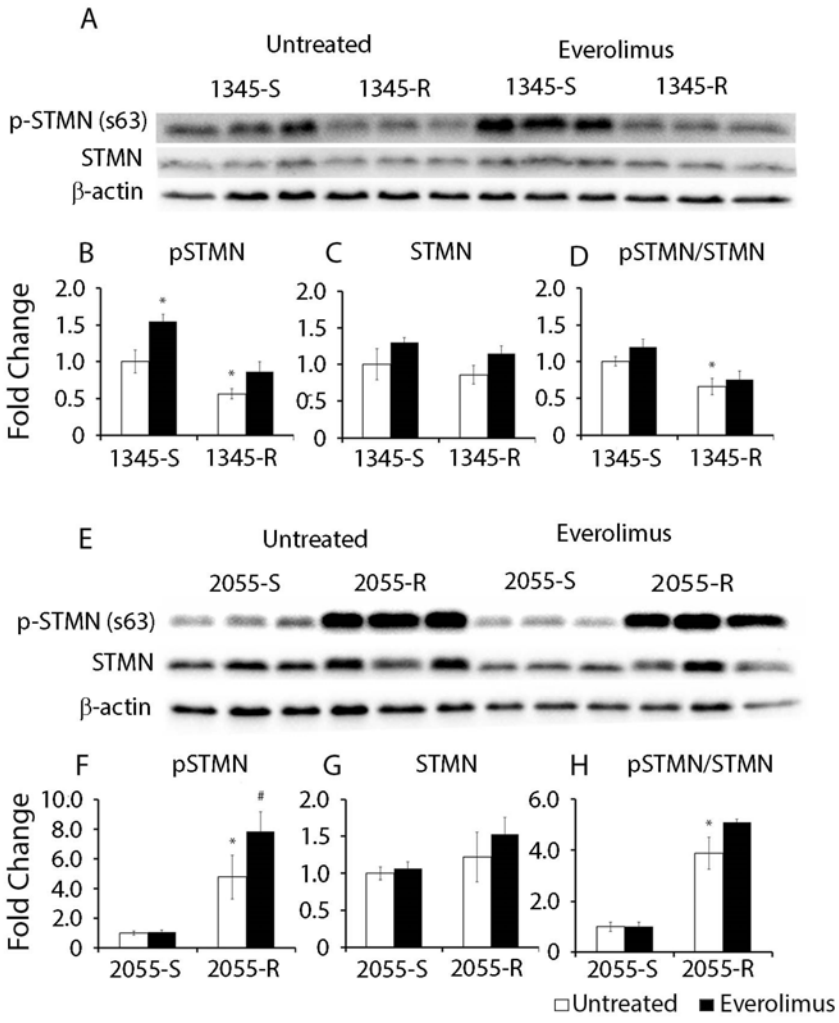

Figure 5.6 Expression of stathmin and phosphorylation of Ser63 in everolimus sensitive and resistant ALL cells with and without everolimus treatment. Protein was isolated from cells recovered from mouse spleens bearing resistant or matched sensitive xenografts 1345-R and 1345-S (A), 2055-S and 2055-R (B). Mice had been treated with everolimus or vehicle 24 h prior to sacrifice. Blots were sequentially probed with antibodies against stathmin phosphorylated on Ser63, total stathmin and β-actin, which was used as a loading control. Band intensity was used to quantify stathmin phosphorylated on Ser63 (B, F), total stathmin (C, G) and ratio of phosphorylated stathmin to total stathmin calculated (D, H). Lysates were run in biological triplicates using students 2 tailed unpaired t-test. * $p < 0.05$ when comparing to untreated sensitive cells, # $p < 0.05$ when comparing to untreated resistant cells.

5.3.3 Differential expression of stathmin through the cell cycle

The expression and activity of stathmin is regulated throughout the cell cycle by a series of inactivating phosphorylation events. To gain insight into the regulation of stathmin during the cell cycle, we used BrdU cell cycle analysis coupled with intracellular phospho-flow cytometry to assess the expression of stathmin and phosphorylation on Ser38 and Ser63.

The expression of total stathmin gradually increased throughout the cell cycle, peaking in the G_2M phase in sensitive and resistant cells from both xenografts (Figure 5.7 and 5.8). Similar to the immunoblotting data, the expression of stathmin was not changed upon development of resistance in 1345 cells. When comparing sensitive and resistant cells, there were no major changes in the phosphorylation status of stathmin in 1345-R cells with small reductions in phosphorylation on both Ser38 and Ser68 in cells in the periphery, most notable in $G_{0/1}$ and S phase cells. However, there was a reduction in total stathmin in 2055-R cells isolated from the spleen and to a lesser extent the bone marrow, a finding that conflicts with the immunoblotting data. Interestingly, there was an increase in total stathmin in 2055-R cells isolated from the blood and increased phosphorylation on Ser38 and Ser68 in all tissues, primarily in $G_{0/1}$ and S phases of the cell cycle. However, the antibodies used in this study to analyse the expression and phosphorylation of stathmin were validated only for use in immunoblotting and not in flow cytometry. While expression and phosphorylation of stathmin was quantifiable by flow cytometry, the lack of validation by BD biosciences and the lack of other sources of intracellular antibodies against stathmin and phosphorylated Ser38 and Ser63, results in an uncertainty into the validity of the flow cytometry results.

Administration of everolimus had little effect on the phosphorylation status of stathmin. In xenograft 1345 there was a small reduction the phosphorylation of Ser38 and even a lesser effect on Ser68, most evident in the sensitive 1345-S cells in the periphery. The exception was an increase in phosphorylation at both sites in 1345-R cells in G_2M isolated from the blood.

Expression of stathmin in 2055-R was significantly decreased all stages of the cell cycle in the spleen and bone marrow, whereas expression was significantly increased in the blood in the S and G_2M phases. Both 2055 and 2055-R phosphorylated stathmin on Ser38 and Ser63 in the G_2M phase in preparation for mitosis, however, phosphorylation of these residues was already apparent in S phase in the everolimus resistant xenograft. Resistant 2055-R cells had a higher level of phosphorylated stathmin than the sensitive parental xenograft in all tissues, except for phosphorylation of Ser38 in the spleen, where 2055-R cells had a significantly lower amount of phosphorylated stathmin. Administration of everolimus had little effect the expression or phosphorylation of stathmin in both sensitive and resistant 2055 cells, although a slight yet significant decrease in total stathmin was found in the spleen and bone marrow of both 2055-S and 2055-R cells.

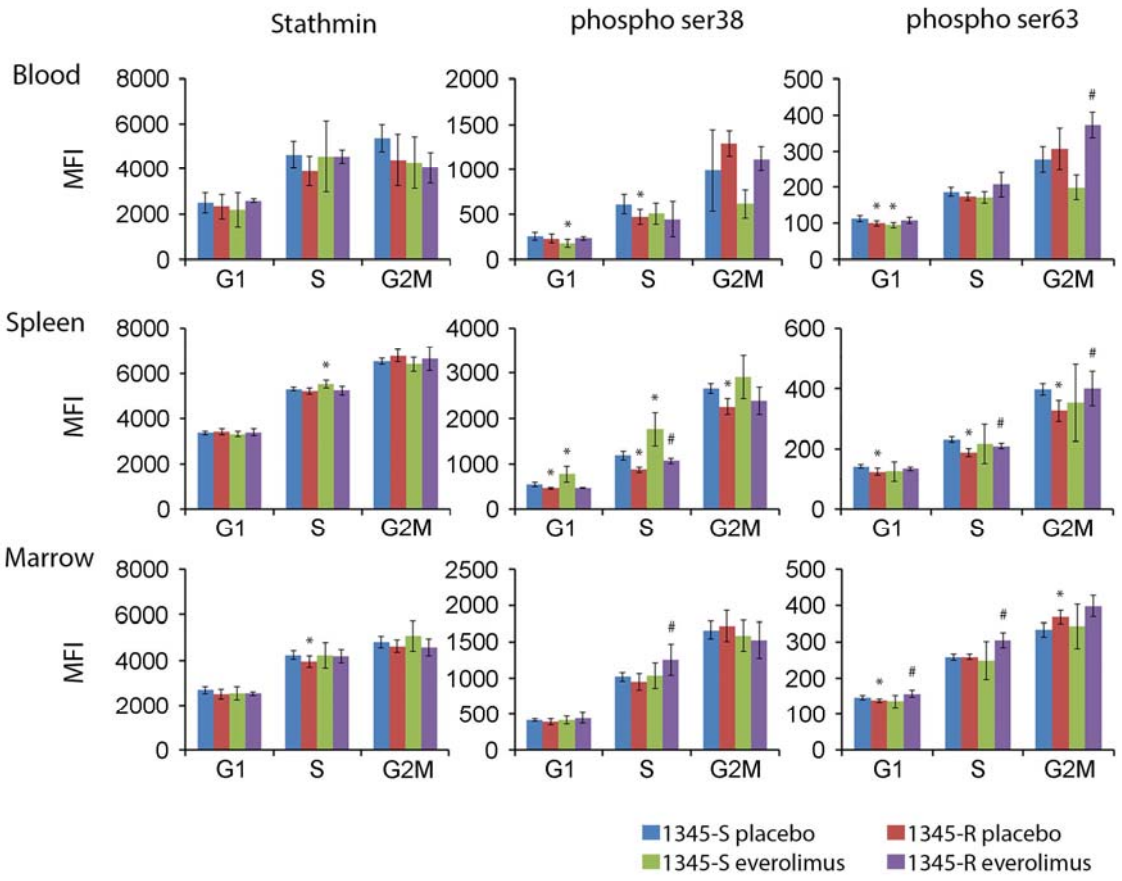

Figure 5.7 Expression and phosphorylation of stathmin on Ser38 and Ser63 throughout the cell cycle in 1345-S and 1345-R. Mice were engrafted with matched sensitive and resistant xenografts and treated with everolimus or vehicle for 24 h prior to sacrifice. Cells were isolated from the indicated tissues and analysed by flow cytometry using gating shown in figure 5.2. Columns represent the average mean fluorescence intensity (MFI) ± SD of 6 biological replicates. *$p < 0.05$ compared to untreated sensitive cells, #$p < 0.05$) compared to untreated resistant cells using Students 2 tailed unpaired t-test.

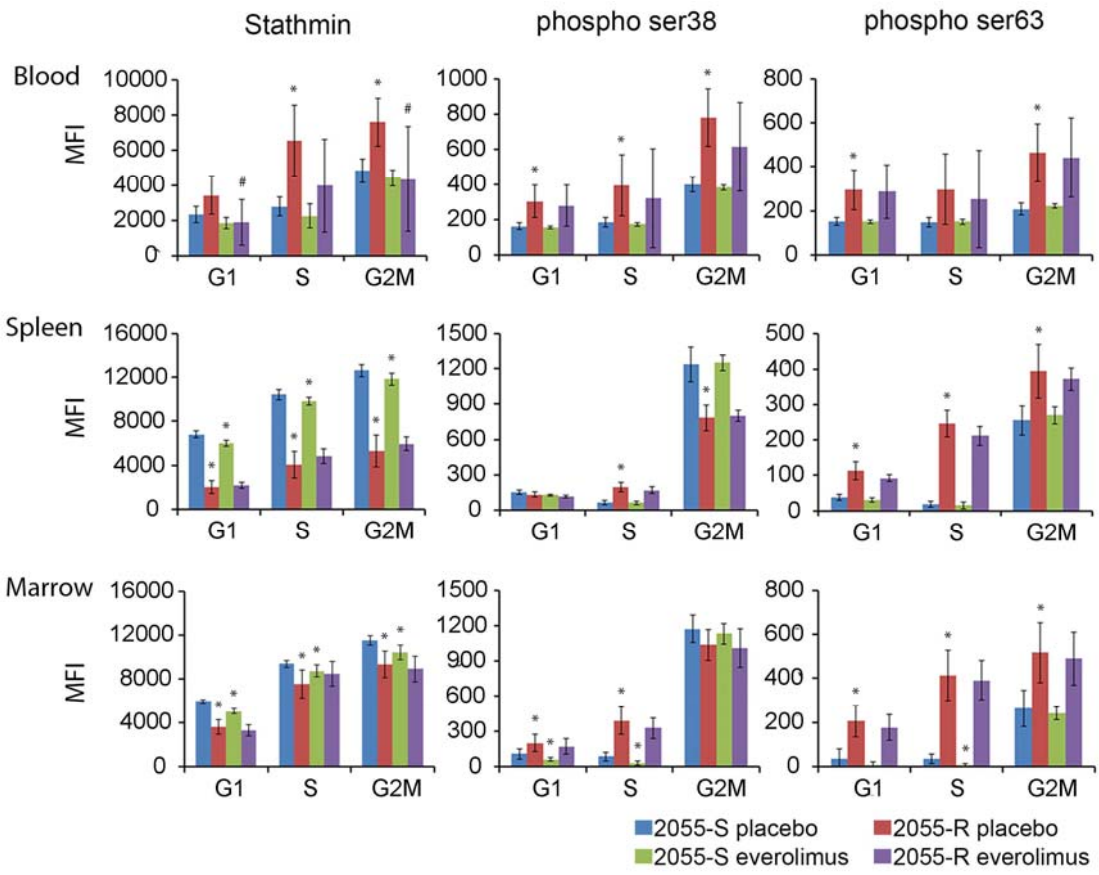

Figure 5.8 Expression of total stathmin and phosphorylation on Ser38 and Ser63 in 2055-S and 2055-R. Mice were engrafted with matched sensitive and resistant xenografts and treated with everolimus or vehicle for 24 h prior to sacrifice. Cells were isolated from the indicated tissues and analysed by flow cytometry using gating shown in figure 5.2. Columns represent the average mean fluorescence intensity (MFI) ± SD of 6 biological replicates. *$p < 0.05$ compared to untreated sensitive cells, #$p < 0.05$) compared to untreated resistant cells using Students 2 tailed unpaired t-test.

5.3.4 Regulation of Stathmin Phosphorylation

Phosphorylation of stathmin is carried out by several kinases throughout the cell cycle, though the best characterized of these are the phosphorylation of the Ser16 and Ser63 by PKA [273, 274] and Ser25 and Ser38 by members of the cyclin dependent kinases CDK1 and CDK2 [275, 276]. We evaluated the expression of the catalytic subunit of PKA (PKA-Cα), CDK1 and CDK2, as well as the respective activating phosphorylation sites of each protein, to assess whether the changes in stathmin phosphorylation in everolimus resistant ALL xenografts may be due to altered expression of these kinases.

Everolimus treatment of 1345-S cells significantly increased the expression of the catalytic subunit of PKA by 1.5 fold (Figure 5.9 C), resulting in a relative decrease in the ratio of phosphorylated to total PKA-Cα (Figure 5.9 D). The proportion of phosphorylated PKA-Cα was significantly decreased in the resistant 1345-R xenograft (Figure 5.9 D), but treatment with everolimus did not to elicit a further decrease (Figure 5.9 D). In contrast to 1345-R, treatment with everolimus and the development of resistance did not alter the expression or phosphorylation of PKA-Cα in the 2055 xenografts.

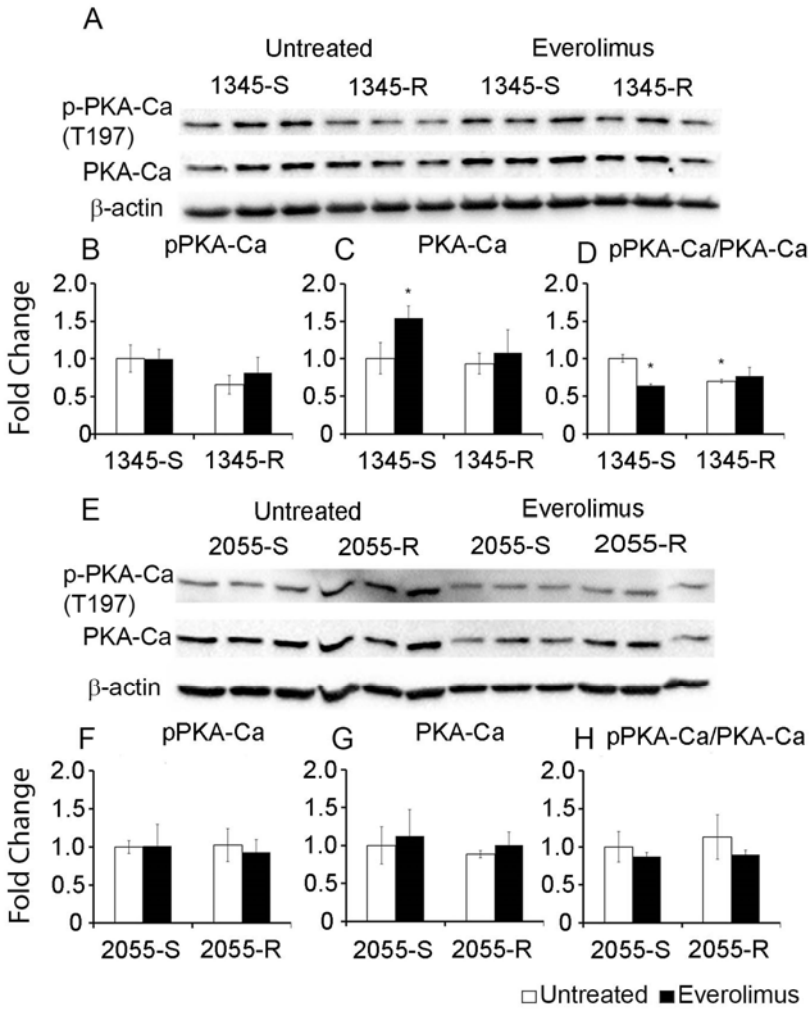

Figure 5.9 Expression and phosphorylation of PKA-Cα on Thr197 in everolimus sensitive and resistant ALL cells with and without everolimus treatment. Protein isolated from resistant xenografts and matched sensitive controls 1345-R and 1345-S (A), 2055-R and 2055-S (E), with and without treatment with everolimus. Blots were sequentially probed with antibodies against PKA-Cα phosphorylated on Thr197 and total PKA-Cα, with β-actin used as a loading control. Band intensity was used to quantify PKA-Cα phosphorylated on Thr197 (B, F) and total PKA-Cα (C, G) and ratio of phosphorylated PKA-Cα to total protein was calculated (D, H). Lysates were run in biological triplicates using students 2 tailed unpaired t-test. *$p < 0.05$ compared to untreated sensitive cells, #$p < 0.05$) compared to untreated resistant cells using Students 2 tailed unpaired t-test.

The basal expression of the cyclin dependent kinases CDK1 and CDK2 and phosphorylation of their respective activation residues at Thr160 and Thr161, remained unchanged with the development of resistance in the 1345 xenograft (Figure 5.10 B - D and 5.11 B - D). In contrast, xenograft 2055-R demonstrated reduced expression of both CDK1 and CDK2 as well as reduced phosphorylation of Thr160 and Thr161 respectively, compared to the parental sensitive xenograft (Figure 5.10 F - H and 5.11 F - H). Administration of everolimus significantly decreased the expression of CDK1 in both sensitive and resistant 2055 xenografts (Figure 5.11 H) leading to a relative increase in the ratio of phosphorylated CDK1 in both 2055-S and 2055-R (Figure 5.10 F). The expression of total CDK2 was upregulated following 24 h of everolimus treatment both 1345-S and 2055-S xenografts (Figure 5.11 C-D, G-H). However, the responses of the resistant xenografts differed with the expression and phosphorylation of CDK2 on Thr160 being significantly reduced in 1345-R cells (Figure 5.11 C-D), while, these parameters were non-significantly increased in 2055-R (Figure 5.11 G-H). However, the ratio of phosphorylated to total CDK2 was significantly reduced in both resistant xenografts (Figure 5.11 D, H). Moreover, the ratio of phosphorylated to total CDK2 was similarly reduced in both the sensitive and resistant forms 1345 and 2055 upon everolimus administration, though this reduction was small, and insignificant in all but xenograft 1345-S.

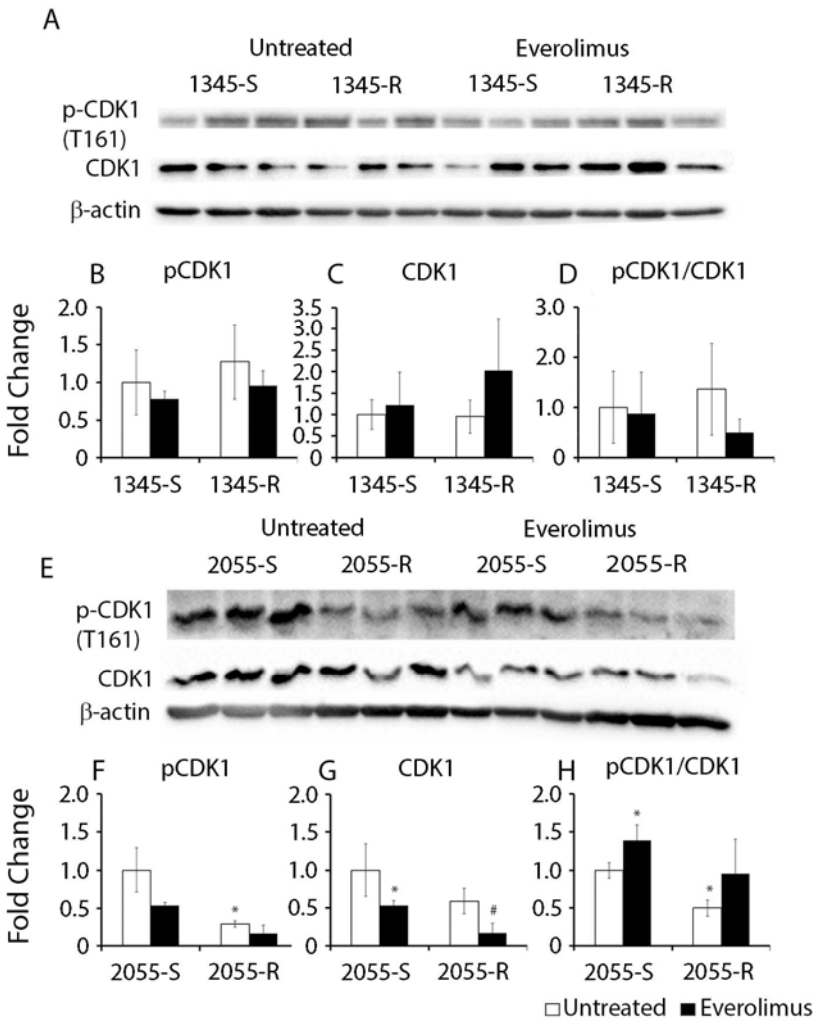

Figure 5.10 Expression and phosphorylation of CDK1 on Thr161 in everolimus sensitive and resistant ALL cells with and without everolimus treatment. Protein isolated from resistant xenografts and matched sensitive controls 1345-R and 1345-S (A), 2055-R and 2055-S (E), with and without treatment with everolimus. Blots were sequentially probed with antibodies against CDK1 phosphorylated on Thr161 and total CDK1, with β-actin used as a loading control. Band intensity was used to quantify CDK1 phosphorylated on Thr161 (B, F) and total CDK1 (C, G) and ratio of phosphorylated CDK1 to total protein was calculated (D, H). Lysates were run in biological triplicates using students 2 tailed unpaired t-test. *$p < 0.05$ compared to untreated sensitive cells, #$p < 0.05$) compared to untreated resistant cells using Students 2 tailed unpaired t-test.

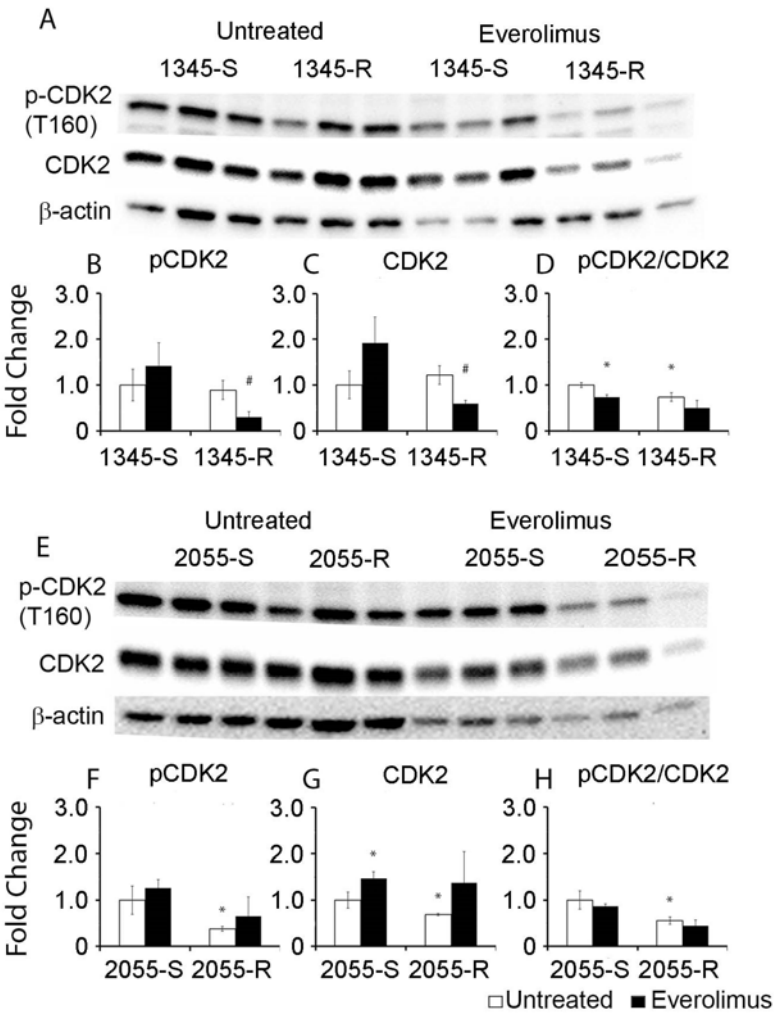

Figure 5.11 Expression and phosphorylation of CDK2 on Thr160 in everolimus sensitive and resistant ALL cells with and without everolimus treatment. Protein isolated from resistant xenografts and matched sensitive controls 1345-R and 1345-S (A), 2055-R and 2055-S (E), with and without treatment with everolimus. Blots were sequentially probed with antibodies against CDK2 phosphorylated on Thr160 and total CDK2, with β-actin used as a loading control. Band intensity was used to quantify CDK2 phosphorylated on Thr160 (B, F) and total CDK2 (C, G) and ratio of phosphorylated CDK2 to total protein was calculated (D, H). Lysates were run in biological triplicates using students 2 tailed unpaired t-test. *$p < 0.05$ compared to untreated sensitive cells, #$p < 0.05$) compared to untreated resistant cells using Students 2 tailed unpaired t-test.

5.4 DISCUSSION

The primary location of hematopoiesis in adults is the bone marrow, which provides a specialised microenvironment that supports the growth and survival of normal and malignant hematopoietic precursors. This supportive environment can offer a sanctuary to leukaemic cells where they can escape the effects of chemotherapy, contributing to resistance [170, 171, 277]. The spleen is a secondary hematopoietic organ that contains a specialized niche that, while different to the bone marrow microenvironment, expresses similar factors such as CXCL12, SCF, VE-Cadherin, PDGFRβ, LepR, TCF21 and VCAM-1 to support the growth and survival of hematopoietic precursors [278-280]. Yet, the prevalence of extramedullary involvement in mice engrafted with human ALL xenografts is varied between xenografts. It is possible that the spleen microenvironment may express factors, different to the bone marrow, which can support the growth of leukemia cell, although such factors are unknown. In times of high stress to the bone marrow, such as trauma, anaemia, infection and leukemia, the spleen is able to support hematopoiesis [278]. Infiltration of malignant cells into the spleen is a common clinical feature of ALL and is often correlated with an elevated white cell count in the peripheral blood [25].

The variability in survival of mice engrafted with the two everolimus resistant xenografts 1345-R and 2055-R, is reflected in the cell cycle distribution of each xenografts. The cell cycle distribution of cells recovered from mice engrafted with 1345-R indicated that these are more proliferative than the sensitive 1345-S cells which corresponded to the more rapid disease progression in 1345-R bearing animals. In contrast, the growth of 2055-R *in vivo* was more subdued and mice survived longer than those engrafted with the parental xenograft, a finding consistent with the high proportion of cells in the $G_{0/1}$ phase of the cell cycle. Everolimus is a cytostatic

compound and induces a $G_{0/1}$ arrest in ALL cells *in vivo* [129]. While 1345-R remained responsive to the cell cycle effects of everolimus, the response of 2055-R cells was significantly reduced with cell cycle inhibition only being detected in cells recovered from the spleen. Furthermore, the differential growth of the xenografts and response to everolimus between the tissues analysed, suggests each tissue offers a specific microenvironment that may affect the growth of the xenografts and their response to everolimus.

Stathmin is an important regulator of the cell cycle that is involved in the G_1-S and the G_2M checkpoints that needs to be phosphorylated for mitosis proceed [281]. The overexpression of stathmin has been identified in numerous malignancies and is correlated to a more proliferative and metastatic phenotype [238-241, 282]. Similarly, stathmin was highly overexpressed in the ALL xenograft 1345-S as well as the everolimus resistant form, 1345-R, compared to normal peripheral blood mononuclear cells. Though, it must be noted that the expression of stathmin in hematopoietic cells decreases as the cells mature [270]. Therefore, CD34 positive immature lymphoblasts at a similar stage of maturation to the malignant cells would have been more appropriate normal comparator for stathmin expression. Nevertheless, the expression and phosphorylation of stathmin, despite significant regulation, was not in line with its predicted effects on the cell cycle in either everolimus resistant xenografts. In addition, both everolimus resistant xenografts demonstrated tissue specific effects on stathmin phosphorylation and expression, further emphasising the possible influence of tissue specific microenvironments on the expression of proteins and the regulation of the cell cycle.

The cyclin dependent kinases CDK1 and CDK2 are important for the proper progression of the cell cycle. Loss of CDK2 in cells can be compensated for by the

recruitment of other cyclin dependant kinases such as CDK1. On the other hand, CDK1 is vital for cell cycle, as it is the master regulator of the G_2M transition [283-285]. Moreover, resistance to everolimus in prostate cancer has been linked to increased expression of CDK1 and CDK2 [143]. In the everolimus resistant ALL xenografts CDK2 activity was lost, while the expression of CDK1 was down regulated solely in 2055-R. The regulation of the cyclin dependent kinases does not explain the increased proliferation of the 1345-R xenograft, indicating multiple mechanisms regulating the cell cycle in the two xenografts.

As CDK1 controls the G_2M transition, its reduction in 2055-R cells recovered from the spleen may be a compensatory mechanism for the increased expression of stathmin and possibly the causative factor behind the strong $G_{0/1}$ accumulation *in vivo*. Nevertheless, despite the strong $G_{0/1}$ accumulation in the blood, spleen and bone marrow, xenograft 2055-R continued to proliferate *in vivo*. The mechanism of how the cells continue to cycle and how these factors contribute to resistance to everolimus remains elusive.

Microenvironments vary between tissues and interaction of ALL xenografts these tissue specific microenvironments may lead to cellular resistance to everolimus. Different xenografts may have a preference for particular microenvironment that may have led to the differential responses between the two xenografts studied. Indeed, disruption of the interaction between ALL cells and the microenvironment using agents such as AMD3100 and G-CSF synergizes with current chemotherapeutic compounds [175, 201], and may be a strategy to overcome potential mechanisms of resistance to everolimus.

CHAPTER 6 EVALUATION OF THE SHORT-TERM EFFECTS OF EVEROLIMUS IN A CLINICAL TRIAL INVOLVING ADULTS WITH REPLAPSED OR REFRACTORY ALL.

6.1 INTRODUCTION

The Akt/mTOR pathway is an important cellular growth pathway that is often over active in many cancers, including ALL [286-288], and offers an attractive target for inhibition in conjunction with conventional chemotherapy.

The allosteric mTOR inhibitor everolimus has been approved for by the Therapeutic Goods Administration (TGA) for clinical use in several malignancies including pancreatic neuroendocrine tumours and renal cell carcinoma, as well as for the treatment of Subependymal giant cell astrocytoma (SEGA), angiomyolipoma and lymphangioleiomyomatosis (LAM) associated with the tuberous sclerosis complex. The efficacy of everolimus is currently being evaluated in several clinical trials for other malignancies including non-small cell lung carcinoma (NCT02321501), chondrosarcoma (NCT02008019), gastroesophageal adenocarcinoma (NCT02138929) and prostate cancer (NCT02125084). The efficacy of everolimus has been demonstrated in pre-clinical models of ALL [65, 125, 128, 289] and while the safety of everolimus has been demonstrated in other hematological malignancies [132], clinical evidence of the safety and efficacy in ALL was lacking.

To assess the safety and efficacy of everolimus in relapsed adult ALL, a single centre, phase I/II clinical trial was conducted through the MD Anderson Cancer Center in Houston, Texas. Patients with relapsed or refractory ALL enrolled into the trial were given everolimus in combination with the intensive chemotherapy regime HyperCVAD, which consists of hyper fractionated cyclophosphamide, vincristine, adriamycin

(doxorubicin) and dexamethasone [133]. We aim to characterise short-term changes induced by everolimus and to determine if these were associated with responses to everolimus as well as the overall clinical outcome.

6.2 METHODS

6.2.1 Patient samples

Peripheral blood mononuclear cells were isolated at the MD Anderson Cancer center by Ficoll-Hypaque density gradient centrifugation (Sigma-Aldrich, St. Louis, MO), before (Cycle 1 Day 0) and 24 hours after (Cycle 1 Day 1) the first dose of everolimus during the first cycle of therapy. Both samples were taken prior to treatment with HyperCVAD chemotherapy. Peripheral blood mononuclear cells were lysed in TRIzol reagent and frozen at -80°C prior to shipping to The Westmead Institute for Medical Research.

6.2.2 miR-21 expression

The expression of human miR-21 was analyzed with the Taqman miRNA expression array system (Life Technologies). RNA was isolated from patient samples using TRizol extraction as described in Chapter 2. Ten nanograms of total RNA was reverse transcribed using Taqman Small RNA assay and MultiScribe reverse transcriptase by incubation with a stem loop primer targeted against miR-21 and the small nucleolar RNA control, snoU6. Samples were sequentially incubated at the following temperatures: 30 min at 16°C, 30 min at 42°C and 5 min at 85°C.

Real time quantitative PCR was then performed on the transcribed product by combining with Taqman Universal PCR master mix (no UNG) and taqman probes targeting miR-21 and snoU6. Reactions were performed in duplicates with the following cycling conditions on the Bio-RAD CFX96 thermocycler: Hot start 95°C for 10 min, 40 cycles of 15 s at 95°C and 1 min at 60°C. Fluorescence was collected at the end of each cycle. Gene expression was calculated using the $2^{-\Delta\Delta ct}$ quantification method [290], normalizing to the average of snoU6.

6.2.3 Expression of miR-21 targets

cDNA was prepared from 400 ng of patient RNA by using the RT^2 First Strand kit. Genomic DNA was removed from samples by incubating with GE buffer for 5 min at 42°C. Samples were reverse transcribed with RC3 reverse transcriptase at 42°C for 15 min and the reaction terminated by incubating tubes at 95°C for 5 min.

The cDNA product was then combined with RT^2 SYBR green qPCR Mastermix and dispensed into a 384 well plate preloaded with target primers. The plate was sealed and centrifuged at 1000 x *g* at RT. Samples were run on the Bio-RAD CFX384 thermocycler using the following program: Hot start 95°C for 10 min, 40 cycles of 15 s at 95°C and 1 min at 60°C, with fluorescence collected at the end of each cycle. Gene expression was calculated by using the $2^{-\Delta\Delta ct}$ quantification method, normalizing to the average of the 5 housekeeping genes included in the array.

6.3 RESULTS

6.3.1: Patient Characteristics

Twenty four patients were enrolled in the study, however, due to lack of patient material, samples from only 15 patients were sent to Australia (Table 6.1). Of the samples sent, the mean age of patients was 29.4 years (range 11-59) and patients received, on average, 2 prior treatments (range 1-4) before enrolment into the trial. Seven patients were diagnosed with pre-B ALL, 7 with pre-T ALL and one mixed phenotype, with varying cytogenetics among patients. Patients remained on the study for an average of 120 days (range 21-800) and received an average of 2 treatment cycles (range 1-4).

Patients were commenced on a dose of 5 mg/kg of everolimus (patients 1-3) and after no serious adverse events were observed, the dose was increased to 10 mg/kg (patients 4-11). Adverse effects were observed at the higher dose of everolimus and therefore the dose was reduced back to 5 mg/kg for the remainder of the trial. Six patients achieved a complete remission (CR), one of which did not completely recover their blood counts (CRi) while another did not recover their platelet counts (CRp). Two patients achieved a partial remission (PR). The remaining 7 patients were classified as non-responders (NR). Peripheral blood samples were taken on day 0 (before everolimus) and day 1 (after one dose).

Table 6.1 Clinical characteristics of patients (N = 15)

No.	Diagnosis	Age	CG	No. Prior treatments/ Regimen		CR1 Duration (months)	Everolimus Dose (mg/day)	No. .Cycles	Clinical Response	Days on Study	S6RP inhib.
1	Pre-T-ALL	29	Del 7, del 17	4	ESHAP, CHOP, AugHCVAD, alloSCT	7	5	2	PR	48	Y
2	Pre-T-ALL	24	Diploid	4	Larson, Nelarabine, other	11	5	2	NR	46	N
3	Pre-B-ALL	52	11q23	1	R-HCVAD	26	5	4	CR	153	Y
4	Pre-B-ALL	27	t(12;16)	1	AugBFM	39	10	1	NR	21	Y
5	Pre-T-ALL	11	del 1, inv 3	1	CCG-1961 w/XRT	12	10	1	NR	28	Y
6	Pre-T-ALL	24	Hyper with 11q23	3	HCVAD, Nelarabine, alloSCT	30	10	4	PR	145	Y
7	Pre-B-ALL	59	Diploid	1	R-CHOP	12	10	2 +mnt	CR	800	N
9	Pre-T-ALL	26	Hyper with +8	2	HCVAD+Nelarabine, MOAD w/ alloSCT	6	10	2	CRi	148	N
10	Pre-B-ALL	24	Del 7, del 17	3	ALL0232, other	12	10	2	NR	49	Y
11	Pre-B-ALL	23	t(2;9)	1	AugBFM	21	10	2	CR	73	Y
14	Pre-B ALL	43	Diploid	4	HCVAD w/FLAG-IDA, Clofarabine, BiTE	9	5	2	NR	64	ND
16	Pre-T-ALL	22	Diploid	1	AugBFM	15	5	4	CR	102	ND
17	Pre-B-ALL	14	IM	3	AALL0232, Bortezomib	11	5	1	NR	29	ND
21	Pre-T-ALL	19	Diploid	1	AugBFM	9	5	2	CRp	68	ND
23	Mixed phenotype	44	Diploid	2	HCVAD w/allo SCT, MorphoSys	7	5	1	NR	26	ND

Abbrevations: CG = cytogenetics, CR = complete remission, PR = partial remission, CRi = complete remission with incomplete counts recovery, CRp = complete remission with incomplete platelets recovery, NR = non responder, mnt = maintenance, ND = not determined

6.3.2: Gene expression analysis by microarray

RNA was isolated from patient samples, quantified by UV spectrophotometry and integrity determined using the Agilent Bioanalyzer (Table 6.2). The RNA isolated from patients 1 to 5, 14, 16, and 17 was not of sufficient quality for microarray analysis (RNA integrity number (RIN) of less than 7). Insufficient initial cell numbers and time RNA was stored in TRizol may have contributed to the lower quality of RNA extracted. An adequate quantity of suitable quality RNA was isolated from patients 6, 7, 9, 10 and 11 (all of which received the higher 10 mg/kg dose of everolimus). These samples were amplified and hybridized to a human gene expression microarray chip. Microarray chips were scanned with the Illumina BeadArray Reader and results imported into BeadStudio where genes were normalised using the average normalisation protocol against internal controls.

Unsupervised hierarchical clustering was performed on genes significantly detected in all samples using the Partek Genomics Suite and Euclidean dissimilarity (Figure 6.1). Of the 5 patients analysed by microarray the 2 patients who achieved CR, 7 and 11, clustered together. Patient 6, a partial responder, also clustered alongside the CR patients while patients 9 and 10 clustered separately. Clustering of all patients, except for the CR patients (7 and 11) was more strongly influenced by the underlying genetics rather than the effects of everolimus treatment. In contrast, clustering of the CR patients 7 and 11 was more heavily influenced by treatment.

Table 6.2 Patient RNA concentration and integrity (N = 15)

No.	Treatment day	Concentration (ng/μl)	A260/280	RIN
1	Day 0	70	1.591	N/A
	Day 1	54	1.688	N/A
2	Day 0	24	1.714	N/A
	Day 1	138	1.769	N/A
3	Day 0	38	1.583	N/A
	Day 1	128	1.455	4.7
4	Day 0	258	1.843	N/A
	Day 1	56	1.750	N/A
5	Day 0	128	1.730	N/A
	Day 1	222	1.820	N/A
6	Day 0	732	1.848	8.7
	Day 1	400	1.724	N/A
7	Day 0	104	1.625	8.8
	Day 1	144	1.565	8.6
9	Day 0	328	1.822	9.7
	Day 1	240	1.818	9.7
10	Day 0	450	1.844	9.4
	Day 1	486	1.898	9.5
11	Day 0	600	1.724	9.2
	Day 1	440	1.833	9.2
14	Day 0	803	1.958	5.5
	Day 1	975	2.002	4
16	Day 0	426	1.941	4.5
	Day 1	389	1.932	4.6
17	Day 0	122	1.800	6.1
	Day 1	24.4	1.600	7.7
21 *	Day 0	816	1.606	N/A
	Day 1	106	1.646	N/A
23 *	Day 0	46.4	1.657	9
	Day 1	83.6	1.672	7.8

Abbreviations: A260/280 – ratio of absorbance at 260 nm and 280 nm, RIN – RNA integrty number. * Samples 21 and 23 were thawed during shipment

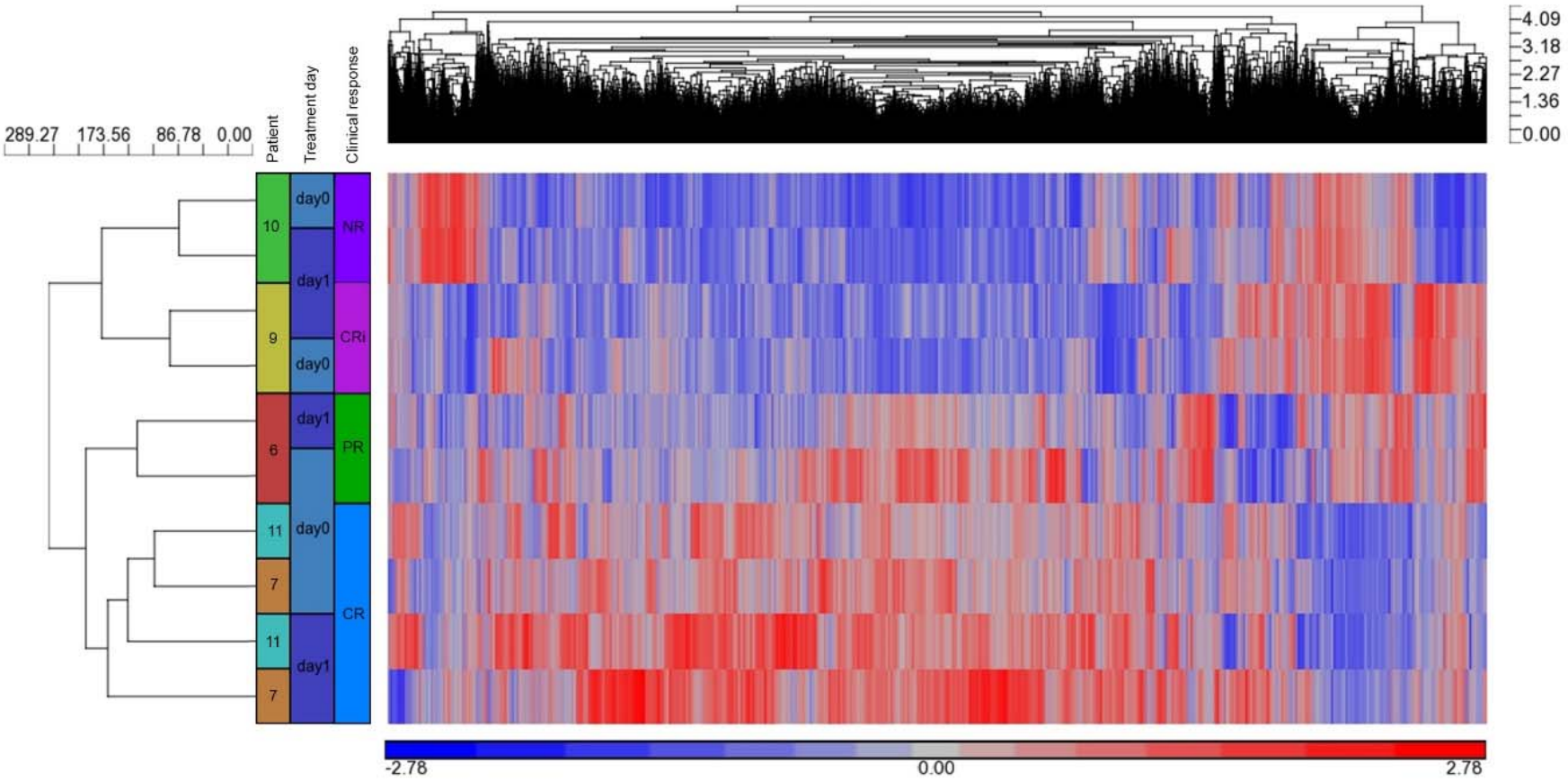

Figure 6.1 Hierarchical clustering of patient samples. Patient samples collected before (Day 0) and 24 h after (Day 1) the first dose of everolimus. Significantly detected genes were segregated using unsupervised hierarchical clustering in the Partek Gene Expression Suite. CR = complete remission, PR = partial remission, CRi = complete remission with incomplete recovery of white blood cell counts, NR = non-responder.

Significantly differentially expressed genes were detected in patients at baseline (day 0) between patients 7 and 11 and the remaining patients. In the two CR patients, 1139 genes were significantly upregulated and 1526 downregulated by more than 1.5 fold as compared to the remaining patients. GSEA was unable to identify any significantly enriched gene sets, however, Metacore identified 50 pathway maps (Table 6.3) and 50 process networks (Table 6.4) that were enriched in CR patients with a FDR of less than 25%. Cell cycle regulation pathways were enriched in both process networks and pathway maps with patients achieving a CR appearing less proliferative (Figure 6.2).

Table 6.3 Top 15 Metacore pathway maps enriched in patients who achieved complete remission (for full table see appendix A.7).

Maps	p-value	FDR
Cell cycle_The metaphase checkpoint	9.644E-22	7.850E-19
Cell cycle_Role of APC in cell cycle regulation	1.869E-19	7.609E-17
Cell cycle_Spindle assembly and chromosome separation	1.217E-13	3.302E-11
Protein folding and maturation_POMC processing	2.695E-12	5.484E-10
Cell cycle_Cell cycle (generic schema)	9.928E-11	1.616E-08
Cell cycle_Transition and termination of DNA replication	1.273E-10	1.727E-08
DNA damage_ATM/ATR regulation of G1/S checkpoint	1.584E-10	1.841E-08
Cell cycle_Role of SCF complex in cell cycle regulation	2.609E-10	2.654E-08
Cell cycle_Start of DNA replication in early S phase	1.792E-09	1.621E-07
Cell cycle_Role of Nek in cell cycle regulation	1.797E-08	1.463E-06
IL-6 signaling in multiple myeloma	2.367E-08	1.751E-06
Cell cycle_Chromosome condensation in prometaphase	2.828E-08	1.919E-06
Cell cycle_Influence of Ras and Rho proteins on G1/S Transition	4.904E-08	3.071E-06
DNA damage_ATM / ATR regulation of G2 / M checkpoint	6.200E-08	3.605E-06
Cell cycle_ESR1 regulation of G1/S transition	2.549E-07	1.383E-05

Table 6.4 Top 15 Metacore process networks enriched in patients who achieved complete remission (for full table see appendix A.8).

Networks	p-value	FDR
Cell cycle_Mitosis	2.704E-28	4.299E-26
Cell cycle_Core	4.171E-27	3.316E-25
Cytoskeleton_Spindle microtubules	1.494E-22	7.921E-21
Cell cycle_S phase	1.177E-19	4.678E-18
Cell cycle_G2-M	1.815E-14	5.772E-13
DNA damage_Checkpoint	2.474E-10	6.557E-09
Cell cycle_Meiosis	2.073E-09	4.709E-08
DNA damage_DBS repair	4.091E-08	8.130E-07
Transcription_mRNA processing	6.874E-07	1.214E-05
DNA damage_MMR repair	2.940E-06	4.674E-05
Transcription_Chromatin modification	6.071E-06	8.776E-05
Cell cycle_G1-S	7.450E-06	9.871E-05
DNA damage_BER-NER repair	4.154E-05	5.081E-04
Cell cycle_G1-S Interleukin regulation	9.372E-05	1.064E-03
Reproduction_Male sex differentiation	1.792E-04	1.900E-03

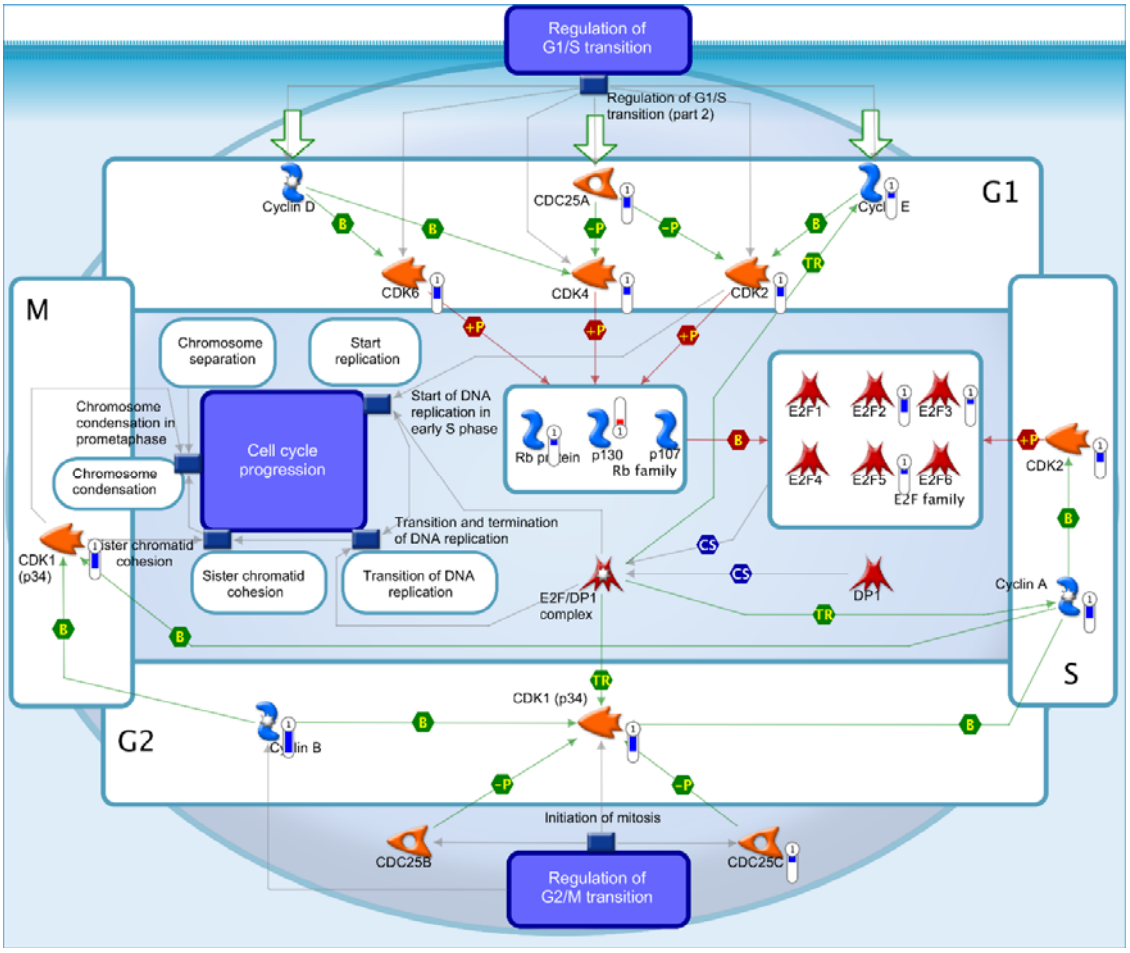

Figure 6.2 Top cell cycle regulation pathway (Cell cycle_Mitosis) in patients achieving complete remission. Red thermometers indicate an increase in expression, while blue thermometers indicate a decreased expression, with the amount of colour indicating the degree of regulation.

The gene signature generated based on the baseline expression of genes in patient who achieved CR was applied to a larger dataset consisting of 280 patients with mixed ALL subtypes and 4 normal controls (GSE28497) [291]. MRD data collected by flow cytometry at day 19 and day 46 was available, however, our CR gene signature was unable to predict MRD outcome at day 19 (Figure 6.3 A) or day 46 (Figure 6.3 B).

GSEA was used to identify gene signatures enriched as a result of treatment with everolimus. In a pooled analysis of array data from all patients, 213 gene signatures were significantly enriched with a FDR of less than 25% following treatment with everolimus. The most significantly enriched were the gene signatures for SMARCA2 ($p<0.001$), ERCC3 ($p<0.002$), TRAIL ($p<0.001$) and 2 gene signatures of miR-21, GABRIELY_MIR21_TARGETS ($p<0.002$) and ATAAGCT MIR-21 ($p<0.004$) (Figure 6.4 A). Micro RNA-21 (miR-21) is a small RNA molecule responsible for the down regulation of many tumour suppressors such as PTEN, and is therefore considered to be an oncogenic microRNA (oncomiR). Due to its oncogenic potential, the GABRIELY_MIR21_TARGETS gene signature was analysed in each patient individually (Figure 6.4 B). The signature was significantly enriched following everolimus treatment in all patients, except patient 11, with a FDR of less than 25%.

RNA from another 2 patients, patient 21 and 23, was arrayed and interrogated by GSEA but failed to generate any gene signatures that were significantly detected with appropriate FDR (q value). Both patients displayed a similar trend in the enrichment curve for the miR-21 gene signature as the initial patient cohort, however, data from neither patient achieved significance with a FDR of less than 25% (Figure 6.4 C). The integrity of RNA isolated from patient 21 could not be quantified and while patient 23 obtained suitable RIN values of 9 for Day 0 and 7.8 for Day 1, the concentration of RNA was much lower than previous samples (Table 6.2). The samples from patients

21 and 23 were thawed during shipment and this may have had detrimental effects on the quality of the RNA obtained from the samples. Additionally, these patients received a lower dose of everolimus than the other patients analysed by microarray, therefore these two patients were excluded from further analysis.

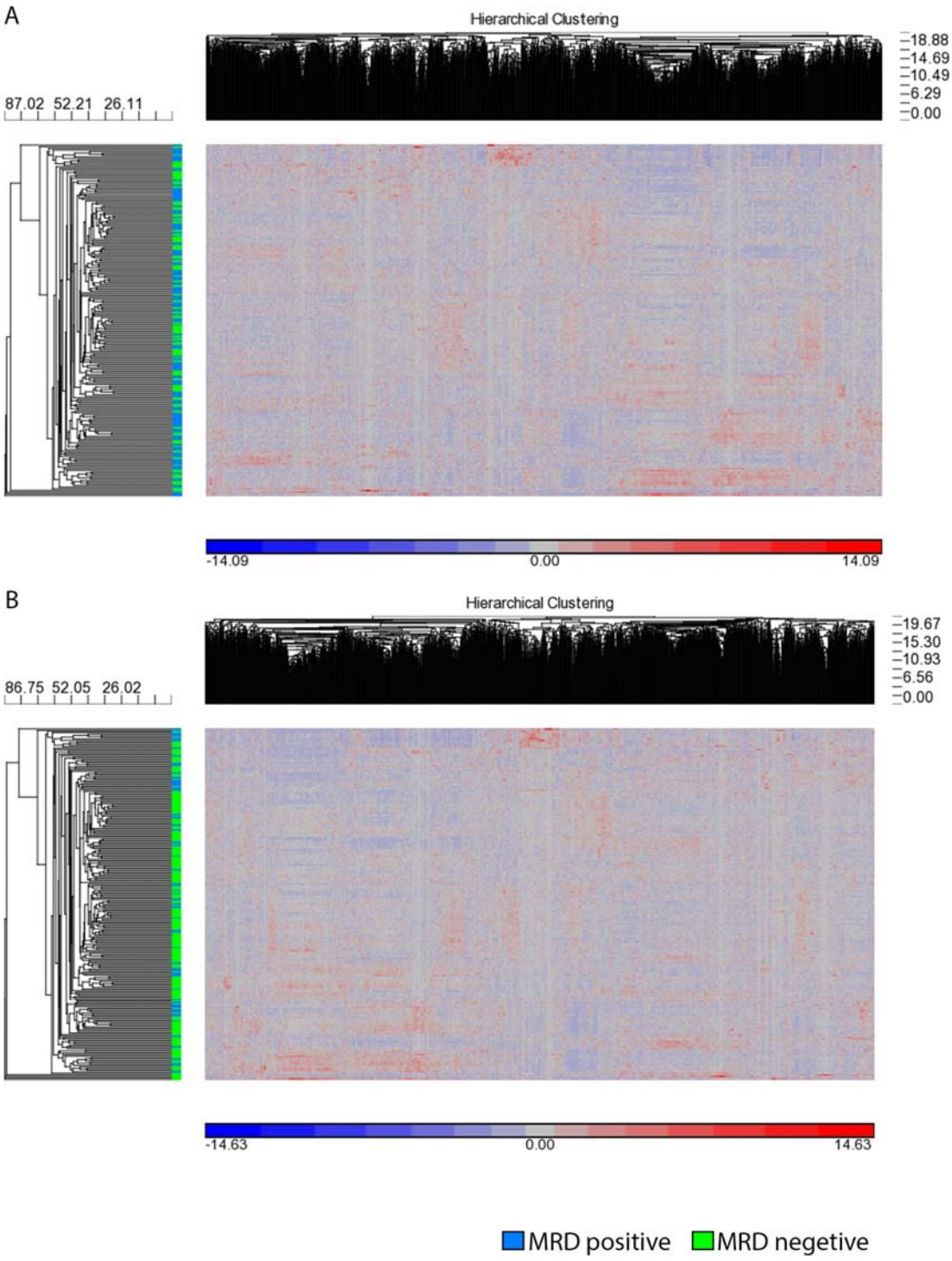

Figure 6.3 CR gene signature does not predict patient MRD status. The CR gene signature was applied to a published dataset of 284 patients with various leukaemia subtypes and MRD assessed at day 19 (A) and 46 (B).

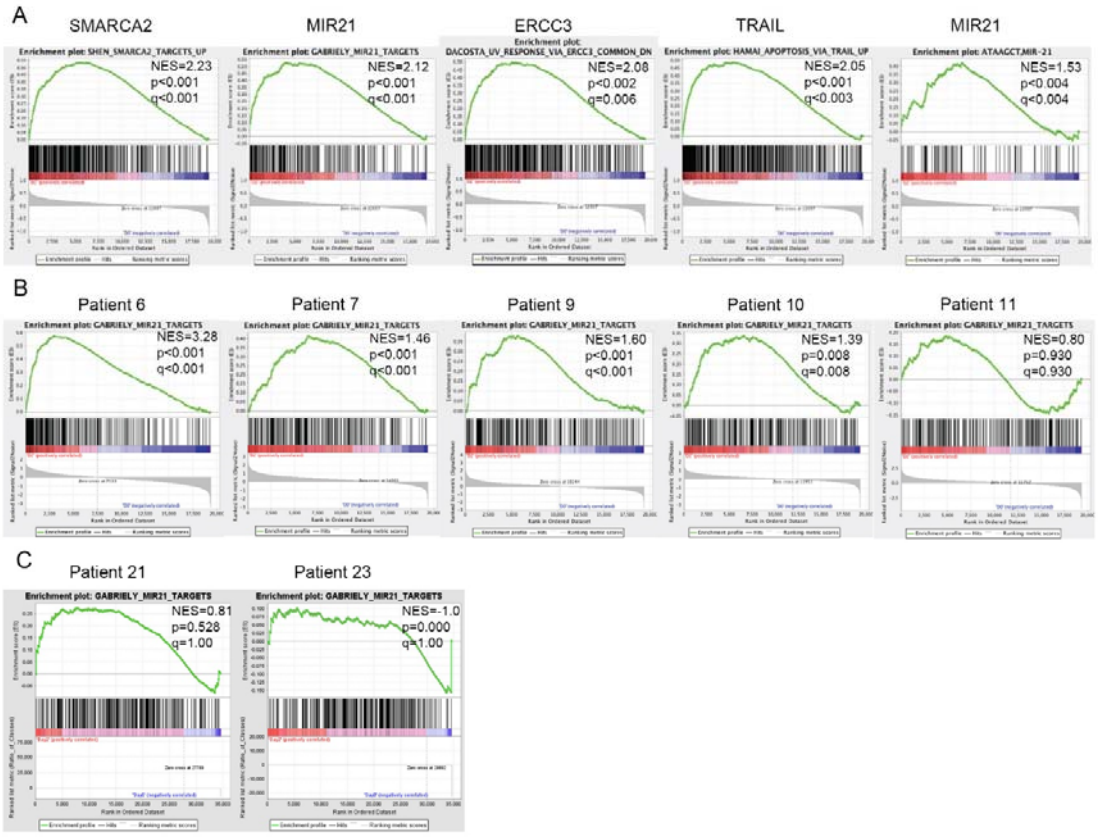

Figure 6.4 GSEA of microarray data of samples collected from (Day 0) and 24 hours after (Day 1) the first dose of everolimus. (A) Columns 1-4 show the top 4 gene signatures (SMARCA2, MIR21, ERCC3, TRAIL) and column 5 the consensus miR-21 signature (GABRIELY_MIR21_TARGETS) when all available samples were analysed. (B) Results for the miR-21 targets for each patient pre- and post-treatment. (C) Consensus miR-21 gene signature in an additional 2 patients.

6.3.3: Expression of miR-21

Expression of miR-21 was assessed using a miR-21 gene expression chip (Methods 2.2.6) in the 5 patients subjected microarray analysis as well as an additional 7 patients, where despite poor quality of the 18s and 26s RNA, small peaks, potentially containing micro RNA, were observed using the Agilent bioanalyser. The signature of miR-21 targets was enriched in day 1 samples from patients 6 to 10, signifying a relative decrease in the activity of miR-21. As observed in the microarray gene signatures, the expression of miR-21 was decreased in patients 6, 7 and 10 after 24 h of everolimus while it was paradoxically increased in patients 9 and 11 (Figure 6.5 A). An increase in miR-21 would be expected to yield decreased expression of downstream targets, yet microarray analysis shows enriched expression in patient 9, a possible explanation may be that the relative expression of miR-21 may be increased but its activity or binding capacity is diminished, leading to the enrichment in target gene expression.

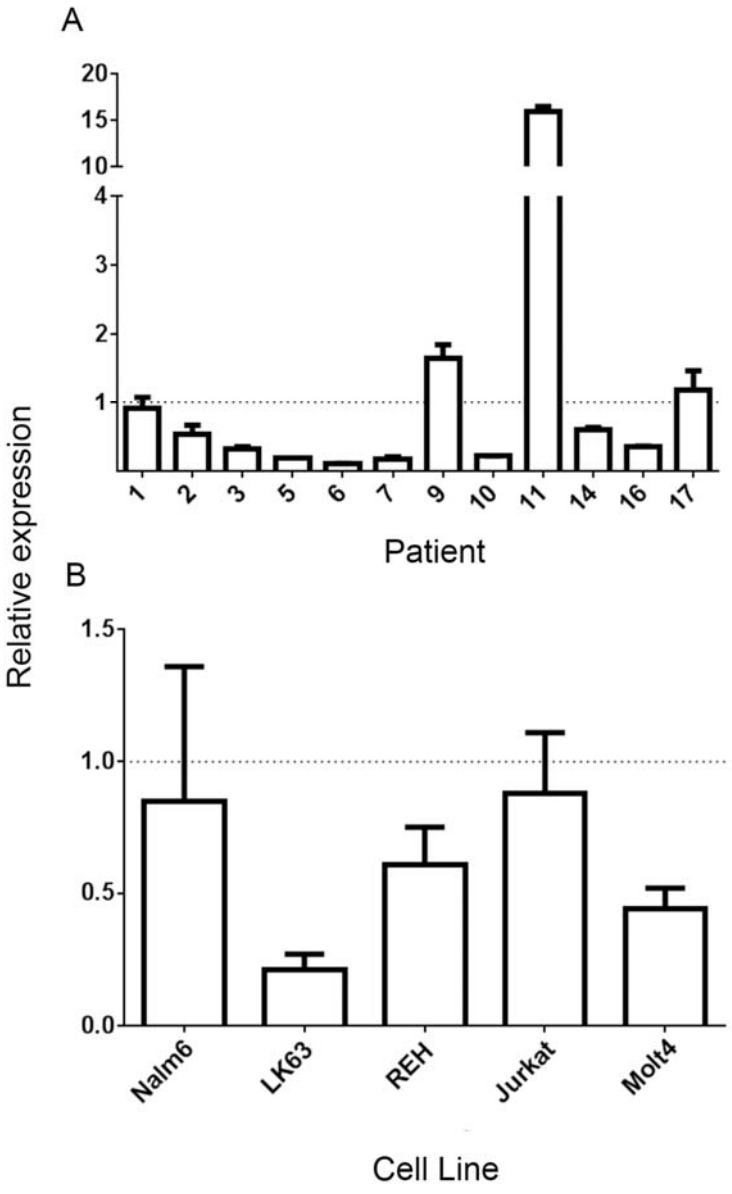

Figure 6.5 miR-21 is downregulated following everolimus treatment. RNA from patients (A) and cell lines (B) before and 24 h after treatment with everolimus was assessed for miR-21 gene expression. miR-21 expression was normalised to the expression of small nucleor RNA U6 (snoU6) and fold change in expression after treatment was calculated with the $2^{-\Delta\Delta ct}$ method.

6.3.4: miR-21 expression and regulation of target genes

As limited patient samples were available, the B and T cell leukemia cell lines NALM6, LK63, REH, Jurkat and Molt4 were used to confirm the effect of everolimus on the expression of miR-21 and its target genes. While LK63, REH and MOLT4 replicated the decrease in miR-21 expression seen in the patient samples after treatment with 4 μM everolimus for 24 h, NALM6 and Jurkat failed to show any significant regulation (Figure 6.5 B). A set of 5 genes regulated by miR-21; PTEN, PEL1, BMPR2, PTAR1 and USP34, were analysed by quantitative RT-PCR to assess the effects of everolimus of miR-21 activity. Two doses of everolimus were used in the cell lines, the *in vitro* IC_{50} dose of 4 μM (Figure 6.6 A), and the peak plasma concentration achieved by the patients enrolled in the trial, 90 nM (Figure 6.6 B). RT-PCR was unsuccessful in demonstrating any effect on these target genes over three separate experiments, despite miR-21 itself being affected in the cell lines.

Due to the unreliability of tissue culture in recapitulating the miR-21 response to everolimus, a more specific array of 86 target sequences was employed to interrogate RNA from two patient samples. Patients 5 and 10 were selected as these patients exhibited differential regulation of miR-21 expression and had sufficient material remaining for analysis. For both patients, the majority of genes analysed were unaffected by treatment with everolimus (Figure 6.7). A small number of these genes were upregulated in patient 5 which may have been due to the effects of miR-21.

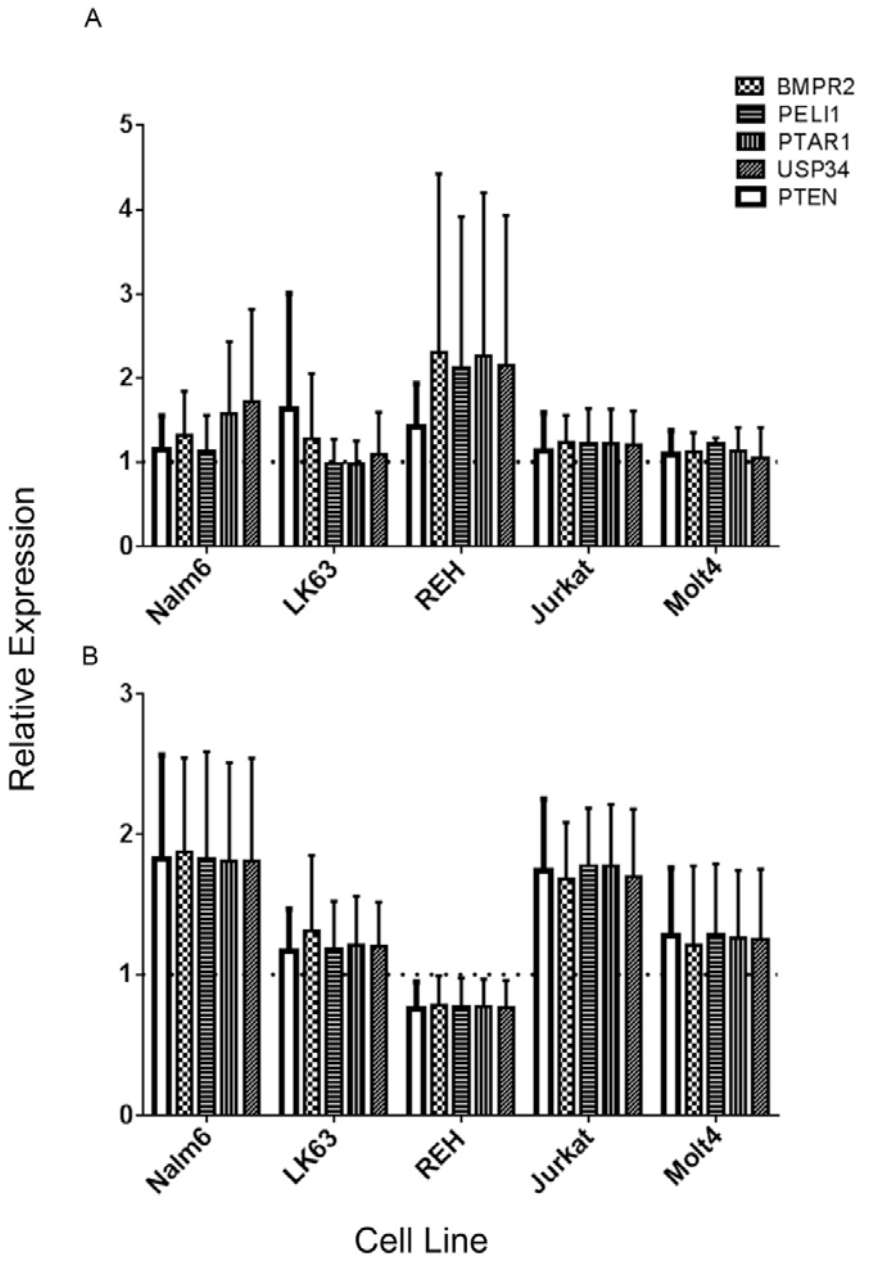

Figure 6.6 Expression of miR-21 targets in cell lines. Cells were treated with everolimus at 4 μM (A) or 90 nM (B) for 24 h and assessed for the expression of the indicated genes by qRT-PCR. Gene expression was normalised to GAPDH and fold change calculated against untreated controls. Bars represent the mean and SD of 3 independent experiments.

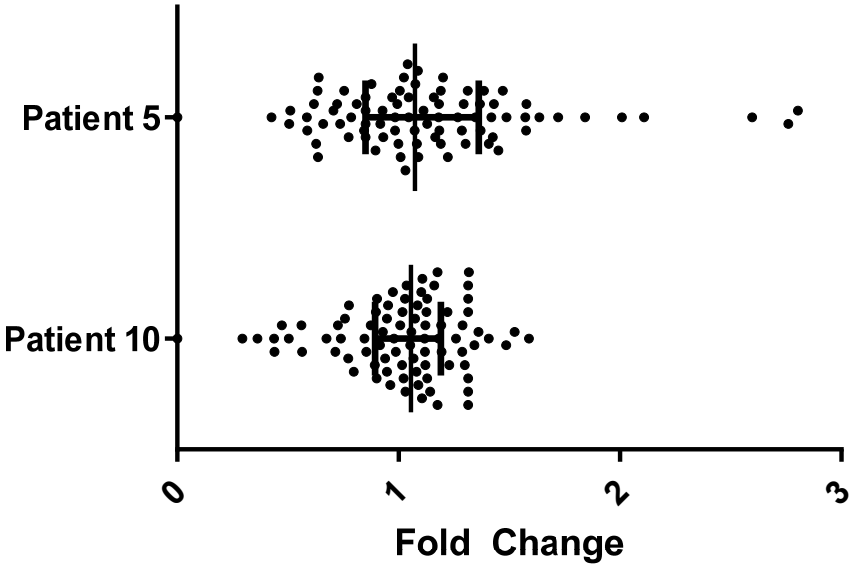

Figure 6.7 Expression of miR-21 targets in patients. Patients were assessed for the expression of 85 target genes of miR-21 by Qiagen RT^2 profiler miR-21 target array. Data represented by a scatter plot with median and interquartile range.

6.4 DISCUSSION

The efficacy of everolimus in treating ALL is well established in pre-clinical models of the disease, however, clinical evidence of its efficacy is lacking. We collaborated with the MD Anderson Cancer Center to investigate the efficacy of everolimus in human ALL and to characterise short-term gene expression changes induced by everolimus and to determine if these correlate with response to mTOR inhibition by everolimus as well as the overall clinical outcome. This project was limited to the analysis of gene expression changes as the only material available was not suitable for other types of studies.

miRNA are small non-coding RNAs that regulate gene expression through binding to the 3' UTR of RNA, and recruit the RNA inducing silencing complex (RISC) to promote RNA degradation [292]. Several miRNAs, such as miR-21, have been reported to have oncogenic potential through the attenuation of tumour suppressor genes such as PTEN. The expression of miR-21 is increased in conditions such as cancer, cardiac injury and response to inflammatory cytokines [293, 294]. Increased levels of miR-21 lead to decreased expression of PTEN, and a subsequent increase in the activity of the downstream signalling pathway of PI3K/Akt/mTOR [295-297]. Pre-clinical studies have highlighted the clinical benefits of miR-21 inhibition as its silencing sensitizes CML cells to imatinib [298] and K562 cells to X-ray irradiation [299].

The genetic signature of miR-21 expression was negatively enriched in patient samples after 24 h of everolimus treatment, suggesting decreased miR-21 activity and thus, an increase in target gene expression. However, the down regulation of miR-21 was not correlated with inhibition of mTOR signalling by everolimus or the overall clinical outcome of patients. ALL is known to induce an inflammatory response in

patients, likely through interaction with the bone marrow microenvironment, leading to the release of pro-inflammatory cytokines such as TNF and IL-6 [300-303]. Everolimus is capable of supressing the immune system and has been successfully used in patients who have undergone a solid organ transplant [304-309]. We hypothesize that the ALL induced inflammation results in increased in miR-21 activity and that the immunosuppressive effects of everolimus abrogate this. The patient samples were taken after a single everolimus dose without chemotherapy, therefore any immunosuppression is a result of mTOR inhibition by everolimus. Nevertheless, these observations arise from a limited patient base and additional patients would need to be studied to confirm whether ALL induced inflammation increases miR-21 expression and activity, and if everolimus abrogates this response.

The gene expression of patients ALL cells was not correlated with inhibition of mTOR by everolimus, although the two patients on whom we had gene expression data that achieved clinical remission exhibited a baseline genetic similarity that separated them from the remainder of the patients. Baseline genetic signatures of patients are gaining increasing attention in order to maximise treatment efficacy through improved risk stratification and optimal therapy selection. However the prognostic power of genetic signatures is limited at the present time [310-312]. Interestingly, one patient who achieved a clinical remission but without recovery of their blood cell counts, failed to separate alongside the other clinical remission patients. However, when the CR gene signature we identified based on the patients studies here was applied to a larger dataset consisting of 180 patients with various ALL subtypes, it was unable to segregate patients based on their MRD status at day 19 or 46. The limited patient dataset used to generate the gene signature severely limits its prognostic capability and acquiring additional gene expression data from more patients is required in order

further strengthen the predictive power of the CR gene signature. Furthermore, the CR gene signature identified in this study may be specific for responses to mTOR inhibition and not applicable to other treatment settings.

The expression of miR-21 and the prognostic power of a baseline gene signature for complete remission may have profound impacts in the clinic, however, the data presented here, although promising, is limited by the number of patients analysed. Gene expression data and corresponding clinical outcome from additional patients will be required to fully characterise miR-21 and the gene signature for complete remission in order to fully elucidate their clinical impact.

CHAPTER 7 CONCLUSION

ALL is one of the success stories of modern oncology with patients achieving high remission rates with current treatment protocols [34, 313]. However, the relapse rate for both children and adults remains high and the outcome for those patients is often very poor [314]. The dose limiting toxicities of current therapies make further intensification impractical and therefore new agents are required in order to further increase patient survival. The mTOR pathway offers an attractive target for novel therapies as it is hyper-activated in many cancers, including ALL [67, 85, 315], and its inhibition is efficacious in prolonging survival in pre-clinical models of ALL [65, 125, 128, 129, 316]. This efficacy has led to the use of everolimus in several clinical trials in many different cancers, including ALL [133]. It has been demonstrated in this thesis that prolonged exposure to the mTOR inhibitor everolimus *in vivo* can result in the development of resistance, with two of three patient derived ALL xenografts displaying resistance. The mechanism by which these cells have developed resistance needs to be characterised and overcome to maximize the clinical application of these agents.

ALL is a clonal disease [190, 191] and resistance is thought to occur through the selection of pre-existing resistant clones that have been exposed to prolonged treatment or through the selection of a clone that has acquired a resistance-conferring trait [192-194]. Several mechanisms by which these clones become resistant to mTOR inhibitors have been proposed, including mutations that reduce the binding capability of the compound and the dysregulation of the expression and/or activity of several proteins up and downstream of mTOR [62, 168, 186, 317]. However, we could not identify, with significant certainty, any mutations solely present within resistant cells. Therefore, it is possible that resistance to everolimus arises due to the aberrant expression or activity of genes or proteins.

The two everolimus resistant xenografts analysed in this study did not appear to share a common resistance phenotype, with the expression of genes and proteins being quite dissimilar. Despite this limited overlap, pathways involved in cellular adhesion were a common feature in both of the everolimus resistant xenografts. Adhesion to the microenvironment provides survival signals that are important for the growth and survival of ALL cells both *in vitro* and *in vivo* [104, 107]. Moreover, increased adhesion has been implicated in the development of resistance to chemotherapeutic compounds [170-172, 176]. Adhesion of ALL cells to the bone marrow microenvironment is highly complex and not fully understood, but interruption of this interaction enhances the efficacy of some therapeutic compounds [175, 201]. Although pathways involved in the regulation of cellular adhesion were repeatedly found to be upregulated in resistant xenografts, the surface factors involved remain elusive.

The difference in survival rates of mice engrafted with the two resistant xenografts and the cell cycle distribution of the resistant cells further exemplified the dissimilar mechanisms by which resistance developed in these cells. Interestingly, there was also discordance amongst the cell cycle profiles of the xenografts between the various tissues analysed. Tissue specific microenvironments, such as those offered by the spleen and bone marrow, likely express different factors and hence provide distinct interactions with ALL cells resulting in different effects on the behaviour of ALL cells [279, 318-320]. Normal hematopoiesis can occur in the spleen under certain circumstances and ALL cells accumulate in this tissue [25, 128, 278]. Analysis of gene and protein expression involved in the development of resistance was performed using leukaemic cells isolated from the spleens of sacrificed animals. If interactions between different microenvironments can have different effects on the behaviour of ALL cells, comparing the gene and protein expression from a single tissue, as done in this thesis,

may not fully characterise the mechanism by which these cells have developed resistance to everolimus. Comparing the expression of genes and proteins from cells isolated from the spleen to others tissues known to support ALL cells such as the liver and bone marrow may further the understanding of how ALL cells behave within various tissue specific microenvironments. Yet, technical challenges limit the use of shotgun based sequencing methods for transcriptome and proteome analysis on some tissues. Mass spectrometry based proteomics requires large amounts of input protein to identify proteins with statistical certainty. In addition, isolating enough cells from tissues such as the blood and liver to identify possible mechanisms of resistance with statistical confidence may not be feasible. The microenvironment within the bone marrow is fairly well characterised, however, it is far from being fully understood, whereas the splenic microenvironment, remains poorly characterised. These microenvironments provided by the various tissues play a major role in the development of resistance to everolimus and additional investigation is required if resistance to everolimus is to be fully understood.

The major limitation of this study is the limited number samples used to characterise resistance to everolimus in both the murine model of ALL as well as human subjects. Assessing additional ALL xenografts for their capability to develop resistance to everolimus and the characterisation those cells may allow this complex puzzle to be unravelled. We were unable to correlate the findings from the murine model of ALL with human patients. The resistance that developed in ALL xenografts was established through the long-term treatment of the animals with everolimus. However, due to the clinical trial protocol and abscence of viable cells from trial patients, we have only analysed the effects of short-term treatment with everolimus. Moreover, many samples sent were not analysed due to degradation of the samples during shipment. Increasing

the number of patients analysed would increase the statistical confidence of the findings. Furthermore, it is possible that long-term follow up of patients with prolonged exposure to everolimus may reveal whether resistance to everolimus will develop in these patients.

A new generation of inhibitors of the kinase region of mTOR offer additional benefits over allosteric mTOR inhibitors such as everolimus, and these are gaining increased attention for clinical use. As they inhibit the kinase region, both mTOR complexes are inhibited, thus eliminating the activation of the negative feedback loop onto Akt. However, resistance to these inhibitors is also beginning to emerge [118, 321]. Increased understanding of the development of resistance to everolimus may also provide insights into the development of resistance to other allosteric inhibiors on mTOR as well as the newer generation of mTOR kinase domain inhbitors. Further work involving additional everolimus resistant ALL xenografts is required to fully understand how resistance to mTOR inhibition develops in these cells. Only then can effective countermeasures be developed that can be translate into the clinic to improve patient outcome.

REFERENCES

1. Karlsson, S. *Hemato-Linné Research Groups: Stefan Karlsson*. 2010 15/02/2010 4/4/2010]; Available from: http://www.med.lu.se/hemato_linne/research_groups/stefan_karlsson.
2. Kiel, M.J. and S.J. Morrison, *Uncertainty in the niches that maintain haematopoietic stem cells.* Nat Rev Immunol, 2008. **8**(4): p. 290-301.
3. Sugiyama, T., et al., *Maintenance of the hematopoietic stem cell pool by CXCL12-CXCR4 chemokine signaling in bone marrow stromal cell niches.* Immunity, 2006. **25**(6): p. 977-88.
4. Passegue, E., et al., *Normal and leukemic hematopoiesis: are leukemias a stem cell disorder or a reacquisition of stem cell characteristics?* Proc Natl Acad Sci U S A, 2003. **100 Suppl 1**: p. 11842-9.
5. Schofield, R., *The relationship between the spleen colony-forming cell and the haemopoietic stem cell.* Blood Cells, 1978. **4**(1-2): p. 7-25.
6. RamÌrez, J., K. Lukin, and J. Hagman, *From hematopoietic progenitors to B cells: mechanisms of lineage restriction and commitment.* Current Opinion in Immunology, 2010. **In Press, Corrected Proof**.
7. Kosan, C. and M. Godmann, *Genetic and Epigenetic Mechanisms That Maintain Hematopoietic Stem Cell Function.* Stem Cells Int, 2016. **2016**: p. 5178965.
8. Warr, M.R., E.M. Pietras, and E. Passegue, *Mechanisms controlling hematopoietic stem cell functions during normal hematopoiesis and hematological malignancies.* Wiley Interdiscip Rev Syst Biol Med, 2011. **3**(6): p. 681-701.
9. Ma, Q., D. Jones, and T.A. Springer, *The chemokine receptor CXCR4 is required for the retention of B lineage and granulocytic precursors within the bone marrow microenvironment.* Immunity, 1999. **10**(4): p. 463-71.
10. Zetterblad, J., et al., *Genomics based analysis of interactions between developing B-lymphocytes and stromal cells reveal complex interactions and two-way communication.* BMC Genomics, 2010. **11**: p. 108.
11. Meffre, E., R. Casellas, and M.C. Nussenzweig, *Antibody regulation of B cell development.* Nat Immunol, 2000. **1**(5): p. 379-85.
12. Nagasawa, T., H. Kikutani, and T. Kishimoto, *Molecular cloning and structure of a pre-B-cell growth-stimulating factor.* Immunology, 1994. **91**(2305-2309).
13. Anthony, B.A. and D.C. Link, *Regulation of hematopoietic stem cells by bone marrow stromal cells.* Trends Immunol, 2014. **35**(1): p. 32-7.
14. Ichii, M., K. Oritani, and Y. Kanakura, *Early B lymphocyte development: Similarities and differences in human and mouse.* World Journal of Stem Cells, 2014. **6**(4): p. 421-431.
15. Ansel, K.M. and J.G. Cyster, *Chemokines in lymphopoiesis and lymphoid organ development.* Current Opinion in Immunology, 2001. **13**(2): p. 172-179.
16. Blank, U. and S. Karlsson, *TGF-beta signaling in the control of hematopoietic stem cells.* Blood, 2015. **125**(23): p. 3542-50.
17. Yamazaki, S. and H. Nakauchi, *Bone marrow Schwann cells induce hematopoietic stem cell hibernation.* Int J Hematol, 2014. **99**(6): p. 695-8.
18. Clark, M.R., et al., *Orchestrating B cell lymphopoiesis through interplay of IL-7 receptor and pre-B cell receptor signalling.* Nat Rev Immunol, 2014. **14**(2): p. 69-80.

19. Johnson, S.E., et al., *Murine and Human IL-7 Activate STAT5 and Induce Proliferation of Normal Human Pro-B Cells.* The Journal of Immunology, 2005. **175**(11): p. 7325-7331.
20. Fry, T.J. and C.L. Mackall, *The many faces of IL-7: from lymphopoiesis to peripheral T cell maintenance.* J Immunol, 2005. **174**(11): p. 6571-6.
21. Kikushige, Y., et al., *Human Flt3 is expressed at the hematopoietic stem cell and the granulocyte/macrophage progenitor stages to maintain cell survival.* J Immunol, 2008. **180**(11): p. 7358-67.
22. Nakamori, Y., et al., *Human bone marrow stromal cells simultaneously support B and T/NK lineage development from human haematopoietic progenitors: a principal role for flt3 ligand in lymphopoiesis.* British Journal of Haematology, 2012. **157**(6): p. 674-686.
23. Linabery, A.M. and J.A. Ross, *Trends in childhood cancer incidence in the U.S. (1992-2004).* Cancer, 2008. **112**(2): p. 416-432.
24. Gaynon, P.S., et al., *Long-term results of the children's cancer group studies for childhood acute lymphoblastic leukemia 1983-2002: a Children's Oncology Group Report.* Leukemia, 2010. **24**(2): p. 285-97.
25. Lustosa de Sousa, D.W., et al., *Acute lymphoblastic leukemia in children and adolescents: prognostic factors and analysis of survival.* Revista Brasileira de Hematologia e Hemoterapia, 2015. **37**(4): p. 223-229.
26. Pulte, D., A. Gondos, and H. Brenner, *Improvement in survival in younger patients with acute lymphoblastic leukemia from the 1980s to the early 21st century.* Blood, 2009. **113**(7): p. 1408-11.
27. Pulte, D., et al., *Survival of adults with acute lymphoblastic leukemia in Germany and the United States.* PLoS One, 2014. **9**(1): p. e85554.
28. Ustwani, O.A., et al., *Clinical updates in adult acute lymphoblastic leukemia.* Crit Rev Oncol Hematol, 2015.
29. Pui, C.-H., L.L. Robison, and A.T. Look, *Acute lymphoblastic leukaemia.* The Lancet. **371**(9617): p. 1030-1043.
30. Ghazavi, F., et al., *Molecular basis and clinical significance of genetic aberrations in B-cell precursor acute lymphoblastic leukemia.* Exp Hematol, 2015. **43**(8): p. 640-53.
31. Mullighan, C.G., *The molecular genetic makeup of acute lymphoblastic leukemia.* Hematology Am Soc Hematol Educ Program, 2012. **2012**: p. 389-96.
32. Pui, C.H., *Recent research advances in childhood acute lymphoblastic leukemia.* J Formos Med Assoc, 2010. **109**(11): p. 777-87.
33. Pui, C.H., et al., *Childhood Acute Lymphoblastic Leukemia: Progress Through Collaboration.* J Clin Oncol, 2015. **33**(27): p. 2938-48.
34. Pui, C.-H., et al., *Pediatric acute lymphoblastic leukemia: where are we going and how do we get there?* Blood, 2012. **120**(6): p. 1165-1174.
35. Boissel, N. and L.S. Sender, *Best Practices in Adolescent and Young Adult Patients with Acute Lymphoblastic Leukemia: A Focus on Asparaginase.* J Adolesc Young Adult Oncol, 2015. **4**(3): p. 118-28.
36. Guru Murthy, G.S., R. Venkitachalam, and P. Mehta, *Trends in survival outcomes of B-lineage acute lymphoblastic leukemia in elderly patients: analysis of Surveillance, Epidemiology, and End Results database.* Leuk Lymphoma, 2015. **56**(8): p. 2296-300.
37. Gokbuget, N. and D. Hoelzer, *.* Semin Hematol, 2009. **46**(1): p. 64-75.

38. Pulte, D., et al., *Recent trends in survival of adult patients with acute leukemia: overall improvements, but persistent and partly increasing disparity in survival of patients from minority groups.* Haematologica, 2013. **98**(2): p. 222-9.
39. Fielding, A.K. and A.H. Goldstone, *Allogeneic haematopoietic stem cell transplant in Philadelphia-positive acute lymphoblastic leukaemia.* Bone Marrow Transplant, 2008. **41**(5): p. 447-53.
40. Roberts, K.G., et al., *Targetable kinase-activating lesions in Ph-like acute lymphoblastic leukemia.* N Engl J Med, 2014. **371**(11): p. 1005-15.
41. Maude, S.L., et al., *Targeting JAK1/2 and mTOR in murine xenograft models of Ph-like acute lymphoblastic leukemia.* Blood, 2012. **120**(17): p. 3510-8.
42. Roberts, K.G., et al., *Genetic alterations activating kinase and cytokine receptor signaling in high-risk acute lymphoblastic leukemia.* Cancer Cell, 2012. **22**(2): p. 153-66.
43. Den Boer, M.L., et al., *A subtype of childhood acute lymphoblastic leukaemia with poor treatment outcome: a genome-wide classification study.* Lancet Oncol, 2009. **10**(2): p. 125-34.
44. Hoelzer, D., *Targeted therapy with monoclonal antibodies in acute lymphoblastic leukemia.* Curr Opin Oncol, 2013. **25**(6): p. 701-6.
45. Jabbour, E., et al., *Monoclonal antibodies in acute lymphoblastic leukemia.* Blood, 2015. **125**(26): p. 4010-6.
46. Portell, C.A. and A.S. Advani, *Antibody therapy for acute lymphoblastic leukemia.* Curr Hematol Malig Rep, 2012. **7**(2): p. 153-9.
47. Batlevi, C.L., et al., *Novel immunotherapies in lymphoid malignancies.* Nat Rev Clin Oncol, 2016. **13**(1): p. 25-40.
48. Cruz, C.R., et al., *Infusion of donor-derived CD19-redirected virus-specific T cells for B-cell malignancies relapsed after allogeneic stem cell transplant: a phase 1 study.* Blood, 2013. **122**(17): p. 2965-73.
49. Davila, M.L., et al., *CD19 CAR-targeted T cells induce long-term remission and B Cell Aplasia in an immunocompetent mouse model of B cell acute lymphoblastic leukemia.* PLoS One, 2013. **8**(4): p. e61338.
50. Kochenderfer, J.N., et al., *B-cell depletion and remissions of malignancy along with cytokine-associated toxicity in a clinical trial of anti-CD19 chimeric-antigen-receptor-transduced T cells.* Blood, 2012. **119**(12): p. 2709-20.
51. Lee, J.C., et al., *In vivo inhibition of human CD19-targeted effector T cells by natural T regulatory cells in a xenotransplant murine model of B cell malignancy.* Cancer Res, 2011. **71**(8): p. 2871-81.
52. Sadelain, M., et al., *CD19 CAR Therapy for Acute Lymphoblastic Leukemia.* Am Soc Clin Oncol Educ Book, 2015: p. e360-3.
53. Nagorsen, D. and P.A. Baeuerle, *Immunomodulatory therapy of cancer with T cell-engaging BiTE antibody blinatumomab.* Exp Cell Res, 2011. **317**(9): p. 1255-60.
54. Newman, M.J. and D.J. Benani, *A review of blinatumomab, a novel immunotherapy.* J Oncol Pharm Pract, 2015.
55. Schlegel, P., et al., *Pediatric posttransplant relapsed/refractory B-precursor acute lymphoblastic leukemia shows durable remission by therapy with the T-cell engaging bispecific antibody blinatumomab.* Haematologica, 2014. **99**(7): p. 1212-9.
56. Topp, M.S., et al., *Safety and activity of blinatumomab for adult patients with relapsed or refractory B-precursor acute lymphoblastic leukaemia: a multicentre, single-arm, phase 2 study*. Lancet Oncol, 2015. **16**(1): p. 57-66.

57. Topp, M.S., et al., *Phase II trial of the anti-CD19 bispecific T cell-engager blinatumomab shows hematologic and molecular remissions in patients with relapsed or refractory B-precursor acute lymphoblastic leukemia.* J Clin Oncol, 2014. **32**(36): p. 4134-40.
58. Zugmaier, G., et al., *Long-term survival and T-cell kinetics in relapsed/refractory ALL patients who achieved MRD response after blinatumomab treatment.* Blood, 2015. **126**(24): p. 2578-84.
59. Henderson, M.J., et al., *Mechanism of relapse in pediatric acute lymphoblastic leukemia.* Cell Cycle, 2008. **7**(10): p. 1315-1320.
60. Ma, X., et al., *Rise and fall of subclones from diagnosis to relapse in pediatric B-acute lymphoblastic leukaemia.* Nat Commun, 2015. **6**: p. 6604.
61. Gingras, A.C., B. Raught, and N. Sonenberg, *Regulation of translation initiation by FRAP/mTOR.* Genes Dev, 2001. **15**(7): p. 807-26.
62. Huang, S., M.A. Bjornsti, and P.J. Houghton, *Rapamycins: mechanism of action and cellular resistance.* Cancer Biol Ther, 2003. **2**(3): p. 222-32.
63. Laplante, M. and David M. Sabatini, *mTOR Signaling in Growth Control and Disease.* Cell, 2012. **149**(2): p. 274-293.
64. Keshwani, M.M., X. Gao, and T.K. Harris, *Mechanism of PDK1-catalyzed Thr-229 phosphorylation of the S6K1 protein kinase.* J Biol Chem, 2009. **284**(34): p. 22611-24.
65. Saunders, P., et al., *The mammalian target of rapamycin inhibitor RAD001 (everolimus) synergizes with chemotherapeutic agents, ionizing radiation and proteasome inhibitors in pre-B acute lymphocytic leukemia.* Haematologica, 2011. **96**(1): p. 69-77.
66. Schalm, S.S. and J. Blenis, *Identification of a Conserved Motif Required for mTOR Signaling.* Current Biology, 2002. **12**(8): p. 632-639.
67. Vivanco, I. and C.L. Sawyers, *The phosphatidylinositol 3-Kinase AKT pathway in human cancer.* Nat Rev Cancer, 2002. **2**(7): p. 489-501.
68. Kim, D.H., et al., *mTOR interacts with raptor to form a nutrient-sensitive complex that signals to the cell growth machinery.* Cell, 2002. **110**(2): p. 163-75.
69. Azim, H., H.A. Azim, Jr., and B. Escudier, *Targeting mTOR in cancer: renal cell is just a beginning.* Target Oncol, 2010. **5**(4): p. 269-80.
70. Bjornsti, M.A. and P.J. Houghton, *The TOR pathway: a target for cancer therapy.* Nat Rev Cancer, 2004. **4**(5): p. 335-48.
71. Findlay, G.M., L.S. Harrington, and R.F. Lamb, *TSC1-2 tumour suppressor and regulation of mTOR signalling: linking cell growth and proliferation?* Current Opinion in Genetics & Development, 2005. **15**(1): p. 69-76.
72. Huang, J. and B.D. Manning, *The TSC1-TSC2 complex: a molecular switchboard controlling cell growth.* Biochem J, 2008. **412**(2): p. 179-90.
73. Kwiatkowski, D.J., *Rhebbing up mTOR: new insights on TSC1 and TSC2, and the pathogenesis of tuberous sclerosis.* Cancer Biol Ther, 2003. **2**(5): p. 471-6.
74. Saucedo, L.J., et al., *Rheb promotes cell growth as a component of the insulin/TOR signalling network.* Nat Cell Biol, 2003. **5**(6): p. 566-71.
75. Magnuson, B., B. Ekim, and D.C. Fingar, *Regulation and function of ribosomal protein S6 kinase (S6K) within mTOR signalling networks.* Biochem J, 2012. **441**(1): p. 1-21.
76. Hay, N. and N. Sonenberg, *Upstream and downstream of mTOR.* Genes Dev, 2004. **18**(16): p. 1926-45.

77. Ali, S.M. and D.M. Sabatini, *Structure of S6 kinase 1 determines whether raptor-mTOR or rictor-mTOR phosphorylates its hydrophobic motif site.* J Biol Chem, 2005. **280**(20): p. 19445-8.
78. Wang, J., et al., *Crystal structures of S6K1 provide insights into the regulation mechanism of S6K1 by the hydrophobic motif.* Biochem J, 2013. **454**(1): p. 39-47.
79. Zhang, H., et al., *Mitogen-independent phosphorylation of S6K1 and decreased ribosomal S6 phosphorylation in senescent human fibroblasts.* Exp Cell Res, 2000. **259**(1): p. 284-92.
80. Julien, L.A., et al., *mTORC1-activated S6K1 phosphorylates Rictor on threonine 1135 and regulates mTORC2 signaling.* Mol Cell Biol, 2010. **30**(4): p. 908-21.
81. Hou, Z., L. He, and R.Z. Qi, *Regulation of s6 kinase 1 activation by phosphorylation at ser-411.* J Biol Chem, 2007. **282**(10): p. 6922-8.
82. Dancey, J., *mTOR signaling and drug development in cancer.* Nat Rev Clin Oncol, 2010. **7**(4): p. 209-19.
83. Oh, W.J. and E. Jacinto, *mTOR complex 2 signaling and functions.* Cell Cycle, 2011. **10**(14): p. 2305-16.
84. Weber, J.D. and D.H. Gutmann, *Deconvoluting mTOR biology.* Cell Cycle, 2012. **11**(2): p. 236-48.
85. Populo, H., J.M. Lopes, and P. Soares, *The mTOR Signalling Pathway in Human Cancer.* Int J Mol Sci, 2012. **13**(2): p. 1886-918.
86. Willems, L., et al., *PI3K and mTOR signaling pathways in cancer: new data on targeted therapies.* Curr Oncol Rep, 2012. **14**(2): p. 129-38.
87. Huang, J., et al., *The TSC1-TSC2 complex is required for proper activation of mTOR complex 2.* Mol Cell Biol, 2008. **28**(12): p. 4104-15.
88. Su, B. and E. Jacinto, *Mammalian TOR signaling to the AGC kinases.* Crit Rev Biochem Mol Biol, 2011. **46**(6): p. 527-47.
89. Heikamp, E.B., et al., *The AGC kinase SGK1 regulates TH1 and TH2 differentiation downstream of the mTORC2 complex.* Nat Immunol, 2014. **15**(5): p. 457-64.
90. Laplante, M. and D.M. Sabatini, *mTOR signaling at a glance.* Journal of Cell Science, 2009. **122**(20): p. 3589-3594.
91. Sarbassov, D.D., S.M. Ali, and D.M. Sabatini, *Growing roles for the mTOR pathway.* Curr Opin Cell Biol, 2005. **17**(6): p. 596-603.
92. Cargnello, M., J. Tcherkezian, and P.P. Roux, *The expanding role of mTOR in cancer cell growth and proliferation.* Mutagenesis, 2015. **30**(2): p. 169-76.
93. Fransecky, L., L.H. Mochmann, and C.D. Baldus, *Outlook on PI3K/AKT/mTOR inhibition in acute leukemia.* Molecular and cellular therapies, 2015. **3**: p. 2.
94. Mahmoud, I.S., et al., *The transforming mutation E17K/AKT1 is not a major event in B-cell-derived lymphoid leukaemias.* Br J Cancer, 2008. **99**(3): p. 488-90.
95. Shojaee, S., et al., *PTEN Is Essential for Normal Cytokine Signaling and Oncogenic Transformation of Pre-B Cells.* Blood, 2014. **124**(21): p. 262-262.
96. Jenkinson, S., et al., *Impact of PTEN abnormalities on outcome in pediatric patients with T-cell acute lymphoblastic leukemia treated on the MRC UKALL2003 trial.* Leukemia, 2016. **30**(1): p. 39-47.
97. Guo, D., et al., *Notch-1 regulates Akt signaling pathway and the expression of cell cycle regulatory proteins cyclin D1, CDK2 and p21 in T-ALL cell lines.* Leuk Res, 2009. **33**(5): p. 678-85.

98. Chan, S.M., et al., *Notch signals positively regulate activity of the mTOR pathway in T-cell acute lymphoblastic leukemia.* Blood, 2007. **110**(1): p. 278-286.
99. Tasian, S.K., D.T. Teachey, and S.R. Rheingold, *Targeting the PI3K/mTOR Pathway in Pediatric Hematologic Malignancies.* Front Oncol, 2014. **4**: p. 108.
100. Dinner, S. and L.C. Platanias, *Targeting the mTOR Pathway in Leukemia.* J Cell Biochem, 2016.
101. Rota, L.M. and T.L. Wood, *Crosstalk of the Insulin-Like Growth Factor Receptor with the Wnt Signaling Pathway in Breast Cancer.* Front Endocrinol (Lausanne), 2015. **6**: p. 92.
102. Batista, A., et al., *Notch pathway is regulated by leukemia microenvironmental cues and positively modulates IL-7 signaling.* Molecular Cancer Therapeutics, 2007. **6**(11 Supplement): p. C295.
103. Chapuis, N., et al., *Perspectives on inhibiting mTOR as a future treatment strategy for hematological malignancies.* Leukemia, 2010. **24**(10): p. 1686-99.
104. Manabe, A., et al., *Bone marrow-derived stromal cells prevent apoptotic cell death in B-lineage acute lymphoblastic leukemia.* Blood, 1992. **79**(9): p. 2370-7.
105. Barata, J.T., et al., *Activation of PI3K is indispensable for interleukin 7-mediated viability, proliferation, glucose use, and growth of T cell acute lymphoblastic leukemia cells.* J Exp Med, 2004. **200**(5): p. 659-69.
106. Juarez, J., et al., *Interaction of interleukin-7 and interleukin-3 with the CXCL12-induced proliferation of B-cell progenitor acute lymphoblastic leukemia.* Haematologica, 2007. **92**(4): p. 450-9.
107. Juarez, J., et al., *Effects of inhibitors of the chemokine receptor CXCR4 on acute lymphoblastic leukemia cells in vitro.* Leukemia, 2003. **17**(17): p. 1294-1300.
108. Ziegler, M.E., et al., *mTORC2 mediates CXCL12-induced angiogenesis.* Angiogenesis, 2016.
109. Yang, X., et al., *Mammalian target of rapamycin inhibitor rapamycin enhances anti-leukemia effect of imatinib on Ph+ acute lymphoblastic leukemia cells.* Eur J Haematol, 2014. **92**(2): p. 111-20.
110. Hirase, C., et al., *Hypersensitivity of Ph-positive lymphoid cell lines to rapamycin: Possible clinical application of mTOR inhibitor.* Leuk Res, 2009. **33**(3): p. 450-9.
111. Tasian, S.K., et al., *Aberrant STAT5 and PI3K/mTOR pathway signaling occurs in human CRLF2-rearranged B-precursor acute lymphoblastic leukemia.* Blood, 2012. **120**(4): p. 833-842.
112. Armengol, G., et al., *4E-binding protein 1: a key molecular "funnel factor" in human cancer with clinical implications.* Cancer Res, 2007. **67**(16): p. 7551-5.
113. Bjornsti, M.A. and P.J. Houghton, *Lost in translation: dysregulation of cap-dependent translation and cancer.* Cancer Cell, 2004. **5**(6): p. 519-23.
114. Populo, H., et al., *mTOR pathway activation in cutaneous melanoma is associated with poorer prognosis characteristics.* Pigment Cell Melanoma Res, 2011. **24**(1): p. 254-7.
115. Hsieh, A.C., et al., *Genetic dissection of the oncogenic mTOR pathway reveals druggable addiction to translational control via 4EBP-eIF4E.* Cancer Cell, 2010. **17**(3): p. 249-61.

116. Hsieh, A.C., et al., *Cell type-specific abundance of 4EBP1 primes prostate cancer sensitivity or resistance to PI3K pathway inhibitors.* Sci Signal, 2015. **8**(403): p. ra116.
117. Truitt, M.L., et al., *Differential Requirements for eIF4E Dose in Normal Development and Cancer.* Cell, 2015. **162**(1): p. 59-71.
118. Mallya, S., et al., *Resistance to mTOR Kinase Inhibitors in Lymphoma Cells Lacking 4EBP1.* PLoS ONE, 2014. **9**(2): p. e88865.
119. Barger, J.F., et al., *S6K1 determines the metabolic requirements for BCR-ABL survival.* Oncogene, 2013. **32**(4): p. 453-61.
120. Perez-Tenorio, G., et al., *Clinical potential of the mTOR targets S6K1 and S6K2 in breast cancer.* Breast Cancer Res Treat, 2011. **128**(3): p. 713-23.
121. Hietakangas, V. and S.M. Cohen, *TOR complex 2 is needed for cell cycle progression and anchorage-independent growth of MCF7 and PC3 tumor cells.* BMC Cancer, 2008. **8**: p. 282.
122. Masri, J., et al., *mTORC2 activity is elevated in gliomas and promotes growth and cell motility via overexpression of rictor.* Cancer Res, 2007. **67**(24): p. 11712-20.
123. Avellino, R., et al., *Rapamycin stimulates apoptosis of childhood acute lymphoblastic leukemia cells.* Blood, 2005. **106**(4): p. 1400-6.
124. Crazzolara, R., K.F. Bradstock, and L.J. Bendall, *RAD001 (Everolimus) induces autophagy in acute lymphoblastic leukemia.* Autophagy, 2009. **5**(5): p. 727-8.
125. Neri, L.M., et al., *Targeting the PI3K/Akt/mTOR signaling pathway in B-precursor acute lymphoblastic leukemia and its therapeutic potential.* Leukemia, 2014. **28**(4): p. 739-48.
126. Teachey, D.T., et al., *The mTOR inhibitor CCI-779 induces apoptosis and inhibits growth in preclinical models of primary adult human ALL.* Blood, 2006. **107**(3): p. 1149-55.
127. Baraz, R., et al., *mTOR inhibition by everolimus in childhood acute lymphoblastic leukemia induces caspase-independent cell death.* PLoS One, 2014. **9**(7): p. e102494.
128. Crazzolara, R., et al., *Potentiating effects of RAD001 (Everolimus) on vincristine therapy in childhood acute lymphoblastic leukemia.* Blood, 2009. **113**(14): p. 3297-306.
129. Saunders, P.O., et al., *RAD001 (everolimus) induces dose-dependent changes to cell cycle regulation and modifies the cell cycle response to vincristine.* Oncogene, 2013. **32**(40): p. 4789-97.
130. Wong, J., et al., *Efficacy of dual PI-3K and mTOR inhibitors in vitro and in vivo in acute lymphoblastic leukemia.* Oncotarget, 2014. **5**(21): p. 10460-72.
131. Teachey, D.T., et al., *mTOR inhibitors are synergistic with methotrexate: an effective combination to treat acute lymphoblastic leukemia.* Blood, 2008. **112**(5): p. 2020-3.
132. Yee, K.W., et al., *Phase I/II study of the mammalian target of rapamycin inhibitor everolimus (RAD001) in patients with relapsed or refractory hematologic malignancies.* Clin Cancer Res, 2006. **12**(17): p. 5165-73.
133. Daver, N., et al., *A Phase I/II Study of the mTOR Inhibitor Everolimus in Combination with HyperCVAD Chemotherapy in Patients with Relapsed/Refractory Acute Lymphoblastic Leukemia.* Clin Cancer Res, 2015. **21**(12): p. 2704-14.

134. Place, A.E., et al., *Phase Ib Trial of the mTOR Inhibitor Everolimus Given in Combination with Multiagent Chemotherapy in Relapsed Acute Lymphoblastic Leukemia.* Blood, 2015. **126**(23): p. 3765-3765.
135. Eng, C.P., S.N. Sehgal, and C. Vezina, *Activity of rapamycin (AY-22,989) against transplanted tumors.* J Antibiot (Tokyo), 1984. **37**(10): p. 1231-7.
136. Choi, J., et al., *Structure of the FKBP12-rapamycin complex interacting with the binding domain of human FRAP.* Science, 1996. **273**(5272): p. 239-42.
137. Cafferkey, R., et al., *Dominant missense mutations in a novel yeast protein related to mammalian phosphatidylinositol 3-kinase and VPS34 abrogate rapamycin cytotoxicity.* Mol Cell Biol, 1993. **13**(10): p. 6012-23.
138. Dumont, F.J., et al., *Dominant mutations confer resistance to the immunosuppressant, rapamycin, in variants of a T cell lymphoma.* Cell Immunol, 1995. **163**(1): p. 70-9.
139. Fruman, D.A., et al., *FK506 binding protein 12 mediates sensitivity to both FK506 and rapamycin in murine mast cells.* Eur J Immunol, 1995. **25**(2): p. 563-71.
140. Guba, M., et al., *Rapamycin inhibits primary and metastatic tumor growth by antiangiogenesis: involvement of vascular endothelial growth factor.* Nat Med, 2002. **8**(2): p. 128-35.
141. Harada, K., et al., *Acquired resistance to temsirolimus in human renal cell carcinoma cells is mediated by the constitutive activation of signal transduction pathways through mTORC2.* Br J Cancer, 2013. **109**(9): p. 2389-95.
142. Juengel, E., et al., *Acetylation of histone H3 prevents resistance development caused by chronic mTOR inhibition in renal cell carcinoma cells.* Cancer Letters, 2012. **324**(1): p. 83-90.
143. Tsaur, I., et al., *The cdk1-cyclin B complex is involved in everolimus triggered resistance in the PC3 prostate cancer cell line.* Cancer Letters, 2011. **313**(1): p. 84-90.
144. Lorenz, M.C. and J. Heitman, *TOR mutations confer rapamycin resistance by preventing interaction with FKBP12-rapamycin.* J Biol Chem, 1995. **270**(46): p. 27531-7.
145. Volarević, S. and G. Thomas, *Role of S6 phosphorylation and S6 kinase in cell growth*, in *Progress in Nucleic Acid Research and Molecular Biology*. 2000, Academic Press. p. 101-127.
146. Dennis, P.B., et al., *The principal rapamycin-sensitive p70(s6k) phosphorylation sites, T-229 and T-389, are differentially regulated by rapamycin-insensitive kinase kinases.* Mol Cell Biol, 1996. **16**(11): p. 6242-51.
147. Kim, E.K., et al., *Phosphorylated S6K1 is a possible marker for endocrine therapy resistance in hormone receptor-positive breast cancer.* Breast Cancer Res Treat, 2011. **126**(1): p. 93-9.
148. Kim, E.K., et al., *Phosphorylated s6 kinase-1: a breast cancer marker predicting resistance to neoadjuvant chemotherapy.* Anticancer Res, 2013. **33**(9): p. 4073-9.
149. De Benedetti, A. and R.E. Rhoads, *Overexpression of eukaryotic protein synthesis initiation factor 4E in HeLa cells results in aberrant growth and morphology.* Proc Natl Acad Sci U S A, 1990. **87**(21): p. 8212-6.
150. Lazaris-Karatzas, A., K.S. Montine, and N. Sonenberg, *Malignant transformation by a eukaryotic initiation factor subunit that binds to mRNA 5' cap.* Nature, 1990. **345**(6275): p. 544-7.

151. Lazaris-Karatzas, A., et al., *Ras mediates translation initiation factor 4E-induced malignant transformation.* Genes Dev, 1992. **6**(9): p. 1631-42.
152. Nathan, C.O., et al., *Analysis of surgical margins with the molecular marker eIF4E: a prognostic factor in patients with head and neck cancer.* J Clin Oncol, 1999. **17**(9): p. 2909-14.
153. Li, B.D., et al., *Overexpression of eukaryotic initiation factor 4E (eIF4E) in breast carcinoma.* Cancer, 1997. **79**(12): p. 2385-90.
154. Nathan, C.O., et al., *Elevated expression of eIF4E and FGF-2 isoforms during vascularization of breast carcinomas.* Oncogene, 1997. **15**(9): p. 1087-94.
155. Martin, M.E., et al., *4E binding protein 1 expression is inversely correlated to the progression of gastrointestinal cancers.* Int J Biochem Cell Biol, 2000. **32**(6): p. 633-42.
156. Pons, B., et al., *The effect of p-4E-BP1 and p-eIF4E on cell proliferation in a breast cancer model.* Int J Oncol, 2011. **39**(5): p. 1337-45.
157. Dilling, M.B., et al., *4E-binding proteins, the suppressors of eukaryotic initiation factor 4E, are down-regulated in cells with acquired or intrinsic resistance to rapamycin.* J Biol Chem, 2002. **277**(16): p. 13907-17.
158. Efeyan, A. and D.M. Sabatini, *mTOR and cancer: many loops in one pathway.* Current opinion in cell biology, 2010. **22**(2): p. 169-176.
159. O'Reilly, K.E., et al., *mTOR Inhibition Induces Upstream Receptor Tyrosine Kinase Signaling and Activates Akt.* Cancer research, 2006. **66**(3): p. 1500-1508.
160. Mi, W., et al., *AKT inhibition overcomes rapamycin resistance by enhancing the repressive function of PRAS40 on mTORC1/4E-BP1 axis.* Oncotarget, 2015. **6**(16): p. 13962-13977.
161. Stratikopoulos, Elias E., et al., *Kinase and BET Inhibitors Together Clamp Inhibition of PI3K Signaling and Overcome Resistance to Therapy.* Cancer Cell, 2015. **27**(6): p. 837-851.
162. Wan, X., et al., *Rapamycin induces feedback activation of Akt signaling through an IGF-1R-dependent mechanism.* Oncogene, 2007. **26**(13): p. 1932-40.
163. Yang, G., et al., *A Positive Feedback Loop between Akt and mTORC2 via SIN1 Phosphorylation.* Cell Rep, 2015. **12**(6): p. 937-43.
164. Mumby, M., *PP2A: unveiling a reluctant tumor suppressor.* Cell, 2007. **130**(1): p. 21-4.
165. Sablina, A.A., et al., *The tumor suppressor PP2A Abeta regulates the RalA GTPase.* Cell, 2007. **129**(5): p. 969-82.
166. Janssens, V. and J. Goris, *Protein phosphatase 2A: a highly regulated family of serine/threonine phosphatases implicated in cell growth and signalling.* Biochem J, 2001. **353**(Pt 3): p. 417-39.
167. Dennis, P.B., S. Fumagalli, and G. Thomas, *Target of rapamycin (TOR): balancing the opposing forces of protein synthesis and degradation.* Curr Opin Genet Dev, 1999. **9**(1): p. 49-54.
168. Kurmasheva, R.T., S. Huang, and P.J. Houghton, *Predicted mechanisms of resistance to mTOR inhibitors.* Br J Cancer, 2006. **95**(8): p. 955-960.
169. Tan, J., et al., *B55beta-associated PP2A complex controls PDK1-directed myc signaling and modulates rapamycin sensitivity in colorectal cancer.* Cancer Cell, 2010. **18**(5): p. 459-71.
170. Correia, A.L. and M.J. Bissell, *The tumor microenvironment is a dominant force in multidrug resistance.* Drug Resistance Updates, 2012. **15**(1–2): p. 39-49.

171. Meads, M.B., L.A. Hazlehurst, and W.S. Dalton, *The bone marrow microenvironment as a tumor sanctuary and contributor to drug resistance.* Clin Cancer Res, 2008. **14**(9): p. 2519-26.
172. Mudry, R.E., et al., *Stromal cells regulate survival of B-lineage leukemic cells during chemotherapy.* Blood, 2000. **96**(5): p. 1926-32.
173. Makrynikola, V., et al., *Migration of acute lymphoblastic leukemia cells into human bone marrow stroma.* Leukemia, 1994. **8**(10): p. 1734-43.
174. Makrynikola, V. and K.F. Bradstock, *Adhesion of precursor-B acute lymphoblastic leukaemia cells to bone marrow stromal proteins.* Leukemia, 1993. **7**(1): p. 86-92.
175. Hsieh, Y.T., et al., *Integrin alpha4 blockade sensitizes drug resistant pre-B acute lymphoblastic leukemia to chemotherapy.* Blood, 2013. **121**(10): p. 1814-8.
176. Juengel, E., et al., *Resistance to the mTOR inhibitor temsirolimus alters adhesion and migration behavior of renal cell carcinoma cells through an integrin alpha5- and integrin beta3-dependent mechanism.* Neoplasia, 2014. **16**(4): p. 291-300.
177. Tsaur, I., et al., *Resistance to the mTOR-inhibitor RAD001 elevates integrin alpha2- and beta1-triggered motility, migration and invasion of prostate cancer cells.* Br J Cancer, 2012. **107**(5): p. 847-55.
178. Schlaepfer, D.D., C.R. Hauck, and D.J. Sieg, *Signaling through focal adhesion kinase.* Progress in Biophysics and Molecular Biology, 1999. **71**(3–4): p. 435-478.
179. Sieg, D.J., et al., *FAK integrates growth-factor and integrin signals to promote cell migration.* Nat Cell Biol, 2000. **2**(5): p. 249-256.
180. Sieg, D.J., C.R. Hauck, and D.D. Schlaepfer, *Required role of focal adhesion kinase (FAK) for integrin-stimulated cell migration.* J Cell Sci, 1999. **112 (Pt 16)**: p. 2677-91.
181. Francois, R.A., et al., *Targeting Focal Adhesion Kinase and Resistance to mTOR Inhibition in Pancreatic Neuroendocrine Tumors.* J Natl Cancer Inst, 2015. **107**(8).
182. Chiong, E., et al., *Effects of mTOR inhibitor everolimus (RAD001) on bladder cancer cells.* Clin Cancer Res, 2011. **17**(9): p. 2863-73.
183. Zitzmann, K., et al., *The novel mTOR inhibitor RAD001 (everolimus) induces antiproliferative effects in human pancreatic neuroendocrine tumor cells.* Neuroendocrinology, 2007. **85**(1): p. 54-60.
184. Yu, C.C., et al., *RAD001 enhances the radiosensitivity of SCC4 oral cancer cells by inducing cell cycle arrest at the G2/M checkpoint.* Anticancer Res, 2014. **34**(6): p. 2927-35.
185. Juengel, E., et al., *HDAC-inhibition counteracts everolimus resistance in renal cell carcinoma in vitro by diminishing cdk2 and cyclin A.* Mol Cancer, 2014. **13**: p. 152.
186. Carew, J.S., K.R. Kelly, and S.T. Nawrocki, *Mechanisms of mTOR inhibitor resistance in cancer therapy.* Target Oncol, 2011. **6**(1): p. 17-27.
187. Wendel, H.G., et al., *Dissecting eIF4E action in tumorigenesis.* Genes Dev, 2007. **21**(24): p. 3232-7.
188. Meric-Bernstam, F. and A.M. Gonzalez-Angulo, *Targeting the mTOR signaling network for cancer therapy.* J Clin Oncol, 2009. **27**(13): p. 2278-87.
189. Sankhala, K. and F.J. Giles, *Potential of mTOR inhibitors as therapeutic agents in hematological malignancies.* Expert Rev Hematol, 2009. **2**(4): p. 399-414.

190. Anderson, K., et al., *Genetic variegation of clonal architecture and propagating cells in leukaemia.* Nature, 2011. **469**(7330): p. 356-361.
191. Nowak, D., et al., *Variegated clonality and rapid emergence of new molecular lesions in xenografts of acute lymphoblastic leukemia are associated with drug resistance.* Exp Hematol, 2015. **43**(1): p. 32-43 e1-35.
192. Inaba, H., M. Greaves, and C.G. Mullighan, *Acute lymphoblastic leukaemia.* Lancet, 2013. **381**(9881): p. 1943-55.
193. Yang, J.J., et al., *Genome-wide copy number profiling reveals molecular evolution from diagnosis to relapse in childhood acute lymphoblastic leukemia.* Blood, 2008. **112**(10): p. 4178-4183.
194. Mullighan, C.G., et al., *Genomic Analysis of the Clonal Origins of Relapsed Acute Lymphoblastic Leukemia.* Science, 2008. **322**(5906): p. 1377-1380.
195. Staubert, C., et al., *Rewired metabolism in drug-resistant leukemia cells: a metabolic switch hallmarked by reduced dependence on exogenous glutamine.* J Biol Chem, 2015. **290**(13): p. 8348-59.
196. Masters, J.R., et al., *Short tandem repeat profiling provides an international reference standard for human cell lines.* Proceedings of the National Academy of Sciences, 2001. **98**(14): p. 8012-8017.
197. Kratz, A. and P. Carninci, *The devil in the details of RNA-seq.* Nat Biotechnol, 2014. **32**(9): p. 882-4.
198. Tsaur, I., et al., *Intensified antineoplastic effect by combining an HDAC-inhibitor, an mTOR-inhibitor and low dosed interferon alpha in prostate cancer cells.* J Cell Mol Med, 2015. **19**(8): p. 1795-804.
199. Shishido, S., H. Bönig, and Y.-M. Kim, *Role of Integrin Alpha4 in Drug Resistance of Leukemia.* Frontiers in Oncology, 2014. **4**: p. 99.
200. Hoofd, C., et al., *CD44 promotes chemoresistance in T-ALL by increased drug efflux.* Exp Hematol, 2016. **44**(3): p. 166-71.e17.
201. Welschinger, R., et al., *Plerixafor (AMD3100) induces prolonged mobilization of acute lymphoblastic leukemia cells and increases the proportion of cycling cells in the blood in mice.* Exp Hematol, 2012.
202. Schaller, M.D., *Cellular functions of FAK kinases: insight into molecular mechanisms and novel functions.* J Cell Sci, 2010. **123**(Pt 7): p. 1007-13.
203. Juliano, R.L., *SIGNAL TRANSDUCTION BY CELL ADHESION RECEPTORS AND THE CYTOSKELETON: Functions of Integrins, Cadherins, Selectins, and Immunoglobulin-Superfamily Members.* Annual Review of Pharmacology and Toxicology, 2002. **42**(1): p. 283-323.
204. Parsons, J.T., A.R. Horwitz, and M.A. Schwartz, *Cell adhesion: integrating cytoskeletal dynamics and cellular tension.* Nature reviews. Molecular cell biology, 2010. **11**(9): p. 633-643.
205. Parmo-Cabañas, M., et al., *Integrin α4β1 involvement in stromal cell-derived factor-1α-promoted myeloma cell transendothelial migration and adhesion: role of cAMP and the actin cytoskeleton in adhesion.* Experimental Cell Research, 2004. **294**(2): p. 571-580.
206. You, D., et al., *FAK mediates a compensatory survival signal parallel to PI3K-AKT in PTEN-null T-ALL cells.* Cell Rep, 2015. **10**(12): p. 2055-68.
207. Hu, Z. and W.B. Slayton, *Integrin VLA-5 and FAK are Good Targets to Improve Treatment Response in the Philadelphia Chromosome Positive Acute Lymphoblastic Leukemia.* Front Oncol, 2014. **4**: p. 112.
208. Sugiyama, H., et al., *p70 S6 kinase sensitivity to rapamycin is eliminated by amino acid substitution of Thr229.* J Immunol, 1996. **157**(2): p. 656-60.

209. Castagna, A., et al., *A proteomic approach to cisplatin resistance in the cervix squamous cell carcinoma cell line A431.* Proteomics, 2004. **4**(10): p. 3246-67.
210. Huber, M., et al., *Comparison of proteomic and genomic analyses of the human breast cancer cell line T47D and the antiestrogen-resistant derivative T47D-r.* Mol Cell Proteomics, 2004. **3**(1): p. 43-55.
211. Karve, T.M. and A.K. Cheema, *Small Changes Huge Impact: The Role of Protein Posttranslational Modifications in Cellular Homeostasis and Disease.* Journal of Amino Acids, 2011. **2011**.
212. Burchmore, R., *Mapping pathways to drug resistance with proteomics.* Expert Review of Proteomics, 2014. **11**(1): p. 1-3.
213. Chen, X., et al., *Quantitative proteomics analysis identifies mitochondria as therapeutic targets of multidrug-resistance in ovarian cancer.* Theranostics, 2014. **4**(12): p. 1164-75.
214. Cho, H.J., et al., *Proteomics-based Strategy to Delineate the Molecular Mechanisms of RhoGDI2-induced Metastasis and Drug Resistance in Gastric Cancer.* Journal of Proteome Research, 2012. **11**(4): p. 2355-2364.
215. Hengel, S.M., et al., *Data-independent Proteomic Screen Identifies Novel Tamoxifen Agonist that Mediates Drug Resistance.* Journal of proteome research, 2011. **10**(10): p. 4567-4578.
216. Candiano, G., et al., *Blue silver: a very sensitive colloidal Coomassie G-250 staining for proteome analysis.* Electrophoresis, 2004. **25**(9): p. 1327-33.
217. Boersema, P.J., et al., *Triplex protein quantification based on stable isotope labeling by peptide dimethylation applied to cell and tissue lysates.* Proteomics, 2008. **8**(22): p. 4624-32.
218. Vincent, E.E., et al., *Akt phosphorylation on Thr308 but not on Ser473 correlates with Akt protein kinase activity in human non-small cell lung cancer.* British Journal of Cancer, 2011. **104**(11): p. 1755-1761.
219. Carracedo, A., et al., *Inhibition of mTORC1 leads to MAPK pathway activation through a PI3K-dependent feedback loop in human cancer.* The Journal of Clinical Investigation, 2008. **118**(9): p. 3065-3074.
220. Sarbassov, D.D., et al., *Phosphorylation and regulation of Akt/PKB by the rictor-mTOR complex.* Science, 2005. **307**(5712): p. 1098-101.
221. Chen, H.N., et al., *PDLIM1 stabilizes the E-cadherin/beta-catenin complex to prevent epithelial-mesenchymal transition and metastatic potential of colorectal cancer cells.* Cancer Res, 2015.
222. Berton, S., et al., *Genetic characterization of p27(kip1) and stathmin in controlling cell proliferation in vivo.* Cell Cycle, 2014. **13**(19): p. 3100-11.
223. Cassimeris, L., *The oncoprotein 18/stathmin family of microtubule destabilizers.* Curr Opin Cell Biol, 2002. **14**(1): p. 18-24.
224. Brown, K.J. and C. Fenselau, *Investigation of doxorubicin resistance in MCF-7 breast cancer cells using shot-gun comparative proteomics with proteolytic 18O labeling.* J Proteome Res, 2004. **3**(3): p. 455-62.
225. Lin, X., et al., *Op18/stathmin is involved in the resistance of taxol among different epithelial carcinoma cell lines.* Cancer Biother Radiopharm, 2014. **29**(9): p. 376-86.
226. Boersema, P.J., et al., *Multiplex peptide stable isotope dimethyl labeling for quantitative proteomics.* Nat Protoc, 2009. **4**(4): p. 484-94.
227. Wan, X., et al., *Rapamycin induces feedback activation of Akt signaling through an IGF-1R-dependent mechanism.* Oncogene, 2006. **26**(13): p. 1932-1940.

228. Cho, W.C., *Contribution of oncoproteomics to cancer biomarker discovery.* Mol Cancer, 2007. **6**: p. 25.
229. Geiger, T., et al., *Proteomic Portrait of Human Breast Cancer Progression Identifies Novel Prognostic Markers.* Cancer Research, 2012. **72**(9): p. 2428-2439.
230. Li, J., et al., *Proteomics and Bioinformatics Approaches for Identification of Serum Biomarkers to Detect Breast Cancer.* Clinical Chemistry, 2002. **48**(8): p. 1296-1304.
231. Mahmoudi, K., A. Ezrin, and C. Hadjipanayis, *Small extracellular vesicles as tumor biomarkers for glioblastoma.* Molecular Aspects of Medicine, 2015. **45**: p. 97-102.
232. Hengel, S.M., et al., *Data-independent proteomic screen identifies novel tamoxifen agonist that mediates drug resistance.* J Proteome Res, 2011. **10**(10): p. 4567-78.
233. Paulitschke, V., et al., *Proteomics approaches to understanding mitogen-activated protein kinase inhibitor resistance in melanoma.* Curr Opin Oncol, 2016.
234. Verrills, N.M., et al., *Proteomic analysis reveals a novel role for the actin cytoskeleton in vincristine resistant childhood leukemia--an in vivo study.* Proteomics, 2006. **6**(5): p. 1681-94.
235. Verrills, N.M., et al., *Proteome analysis of vinca alkaloid response and resistance in acute lymphoblastic leukemia reveals novel cytoskeletal alterations.* J Biol Chem, 2003. **278**(46): p. 45082-93.
236. Xu, F., et al., *An investigation of heat shock protein 27 and P-glycoprotein mediated multi-drug resistance in breast cancer using liquid chromatography-tandem mass spectrometry-based targeted proteomics.* Journal of Proteomics, 2014. **108**: p. 188-197.
237. Yoon, S.-O. and Philippe P. Roux, *Rapamycin Resistance: mTORC1 Substrates Hold Some of the Answers.* Current Biology, 2013. **23**(19): p. R880-R883.
238. Belletti, B. and G. Baldassarre, *Stathmin: a protein with many tasks. New biomarker and potential target in cancer.* Expert Opin Ther Targets, 2011. **15**(11): p. 1249-66.
239. Brattsand, G., et al., *Quantitative analysis of the expression and regulation of an activation-regulated phosphoprotein (oncoprotein 18) in normal and neoplastic cells.* Leukemia, 1993. **7**(4): p. 569-79.
240. Miceli, C., et al., *Cell cycle inhibition therapy that targets stathmin in in vitro and in vivo models of breast cancer.* Cancer Gene Ther, 2013. **20**(5): p. 298-307.
241. Mistry, S.J. and G.F. Atweh, *Therapeutic interactions between stathmin inhibition and chemotherapeutic agents in prostate cancer.* Mol Cancer Ther, 2006. **5**(12): p. 3248-57.
242. Challa, A.A. and B. Stefanovic, *A Novel Role of Vimentin Filaments: Binding and Stabilization of Collagen mRNAs.* Molecular and Cellular Biology, 2011. **31**(18): p. 3773-3789.
243. Havel, L.S., et al., *Vimentin regulates lung cancer cell adhesion through a VAV2-Rac1 pathway to control focal adhesion kinase activity.* Oncogene, 2015. **34**(15): p. 1979-90.
244. Satelli, A. and S. Li, *Vimentin in cancer and its potential as a molecular target for cancer therapy.* Cell Mol Life Sci, 2011. **68**(18): p. 3033-46.

245. Tezcan, O. and U. Gunduz, *Vimentin silencing effect on invasive and migration characteristics of doxorubicin resistant MCF-7 cells.* Biomed Pharmacother, 2014. **68**(3): p. 357-64.
246. Wei, J., et al., *Overexpression of vimentin contributes to prostate cancer invasion and metastasis via src regulation.* Anticancer Res, 2008. **28**(1a): p. 327-34.
247. Maxwell, S.A., E.M. Cherry, and K.J. Bayless, *Akt, 14-3-3zeta, and vimentin mediate a drug-resistant invasive phenotype in diffuse large B-cell lymphoma.* Leuk Lymphoma, 2011. **52**(5): p. 849-64.
248. Haslehurst, A.M., et al., *EMT transcription factors snail and slug directly contribute to cisplatin resistance in ovarian cancer.* BMC Cancer, 2012. **12**(1): p. 1-10.
249. Li, J., et al., *miR-27a regulates cisplatin resistance and metastasis by targeting RKIP in human lung adenocarcinoma cells.* Molecular Cancer, 2014. **13**(1): p. 1-9.
250. Bauer, K., et al., *Human CLP36, a PDZ-domain and LIM-domain protein, binds to alpha-actinin-1 and associates with actin filaments and stress fibers in activated platelets and endothelial cells.* Blood, 2000. **96**(13): p. 4236-45.
251. Tamura, N., et al., *The PDZ-LIM protein CLP36 is required for actin stress fiber formation and focal adhesion assembly in BeWo cells.* Biochem Biophys Res Commun, 2007. **364**(3): p. 589-94.
252. Vallenius, T., K. Luukko, and T.P. Makela, *CLP-36 PDZ-LIM protein associates with nonmuscle alpha-actinin-1 and alpha-actinin-4.* J Biol Chem, 2000. **275**(15): p. 11100-5.
253. Liu, Z., et al., *PDZ and LIM domain protein 1(PDLIM1)/CLP36 promotes breast cancer cell migration, invasion and metastasis through interaction with alpha-actinin.* Oncogene, 2015. **34**(10): p. 1300-11.
254. Alaiya, A., M. Al-Mohanna, and S. Linder, *Clinical cancer proteomics: promises and pitfalls.* J Proteome Res, 2005. **4**(4): p. 1213-22.
255. Verrills, N.M., *Clinical proteomics: present and future prospects.* Clin Biochem Rev, 2006. **27**(2): p. 99-116.
256. Bunai, K. and K. Yamane, *Effectiveness and limitation of two-dimensional gel electrophoresis in bacterial membrane protein proteomics and perspectives.* J Chromatogr B Analyt Technol Biomed Life Sci, 2005. **815**(1-2): p. 227-36.
257. Vélez, P., et al., *A 2D-DIGE-based proteomic analysis reveals differences in the platelet releasate composition when comparing thrombin and collagen stimulations.* Scientific Reports, 2015. **5**: p. 8198.
258. Wu, W.W., et al., *Comparative study of three proteomic quantitative methods, DIGE, cICAT, and iTRAQ, using 2D gel- or LC-MALDI TOF/TOF.* J Proteome Res, 2006. **5**(3): p. 651-8.
259. Chen, H.S., et al., *Enhanced characterization of complex proteomic samples using LC-MALDI MS/MS: exclusion of redundant peptides from MS/MS analysis in replicate runs.* Anal Chem, 2005. **77**(23): p. 7816-25.
260. Wang, H., et al., *Comparison of extensive protein fractionation and repetitive LC-MS/MS analyses on depth of analysis for complex proteomes.* J Proteome Res, 2010. **9**(2): p. 1032-40.
261. Deeb, S.J., et al., *Super-SILAC allows classification of diffuse large B-cell lymphoma subtypes by their protein expression profiles.* Mol Cell Proteomics, 2012. **11**(5): p. 77-89.

262. Geiger, T., et al., *Super-SILAC mix for quantitative proteomics of human tumor tissue.* Nat Methods, 2010. **7**(5): p. 383-5.
263. Tebbe, A., et al., *Systematic evaluation of label-free and super-SILAC quantification for proteome expression analysis.* Rapid Commun Mass Spectrom, 2015. **29**(9): p. 795-801.
264. Mihara, K., et al., *Development and functional characterization of human bone marrow mesenchymal cells immortalized by enforced expression of telomerase.* Br J Haematol, 2003. **120**(5): p. 846-9.
265. Schittek, B., K. Rajewsky, and I. Forster, *Dividing cells in bone marrow and spleen incorporate bromodeoxyuridine with high efficiency.* Eur J Immunol, 1991. **21**(1): p. 235-8.
266. Welschinger, R. and L.J. Bendall, *Temporal Tracking of Cell Cycle Progression Using Flow Cytometry without the Need for Synchronization.* J Vis Exp, 2015(102): p. e52840.
267. Iancu, C., et al., *Effects of stathmin inhibition on the mitotic spindle.* J Cell Sci, 2001. **114**(Pt 5): p. 909-16.
268. Manna, T., et al., *Regulation of microtubule dynamic instability in vitro by differentially phosphorylated stathmin.* J Biol Chem, 2009. **284**(23): p. 15640-9.
269. Rubin, C.I. and G.F. Atweh, *The role of stathmin in the regulation of the cell cycle.* J Cell Biochem, 2004. **93**(2): p. 242-50.
270. Machado-Neto, J.A., S.T. Olalla Saad, and F. Traina, *Stathmin 1 in normal and malignant hematopoiesis.* BMB Reports, 2014. **47**(12): p. 660-665.
271. Alli, E., et al., *Reversal of stathmin-mediated resistance to paclitaxel and vinblastine in human breast carcinoma cells.* Mol Pharmacol, 2007. **71**(5): p. 1233-40.
272. Larsson, N., et al., *Control of microtubule dynamics by oncoprotein 18: dissection of the regulatory role of multisite phosphorylation during mitosis.* Mol Cell Biol, 1997. **17**(9): p. 5530-9.
273. Gradin, H.M., et al., *Regulation of microtubule dynamics by extracellular signals: cAMP-dependent protein kinase switches off the activity of oncoprotein 18 in intact cells.* J Cell Biol, 1998. **140**(1): p. 131-41.
274. Yip, Y.Y., et al., *cAMP-dependent protein kinase and c-Jun N-terminal kinase mediate stathmin phosphorylation for the maintenance of interphase microtubules during osmotic stress.* J Biol Chem, 2014. **289**(4): p. 2157-69.
275. Beretta, L., T. Dobransky, and A. Sobel, *Multiple phosphorylation of stathmin. Identification of four sites phosphorylated in intact cells and in vitro by cyclic AMP-dependent protein kinase and p34cdc2.* J Biol Chem, 1993. **268**(27): p. 20076-84.
276. Brattsand, G., et al., *Cell-cycle-regulated phosphorylation of oncoprotein 18 on Ser16, Ser25 and Ser38.* Eur J Biochem, 1994. **220**(2): p. 359-68.
277. Meads, M.B., R.A. Gatenby, and W.S. Dalton, *Environment-mediated drug resistance: a major contributor to minimal residual disease.* Nat Rev Cancer, 2009. **9**(9): p. 665-74.
278. Johns, J.L. and M.M. Christopher, *Extramedullary hematopoiesis: a new look at the underlying stem cell niche, theories of development, and occurrence in animals.* Vet Pathol, 2012. **49**(3): p. 508-23.
279. Inra, C.N., et al., *A perisinusoidal niche for extramedullary haematopoiesis in the spleen.* Nature, 2015. **527**(7579): p. 466-471.

280. Yamamoto, K., et al., *Extramedullary hematopoiesis: Elucidating the function of the hematopoietic stem cell niche (Review).* Mol Med Rep, 2016. **13**(1): p. 587-91.
281. Sherbert, G.V. and F. Cajone, *Stathmin in Cell Proliferation and Cancer Progression.* Cancer Genomics - Proteomics, 2005. **2**(4): p. 227-237.
282. Wik, E., et al., *High phospho-Stathmin(Serine38) expression identifies aggressive endometrial cancer and suggests an association with PI3K inhibition.* Clin Cancer Res, 2013. **19**(9): p. 2331-41.
283. Castedo, M., et al., *Cyclin-dependent kinase-1: linking apoptosis to cell cycle and mitotic catastrophe.* Cell Death Differ, 2002. **9**(12): p. 1287-93.
284. Neganova, I., et al., *CDK1 plays an important role in the maintenance of pluripotency and genomic stability in human pluripotent stem cells.* Cell Death Dis, 2014. **5**: p. e1508.
285. Santamaria, D., et al., *Cdk1 is sufficient to drive the mammalian cell cycle.* Nature, 2007. **448**(7155): p. 811-815.
286. Abdel-Karim, I.A. and F.J. Giles, *Mammalian Target of Rapamycin as a Target in Hematological Malignancies.* Current Problems in Cancer, 2008. **32**(4): p. 161-177.
287. Alayev, A. and M.K. Holz, *mTOR signaling for biological control and cancer.* J Cell Physiol, 2013. **228**(8): p. 1658-64.
288. Guertin, D.A. and D.M. Sabatini, *Defining the role of mTOR in cancer.* Cancer Cell, 2007. **12**(1): p. 9-22.
289. Kuwatsuka, Y., et al., *The mTOR inhibitor, everolimus (RAD001), overcomes resistance to imatinib in quiescent Ph-positive acute lymphoblastic leukemia cells.* Blood Cancer J, 2011. **1**(5): p. e17.
290. Livak, K.J. and T.D. Schmittgen, *Analysis of relative gene expression data using real-time quantitative PCR and the 2(-Delta Delta C(T)) Method.* Methods, 2001. **25**(4): p. 402-8.
291. Coustan-Smith, E., et al., *New markers for minimal residual disease detection in acute lymphoblastic leukemia.* Blood, 2011. **117**(23): p. 6267-76.
292. Bartel, D.P., *MicroRNAs: genomics, biogenesis, mechanism, and function.* Cell, 2004. **116**(2): p. 281-97.
293. Sheedy, F.J., *Turning 21: Induction of miR-21 as a Key Switch in the Inflammatory Response.* Front Immunol, 2015. **6**: p. 19.
294. Loffler, D., et al., *Interleukin-6 dependent survival of multiple myeloma cells involves the Stat3-mediated induction of microRNA-21 through a highly conserved enhancer.* Blood, 2007. **110**(4): p. 1330-3.
295. Cingarlini, S., et al., *Profiling mTOR pathway in neuroendocrine tumors.* Target Oncol, 2012. **7**(3): p. 183-8.
296. Meng, F., et al., *MicroRNA-21 regulates expression of the PTEN tumor suppressor gene in human hepatocellular cancer.* Gastroenterology, 2007. **133**(2): p. 647-58.
297. Pan, Y., et al., *Oncogenic microRNAs in the genesis of leukemia and lymphoma.* Curr Pharm Des, 2014. **20**(33): p. 5260-7.
298. Wang, W.Z., et al., *Silencing of miR-21 sensitizes CML CD34(+) stem/progenitor cells to imatinib-induced apoptosis by blocking PI3K/AKT pathway.* Leuk Res, 2015. **39**(10): p. 1117-24.
299. Zhou, L., et al., *MicroRNA-21 is involved in X-ray irradiation resistance in K562 leukaemia cells.* Hematology, 2015. **20**(6): p. 343-8.

300. Espinoza-Hernandez, L., et al., *In vitro characterization of the hematopoietic system in pediatric patients with acute lymphoblastic leukemia.* Leuk Res, 2001. **25**(4): p. 295-303.
301. Giles, F.J., et al., *The role of inflammation in leukaemia.* Adv Exp Med Biol, 2014. **816**: p. 335-60.
302. Pituch-Noworolska, A., et al., *The IL-6 gene expression by leukemic cells from acute lymphoblastic leukemia common and T type and modulation of IL-6 production by TNF.* Haematologia (Budap), 1998. **29**(2): p. 101-14.
303. Vilchis-Ordonez, A., et al., *Bone Marrow Cells in Acute Lymphoblastic Leukemia Create a Proinflammatory Microenvironment Influencing Normal Hematopoietic Differentiation Fates.* Biomed Res Int, 2015. **2015**: p. 386165.
304. Budde, K., et al., *Everolimus-based, calcineurin-inhibitor-free regimen in recipients of de-novo kidney transplants: an open-label, randomised, controlled trial.* Lancet, 2011. **377**(9768): p. 837-47.
305. Cibrik, D., et al., *Randomized trial of everolimus-facilitated calcineurin inhibitor minimization over 24 months in renal transplantation.* Transplantation, 2013. **95**(7): p. 933-42.
306. Ganschow, R., et al., *The role of everolimus in liver transplantation.* Clin Exp Gastroenterol, 2014. **7**: p. 329-43.
307. Gonzalez, F. and R. Valjalo, *Combining cytochrome P-450 3A4 modulators and cyclosporine or everolimus in transplantation is successful.* World J Transplant, 2015. **5**(4): p. 338-47.
308. Patel, J.K. and J.A. Kobashigawa, *Everolimus: an immunosuppressive agent in transplantation.* Expert Opin Pharmacother, 2006. **7**(10): p. 1347-55.
309. Vitiello, D., et al., *Effect of everolimus on the immunomodulation of the human neutrophil inflammatory response and activation.* Cell Mol Immunol, 2015. **12**(1): p. 40-52.
310. Bhojwani, D., et al., *Gene expression signatures predictive of early response and outcome in high-risk childhood acute lymphoblastic leukemia: A Children's Oncology Group Study [corrected].* J Clin Oncol, 2008. **26**(27): p. 4376-84.
311. Holleman, A., et al., *Gene-Expression Patterns in Drug-Resistant Acute Lymphoblastic Leukemia Cells and Response to Treatment.* New England Journal of Medicine, 2004. **351**(6): p. 533-542.
312. Teuffel, O., et al., *Gene expression profiles and risk stratification in childhood acute lymphoblastic leukemia.* Haematologica, 2004. **89**(7): p. 801-8.
313. Peters, C., et al., *Stem-cell transplantation in children with acute lymphoblastic leukemia: A prospective international multicenter trial comparing sibling donors with matched unrelated donors-The ALL-SCT-BFM-2003 trial.* J Clin Oncol, 2015. **33**(11): p. 1265-74.
314. Krentz, S., et al., *Prognostic value of genetic alterations in children with first bone marrow relapse of childhood B-cell precursor acute lymphoblastic leukemia.* Leukemia, 2013. **27**(2): p. 295-304.
315. Chu, E.C. and A.S. Tarnawski, *PTEN regulatory functions in tumor suppression and cell biology.* Med Sci Monit, 2004. **10**(10): p. RA235-41.
316. Badura, S., et al., *Differential effects of selective inhibitors targeting the PI3K/AKT/mTOR pathway in acute lymphoblastic leukemia.* PLoS One, 2013. **8**(11): p. e80070.
317. Huang, S. and P.J. Houghton, *Mechanisms of resistance to rapamycins.* Drug Resist Updat, 2001. **4**(6): p. 378-91.

318. Burger, J. and T. Kipps, *CXCR4: a key receptor in the crosstalk between tumor cells and their microenvironment.* Blood, 2006. **107**(5): p. 1761-1767.
319. Li, Z. and L. Li, *Understanding hematopoietic stem-cell microenvironments.* Trends in Biochemical Sciences, 2006. **31**(10): p. 589-595.
320. Nagasawa, T., *Microenvironmental niches in the bone marrow required for B-cell development.* Nat Rev Immunol, 2006. **6**(2): p. 107-16.
321. Ducker, G.S., et al., *Incomplete inhibition of phosphorylation of 4E-BP1 as a mechanism of primary resistance to ATP-competitive mTOR inhibitors.* Oncogene, 2014. **33**(12): p. 1590-600.

APPENDIX

Table A.1 Genes up-regulated 2-fold or greater in 1345-R by transcriptome

Gene	R/S
MLLT4	53.97
ITGA6	45.62
CR1	44.91
H1F0	35.49
LOC100130992	28.62
JMJD7-PLA2G4B	27.94
RAI14	27.50
FOSB	25.69
ANKRD6	21.15
ITGA8	20.00
NNAT	18.99
NOS1	17.82
STON1-GTF2A1L	17.81
EGR2	17.69
NR4A1	17.11
FOS	17.10
TTC28	16.41
AFF2	15.53
PTGDR	15.14
LOC100132215	13.92
CABLES1	13.68
CNR1	13.55
CHPF	12.89
KCNMB2	12.52
SDK2	12.31
LITAF	11.75
PCDH18	11.29
TSC22D3	11.05
MPP7	10.99
EGR1	10.71
POU3F3	10.54
PPIL6	10.27
LOC100507433	10.19
IL1B	10.12
CTNNA1	10.04
IGSF9	9.94
ACTR3C	9.76
SPAG6	9.70
ARHGAP29	9.58
SMN1	9.42
SMN1	9.42
LOC63930	9.26
PARVG	8.94
MYLK	8.87
CSF1	8.87
LRRN2	8.86
GRASP	8.54
DYSF	8.47
SNED1	8.32
IL18BP	8.28
VGF	8.12
RAVER2	8.10
NSUN7	8.07
BCL2A1	8.06
DPEP1	7.85
DNAJA4	7.78
SPRY4	7.63
JUN	7.59
TRIM74	7.58
NEK6	7.53
FLT1	7.46
SEMA4C	7.40
TRIB3	7.39
SORBS2	7.22
SLC16A3	7.12
ZNF154	7.11
PYROXD2	6.80
SORBS3	6.67
ODZ1	6.62
RASD1	6.45
ZNF626	6.44
GZMA	6.39
DGCR9	6.38
38596	6.37
RHOB	6.02
CACNA2D2	5.99
LRRC38	5.99
CD69	5.82
NR4A2	5.66
RGS16	5.61

ZIC2	5.58
OPTN	5.44
EHD3	5.36
LOC100507140	5.23
C11orf75	5.23
MDK	5.22
PRKCQ	5.20
TNFSF12	5.15
C11orf92	5.11
LOC100507254	5.08
IL24	4.94
SPRY1	4.92
CDC42EP4	4.91
HAPLN3	4.88
NRN1	4.86
ADAMTS18	4.85
GUSBP9	4.81
GUSBP9	4.81
CSRNP1	4.81
TPBG	4.80
HIST1H2BC	4.78
FAM134B	4.78
GOLGA7B	4.75
KLF6	4.74
RAB15	4.68
NEIL1	4.67
C9orf47	4.63
LTK	4.57
PTK2	4.56
NKPD1	4.53
HMX2	4.47
C15orf52	4.44

FBXO39	4.39
HAR1B	4.39
AHRR	4.38
CAPN3	4.36
PHOX2B	4.35
CYS1	4.35
PNPLA7	4.35
TCP11L2	4.34
HIST2H2BF	4.29
PCDHGC3	4.27
HAR1A	4.20
C1orf187	4.19
BTG2	4.17
KLF2	4.17
C11orf66	4.14
MUC20	4.13
CTGF	4.07
PALLD	4.05
PPP1R15A	4.00
SMAD3	3.98
C5orf62	3.97
ATF5	3.97
SERPINB9	3.97
SH3TC1	3.96
ESM1	3.96
39692	3.92
FLJ39639	3.91
PANX2	3.91
HLX	3.89
PTPRN2	3.88
HTR3A	3.85
BMPR2	3.83

IL8	3.80
TMEM99	3.77
HIST1H2AK	3.75
ISG20	3.75
GPR114	3.73
OBSCN	3.71
LOC100130451	3.70
HIST1H2AC	3.70
PTGER4	3.68
RAB37	3.63
AIM1L	3.56
MTUS2	3.55
FLJ36644	3.55
ISM1	3.55
HLA-DQB1	3.54
LOC653160	3.53
ZNF704	3.51
FAIM3	3.50
TREML2	3.50
LOC100506585	3.49
LOC541473	3.48
MORN1	3.46
NDRG1	3.46
KLKB1	3.45
KBTBD11	3.43
CDKN1C	3.43
AOX2P	3.40
CRYM	3.40
CYP21A2	3.38
LGR6	3.37
LOC284749	3.36
SPTLC3	3.34

FCGRT	3.34
RNF224	3.34
AMIGO1	3.31
LSP1	3.30
CELF6	3.30
CBLN3	3.28
NCRNA00114	3.28
CNR2	3.28
FAM57B	3.28
C11orf93	3.26
KIAA1683	3.26
SCARF1	3.26
HCG26	3.25
ZYX	3.25
MGAT5B	3.24
IDUA	3.24
PTPRF	3.23
PREX1	3.23
FAM110C	3.22
C19orf18	3.22
FBN1	3.21
BLOC1S1-RDH5	3.20
NCRNA00304	3.19
BAI2	3.19
LOC100130093	3.19
GPA33	3.18
MYO15B	3.15
BAGE3	3.15
GPR56	3.15
FBXO44	3.15
SPNS3	3.13
RIMS3	3.12

PLEK	3.12
C3orf47	3.12
LYZ	3.12
MVP	3.12
HIST1H2BJ	3.11
CD226	3.10
PATL2	3.10
DNTT	3.10
FLJ46906	3.08
COL18A1	3.08
C11orf21	3.08
PARP3	3.07
ZNF853	3.07
FLJ20021	3.07
PLGLB2	3.07
PLGLB2	3.07
CBX7	3.06
SH3BP5	3.05
GPR150	3.04
FLJ22536	3.04
LGALS3	3.04
LOC100129034	3.04
PNRC1	3.03
CYP2E1	3.03
PCDHGA5	3.02
TAS2R4	3.01
RGS1	3.01
CBWD3	3.01
RSAD2	3.00
MYO7B	3.00
ABTB1	3.00
PYY2	2.99

IER2	2.95
PIP5KL1	2.95
DEFA3	2.94
HIST2H4A	2.93
HIST2H4A	2.93
HLA-DQA2	2.93
BCL3	2.93
HIST2H2BE	2.92
PLEKHG1	2.92
FAT1	2.92
C9orf173	2.92
DENND3	2.91
ZFP36	2.90
APOBEC3B	2.90
DUSP2	2.90
SMTNL1	2.89
REM2	2.88
ATHL1	2.87
PPP1R16B	2.86
HIST1H3B	2.85
TMEM136	2.85
ZFP36L1	2.85
HIST1H1D	2.84
HRH2	2.82
FLJ45244	2.82
HIST1H2BG	2.82
ZMAT1	2.81
TPM2	2.81
YPEL5	2.81
C17orf109	2.80
PLXNC1	2.78
SDC2	2.78

FRMPD1	2.77
WBP2NL	2.76
SH3BP2	2.76
TP53INP1	2.76
LOC100289511	2.76
LTF	2.76
CARD11	2.73
CCDC136	2.73
IL3RA	2.72
IL3RA	2.72
ATP6V1C2	2.72
EXD3	2.72
LOC100289187	2.72
SLC45A4	2.71
LOC100131234	2.69
RALB	2.68
CCDC121	2.68
C17orf103	2.67
CCDC122	2.67
LOC100270804	2.67
LOC100129387	2.66
PGCP	2.66
LOC100129722	2.66
YPEL3	2.66
NKG7	2.65
C10orf57	2.65
TCL1B	2.65
PCDHGB6	2.65
IGSF3	2.65
NAV1	2.65
DEFA1	2.65
DEFA1	2.65

DEFA1B	2.65
APOLD1	2.65
S100A8	2.65
BTNL9	2.65
C21orf96	2.65
FFAR1	2.65
PTP4A3	2.64
MAPK8IP2	2.64
CALCOCO1	2.64
GAPDHS	2.64
LAPTM4B	2.64
TSSK3	2.63
RRBP1	2.62
CD82	2.62
LOC644554	2.62
LAX1	2.62
ETV5	2.61
GSN	2.60
LOC100506713	2.60
LOC100505783	2.60
GATS	2.60
SKI	2.60
S100A12	2.60
LOC400960	2.60
LOC100130357	2.58
GTF2IRD2	2.58
SLC37A1	2.58
ETV4	2.57
ANK1	2.57
MXRA8	2.56
LOC282997	2.55
HLA-F	2.54

GPR3	2.54
BMF	2.53
CDH24	2.53
C1QL1	2.52
NCRNA00086	2.52
SIRT2	2.52
DNAJB2	2.51
C17orf108	2.51
SCARNA9	2.51
HCG27	2.51
ZNF177	2.50
HVCN1	2.50
ALOX5AP	2.50
COMMD3-BMI1	2.50
RUNDC2C	2.50
JUND	2.49
PCDHGA6	2.49
TPST1	2.49
PDLIM2	2.49
AK1	2.48
C5orf45	2.48
NAV2	2.48
CBFA2T3	2.47
LOC100131691	2.47
PCDHGB2	2.47
LOXL2	2.47
GTF2IRD2P1	2.47
APITD1-CORT	2.47
LBH	2.47
HIST1H3D	2.46
SVIL	2.46
HLA-H	2.45

HLA-DMB	2.45
NFKBIZ	2.45
PPAP2A	2.44
EFCAB4A	2.44
PCDH9	2.44
CHAC1	2.43
TMEM234	2.43
PLIN4	2.42
HLA-DQA1	2.42
LOC254100	2.42
ZNF528	2.42
SLC22A18	2.41
LHFPL2	2.41
SAP25	2.41
VN1R1	2.40
CATSPER3	2.40
FLJ10038	2.39
KRTAP5-9	2.39
GTF2IRD2B	2.39
CXCL16	2.39
SIK1	2.39
CASKIN2	2.39
C1orf220	2.38
LPAR6	2.37
ABCG1	2.37
NCRNA00163	2.37
CD200	2.37
PCDHGA7	2.36
LSR	2.36
C21orf122	2.36
GYLTL1B	2.36
LOC100188949	2.36

LOC100131096	2.36
FSCN2	2.36
LAIR1	2.35
HERC2P4	2.35
LOC100131564	2.35
AKAP2	2.35
LOC100131089	2.35
HCP5	2.35
RHBDL1	2.34
MAST4	2.34
PBXIP1	2.34
ZCWPW1	2.34
POPDC2	2.33
LOC100506826	2.32
PDE1B	2.32
QSOX2	2.32
PLEC	2.32
PROX1	2.32
LOC100499489	2.32
MTSS1L	2.31
FAM46C	2.31
CD27	2.31
TMEM44	2.30
LRRC37A3	2.30
LOC643770	2.29
TM6SF1	2.29
ARSD	2.29
QRICH2	2.29
LOC645431	2.28
NCRNA00321	2.28
CIITA	2.28
GAS2L3	2.28

TAS1R3	2.28
FMO5	2.28
RGL4	2.28
SH2D4B	2.27
LOC284454	2.27
ABCA1	2.27
P2RX1	2.27
KLF8	2.27
GPT	2.27
C14orf28	2.26
CAPS	2.26
EBLN2	2.26
RGS2	2.26
B3GNT9	2.26
GZMK	2.26
TEX21P	2.26
LY6G5C	2.25
GLT1D1	2.25
CROCCP3	2.25
C1orf228	2.25
MMP11	2.25
FCRLA	2.25
AMY2B	2.24
SNX24	2.24
KDM5B	2.23
B3GALTL	2.23
ZMYND10	2.23
TK2	2.23
SPRY2	2.23
NFATC4	2.23
CACNB4	2.23
ABCA2	2.22

NCF1C	2.22
LOC728739	2.22
LOC100129726	2.21
ADAP1	2.21
LOC100216545	2.21
LOC338799	2.21
SPP1	2.21
RPS10P7	2.21
RPL21P28	2.21
LAPTM5	2.21
LTB	2.21
HIST1H2BN	2.20
LOC100128288	2.20
ACTN1	2.20
LILRB2	2.19
LOC146880	2.19
WDR78	2.19
RDX	2.19
FLJ40852	2.19
FAM19A1	2.19
GPR52	2.19
HLA-DOA	2.18
YJEFN3	2.18
LOC100101266	2.18
PLAGL1	2.17
HCFC1R1	2.17
DNAJC2	2.17
HLA-DPB1	2.17
LOC728724	2.17
ZBTB46	2.17
FAM167A	2.17
KRBA2	2.17

CHKB-CPT1B	2.16
HIST1H2BK	2.16
PIK3R5	2.16
TLE3	2.16
LAMA3	2.15
SLC23A1	2.15
C5orf41	2.15
LOC100129917	2.15
RNF215	2.15
ADAM8	2.14
C21orf15	2.14
CPT1B	2.14
HIST1H3H	2.14
PRKCB	2.14
C8orf84	2.14
FAM167B	2.13
ARL4C	2.13
JUNB	2.13
MYLIP	2.13
ATF3	2.13
GJA9-MYCBP	2.13
LOC389634	2.13
OPRL1	2.13
LOC728175	2.12
DNAJC1	2.12
C1RL	2.12
HLA-E	2.12
TNFRSF14	2.12
PCDHGB3	2.12
BTG1	2.12
TXK	2.12
ST3GAL1	2.12

AACS	2.12
B3GALT4	2.12
LOC100507557	2.11
ARSA	2.11
HIST2H2BC	2.11
MACROD2	2.10
ABR	2.10
LILRA2	2.09
SCARF2	2.09
MMP25	2.09
IGLL5	2.09
NFATC2	2.09
IGF1R	2.09
DTX1	2.09
HSD17B11	2.08
PTPRJ	2.08
ARL4A	2.08
SEC31B	2.08
HEATR7A	2.08
LOC100507331	2.08
CD72	2.07
YPEL2	2.07
DUSP1	2.07
NFIL3	2.07
IL11RA	2.07
FLJ45983	2.07
SLC31A2	2.07
FAM180B	2.06
LHPP	2.06
HOOK2	2.06
ZNF671	2.06
HLA-F-AS1	2.06

ZNF862	2.06
GPR35	2.06
ZMYND11	2.06
LOC202181	2.06
CD74	2.06
CMTM8	2.05
CA5B	2.05
CD160	2.05
LOC100129148	2.05
PCSK4	2.05
LOC283624	2.04

SUPT7L	2.04
LOC154822	2.04
HIST1H2BD	2.04
ANKRD36BP2	2.03
NBEA	2.03
TRAF1	2.03
MTMR9LP	2.03
C20orf165	2.03
FAM84B	2.03
ITM2A	2.03
STARD5	2.02

CNNM4	2.02
NCRNA00115	2.01
MASP2	2.01
LOC100131655	2.01
CD22	2.01
ACP2	2.01
PDE3B	2.01
C6orf164	2.01
CLSTN3	2.00

Table A.2 Genes down-regulated 2-fold or greater in 1345-R by transcriptome

Gene	R/S
ADAM23	176.58
LRRC26	79.74
PHOSPHO2-KLHL23	31.90
SNHG5	23.69
SNHG4	17.34
RNF130	13.86
MOCS2	13.19
HSD17B8	12.90
SHOX2	12.89
SPG20	12.04
LOC100133957	11.91
C16orf5	11.58
RNF144B	11.52
ODF2L	11.03
GUSBP2	10.86
FERMT1	10.62
GUSBP4	10.33
ZNF540	10.32
DDN	9.65
PHLDA3	9.49
CXorf57	8.81
APOBEC3H	8.25
SEC61G	7.87
SOX11	7.57
SKAP1	7.57
LIMA1	7.42
METTL7B	7.33
BEST3	7.13
CDKN1A	7.13
ZSCAN18	7.12
MCAM	7.05
CD163L1	6.69
TTC8	6.58
ALOX5	6.52
PRR4	6.51
RPF2	6.49
C6orf108	6.31
C20orf160	6.29
VDR	6.19
FAM169A	6.00
PRPF40B	5.76
TP63	5.64
BCKDHB	5.51
SAMHD1	5.36
KRT10	5.33
ITGB7	5.28
VCL	5.24
LOC344595	5.23
ASB14	5.21
MTHFD1L	5.10
ZNF565	5.04
TMEM237	4.99
NOL7	4.96
LY6E	4.96
MACC1	4.89
KRTCAP3	4.89
OXCT2	4.83
C6orf125	4.71
IGJ	4.69
TUBB4	4.65
BBS9	4.64
CENPV	4.63
DPCD	4.51
KBTBD8	4.49
VARS	4.48
DHRS3	4.46
SCO2	4.42
RAB34	4.41
SKAP2	4.35
MUTED	4.35
RPS18	4.33
PLIN2	4.24
RARS2	4.17
PFKM	4.13
FAM164A	4.11
IFI30	4.04
CSNK2B	4.03
SLC25A23	3.97
FAH	3.93
APOM	3.91
FDXR	3.89
IKZF4	3.88
DDX43	3.88
THOC6	3.84

PAK1IP1	3.81
RPA3	3.81
COX7A2	3.80
MYO1F	3.78
DCBLD2	3.76
STK33	3.75
PRIM2	3.73
GCAT	3.68
C4orf32	3.66
PRPS1L1	3.63
GDAP1	3.60
CRYZ	3.58
ACAT2	3.56
ECI2	3.55
CD96	3.55
SLC29A1	3.55
POLR1C	3.55
KDELC1	3.54
PTRH1	3.53
GMDS	3.52
DAZL	3.51
PYCR1	3.50
GNGT2	3.50
STOM	3.49
WDR46	3.49
SBF2	3.48
DHX32	3.47
CKMT2	3.46
PHPT1	3.45
FAM162A	3.45
TNFRSF21	3.44
EDA2R	3.42

KLHL14	3.41
PI4K2A	3.40
STAP1	3.39
NDUFA4	3.38
GPR176	3.38
C14orf132	3.37
RPS27L	3.36
TLN2	3.35
OSBPL1A	3.32
PEX7	3.31
ORC3	3.29
ACTA2	3.29
GARS	3.29
HAAO	3.29
FKBP11	3.28
C3orf39	3.28
VARS2	3.28
DGCR6	3.28
ZNF571	3.27
URGCP	3.26
S100A11	3.26
CCT6A	3.26
PFDN6	3.26
EIF3B	3.25
BROX	3.24
NME1	3.23
THAP9	3.22
MREG	3.21
B3GNT5	3.21
CYTIP	3.17
MPEG1	3.16
MRPS28	3.14

NT5DC3	3.14
NDUFAF2	3.10
PMS2	3.10
UAP1	3.09
POLD2	3.08
MAP1B	3.07
MRPL2	3.07
NTPCR	3.07
GCLC	3.06
DDX60	3.06
FAS	3.05
ZNF542	3.03
PSMA2	3.02
LOC100271831	3.02
SESN1	3.02
GUK1	3.01
CD3EAP	3.00
C3orf78	3.00
SARS2	2.99
RPAP3	2.98
OGDH	2.98
HRSP12	2.96
MINA	2.96
UBE2CBP	2.94
CSRP2	2.94
HERC5	2.92
DCXR	2.91
RASA4P	2.91
WBP5	2.91
ABCF1	2.91
CCDC74A	2.91
C9orf64	2.91

TRIM58	2.90
CENPW	2.88
HSP90AB1	2.88
MYL4	2.88
FOSL1	2.87
ARHGAP18	2.87
FH	2.87
NUDT1	2.85
LACE1	2.85
RPL26L1	2.84
NOP16	2.84
PSMB1	2.84
TMEM14A	2.83
MRPS18B	2.82
BZW2	2.82
XPO5	2.80
ALDH1B1	2.80
PMPCB	2.80
LRFN3	2.78
C3orf26	2.77
MT2A	2.76
TCP1	2.76
PACSIN3	2.75
NQO1	2.75
NPL	2.75
BOLA3	2.75
C7orf44	2.74
CCDC167	2.74
METTL1	2.74
VWCE	2.73
EFNB1	2.73
GMNN	2.73

LOC649330	2.73
ZNF670	2.73
MT1X	2.72
ADCY9	2.72
MVK	2.70
LYSMD1	2.70
OXER1	2.68
KLHL3	2.68
POLR3G	2.68
CNIH4	2.68
MLKL	2.67
SCAMP5	2.67
TOE1	2.66
TOMM7	2.66
RIOK1	2.66
REC8	2.66
PUS7	2.66
NPM3	2.66
KIAA0664	2.65
FAM26F	2.65
RPP40	2.63
ADAM15	2.63
C6orf192	2.63
LOC92659	2.62
MRPL55	2.61
TRMT11	2.61
GALE	2.60
ARL6	2.60
HEATR1	2.60
BBC3	2.60
CUTA	2.59
CLCN5	2.59

SH2D2A	2.58
SCCPDH	2.58
B3GNT7	2.58
GPR126	2.58
ENDOG	2.58
POMT1	2.57
TNNI3K	2.57
GTF2H4	2.57
DDX56	2.57
RDBP	2.57
HSPE1	2.56
ELMO1	2.56
C1QBP	2.56
PTPRZ1	2.55
ARF3	2.55
TUBA1C	2.54
LOC100286844	2.54
COQ3	2.53
HEATR2	2.53
ABHD16A	2.53
IPO4	2.53
AIF1	2.52
PALM2	2.52
HSPD1	2.52
B7H6	2.51
C12orf41	2.51
TMEM183B	2.51
TTN	2.51
RCAN1	2.50
SNRPC	2.50
HPDL	2.50
CDKAL1	2.50

MAP4K4	2.50
AS3MT	2.50
TCTN2	2.50
TTK	2.49
BCL2L12	2.49
SLC16A10	2.49
PHF14	2.49
CKB	2.48
PYGL	2.47
ZBTB7B	2.47
SMARCD1	2.47
MCM3	2.46
PDF	2.46
FARS2	2.46
NLN	2.46
ZNF239	2.46
SENP1	2.46
MCRS1	2.45
PRKAR1B	2.45
SLC35A4	2.45
DYNC2LI1	2.45
TSFM	2.44
MSH5	2.44
MRPL1	2.44
PSMG1	2.44
DDX21	2.44
SLC39A4	2.43
LSS	2.43
NT5C3L	2.43
C7orf30	2.43
MAGI1	2.43
HCN3	2.42

DHCR7	2.42
RWDD1	2.42
ACAT1	2.42
NUDT3	2.42
AFAP1L1	2.41
EIF3IP1	2.41
C7orf50	2.41
EPHX1	2.41
HOMER1	2.41
ARMC9	2.41
TMEM106C	2.40
TRAP1	2.40
VPRBP	2.40
FAM127A	2.40
S100A4	2.40
TUBA1B	2.39
HSD17B6	2.39
SLC40A1	2.38
ADSS	2.38
GPR65	2.38
MRPL12	2.38
MIF	2.38
ITSN1	2.37
PELO	2.37
NT5DC1	2.36
GBP1	2.36
EIF1AD	2.36
APITD1	2.36
RRP36	2.35
GLRX2	2.35
MRPL4	2.35
KAZN	2.35

RANBP1	2.34
CHCHD2	2.34
EBNA1BP2	2.34
ACOT7	2.34
WDR18	2.33
C6orf26	2.33
C16orf59	2.33
ZSCAN5A	2.33
DOCK9	2.33
PSMA3	2.33
RPS12	2.32
UBE2E3	2.32
CLCN6	2.32
PCYT2	2.32
TFAP2C	2.31
GSTP1	2.31
CCDC58	2.30
GADD45GIP1	2.30
CCZ1	2.29
PHF10	2.29
C16orf88	2.29
MEF2B	2.29
LOC100287722	2.29
PHB	2.29
NELL1	2.29
XRCC5	2.29
AHCY	2.28
EDARADD	2.28
IQCK	2.28
RRP12	2.28
C15orf63	2.28
GCSH	2.28

C7orf28B	2.28
KLHL5	2.28
TTLL12	2.27
BLVRB	2.27
IPO11	2.27
MRPL39	2.27
C12orf62	2.27
SNORA40	2.27
NDUFS5	2.27
ZNF643	2.27
ACN9	2.27
FARSB	2.26
CCDC86	2.26
HSPBP1	2.26
THG1L	2.26
PLTP	2.26
CCDC51	2.25
HOPX	2.25
ROR1	2.25
SCFD2	2.25
FAM54A	2.25
NVL	2.25
ASCC3	2.25
L2HGDH	2.24
CACNB2	2.24
BYSL	2.23
SMYD3	2.23
UCHL5	2.23
SRM	2.23
GCHFR	2.23
DIP2B	2.23
ENO1	2.23

MIPEP	2.22
ZNRD1	2.22
PARP1	2.22
TRIP10	2.22
UTP20	2.22
MRPS7	2.22
CLASP2	2.22
WDR12	2.22
FKBP5	2.21
DDX39B	2.21
DUSP15	2.21
GTF3C6	2.21
KCNN4	2.21
EIF2B3	2.21
MDN1	2.20
SDF2L1	2.20
NUP133	2.19
DCTPP1	2.19
GPN1	2.19
C2orf47	2.19
MAF	2.19
NFS1	2.19
ZNF43	2.18
ABCB10	2.18
ISOC2	2.18
LCMT2	2.18
PRKAG1	2.18
MTFP1	2.18
GEMIN5	2.17
ASB8	2.17
LYRM4	2.17
AIMP2	2.17

RAD51L3-RFFL	2.17
TACO1	2.16
RTEL1	2.16
RPS2P32	2.16
LTV1	2.16
TOMM40	2.16
CSE1L	2.16
LDHA	2.16
PDP2	2.16
ALDOA	2.16
DDX23	2.15
GBP2	2.15
GPI	2.14
GCDH	2.14
ORC1	2.14
HK2	2.14
BAG6	2.14
MAP1A	2.13
SNAPC2	2.13
CYB5R4	2.13
SKIV2L	2.13
ATPAF1	2.13
UGT3A2	2.13
EEF1E1	2.13
PSD3	2.13
MRM1	2.13
MRTO4	2.13
L3MBTL3	2.12
MRPL11	2.12
NME2	2.12
RFC4	2.12
EARS2	2.12

TMCO7	2.12
MRPS18A	2.12
RCOR2	2.12
NDUFAF4	2.11
HMBS	2.11
TBRG4	2.11
HMGA1	2.11
LGALS3BP	2.11
ATP5G1	2.11
TBXA2R	2.11
SMAP1	2.11
POLR2J4	2.10
PAQR9	2.10
GNL1	2.10
NCL	2.10
KHK	2.10
KIAA0114	2.10
RPS26	2.09
PSMD1	2.09
HDAC2	2.09
MRPL27	2.09
LARS2	2.09
AKR1B1	2.09
DHX57	2.09
PARS2	2.09
TTC23	2.08
PPP2R1B	2.08
PPIL1	2.08
LOC344967	2.08
C20orf27	2.08
EIF5A	2.08
ATF1	2.08

DHX16	2.07
FECH	2.07
FBXW9	2.07
SELRC1	2.07
TBCE	2.07
FABP5	2.06
RABEPK	2.06
DIAPH3	2.06
SNRPF	2.06
ACADSB	2.06
NPW	2.06
GRWD1	2.06
RPL23AP82	2.06
PGK1	2.05
AKR7A2	2.05
SIP1	2.05
CISD1	2.05
VPS41	2.05
THNSL1	2.05
PDCD2L	2.05
RRP1B	2.04
BDH1	2.04
MRPL47	2.04
C8orf59	2.04
TALDO1	2.04
SYNCRIP	2.04
LOC388564	2.04
GLO1	2.04
MAPK13	2.04
GGH	2.04
KBTBD7	2.04
CCDC124	2.03

HYAL2	2.03
RRP9	2.03
HNRNPA2B1	2.03
SLC38A2	2.03
EHMT2	2.03
GBAS	2.03
HSPA9	2.03
CHI3L2	2.03
PPP1R14B	2.03
TUBA1A	2.03
PRELID1	2.03
PMF1-BGLAP	2.03
TUBB3	2.02
PGAM4	2.02
GNL3	2.02
SF3A3	2.02
BAG4	2.02
PPA2	2.02
MIS18A	2.02
SPRYD7	2.02
HSPH1	2.02
PA2G4P4	2.02
GAPT	2.01
PSMD11	2.01
CHCHD4	2.01
RPS26P11	2.01
HIST1H1B	2.01
MTHFD1	2.01
ALG14	2.01
AGK	2.00
TUBG2	2.00
WDR3	2.00

RMND1	**2.00**
PFAS	**2.00**

Table A.3 Metacore pathway maps in the transcriptome data

Maps	p-value	FDR
Transcription_Role of AP-1 in regulation of cellular metabolism	**2.948E-07**	**2.287E-04**
Cytoskeleton remodeling_Cytoskeleton remodeling	**4.952E-06**	**1.922E-03**
Cytoskeleton remodeling_TGF, WNT and cytoskeletal remodeling	**1.677E-05**	**4.337E-03**
Inhibition of neutrophil migration by proresolving lipid mediators in COPD	**5.898E-05**	**1.144E-02**
Reproduction_GnRH signaling	**8.004E-05**	**1.242E-02**
NETosis in SLE	**1.465E-04**	**1.722E-02**
Cell adhesion_Integrin-mediated cell adhesion and migration	**1.553E-04**	**1.722E-02**
Neurophysiological process_Corticoliberin signaling via CRHR1	**2.219E-04**	**2.027E-02**
Immune response_ETV3 affect on CSF1-promoted macrophage differentiation	**2.350E-04**	**2.027E-02**
Transcription_Role of VDR in regulation of genes involved in osteoporosis	**2.845E-04**	**2.208E-02**
Immune response_HSP60 and HSP70/ TLR signaling pathway	**4.282E-04**	**2.858E-02**
HBV signaling via protein kinases leading to HCC	**4.458E-04**	**2.858E-02**
Immune response_MIF-induced cell adhesion, migration and angiogenesis	**5.414E-04**	**2.858E-02**
Immune response_MIF - the neuroendocrine-macrophage connector	**5.414E-04**	**2.858E-02**
Development_Keratinocyte differentiation	**5.799E-04**	**2.858E-02**
Role of Endothelin-1 in inflammation and vasoconstriction in Sickle cell disease	**6.569E-04**	**2.858E-02**
Development_Regulation of cytoskeleton proteins in oligodendrocyte differentiation and myelination	**7.735E-04**	**2.858E-02**
Stimulation of TGF-beta signaling in lung cancer	**7.507E-04**	**2.858E-02**
Cell adhesion_Chemokines and adhesion	**6.864E-04**	**2.858E-02**
Immune response_MIF-mediated glucocorticoid regulation	**7.343E-04**	**2.858E-02**
LRRK2 and immune function in Parkinson's disease	**7.343E-04**	**2.858E-02**
Immune response_C5a signaling	**1.022E-03**	**3.604E-02**
CFTR folding and maturation (normal and CF)	**1.211E-03**	**4.087E-02**
Signal transduction_Activin A signaling regulation	**1.360E-03**	**4.399E-02**
Transcription_Transcription regulation of aminoacid metabolism	**1.524E-03**	**4.549E-02**
Immune response_IL-1 signaling pathway	**1.806E-03**	**5.190E-02**

Glycolysis and gluconeogenesis (short map)	2.149E-03	5.380E-02
Cytoskeleton remodeling_Neurofilaments	1.524E-03	4.549E-02
Immune response_TNF-R2 signaling pathways	2.097E-03	5.380E-02
Cell adhesion_Histamine H1 receptor signaling in the interruption of cell barrier integrity	2.097E-03	5.380E-02
Cell adhesion_Cadherin-mediated cell adhesion	1.895E-03	5.251E-02
Signal transduction_PTMs in IL-17-induced CIKS-independent signaling pathways	2.425E-03	5.881E-02
Immune response_Oncostatin M signaling via MAPK in human cells	2.735E-03	6.241E-02
Immune response_Antigen presentation by MHC class II	2.644E-03	6.218E-02
dATP/dITP metabolism	3.913E-03	7.786E-02
Immune response_IL-18 signaling	3.790E-03	7.739E-02
Regulation of degradation of wtCFTR	3.132E-03	6.943E-02
Immune response_IL-2 activation and signaling pathway	3.653E-03	7.739E-02
Regulation of degradation of deltaF508-CFTR in CF	3.732E-03	7.739E-02
Cell adhesion_Gap junctions	4.090E-03	7.935E-02
Development_Oligodendrocyte differentiation from adult stem cells	4.706E-03	8.695E-02
Chemotaxis_Inhibitory action of lipoxins on IL-8- and Leukotriene B4-induced neutrophil migration	4.706E-03	8.695E-02
Signal transduction_Activation of PKC via G-Protein coupled receptor	5.313E-03	9.371E-02
Immune response_IL-3 activation and signaling pathway	4.852E-03	8.756E-02
Nociception_Nociceptin receptor signaling	6.097E-03	1.007E-01
Cell cycle_Role of Nek in cell cycle regulation	5.712E-03	9.637E-02
Cell cycle_Start of DNA replication in early S phase	5.712E-03	9.637E-02
Regulation of Tissue factor signaling in cancer	6.528E-03	1.055E-01
Development_BMP signaling	6.679E-03	1.058E-01
Glycolysis and gluconeogenesis p.3	7.220E-03	1.099E-01

Table A.4 Genes regulated in common between resistant xenografts identified by microarray

GENE	2055-S	2055-R	2055-S eve	2055-R eve	1345-S	1345-R	1345-S eve	1345-R eve
A2M	1.00	-2.21	1.45	-2.69	1.00	0.89	1.22	1.34
AADACL4	1.00	-33.59	-3.88	-52.90	1.00	0.65	0.71	0.48
ABCD4	1.00	1.31	0.68	1.48	1.00	-2.41	-2.36	-1.59
ADAM33	1.00	0.77	0.87	0.69	1.00	-5.38	-8.80	-5.47
ADAP1	1.00	-3.94	0.00	-3.87	1.00	0.35	1.84	0.80
AGXT2L1	1.00	-3.69	1.21	-1.81	1.00	0.17	0.77	1.01
ALDH1A1	1.00	-94.44	2.36	-93.51	1.00	-0.28	1.28	-0.37
ALDH3B1	1.00	-26.45	0.63	-25.03	1.00	1.66	3.50	2.30
ANKRD55	1.00	-4.87	0.98	-4.77	1.00	0.75	0.66	0.72
ANTXR2	1.00	-18.12	1.67	-25.20	1.00	1.51	1.07	1.38
ARHGAP22	1.00	-7.22	0.63	-3.15	1.00	1.74	5.21	3.03
ARHGEF17	1.00	-28.62	1.56	-44.93	1.00	-52.44	-50.12	66.27
ARHGEF3	1.00	-21.48	-0.17	-23.53	1.00	0.46	0.56	0.76
ARHGEF5	1.00	-7.72	1.16	-7.80	1.00	1.12	0.99	0.91
ARHGEF5L	1.00	-584.54	-2.88	-593.93	1.00	-0.63	2.17	-1.04
ATP10D	1.00	-0.62	0.23	-0.38	1.00	-6.38	-19.33	-13.36
B3GALTL	1.00	9.34	0.24	6.48	1.00	-3.53	1.13	-6.32
BATF	1.00	-4.59	1.56	-4.34	1.00	2.16	2.09	1.83
BGN	1.00	-3.46	0.43	-3.87	1.00	1.59	19.67	32.80
BRSK1	1.00	2.81	0.69	3.73	1.00	-30.68	-16.99	-34.05
C18ORF51	1.00	-443.44	-0.48	-341.19	1.00	0.56	0.37	0.20
C1ORF115	1.00	-166.45	1.45	-169.25	1.00	0.77	1.70	1.77
C1QTNF3	1.00	1.14	0.80	1.19	1.00	-3.20	-2.46	-3.71
C20ORF197	1.00	-5.65	-0.54	-28.21	1.00	0.68	-0.46	-0.01
C2ORF55	1.00	-25.98	2.02	-41.62	1.00	0.48	1.07	0.44

C5ORF42	1.00	1.96	0.47	2.44	1.00	-16.36	-22.03	-37.83
C6ORF59	1.00	-3.32	0.20	-3.58	1.00	0.58	2.27	1.28
CA8	1.00	-3.00	0.77	-2.76	1.00	1.00	1.35	1.18
CAP2	1.00	-13.82	0.42	-29.42	1.00	0.98	1.64	3.35
CARD6	1.00	2.56	1.07	1.65	1.00	-6.50	0.54	-1.87
CCDC71	1.00	0.54	0.34	0.69	1.00	-3.43	-4.46	-5.65
CCDC89	1.00	12.35	1.30	13.89	1.00	-2.80	6.93	-1.55
CCND1	1.00	-17.12	1.19	-18.20	1.00	-0.08	-0.34	-1.02
CCND2	1.00	-116.76	1.30	-126.27	1.00	-0.51	-1.08	-0.86
CD1C	1.00	-30.50	4.91	-48.42	1.00	-1.27	-0.62	0.30
CD244	1.00	2.80	0.61	3.34	1.00	-9.76	-3.40	-2.24
CD247	1.00	-49.55	-2.06	-38.59	1.00	4.88	-0.62	2.47
CD300A	1.00	-7.22	0.57	-10.71	1.00	1.48	1.69	1.75
CD300LF	1.00	-12.80	7.26	-16.98	1.00	1.61	0.48	2.62
CD3D	1.00	-27.86	1.04	-35.60	1.00	1.25	0.52	0.66
CD93	1.00	-2980.36	2.17	-3502.35	1.00	0.53	1.85	1.49
CEACAM1	1.00	-149.60	0.24	-206.94	1.00	2.59	0.92	0.38
CEACAM6	1.00	-13.44	2.96	-11.71	1.00	1.75	1.25	0.46
CENTG2	1.00	-147.41	0.11	-149.02	1.00	-4.05	1.28	-1.75
CGNL1	1.00	-28.41	0.89	-32.55	1.00	0.87	1.21	0.78
CITED4	1.00	-35.30	1.12	-38.72	1.00	0.20	-0.55	-0.42
CPVL	1.00	-13.79	1.43	-13.45	1.00	0.60	0.68	1.43
CSGALNACT1	1.00	-14.97	1.59	-26.23	1.00	0.66	1.36	0.77
CTDSPL	1.00	-23.06	0.99	-21.05	1.00	2.71	4.08	4.25
CXCR3	1.00	-4204.87	26.07	-3707.50	1.00	1.54	0.81	-0.07
CYTSB	1.00	-9.55	0.92	-10.18	1.00	0.08	-0.05	1.31
DEFA5	1.00	0.83	0.80	0.65	1.00	-34.48	-408.27	-177.86
DHDH	1.00	-123.35	4.56	-177.95	1.00	1.78	2.70	4.72
DNER	1.00	-7.06	1.02	-17.26	1.00	1.26	0.52	1.38

DUSP3	1.00	-30.83	1.07	-33.78	1.00	0.32	0.49	0.34
ECM2	1.00	-5.95	0.71	-8.23	1.00	0.38	0.28	1.12
EEPD1	1.00	-6.42	0.21	-7.44	1.00	0.15	1.91	1.73
EFCAB2	1.00	2.25	0.76	2.75	1.00	-22.98	-3.37	-11.25
EFNB1	1.00	-57.49	-1.06	-63.01	1.00	-1.08	-1.32	-1.00
EMILIN1	1.00	-3.38	1.54	-3.15	1.00	1.51	2.01	1.64
ENOSF1	1.00	-28.93	0.91	-20.49	1.00	0.77	0.83	0.98
ERV3	1.00	3.13	0.81	3.21	1.00	-7.88	1.74	-6.53
FAM46B	1.00	-86.71	7.38	-98.87	1.00	0.57	-15.41	-9.11
FAM89A	1.00	-515.15	0.19	-599.81	1.00	-2.35	0.52	-2.77
FAM90A1	1.00	-3.80	0.54	-4.10	1.00	0.43	1.22	0.92
FGD5	1.00	-75.08	-7.35	-123.84	1.00	0.17	0.88	0.06
FGD6	1.00	-3.34	0.50	-4.62	1.00	0.40	0.22	0.84
FLJ11795	1.00	-4.40	0.78	-5.06	1.00	0.93	1.58	1.12
FLJ23834	1.00	-35.94	1.11	-39.86	1.00	0.77	0.93	1.14
FLJ35220	1.00	-0.14	0.38	0.08	1.00	-2.12	4.28	-0.20
FLJ37228	1.00	0.57	0.66	0.34	1.00	-81.17	-54.76	-55.80
FLJ41649	1.00	-19.70	-0.31	-17.94	1.00	1.87	0.23	0.22
FLJ46020	1.00	-12.74	-1.71	-9.79	1.00	-1.05	-0.82	-2.29
FSTL5	1.00	-82.94	1.67	-98.07	1.00	1.23	1.14	0.52
GALNT11	1.00	-15.72	1.85	-10.97	1.00	0.91	1.12	0.86
GANC	1.00	1.82	0.75	2.08	1.00	-4.45	-3.62	-8.63
GBA3	1.00	-9.67	0.77	-8.34	1.00	1.03	1.04	1.24
GDF9	1.00	1.63	1.16	1.93	1.00	-27.16	-21.93	-24.39
GDPD5	1.00	-9.49	1.11	-7.99	1.00	0.73	0.72	0.69
GIMAP6	1.00	13.15	1.42	16.19	1.00	-3.66	-1.11	-4.36
GLIPR1	1.00	-81.45	6.67	-105.12	1.00	0.99	0.39	1.41
GPR68	1.00	-37.60	0.46	-51.99	1.00	0.78	1.90	1.03
GPRC5B	1.00	0.78	0.67	0.44	1.00	-18.75	-24.22	-20.31

GRAP2	1.00	-7.19	0.70	-8.56	1.00	1.48	1.14	1.79
GUCY1B3	1.00	9.11	-0.24	9.58	1.00	-40.97	-67.02	-23.53
HEY2	1.00	-25.84	2.62	-36.28	1.00	0.68	0.94	0.67
HGF	1.00	-14.40	1.64	-17.91	1.00	0.57	0.45	0.12
HPD	1.00	29.02	0.44	33.08	1.00	-428.73	-637.03	-308.04
HS.151692	1.00	-21.46	-0.32	-13.15	1.00	14.77	9.40	19.82
HS.155579	1.00	1.44	1.11	0.57	1.00	-5.31	-6.72	-5.48
HS.175285	1.00	0.89	0.80	0.29	1.00	-6.27	-3.79	-4.75
HS.18849	1.00	1.01	0.66	0.84	1.00	-9.33	-5.68	-0.90
HS.189987	1.00	-5.78	1.19	-5.82	1.00	-0.29	1.22	-0.15
HS.193557	1.00	-7.92	-0.64	-7.17	1.00	0.34	1.55	0.42
HS.222909	1.00	-3.77	0.04	-4.94	1.00	0.39	-1.43	2.07
HS.439578	1.00	-42.37	-11.85	-69.76	1.00	5.21	8.14	0.89
HS.482960	1.00	-28.49	3.95	-29.32	1.00	0.57	0.96	0.44
HS.536336	1.00	1.31	1.60	1.83	1.00	-8.33	-6.88	-13.15
HS.564658	1.00	1.29	1.62	1.17	1.00	-4.78	-5.87	-2.81
HS3ST1	1.00	-3.61	-0.30	-4.53	1.00	0.24	-0.35	-0.07
HTR7	1.00	-8.03	1.53	-6.30	1.00	0.63	-1.03	0.24
IFFO2	1.00	2.32	1.00	3.26	1.00	-10.59	-10.49	-3.04
IL18R1	1.00	-10.22	1.29	-37.43	1.00	0.71	0.08	0.00
IL18RAP	1.00	-9.14	0.85	-29.23	1.00	-0.54	0.12	-0.92
IL1B	1.00	0.59	1.63	0.71	1.00	-4.14	1.66	-8.01
INSL3	1.00	-11.91	5.01	-17.10	1.00	1.01	1.19	0.73
IQSEC2	1.00	-6.10	0.40	-14.18	1.00	0.13	0.70	0.68
IRGM	1.00	-8.97	1.30	-10.32	1.00	0.77	0.99	-0.46
JPH1	1.00	-5.16	1.20	-2.20	1.00	1.23	0.45	1.22
JPH3	1.00	-5.87	0.46	-6.80	1.00	5.37	17.69	7.60
KANK3	1.00	-10.56	0.40	-12.82	1.00	-1.09	-0.20	-0.35
KDM4D	1.00	1.35	0.83	1.56	1.00	-3.48	-7.41	-5.49

KDM6B	1.00	2.29	1.00	3.25	1.00	-3.10	6.35	3.21
KIAA1199	1.00	-20.99	0.86	-21.92	1.00	1.14	1.06	1.34
KIAA1324L	1.00	-16.25	1.40	-20.46	1.00	0.53	0.87	0.85
KIAA1522	1.00	1.25	1.04	1.45	1.00	-3.58	-3.91	-6.07
KIF17	1.00	-13.21	0.90	-13.36	1.00	0.45	1.14	0.78
KIT	1.00	0.26	0.23	0.59	1.00	-2.38	-3.08	2.82
KL	1.00	-17.35	2.71	-17.53	1.00	-6.97	-1.55	-7.63
KLHL38	1.00	0.57	0.63	2.31	1.00	-44.81	-64.31	-37.86
LARP6	1.00	-17.16	1.14	-17.76	1.00	0.38	1.07	0.62
LGALS7B	1.00	-2.76	0.84	-3.07	1.00	0.63	0.45	0.56
LOC100129354	1.00	-20.43	-2.39	-16.51	1.00	1.81	2.36	0.53
LOC100129977	1.00	0.60	0.74	0.52	1.00	-44.45	-63.78	-33.72
LOC100131250	1.00	1.50	0.61	1.24	1.00	-238.42	-287.95	-304.44
LOC100132532	1.00	-13.40	0.85	-15.05	1.00	-2.04	-4.41	-4.56
LOC100133214	1.00	0.52	0.22	0.64	1.00	-2.65	-4.10	-9.81
LOC100134728	1.00	1.32	1.12	1.84	1.00	-2.48	0.39	-0.44
LOC144481	1.00	-1161.86	25.16	-1398.41	1.00	2.78	-0.32	-0.63
LOC154822	1.00	-23.28	1.79	-33.77	1.00	-0.32	0.80	-3.02
LOC338829	1.00	0.57	0.66	0.94	1.00	-2.85	-0.67	-0.78
LOC388820	1.00	0.92	1.57	1.24	1.00	-7.83	2.52	-0.27
LOC389000	1.00	1.53	1.06	1.85	1.00	-2.67	-8.12	-4.20
LOC389641	1.00	63.70	-5.83	46.01	1.00	-2.70	0.34	-2.08
LOC391427	1.00	24.02	-6.39	40.48	1.00	-3.61	0.97	-2.47
LOC440508	1.00	1.21	1.50	1.03	1.00	-8.49	-11.87	-9.27
LOC54103	1.00	29.11	0.44	36.04	1.00	-2.68	1.90	-2.04
LOC641744	1.00	-6.09	-0.82	-7.72	1.00	-1.74	0.73	-0.98
LOC641926	1.00	1.10	0.48	0.86	1.00	-7.38	-2.36	-3.15
LOC642083	1.00	3.29	0.35	3.22	1.00	-105.08	123.25	36.82
LOC642833	1.00	0.47	0.43	0.81	1.00	-16.83	-7.62	-1.31

LOC643918	1.00	0.68	0.34	0.84	1.00	-2.83	-4.40	-3.05
LOC644477	1.00	0.77	1.32	1.51	1.00	-9.67	-33.89	-145.72
LOC646128	1.00	0.37	1.02	0.65	1.00	-8.09	-7.42	-8.05
LOC646576	1.00	-18.79	0.13	-24.46	1.00	1.48	-4.79	0.49
LOC646855	1.00	0.46	0.32	0.27	1.00	-4.23	-19.18	-4.42
LOC647050	1.00	0.56	1.00	1.03	1.00	-2.81	-7.81	-10.77
LOC647219	1.00	1.33	1.11	1.12	1.00	-31.57	-120.05	-81.75
LOC648745	1.00	0.38	-0.44	1.17	1.00	-2.68	-1.49	1.24
LOC648982	1.00	-26.96	-7.81	-41.12	1.00	1.24	0.82	1.08
LOC650620	1.00	0.81	1.00	0.67	1.00	-4.16	-2.78	-3.63
LOC728022	1.00	0.52	0.42	0.70	1.00	-8.54	-11.97	-7.56
LOC728910	1.00	55.47	-1.76	87.08	1.00	-3.55	-2.23	0.03
LOC729313	1.00	0.84	0.70	0.96	1.00	-4.40	-76.16	-49.14
LOC729715	1.00	0.51	0.77	0.79	1.00	-3.57	-8.50	-21.41
LOC729806	1.00	1.76	0.45	2.10	1.00	-8.46	-15.00	-5.35
LOC730241	1.00	0.60	1.29	0.72	1.00	-2.62	-0.52	-0.85
LOC730281	1.00	2.09	3.74	4.24	1.00	-4.61	-22.77	-15.28
LOC730517	1.00	-107.16	-10.11	-177.90	1.00	0.18	0.73	0.13
LOC732371	1.00	4.41	1.08	3.01	1.00	-5.09	-2.70	-0.30
LOXL1	1.00	-7.42	0.64	-5.94	1.00	0.77	1.07	0.74
LRP3	1.00	-6.05	1.11	-2.15	1.00	0.73	1.54	0.82
LRRC3B	1.00	-3.79	-0.55	-4.30	1.00	-1.68	1.00	-0.63
MAML2	1.00	-6.18	-1.10	-9.70	1.00	-0.34	0.12	0.98
MAST4	1.00	-5.97	1.52	-5.89	1.00	1.96	0.38	1.16
MEGF11	1.00	6.04	-0.98	2.42	1.00	-2.08	5.78	4.85
MGC42367	1.00	-17.99	1.32	-30.86	1.00	1.04	1.08	0.70
MKRN3	1.00	-12.12	0.60	-15.85	1.00	0.55	0.83	0.89
MMP28	1.00	-39.04	0.66	-45.69	1.00	0.56	-0.12	-1.03
MOCS3	1.00	0.21	0.46	0.06	1.00	-14.57	-16.12	-12.60

MOSC2	1.00	-21.27	2.02	-16.89	1.00	1.63	0.99	0.73
MPO	1.00	-200.23	0.96	-219.46	1.00	-1.51	-0.16	0.09
MST1R	1.00	-2.79	1.02	-3.54	1.00	0.78	1.07	0.84
MYOF	1.00	-17.46	-0.45	-18.17	1.00	1.04	2.31	0.83
MYOZ3	1.00	10.65	0.16	6.81	1.00	-2.71	-0.07	-0.81
N4BP3	1.00	-0.22	0.54	-0.13	1.00	-2.24	12.56	3.93
NBL1	1.00	-7654.19	-67.51	-6464.02	1.00	1.39	-1.10	0.10
NCF1B	1.00	73.03	-3.99	109.06	1.00	-2.22	0.95	8.13
NCRNA00119	1.00	0.67	0.87	0.60	1.00	-13.09	-2.52	-16.01
NFIA	1.00	0.17	0.55	0.33	1.00	-6.62	-0.55	-3.92
NIPSNAP3B	1.00	-46.27	3.45	-66.61	1.00	0.43	0.68	0.76
NLRP11	1.00	-8.59	1.68	-8.00	1.00	1.59	1.75	1.48
NPY	1.00	-37.24	1.29	-96.79	1.00	0.83	1.52	0.94
OPLAH	1.00	-5.24	1.08	-7.11	1.00	0.42	1.08	0.34
OR2A20P	1.00	-50.03	-1.29	-56.92	1.00	-3.55	-3.01	-2.94
OR2A42	1.00	4.27	0.85	5.26	1.00	-3.87	3.79	0.25
OR2A9P	1.00	-81.53	-1.72	-100.41	1.00	-3.21	6.87	-7.14
OR7D2	1.00	-16.39	1.84	-25.33	1.00	0.87	0.67	0.66
OSBPL10	1.00	-6.07	3.17	-6.14	1.00	0.83	1.19	0.80
PC	1.00	-5.36	0.52	-3.16	1.00	0.84	1.22	1.23
PDCD1	1.00	-3.18	1.24	-4.48	1.00	0.77	1.22	0.98
PDGFRB	1.00	-27.77	1.38	-27.55	1.00	1.16	2.24	0.87
PDK4	1.00	-8.60	-0.33	-20.50	1.00	-0.79	1.39	3.12
PIK3R6	1.00	-285.39	-33.16	-307.07	1.00	-0.28	0.03	1.61
PION	1.00	-46.85	1.17	-68.49	1.00	11.29	18.24	15.14
PLAUR	1.00	2.62	0.42	2.57	1.00	-4.33	11.03	-13.02
PLCH1	1.00	4.54	0.96	8.41	1.00	-4.03	0.21	-1.40
PLCL1	1.00	-3.27	-1.18	-3.25	1.00	0.86	1.03	0.11
PLEKHA5	1.00	-15.94	-2.66	-20.42	1.00	1.17	2.59	1.66

PLEKHG7	1.00	0.98	0.89	1.21	1.00	-4.33	-6.11	-0.84
PLK2	1.00	-4.64	1.91	-4.85	1.00	2.03	3.59	-1.36
PLXNA1	1.00	-2.22	1.34	-1.72	1.00	0.87	1.05	1.12
PNOC	1.00	-24.13	0.19	-32.52	1.00	2.09	1.56	1.33
PNPLA4	1.00	-2.11	0.97	-3.59	1.00	1.51	0.61	1.50
PODXL2	1.00	-6.97	0.29	-5.54	1.00	0.30	0.04	0.17
PON2	1.00	-142.41	-1.50	-201.06	1.00	0.57	0.71	-2.68
POU2F2	1.00	-9.11	4.79	-11.43	1.00	0.99	0.75	0.95
PPFIBP2	1.00	-3.87	0.99	-6.63	1.00	1.73	0.73	1.28
PPIL2	1.00	0.81	1.08	2.00	1.00	-3.15	-13.77	-11.55
PRAM1	1.00	-3.63	0.72	-9.90	1.00	0.50	0.25	0.95
PRL	1.00	-4.69	1.37	-5.71	1.00	-0.57	0.18	1.66
PROM1	1.00	24.40	2.22	31.54	1.00	-25.58	-7.37	-4.79
PRSSL1	1.00	38.62	0.86	47.26	1.00	-2.73	0.22	-1.50
PSTPIP1	1.00	-14.96	0.35	-20.56	1.00	1.25	0.68	1.09
PTPRO	1.00	-3.46	0.91	-5.30	1.00	1.94	2.78	2.34
PVRL2	1.00	-10.65	-0.27	-14.06	1.00	0.16	1.07	0.82
RAB11B	1.00	1.26	1.41	1.28	1.00	-2.11	-2.50	-1.60
RAB17	1.00	-8.97	0.79	-18.42	1.00	0.84	1.32	0.89
RAB3IL1	1.00	-5.41	1.25	-5.08	1.00	0.36	1.30	0.92
RADIL	1.00	-32.64	-1.26	-47.10	1.00	-0.08	-0.71	1.09
RBM47	1.00	-2.60	0.88	-3.27	1.00	0.47	0.96	1.23
RENBP	1.00	12.83	0.81	13.23	1.00	-3.39	-0.36	-3.05
RFX2	1.00	0.99	0.39	1.42	1.00	-56.26	-45.92	14.09
RNF157	1.00	1.91	1.31	1.88	1.00	-2.10	-2.56	-6.86
RNF165	1.00	-248.22	-14.61	-239.57	1.00	5.85	3.15	38.91
ROR2	1.00	-73.73	1.29	-100.37	1.00	0.74	0.56	0.59
S100A16	1.00	-854.01	-2.20	-941.01	1.00	0.13	0.25	-0.36
SCARNA2	1.00	-13.53	1.96	-9.40	1.00	0.02	0.65	0.23

SCHIP1	1.00	-2.35	0.93	-2.19	1.00	1.21	0.47	0.55
SCML4	1.00	9.93	2.12	13.32	1.00	-3.53	0.03	-4.89
SEMA6A	1.00	-33.36	-1.39	-39.99	1.00	3.50	4.15	2.34
SFRP5	1.00	-0.21	0.67	-0.38	1.00	-16.49	-11.28	-19.76
SH2D3A	1.00	0.24	1.41	0.54	1.00	-7.48	6.24	-6.77
SH3RF1	1.00	-18.51	1.36	-24.17	1.00	0.42	1.46	0.32
SHISA2	1.00	-7.85	-0.08	-7.83	1.00	-0.21	-1.71	1.57
SHROOM3	1.00	-3.88	1.15	-5.40	1.00	1.48	0.39	0.97
SIPA1L2	1.00	-72.36	1.40	-124.95	1.00	0.47	0.71	0.04
SIRPA	1.00	-22.75	1.05	-29.76	1.00	0.89	1.40	0.78
SLC12A7	1.00	-5.66	-0.14	-10.86	1.00	0.94	1.00	0.74
SLC30A4	1.00	-6.18	-1.41	-10.53	1.00	0.46	0.46	1.41
SMOX	1.00	23.20	0.76	27.66	1.00	-10.53	-0.59	-4.07
SNX24	1.00	0.73	0.80	1.02	1.00	-5.77	-5.11	-8.47
SPATA13	1.00	45.73	-16.08	67.90	1.00	-4.67	0.16	-1.76
STAP2	1.00	-2.09	-0.01	-1.56	1.00	-0.69	-0.51	0.47
STON1	1.00	-27.12	18.51	-67.37	1.00	0.90	0.19	0.17
STS	1.00	3.26	1.44	4.09	1.00	-41.42	-16.60	-13.84
SYNGR1	1.00	-32.24	1.50	-28.42	1.00	1.13	0.16	0.42
SYT1	1.00	-14.92	1.41	-13.40	1.00	0.31	0.97	0.61
TAKR	1.00	-10.21	1.94	-10.54	1.00	0.61	1.12	0.88
TANC2	1.00	-40.38	0.64	-34.67	1.00	-4.48	-1.86	-3.73
TBC1D9	1.00	-5.75	0.70	-5.86	1.00	0.83	0.67	1.21
TBKBP1	1.00	-32.51	0.76	-40.85	1.00	0.59	0.67	0.37
TBX10	1.00	0.54	0.83	0.61	1.00	-61.68	-83.79	-43.82
TCF7L2	1.00	-1639.47	-62.76	-1691.71	1.00	1.44	-1.04	0.48
TES	1.00	-6.18	0.33	-7.53	1.00	1.28	2.56	1.45
TMEM121	1.00	0.57	1.23	0.91	1.00	-26.99	10.44	-8.64
TMEM128	1.00	5.58	1.01	8.33	1.00	-6.72	-1.76	-5.62

TMEM133	1.00	-8.43	0.60	-8.23	1.00	0.57	-0.10	0.75
TMEM144	1.00	-2.25	1.13	-1.47	1.00	0.96	1.01	0.90
TMEM16A	1.00	4.46	0.43	11.82	1.00	-5.70	-5.56	-22.28
TMEM170B	1.00	8.12	0.57	9.18	1.00	-4.25	12.94	4.72
TMEM38A	1.00	0.80	1.07	0.47	1.00	-42.11	-5.17	-29.13
TMEM71	1.00	-53.91	2.51	-109.69	1.00	151.94	-84.01	64.64
TMOD1	1.00	-66.55	12.03	-45.79	1.00	-0.54	-1.22	0.23
TNFRSF1B	1.00	-13.49	0.64	-16.95	1.00	0.40	0.80	1.00
TPSB2	1.00	0.52	0.53	0.43	1.00	-2.27	2.02	5.93
TRH	1.00	178.88	-0.82	257.63	1.00	-36.97	-33.67	-41.51
TRPM4	1.00	-10.14	2.42	-16.12	1.00	3.27	2.78	3.66
TRPM8	1.00	-87.11	-0.86	-171.46	1.00	-0.29	0.04	0.07
TSHZ2	1.00	-108.07	-2.73	-205.63	1.00	-0.21	2.46	1.40
TTYH1	1.00	-3.67	0.97	-2.56	1.00	0.31	0.89	0.18
TYROBP	1.00	-6.52	-0.26	-11.06	1.00	0.98	0.98	0.34
VCX-C	1.00	2.20	1.35	2.22	1.00	-2.92	4.62	4.88
WIPI1	1.00	-3.38	1.30	-10.33	1.00	0.98	0.47	0.96
ZBTB46	1.00	-0.16	0.94	0.16	1.00	-2.64	-3.69	-8.11
ZC3H12D	1.00	0.79	0.28	1.25	1.00	-17.89	-7.21	-4.20
ZNF135	1.00	-18.36	1.48	-23.53	1.00	0.66	1.02	0.60
ZNF287	1.00	0.00	0.19	0.10	1.00	-677.39	-2301.56	-831.43
ZNF354C	1.00	-10.41	0.76	-13.87	1.00	5.42	1.68	1.39
ZNF397OS	1.00	1.83	0.76	1.75	1.00	-55.08	-82.84	-83.11
ZNF467	1.00	-11.87	2.23	-15.44	1.00	1.18	1.22	1.25
ZNF471	1.00	-6.02	0.69	-7.19	1.00	1.12	1.20	0.51
ZNF521	1.00	-2.15	0.91	-1.01	1.00	1.37	1.62	1.52
ZNF667	1.00	-8.87	0.61	-10.44	1.00	1.18	2.08	1.24

Table A.5 Pathway maps of genes commonly regulated in resistant xenografts found by microarray and transcriptome.

Maps	p-value	FDR
Cell adhesion_Cadherin-mediated cell adhesion	**1.058E-05**	**9.154E-04**
Cell adhesion_Chemokines and adhesion	**2.068E-05**	**9.154E-04**
Cytoskeleton remodeling_Cytoskeleton remodeling	**2.237E-05**	**9.154E-04**
HBV signaling via protein kinases leading to HCC	**2.876E-05**	**9.154E-04**
Development_Gastrin in differentiation of the gastric mucosa	**3.390E-05**	**9.154E-04**
Cell adhesion_Histamine H1 receptor signaling in the interruption of cell barrier integrity	**5.661E-05**	**1.274E-03**
Cell adhesion_Integrin-mediated cell adhesion and migration	**6.879E-05**	**1.327E-03**
Muscle contraction_Oxytocin signaling in uterus and mammary gland	**1.482E-04**	**2.501E-03**
Development_VEGF signaling via VEGFR2 - generic cascades	**3.649E-04**	**5.473E-03**
Cell adhesion_Endothelial cell contacts by non-junctional mechanisms	**7.481E-04**	**9.891E-03**
Cytoskeleton remodeling_TGF, WNT and cytoskeletal remodeling	**8.257E-04**	**9.891E-03**
Cell adhesion_Endothelial cell contacts by junctional mechanisms	**8.792E-04**	**9.891E-03**
Cytoskeleton remodeling_Fibronectin-binding integrins in cell motility	**1.252E-03**	**1.207E-02**
NETosis in SLE	**1.252E-03**	**1.207E-02**
Neurophysiological process_Thyroliberin in cell hyperpolarization and excitability	**1.595E-03**	**1.436E-02**
Apoptosis and survival_Anti-apoptotic action of Gastrin	**2.401E-03**	**1.907E-02**
Development_VEGF signaling and activation	**2.401E-03**	**1.907E-02**
Immune response_MIF - the neuroendocrine-macrophage connector	**2.744E-03**	**2.058E-02**
Oxidative stress_Role of IL-8 signaling pathway in respiratory burst	**2.985E-03**	**2.098E-02**
Cytoskeleton remodeling_Integrin outside-in signaling	**3.109E-03**	**2.098E-02**
Development_Gastrin in cell growth and proliferation	**4.934E-03**	**3.172E-02**
Development_Positive regulation of STK3/4 (Hippo) pathway and negative regulation of YAP/TAZ function	**6.251E-03**	**3.615E-02**
Inhibition of neutrophil migration by proresolving lipid mediators in COPD	**6.251E-03**	**3.615E-02**

Development_EGFR signaling pathway	**6.426E-03**	**3.615E-02**
Nociception_Nociceptin receptor signaling	**7.333E-03**	**3.960E-02**
Cell adhesion_Role of CDK5 in cell adhesion	**1.537E-02**	**7.982E-02**
Immune response_Regulatory role of C1q in platelet activation	**2.550E-02**	**1.104E-01**
G-protein signaling_RhoB regulation pathway	**2.718E-02**	**1.104E-01**
Transcription_Transcription factor Tubby signaling pathways	**2.885E-02**	**1.104E-01**
Cell cycle_Chromosome condensation in prometaphase	**3.553E-02**	**1.104E-01**
Cytoskeleton remodeling_ESR1 action on cytoskeleton remodeling and cell migration	**3.719E-02**	**1.104E-01**
Cell cycle_Sister chromatid cohesion	**3.719E-02**	**1.104E-01**
Development_Delta- and kappa-type opioid receptors signaling via beta-arrestin	**3.885E-02**	**1.104E-01**
Development_GDNF signaling	**4.050E-02**	**1.104E-01**
Cell cycle_Initiation of mitosis	**4.216E-02**	**1.104E-01**
Development_Angiotensin signaling via beta-Arrestin	**4.216E-02**	**1.104E-01**
Transcription_Transcription regulation of aminoacid metabolism	**4.216E-02**	**1.104E-01**
Neurophysiological process_Dopamine D2 receptor transactivation of PDGFR in CNS	**4.381E-02**	**1.104E-01**
Neurophysiological process_nNOS signaling in neuronal synapses	**4.875E-02**	**1.104E-01**

Table A.6 Process networks of genes commonly regulated in resistant xenografts found by microarray and transcriptome

Networks	p-value	FDR
Cell adhesion_Cadherins	8.305E-09	5.647E-07
Cell adhesion_Cell junctions	5.071E-05	1.724E-03
Cytoskeleton_Regulation of cytoskeleton rearrangement	9.073E-05	2.057E-03
Cell adhesion_Integrin-mediated cell-matrix adhesion	1.900E-04	3.230E-03
Development_Neuromuscular junction	5.246E-04	7.134E-03
Cytoskeleton_Actin filaments	1.033E-03	1.143E-02
Signal transduction_Oxytocin signaling	1.420E-03	1.143E-02
Cell cycle_G1-S Growth factor regulation	1.513E-03	1.143E-02
Cell adhesion_Amyloid proteins	1.513E-03	1.143E-02
Signal Transduction_Cholecystokinin signaling	2.589E-03	1.688E-02
Inflammation_Protein C signaling	2.731E-03	1.688E-02
Cell adhesion_Platelet aggregation	7.931E-03	4.444E-02
Cell adhesion_Glycoconjugates	8.496E-03	4.444E-02
Muscle contraction	1.017E-02	4.939E-02
Cell adhesion_Synaptic contact	1.202E-02	5.451E-02
Inflammation_Neutrophil activation	1.825E-02	7.062E-02
Cytoskeleton_Intermediate filaments	1.917E-02	7.062E-02
Immune response_Phagocytosis	1.987E-02	7.062E-02
Cytoskeleton_Macropinocytosis and its regulation	2.099E-02	7.062E-02
Reproduction_Spermatogenesis, motility and copulation	2.131E-02	7.062E-02
Development_Neurogenesis_Axonal guidance	2.181E-02	7.062E-02
Reproduction_Male sex differentiation	2.518E-02	7.784E-02

Table A.7 Pathway maps enriched in CR patients

Maps	p-value	FDR
Cell cycle_The metaphase checkpoint	9.644E-22	7.850E-19
Cell cycle_Role of APC in cell cycle regulation	1.869E-19	7.609E-17
Cell cycle_Spindle assembly and chromosome separation	1.217E-13	3.302E-11
Protein folding and maturation_POMC processing	2.695E-12	5.484E-10
Cell cycle_Cell cycle (generic schema)	9.928E-11	1.616E-08
Cell cycle_Transition and termination of DNA replication	1.273E-10	1.727E-08
DNA damage_ATM/ATR regulation of G1/S checkpoint	1.584E-10	1.841E-08
Cell cycle_Role of SCF complex in cell cycle regulation	2.609E-10	2.654E-08
Cell cycle_Start of DNA replication in early S phase	1.792E-09	1.621E-07
Cell cycle_Role of Nek in cell cycle regulation	1.797E-08	1.463E-06
IL-6 signaling in multiple myeloma	2.367E-08	1.751E-06
Cell cycle_Chromosome condensation in prometaphase	2.828E-08	1.919E-06
Cell cycle_Influence of Ras and Rho proteins on G1/S Transition	4.904E-08	3.071E-06
DNA damage_ATM / ATR regulation of G2 / M checkpoint	6.200E-08	3.605E-06
Cell cycle_ESR1 regulation of G1/S transition	2.549E-07	1.383E-05
Cell cycle_Initiation of mitosis	3.587E-07	1.825E-05
DNA damage_Role of Brca1 and Brca2 in DNA repair	5.110E-07	2.447E-05
Development_Thrombopoietin-regulated cell processes	3.668E-06	1.659E-04
Immune response_Signaling pathway mediated by IL-6 and IL-1	3.938E-06	1.687E-04
Inhibition of neutrophil migration by proresolving lipid mediators in COPD	6.179E-06	2.515E-04
Signal transduction_Additional pathways of NF-kB activation (in the cytoplasm)	7.520E-06	2.915E-04
Mitogenic action of Estradiol / ESR1 (nuclear) in breast cancer	1.232E-05	4.559E-04
Apoptosis and survival_DNA-damage-induced apoptosis	1.292E-05	4.573E-04
Immune response_BCR pathway	1.635E-05	5.547E-04
Development_NOTCH1-mediated pathway for NF-KB activity modulation	1.792E-05	5.836E-04

Role of B cells in SLE	2.096E-05	6.488E-04
Transcription_Role of heterochromatin protein 1 (HP1) family in transcriptional silencing	2.232E-05	6.488E-04
Reproduction_Progesterone-mediated oocyte maturation	2.232E-05	6.488E-04
Transcription_Ligand-dependent activation of the ESR1/SP pathway	2.659E-05	7.215E-04
Immune response_IL-4 - antiapoptotic action	2.659E-05	7.215E-04
Apoptosis and survival_Apoptotic TNF-family pathways	4.008E-05	1.053E-03
Cell cycle_Sister chromatid cohesion	5.324E-05	1.354E-03
Cell cycle_Regulation of G1/S transition (part 1)	6.358E-05	1.568E-03
Transport_RAN regulation pathway	6.908E-05	1.654E-03
Cytoskeleton remodeling_TGF, WNT and cytoskeletal remodeling	8.164E-05	1.899E-03
Inflammatory factors-induced expression of mucins in normal and asthmatic epithelium	8.938E-05	1.966E-03
Signal transduction_NF-kB activation pathways	8.938E-05	1.966E-03
Development_Regulation of cytoskeleton proteins in oligodendrocyte differentiation and myelination	1.066E-04	2.283E-03
Proteolysis_Putative SUMO-1 pathway	1.134E-04	2.334E-03
Immune response_Inhibitory action of Lipoxins on pro-inflammatory TNF-alpha signaling	1.147E-04	2.334E-03
Immune response_HMGB1/RAGE signaling pathway	1.407E-04	2.763E-03
Immune response_HMGB1 release from the cell	1.448E-04	2.763E-03
Development_Leptin signaling via PI3K-dependent pathway	1.460E-04	2.763E-03
Immune response_LTBR1 signaling	1.612E-04	2.983E-03
DNA damage_Inhibition of telomerase activity and cellular senescence	1.695E-04	2.999E-03
DNA damage_Mismatch repair	1.695E-04	2.999E-03
Immune response_IL-6 signaling pathway	2.134E-04	3.584E-03
Aberrant B-Raf signaling in melanoma progression	2.159E-04	3.584E-03
dCTP/dUTP metabolism	2.200E-04	3.584E-03
Immune response_IL-2 activation and signaling pathway	2.309E-04	3.584E-03

Table A.8 Process networks enriched in CR patients

Networks	p-value	FDR
Cell cycle_Mitosis	2.704E-28	4.299E-26
Cell cycle_Core	4.171E-27	3.316E-25
Cytoskeleton_Spindle microtubules	1.494E-22	7.921E-21
Cell cycle_S phase	1.177E-19	4.678E-18
Cell cycle_G2-M	1.815E-14	5.772E-13
DNA damage_Checkpoint	2.474E-10	6.557E-09
Cell cycle_Meiosis	2.073E-09	4.709E-08
DNA damage_DBS repair	4.091E-08	8.130E-07
Transcription_mRNA processing	6.874E-07	1.214E-05
DNA damage_MMR repair	2.940E-06	4.674E-05
Transcription_Chromatin modification	6.071E-06	8.776E-05
Cell cycle_G1-S	7.450E-06	9.871E-05
DNA damage_BER-NER repair	4.154E-05	5.081E-04
Cell cycle_G1-S Interleukin regulation	9.372E-05	1.064E-03
Reproduction_Male sex differentiation	1.792E-04	1.900E-03
Reproduction_Progesterone signaling	2.776E-04	2.759E-03
Cytoskeleton_Regulation of cytoskeleton rearrangement	3.281E-04	3.069E-03
Cell adhesion_Cadherins	4.427E-04	3.910E-03
Inflammation_IL-4 signaling	6.922E-04	5.793E-03
Apoptosis_Death Domain receptors & caspases in apoptosis	1.060E-03	8.430E-03
Proliferation_Positive regulation cell proliferation	1.118E-03	8.464E-03
Cytoskeleton_Cytoplasmic microtubules	1.503E-03	1.086E-02
Apoptosis_Apoptotic nucleus	1.792E-03	1.221E-02
Immune response_Phagosome in antigen presentation	1.843E-03	1.221E-02
Signal transduction_WNT signaling	2.135E-03	1.358E-02

Inflammation_MIF signaling	**2.482E-03**	**1.518E-02**
Proliferation_Lymphocyte proliferation	**3.208E-03**	**1.889E-02**
Cell cycle_G0-G1	**4.661E-03**	**2.647E-02**
DNA damage_Core	**5.574E-03**	**3.056E-02**
Signal transduction_ESR1-nuclear pathway	**6.099E-03**	**3.232E-02**
Development_Regulation of telomere length	**6.522E-03**	**3.244E-02**
Reproduction_Feeding and Neurohormone signaling	**6.529E-03**	**3.244E-02**
Cell cycle_G1-S Growth factor regulation	**7.326E-03**	**3.530E-02**
Immune response_Antigen presentation	**8.752E-03**	**4.093E-02**